Department of Analytical Chemistry
Institute for Nuclear Sciences

INVESTIGATION OF THE OPTICALLY STIMULATED LUMINESCENCE DATING METHOD FOR APPLICATION TO YOUNG GEOLOGICAL SEDIMENTS

Dimitri Vandenberghe

Thesis submitted in fulfilment of the requirements for the degree of
Doctor (PhD) of Science: Chemistry

Promoter: Dr. F. De Corte
Co-promoter: Prof. Dr. P. Van den haute

Academic year: 2003-2004

DANKWOORD

Dr. F. De Corte dank ik voor de kans die hij mij heeft gegeven dit doctoraat te starten, en om de taak van promotor op zich te nemen. De manier waarop hij mij vertrouwd maakte met het nucleair-analytisch onderzoek, zonder hierbij de wetenschap nog moeilijker te maken dan ze al is, kon ik enorm waarderen. Dit doctoraatswerk is het allerlaatste proefschrift waarin de k_0-methode werd toegepast, gebruik makend van reactor Thetis. Bovendien was ik waarschijnlijk ook de laatste doctoraatsstudent die Frans onder zijn konijnenvleugeltjes nam. Ik heb dan ook mijn uiterste best gedaan om van deze thesis iets te maken waar hij terecht trots kan op zijn.
Ik wil Frans vooral bedanken voor het vertrouwen dat hij mij schonk en voor zijn onvoorwaardelijke steun, zowel professioneel als daarbuiten.

Ik dank Prof Dr. P. Van den haute om de taak van co-promotor op zich te nemen en voor de ondersteuning bij het veldwerk. Verder dank ik hem voor de vele interessante toelichtingen bij de geologie en geochronologie, en voor de interessante wetenschappelijke discussies.

Prof Dr. Em. R. Dams en Prof Dr. K. Strijckmans wens ik te bedanken voor het ter beschikking stellen van de infrastructuur.

Dr. C. Kasse (Vrije Universiteit, Amsterdam) wil ik in het algemeen bedanken voor de productieve samenwerking. Meer in het bijzonder dank ik hem voor zijn hulp bij de keuze van de bemonsteringslocaties en bij het veldwerk. Zonder zijn bijdrage had ik het geologisch aspect van dit onderzoek niet zo stevig kunnen onderbouwen.

I would like to thank Prof. Dr. A.S. Murray (the Nordic Laboratory for Luminescence Dating) for his support throughout this entire work. I am very grateful for his willingness to participate in the interlaboratory comparison, for the stimulating discussions, and for sharing thoughts and Duvel...

I also wish to thank Dr. M. Fuchs (Universität Bayreuth) for participating in the laboratory intercomparison and for providing samples. I really enjoyed our discussions, scientific or otherwise, even more so as these were often accompanied by a few beers.

Grateful acknowledgement is made to Prof. Dr. G. Wagner and co-workers at the Max Planck Institut for the cordial manner by which they have received us in Heidelberg. I wish to thank especially Dr. A. Kadereit en Dr. R. Kalchgruber for the valuable discussions, and for providing samples and literature.
More in general, I would like to express my gratitude to all members of the German luminescence dating community, for having me at their meetings and for the warm manner by which they welcomed me there. I thank them for the many useful discussions and suggestions, and for the great time before, in between and after scientific sessions.

I thank Till Fink for sending a copy of his thesis and for the unforgettable time in Marburg.

Grateful acknowledgement is made to Dr. L. Bøtter-Jensen and his co-workers (Risø National Laboratory) for allowing me to visit their lab. I wish to express my sincere thanks to Henrik Christiansen for providing technical support and for answering all the questions I had regarding the OSL-measurement apparatus.

I thank Dr. J.M. Olley for the “Radial plot” program, and Prof. Dr. D.J. Huntley for the Dose-Intercept program.

I am grateful to Dr. M.D. Bateman for allowing me access to his unpublished data of the Grubbenvorst sands.

I would also like to thank the many luminescence workers around the world that shared ideas with me, provided me with reading material, and bothered to reply to my sometimes time-consuming questionnaires.

Alle collega-doctorandi dank ik voor de aangename werksfeer op het INW; in het bijzonder Jan en Marijn voor de leuke gesprekken en voor het blijven hangen op recepties en feestjes. I am grateful to S.M. Hossain, who was my nearest colleague for about four years. His kind and warm companionship made the long hours at the office much more agreeable. His work on the determination of the annual dose-rate was essential for the preparation of this thesis.

Collega-doctorandus Jan-Pieter wil ik bedanken voor de interessante gesprekken en de hulp bij verschillende geologisch facetten van het onderzoek, voor de vriendschap na de werkuren en zijn liefde voor de tripel.

Caroline, Mathieu en Herman wens ik te bedanken voor de indirecte bijdrage die ze met hun Licentiaatsthesis aan dit werk hebben geleverd, en voor hun aangenaam gezelschap.

Zonder de nauwgezette hulp van Jochem bij nagenoeg alle praktische aspecten van dit onderzoek, was dit werk zowel kwalitatief als kwantitatief heel wat minder uitgebreid geweest. Ik ben hem vooral zeer dankbaar voor zijn onvoorwaardelijke vriendschap.

Ing. A. “Tony” De Wispelaere dank ik voor zijn bereidwillige, efficiënte en vriendelijke hulp bij de bestralingen en bij allerhande meet- en rekenwerk.

Alle administatrieve en technische personeelsleden hebben op de één of andere manier bijgedragen tot de totstandkoming van dit werk. Ze zorgden ook voor pret en (veel…) verzet. Ik wil Marc bedanken voor het maken van verschillende monsterhouders en voor het boren van de vele (soms te veel…) gaten, en Maurice voor het blazen van de flotatiecel (een waarachtig artisanaal kunstwerk). Chantal was onmisbaar bij de administratie en ik ben haar ook dankbaar voor de babbels. Lucien dank ik voor het soigneren van Berta en Amanda, voor de occasionele pint en voor de reddende plukjes tabak. Jacques, Rudy en Jos dank ik voor de hulp bij de bestralingen. Zonder Rudy waren bovendien ook mijn weerstanden waarschijnlijk meer dan eens gesmolten, en ik dank hem voor zijn snelle bijstand. Jos wens ik te bedanken voor zijn hulp bij allerlei software problemen, en vooral om mij op tijd uit de illegaliteit van het downloaden te redden. Alhoewel reeds een aantal jaren niet meer op het INW werkzaam, dank ik Ruth voor de overlevering van haar praktische kennis met betrekking tot de monstervoorbereiding, haar aangenaam gezelschap in de donkere kamer en tijdens het studieverblijf in Risø. Jan, Johan en Roger dank ik voor de aangename keuvels. Hugo Palmans wens ik te bedanken voor het uitvoeren van de gamma bestralingen.

Tot slot wens ik mijn familie te bedanken, in het bijzonder Barbara, mama en Ethel. Zonder hun liefde en constante steun, hun begrip voor de vele overuren, en hun eindeloos geduld met mijn luimen, was dit werk nooit voltooid.

Dit onderzoek kwam tot stand met de financiële steun van het Fonds voor Wetenschappelijk Onderzoek, het Bijzonder Onderzoeksfonds van de Universiteit Gent, en Wilfried Hoste.

CONTENTS

INTRODUCTION

The exact reconstruction of past events and processes plays a very important role in a number of scientific disciplines, such as geology and archaeology. An accurate and precise knowledge of the time when certain events took place, of the duration of certain phases or periodicities, and of the rate at which certain processes are active, forms the indispensable basis for every good reconstruction. Hence, the time factor is of primary importance to these scientific disciplines, and the need for geo(archaeo-) chronometric techniques is high. Nowadays, a broad spectrum of chronometric techniques is available, each with its own possibilities and limitations.

A dating method that seems to bring about a real break-through in the chronometry of the last 100 ka is the optically stimulated luminescence (OSL) dating method. Optical dating is used increasingly as a means of establishing the deposition chronology of sediment. It is unique because it uses the constituent mineral grains of the sediment itself (quartz, feldspars) instead of the associated material (such as ^{14}C) that is often scarce or less reliable.

Luminescence dating was originally developed in the 1960's and early 1970's for determining the age of ancient ceramics (Aitken et al., 1964, 1968; Fleming, 1966, 1970; Zimmerman, 1966, 1971; Mejdahl, 1969). The phenomenon used was thermoluminescence (TL), i.e. the light (luminescence) emitted by a sample when it is heated. Subsequent applications involved the dating of various other types of heated archaeological materials, such as burnt flint and stones (for summaries, see Aitken, 1985; Roberts, 1997; and Wagner, 1998), and the method became firmly established for testing the authenticity of art ceramics (Stoneham, 1991). Wintle and Huntley (1979, 1980) were the first to present a workable TL dating technique for determining the time of deposition of sediments. This first application was to deep-sea sediments, but the technique was subsequently extended to a wide range of aeolian and aquatic clastic sediments (see e.g. the review by Prescott and Robertson, 1997). The dating of sediments became the mainstream area of luminescence dating research. In 1985, Huntley et al. discovered that

the dating signal could be stimulated from sedimentary minerals by exposing them to light, instead of heat. Huntley et al.'s pilot work suggested this optically stimulated luminescence (or optical) dating method to be a better means for dating sediments, offering additional practical and methodological advantages. These expectations were soon fulfilled, and nowadays, optical dating has replaced the use of TL almost completely. Especially over the last few years, the method has undergone major developments and enhancements in instrumentation, measurement procedures and the preferred mineral (Bøtter-Jensen et al., 2003a).

Optical dating is thus a relative young method, and it has not yet entirely outgrown its developmental state. Nevertheless, owing to the methodological progress made over recent years, enhanced confidence can be placed in the accuracy of the age results (Murray and Olley, 2002). An increased precision is furthermore available from advanced and sophisticated laboratory procedures for measuring OSL. As a consequence, the method has – notwithstanding its adolescence – already found a considerable application in archaeology and Quaternary geology, and its popularity continues to grow.

Despite this increasing international success, optical dating was, however, not yet applied in our laboratory (or, for that matter, in Belgium). Up to 1999, all the luminescence research was still performed using TL. Although this led to TL ages for some important Belgian loess sections at Kesselt, Rocourt, Harmignies and Momalle (Vancraeynest, 1998; Van den haute et al., 1998, 2003) and for aeolian dune sands from the southern African Kalahari (Munyikwa et al., 2000), our laboratory did lag behind in the immense progress that was being made in luminescence dating technology.

The overriding objective of this thesis, therefore, was to catch up with all these developments, and to set up a laboratory that applies luminescence dating according to the state of the art. In essence, this consisted of the implementation of the optical dating method at the Ghent luminescence dating laboratory, in the first instance for the practical purpose of obtaining accurate and reliable age information for the Late Pleniglacial to Holocene aeolian phases of coversand and drift sand deposition in the West-European lowlands. The implementation and dating research were taken up as an interdisciplinary

co-operation between the Department of Analytical Chemistry (Institute for Nuclear Sciences) and the Department of Geology and Soil Sciences (Laboratory for Mineralogy, Petrology & Micropedology) of the Ghent University.

In Chapter 1 of this thesis, the basic principles of the luminescence process are briefly described, with an explanation of how the phenomenon can be used for dating. Quartz is the dosimeter that has been used throughout this work, and the most important OSL properties of this mineral are discussed in Chapter 2. Although this chapter is based on a study of the literature, it contains results from own research to illustrate some of these properties more clearly. Chapter 3 deals with the two quantities that need to be experimentally determined to arrive at an OSL age, namely the equivalent and the annual dose. An overview is presented of the different measurement protocols and procedures for equivalent dose (D_e) determination, with specific attention to those that have been developed for quartz. Some results from own research are used for the sake of illustration. The most recently developed protocols allow obtaining many values of D_e for a single sample, and a discussion on the interpretation of these data is included. The determination of the annual dose, on the other hand, is the same in TL and OSL dating. Therefore, only the basic notions are covered. As no well-established experience was available in our laboratory for the dating of coarse quartz grains (90-125 μm), however, the specific aspects associated with the evaluation of the annual dose to such grains are discussed in some greater detail.

The actual implementation of the optical dating method in our laboratory is described in Chapter 4. The implementation consisted of the exploration of various aspects of the method, by applying it to quartz grains extracted from a sequence of Upper-Pleniglacial to Late-glacial coversands exposed at the locality of Ossendrecht (SW Netherlands). This site was chosen because a number of radiocarbon dates and earlier luminescence dates are available that provide independent age control, and hence a means for validating other dating procedures.

Finally, Chapter 5 deals with the application of the optical dating method to a sequence of Upper-Weichselian coversands exposed at the locality of Grubbenvorst (SE Netherlands). The exposed sediments bear witness to the landscape evolution in the southeastern Netherlands during the Upper Pleniglacial and Late-glacial. Therefore, the site is

considered as a type locality of considerable importance. Because of the lack of datable organic material, however, no absolute age information is available for the Grubbenvorst section. Using the experience gained in the pilot study (Chapter 4), optical dating was applied to these sediments to establish an improved and reliable chronology for this site. This serves to illustrate the important contribution that the method can make to palaeoclimatic research in our West European lowlands.

– CHAPTER 1 –

ESSENTIALS OF LUMINESCENCE DATING

1.1. General principles of luminescence dating

Luminescence dating belongs to the category of the so-called radiation dosimetric dating methods, which are based on the time-dependent accumulation of radiation damage in minerals. Other members belonging to this family of dating methods are, for instance, fission-track dating and electron spin resonance dating. The radiation damage is the result of the exposure to a low-level of ionising radiation that is omnipresent in nature. The longer a mineral is exposed to this fluence of radiation, the greater the radiation damage. The intensity of the radiation damage is consequently a measure for the total dose (the total amount of energy absorbed from the ionising radiation) the mineral has received over a certain period of time.

In luminescence dating, the intensity of the radiation damage is detected as a small amount of light, which is called luminescence. The radiation damage, and hence the latent luminescence signal, can be removed, or set to zero, by exposure to heat or light. For ancient pottery, for instance, the 'zeroing' took place during manufacturing, when it was baked in an oven. In the context of sediment dating, the zeroing event was the exposure to daylight during erosion, transport and deposition of the mineral grains. This zeroing through exposure to sunlight is also called bleaching. Once the zeroing agent is no longer operative, the luminescence signal can start to build up again. For instance, in the case of sedimentary mineral grains, the clock starts ticking anew when they are shielded from the sunlight by burial under other grains deposited on top of them.

The latent luminescence signal can also be released in the laboratory using the same zeroing agents, heat or light. At this point, however, the luminescence signal that is being emitted will be recorded. If the signal is set free by applying heat, the resulting luminescence is called thermoluminescence (TL). If the measured signal results from exposure of the mineral grains to a beam of light, the emitted luminescence is termed optically stimulated luminescence (OSL).

The luminescence signal measured in the laboratory is thus related to the dose the mineral has received since the last zeroing event. For sediments, the last zeroing event was their exposure to sunlight at deposition. If also the rate is determined at which the dose has been absorbed (or, in other words, the radiation damage was created), then it is possible to calculate an age. This age refers to the time that has elapsed between the moment that a sediment was deposited and the moment of sampling for analysis. This is illustrated in Figure 1.1.

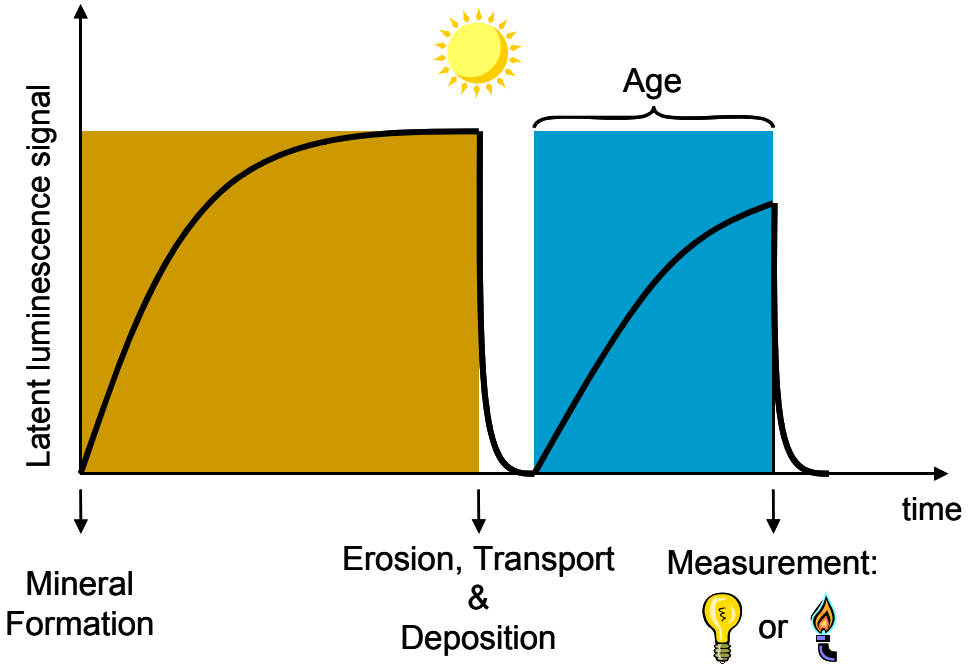

Figure 1.1: Schematic representation of the event that is being dated in the luminescence dating of sediments. Minerals are continuously exposed to a low-level of natural radioactivity, through which they can acquire a latent luminescence signal. During erosion, transport and deposition, the minerals are exposed to sunlight and all the previously accumulated luminescence is removed ("bleaching"). Once shielded from the sunlight, the signal starts to build up again, until the moment of measurement in the laboratory. The age that is being determined is consequently the time that has elapsed between these two zeroing events. The luminescence is measured in the laboratory by exposing the mineral grains to light or heat, and is then termed optically stimulated luminescence (OSL) or thermally stimulated luminescence (thermoluminescence or TL), respectively.

1.2. Mechanism

Although reality is much more complicated and in fact poorly understood, the main processes causing luminescence can be described in terms of the energy level diagram for non-conducting ionic crystalline materials (Figure 1.2; Aitken, 1998).

In this model, electrons are associated with discrete ranges of energy, which are called bands. The lowest energy band is the valence band; the highest energy band is the conduction band. The gap between the two is the so-called 'forbidden zone'. In an ideal crystal, no electron occupies a position in this zone. In any natural crystal, however, defects are present that disturb the perfectly ordered crystalline structure. Many types of imperfections are possible such as impurities (either as substitutionals or in interstitial positions) or missing atoms. These defects give rise to the presence of energy levels within the forbidden zone. Whereas the conduction and the valence band extend throughout the crystal, the defect states are associated with the defects themselves, and are therefore called localized energy levels. These localized energy levels are the key to the luminescence phenomenon, as they carry the memory of exposure to nuclear radiation. In other words, luminescence requires the existence of lattice defects.

In nature, a low level of nuclear radiation is omnipresent. This radiation has an ionizing effect and, upon interaction with the crystal, can raise an electron from the valence band into the conduction band [Figure 1.2(a)]. For every electron that is created, an electron vacancy, termed a hole, is left behind and both the electron and hole are free to move through the crystal. In this way, energy of the nuclear radiation is taken up. The energy can be released again (usually as heat) by recombination. Although most charges indeed do recombine directly, another possibility is that the electron and the hole are trapped at the defect centers. In this case, the nuclear energy is stored temporarily in the crystal lattice and the system is said to be in a metastable situation [Figure 1.2(b)]. Energy is required to remove the electrons out of the traps and to return the system to a stable situation. The amount of energy that is necessary, is determined by the depth E of the trap below the conduction band. This trap depth consequently determines how long an electron will stay in the trap. To empty deeper traps, more energy will be required and those traps are more stable over time. For dating, we are only concerned in those traps deep enough (i.e. ~1.6 eV or more) for the lifetime to be at least several million years (see Section 1.3).

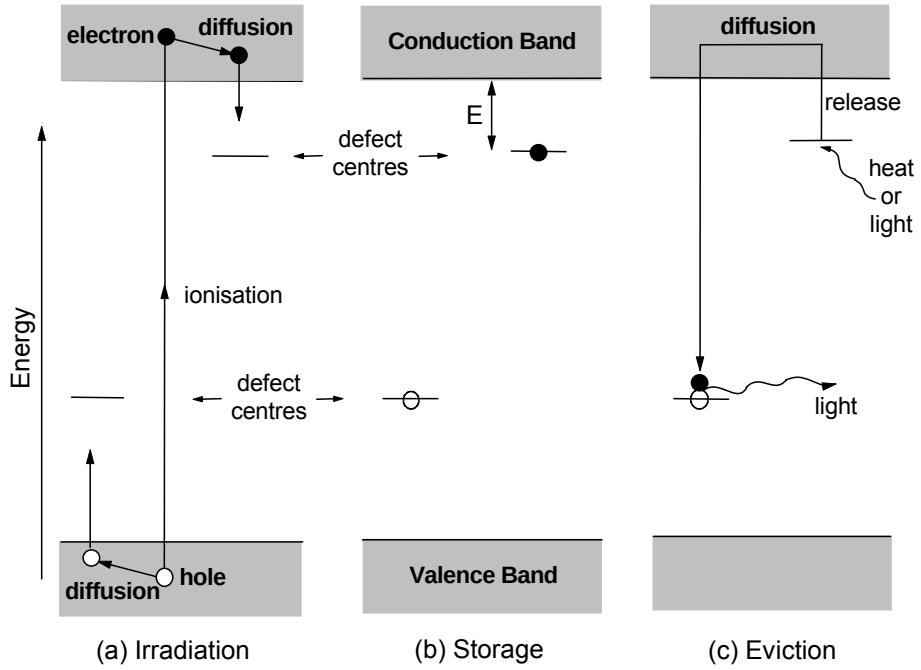

Figure 1.2: Energy-level representation of the luminescence process (adopted from Aitken, 1998). ○: hole; ●: electron.

By exposing the crystal to heat or light, the trapped electrons may absorb enough energy to bridge the barrier to the conduction band [Figure 1.2(c)]. Once evicted, they can be trapped again, or they can recombine with holes in the so-called recombination centers. These are defect sites attractive to electrons. The recombination can result in either the emission of heat (non-radiative recombination) or light (radiative recombination). The defect sites where the radiative recombination occurs are called luminescence centers, and the resulting light is termed thermoluminescence or optically stimulated luminescence, depending on whether heat or light, respectively, were used to release the electrons from the traps. The amount of light emitted is proportional to the amount of electrons stored in defects, and hence to the amount of energy absorbed from nuclear radiation. Since the energy is absorbed at a certain rate, the intensity is related to the time of accumulation; the longer the material is exposed, the more signal is acquired. The colour (wavelength) of the emitted luminescence depends on the type of luminescence center where the recombination takes place.

The details of how luminescence is produced in any given mineral are at present poorly understood. It is only for crystals grown in the laboratory under strict controlled

conditions of impurity content and heat treatment that a more complete picture can be obtained. Nevertheless, the main features of the mechanism by which luminescence is produced, and of how the phenomenon can be exploited for dating purposes, can be understood from the simplified representation given above. It can be added that other types of insulators (such as glasses), as well as semi-conductors also exhibit luminescence; metals, on the other hand, do not. For more complex and detailed accounts on the physical theory, reference is made to McKeever (1985), Chen and McKeever, (1997) and Bøtter Jensen et al. (2003a).

1.3. Signal growth and trap stability

From the previous section it is clear that the intensity of the luminescence signal is proportional to the number of electrons trapped: the longer the irradiation time, the more electrons will have become trapped and the higher the luminescence intensity. There are however two limitations. First of all, the total number of traps that is available for storing the charge is limited. Consequently, under continuous irradiation, the available traps are gradually filled and eventually saturation will be reached. A second limitation is that electrons are also spontaneously evicted from their traps, a process which is termed 'thermal fading' (see later).

Taking both effects of thermal fading and saturation into account, the growth of the luminescence intensity (I) as a function of time can be described by the following equation (Wagner, 1995):

$$I(t) = S \times \dot{D} \times \tau \times (1 - e^{-\frac{t}{\tau}}) \qquad (1.1)$$

with:

S = the sensitivity; the amount of luminescence per unit of dose

$\dot{D}$ = the dose rate; the dose received per unit of time

τ = the apparent mean lifetime

t = the time span of signal accumulation

The term $S \times \dot{D}$ refers to the increase in luminescence intensity due to the filling of the traps, while the term $\tau \times (1 - e^{-\frac{t}{\tau}})$ takes the saturation and thermal fading effects into account. Equation 1.1 can be simplified to:

$$I(t) = I_{max} \times (1 - e^{-\frac{t}{\tau}}) \tag{1.2}$$

with $I_{max} = S \times \dot{D} \times \tau$, i.e. the maximum intensity that can be built up and measured.

The apparent mean lifetime τ can be written as (see e.g. Wagner, 1995; Vancraeynest, 1998):

$$\tau = \frac{\tau_S \times \tau_T}{\tau_S + \tau_T} \tag{1.3}$$

with τ_s a decay constant taking into account that the number of traps is limited and τ_T the mean lifetime. The mean lifetime is the average residence time of electrons in a given type of trap and at a temperature T.

It is clear from the above that both the saturation characteristic (τ_s) and the long-term stability of the signal (τ_T) determine the highest intensity to which a luminescence signal can grow, and hence also the upper dating limit that can be attained.

The saturation dose depends, to a first approximation, on the mineral under consideration. Quartz, for instance, generally saturates at a much lower dose compared to feldspars. Prescott and Robertson (1997) mention an age limit of 100-200 ka for quartz, while feldspars could possibly provide ages up to 1 Ma, if they do not suffer from anomalous fading (see Section 1.4). However, if the quartz minerals are exposed to a very low-level of natural radioactivity, the traps are also less rapidly filled, which extends the age range over which this mineral can be used. For instance, a low dose rate enabled Huntley et al.

(1993, 1994) and Huntley and Prescott (2001), to obtain quartz-based luminescence ages as old as ~700-800 ka.

Investigations that have been carried out over the last few years, however, suggest that, at least in the case of quartz, the saturation dose is not a general property of a sample under consideration, but can vary from grain to grain. Furthermore, different components of the luminescence emitted by quartz have been found to exhibit different saturation characteristics. All these studies suggest that quartz could be useful over a larger age range than was previously thought. These issues will be further addressed in Chapter 2.

Besides the limitations imposed by signal saturation, the mean lifetime also restricts the age range over which a luminescence signal can be used for dating; the luminescence signal employed should be sufficiently stable. By this, it is meant that only those traps should be sampled during the measurement from which there has been a negligible loss of electrons over the time span that is being dated. It is usually said that unstable luminescence arises from shallow traps while stable luminescence arises from deep traps. The probability for electrons to escape from a deep trap is low, and the lifetime (τ_T) is correspondingly high. The possibility exists though, owing to the random chance of an abnormally large energetic lattice vibration causing the eviction. At a constant temperature, the number of trapped electrons, n, exponentially decays with time according to:

$$n(t_2) = n(t_1) \times e^{-\frac{t_2 - t_1}{\tau_T}} \qquad (1.4)$$

In the context of dating, the time interval t_2-t_1 of interest is the age of the sample. However, when calculating the fraction of electrons that spontaneously escapes during this period of time, it must be taken into account that there are no electrons in their traps at time zero [i.e. at $t_1 = 0$, $n(t_1) = 0$] and that they become trapped at a uniform rate thereafter. For such a situation, it can be shown to a good approximation (Aitken, 1985) that the fractional loss of luminescence due to escape during the sample's age span, t_s (= t_2-t_1), is given by $\frac{1}{2}(t_s/\tau_T)$ as long as t_s does not exceed one third of τ_T. This means that to avoid an age underestimation by e.g. 5%, the lifetime consequently needs to be at least 10 times the age.

The spontaneous signal loss with time is termed thermal fading because of the dependency of the lifetime on the burial temperature. For first order kinetics, this temperature dependency is defined through the following equation:

$$\tau_T = s^{-1} \times e^{\frac{E}{k \times T}} \tag{1.5}$$

with:

s = the frequency or pre-exponential factor (in s^{-1}); this may be thought of as the number of attempts to escape per second
E = the depth of the trap (in eV)
T = the absolute temperature (in K)
k = Bolzmann's constant (8.6173×10^{-5} eV K^{-1})

Techniques for the evaluation in the laboratory of the main kinetic parameters, such as E and s, from which the lifetime is predicted, can be found in Chen (1976), McKeever (1985) and Chen and McKeever (1997), and references therein.
Predicting lifetimes is useful as it helps to establish the likely time range over which a given signal from a given mineral will be useful. It is also important because a measured optically stimulated luminescence signal does not contain any intrinsic information with regard to its stability. The OSL signal arises from electrons that are evicted out of all traps that are sensitive to the light employed for stimulation, whether these traps are deep (stable) or not (unstable). It can be noted that this is quite contrary to the situation in TL. In the latter case, the luminescence is recorded as a function of temperature. The curve so obtained is termed a glow curve, and this consequently can be interpreted as a plot of luminescence versus trap stability (as temperature increases, progressively deeper – and hence more stable – traps are being sampled; see e.g. Aitken, 1985 and Vancraeynest, 1998). Apart from rather physically oriented measurements, evidence for a signal from sufficiently stable traps being used can also be gained more empirically, from the dating of materials of known age. Some further considerations regarding signal stability and lifetimes that are directly relevant to the present work are discussed in Chapter 2.

In nature, the filling rate of the traps is low. As the shallow traps loose their electrons rather quickly, this means that the luminescence signal measured from a natural sample will be primarily associated with deep traps. Thermal fading will become visible and will lead to an age shortfall when the age of the sample is significant compared to the lifetime of the electrons in the traps that are being sampled during the measurement of the natural luminescence signal.

For reasons outlined in Chapter 3, however, it is also necessary to irradiate the sample in the laboratory, and to compare the artificial luminescence signals so induced with the natural signal. In the laboratory, the doses are administered to the samples at a much higher rate than in nature. Now, the shallow traps will be filled and, owing to the short time scale over which the experiments are carried out, they may contribute significantly to the artificial signal. Therefore it is necessary to remove this unstable "contaminating" luminescence by emptying the shallow traps before the signal is measured. This emptying is usually accomplished by heating the sample prior to measurement. This treatment is called preheating and it will be further discussed in Chapter 3, together with the additional reasons for why it is necessary.

1.4. Anomalous fading

Equation 1.5 describes the expected mean lifetime of an electron in a trap of depth E and escape frequency s at a storage temperature T. For deep traps and at low temperatures, the lifetime will consequently be quite large and leakage of electrons from these traps will be low. However, it has been observed for many materials that the electrons are released from their traps at a much faster rate than predicted by equation 1.5. This fading of the luminescence signal is therefore termed 'anomalous' (abnormal) fading.

For natural minerals relevant to dating, the result of anomalous fading is an age shortfall, regardless of whether TL or OSL signals are being used. The effect was first observed by Wintle et al. (1971) and Wintle (1973), when trying to date feldspars extracted from volcanic lava with TL. The ages obtained were significantly lower than the accepted ages for the lava flows. The effect has subsequently been observed and investigated in a number of studies such as by Wintle (1977), Clark and Templer (1988), Spooner (1992; 1994a), Visocekas (2000) and Auclair et al. (2003).

A number of natural dosimeters, most notably zircon and several types of feldspar, suffer from anomalous fading. It is generally accepted, however, that quartz is not affected by this phenomenon. Wintle (1973) reported no loss in TL after storage of the quartz for 2 years, while Roberts et al. (1994a) did not detect any loss in the OSL from quartz after 70 days storage at room temperature. Readhead (1988) found anomalous fading of TL in quartz from southeastern Australia, but Fragoulis and Stoebe (1990) and Fragoulis and Readhead (1991) subsequently found fading feldspar inclusions to be present in these quartz grains.

Of all the mechanisms that have been proposed to explain anomalous fading, quantum mechanical tunneling of electrons to nearby recombination centers is probably the most accepted one. For more details on this, and other suggested explanations, reference is made to Aitken (1985, Appendix F), Aitken (1998, Appendix D), McKeever (1985), Chen and McKeever (1997) and Bøtter-Jensen et al. (2003a). These publications also provide a comprehensive overview on the reported observations of the effect, and address practical issues that are relevant in a dating context, such as ways to detect, overcome or correct for anomalous fading. Recent work on the correction for fading in feldspar minerals is that by Auclair et al. (2003) and Lamothe et al. (2003).

1.5. Stimulation of the signal

From Section 1.2 it is clear that the same production mechanism is responsible for the two luminescence phenomena, TL and OSL, and that the only difference lies in the way the electrons are stimulated out of their traps.

In OSL, the electron escapes from its trap as the result of the absorption of a photon of light with a sufficient energy. The rate of eviction depends on the intensity of the stimulating light and the sensitivity of the trap to light. There is also a dependency on the temperature of the sample (see Chapter 2).
The intensity refers to the number of photons arriving within a certain time. It can easily be understood that the more photons arrive per unit of time, the more electrons will be stimulated out of their traps. The light-sensitivity of a trap can be understood by

imagining the traps as baskets and the stimulating light photons as balls. Not all baskets have the same diameter; some are large whereas others are small. The balls will obviously have the highest probability of going into the largest baskets. These large baskets hence represent the most light-sensitive traps. The light-sensitivity of a trap is not well described by the trap depth E; it depends on other characteristics of the trap, as well as on the wavelength of the stimulating light (Aitken, 1998). In general, shorter wavelengths (higher energy) are more effective in stimulating electrons from their traps.

It would consequently seem advantageous to use a short wavelength for stimulation. However, an important limitation to the wavelengths that can be used for stimulation is imposed by the wavelength of the emitted luminescence. Indeed, when detecting the luminescence emitted by a sample, one clearly has to avoid a situation in which it is diluted by the stimulating light. Consequently, stimulation and luminescence emission wavelength regions need to be well separated from each other. Furthermore, the wavelength of the luminescence signal that is used for dating should be shorter than the one used for stimulation. This is to avoid the possibility of measuring luminescence from electrons which are not detrapped, as zero setting is in doubt for such a signal (Aitken, 1998). From these latter points of view, it would hence be advantageous to use longer stimulation wavelengths, as then a larger range of wavelengths becomes available for luminescence detection without any risk of measuring the stimulating light as well.

Finally, the type of mineral that is under investigation also plays a role in the selection of the most appropriate light source for stimulation. A given wavelength can be effective for stimulating a luminescence signal from some minerals, whereas for other minerals, it proves to be not suitable.

From the above considerations, it was found that for quartz, for instance, stimulation by visible light with a wavelength somewhere in the blue to green region of the spectrum is appropriate. For feldspathic minerals, but not for quartz, on the other hand, it has been found that long wavelengths, in the infrared region (800-900 nm) also can be used (Hütt et al., 1988). It can be mentioned here that longer wavelengths can also be effective, if the temperature of the sample is raised. This effect is called thermal assistance and will receive some further attention in Chapter 2.

Depending on the wavelength used for stimulation, the resulting luminescence is termed **i**nfra**r**ed **s**timulated **l**uminescence (IRSL), **b**lue-plus-**g**reen **s**timulated **l**uminescence (BGSL), **g**reen **l**ight **s**timulated **l**uminescence (GLSL or GSL) or **b**lue **l**ight **s**timulated **l**uminescence (BLSL or BSL). OSL generally refers to any luminescence signal that is obtained via stimulation with light, regardless of the wavelength. In some literature, however, the term OSL should be read as encompassing visible stimulation wavelengths only. To avoid confusion, it is therefore perhaps more appropriate to specify the stimulation wavelength, for example as OSL (514.5 nm).

1.6. Minerals used for optical dating

Feldspars and quartz are the most widely used minerals in the optical dating of sediments. Both types have been found to emit OSL signals that can be used for dating. The choice of the mineral that is being used usually depends on the availability within a sample, and the age of the sediments. Quartz saturates at lower doses than feldspars, and so the use of feldspar might prove to be advantageous for dating older deposits. Whereas for sand-sized grains (of ~0.1 mm in diameter), the different mineral fractions can be easily separated from each other, this is not the case for silt-sized grains (of ~0.01 mm in diameter). Usually, the measurements are then carried out on the polymineral fine fraction, which is a mixture of all kinds of minerals with a grain size within the range 4-11 μm.

Zircon (Smith et al., 1986; Smith, 1988) and apatite (Smith et al., 1986) have been found to emit OSL as well, but apart from these studies, their applicability for dating purposes does not seem to have been further investigated. Compared to feldspar and quartz, these minerals occur in sediments in much smaller quantities, which limits their use in any case. Finally, it is perhaps worth mentioning that also glass extracted from volcanic ash deposits has been found to emit OSL (Berger and Huntley, 1994; Berger and Neil, 1999). Encouraging initial results were obtained, but further work is necessary to establish the full extent to which this glass might be suitable for optical dating.

– CHAPTER 2 –

OSL FROM QUARTZ

Quartz is the dosimeter that has been used throughout this work. This mineral was chosen because of its abundance in the sediments to be investigated, and because it has certain advantages with regard to microdosimetry and anomalous fading. Furthermore, over the last seven years or so, considerable progress has been made in the understanding of its luminescence properties, through which it nowadays has become the preferred mineral for dating purposes. In this chapter, the key features of the quartz OSL signal are discussed.

2.1. Stimulation of quartz

A stimulation spectrum yields information on the efficiency by which a certain wavelength is able to stimulate a certain mineral. For instance, Hütt et al. (1988) discovered in this manner that infrared light could be used for stimulating feldspars, but not for quartz. Knowledge of the stimulation spectra is however not only important because it allows the selection of a specific mineral, but also for optimising the stimulation wavelength to obtain a maximum light output.

Bøtter-Jensen et al. (1994) investigated the stimulation efficiency of quartz at different wavelengths. They found an increase in signal intensity (I) with decreasing stimulation wavelength (increasing energy), as is shown in Figure 2.1. Stimulation spectra were also published by Ditlefsen and Huntley (1994; further elaborated by Huntley et al., 1996) and Kuhn et al. (2000), with no significant differences. It can be seen in Figure 2.1 that there is a slight change in response at around 500-520 nm. The reason for this "knee" is still poorly understood. The same observation was made by Kuhn et al. (2000) who, consequently, recommended avoiding stimulation with wavelengths in this region to minimize additional scatter in the luminescence output from identical samples.

The stimulation spectrum also shows that practically no luminescent signal is to be expected when quartz is stimulated with infrared light. Spooner (1994b) also found that wavelengths greater than 690 nm are inefficient for stimulating a luminescence signal

from quartz. This is quite opposite to the situation for feldspars, for which also infrared light in between 800 and 900 nm can be used.

Godfrey-Smith et al. (1988) and Godfrey-Smith and Cada (1996), however, did observe an IRSL signal from quartz, which they attributed to charge-compensated Al impurities in the quartz lattice, rather than to the feldspathic microinclusions that were found to be present within the quartz grains. Up to now, however, apart from these rather isolated reports, no other evidence for a substantial IRSL signal originating at room temperature from the quartz lattice itself has been reported in literature.

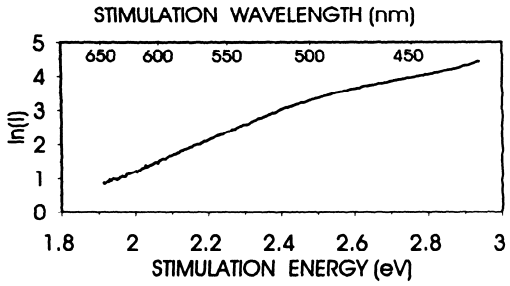

Figure 2.1: Optical stimulation spectrum of quartz (from Bøtter-Jensen et al., 1994).

The experimental data shown in Figure 2.1 are seemingly in contradiction with the theoretical expectation that for quartz ~400 nm is the maximum wavelength for which eviction should occur (see e.g. Chen and McKeever, 1997, p. 218, or Aitken, 1998, p. 16 and 34, for further explanation). However, raising the sample temperature increases the rate at which electrons are evicted from their traps. This phenomenon is termed “thermal assistance” and allows lower photon energies (i.e. longer wavelengths) to be effective as well for stimulating luminescence. Provided that the sample temperature is sufficiently high, luminescence can then be observed even under IR stimulation. Thermal assistance has been documented by a number of authors, such as Spooner (1994b), Huntley et al. (1996), Bailey et al. (1997) and Bailey (1998).

A variety of light sources have been used throughout the years for stimulating OSL from quartz. At first, the 514.5 nm line from an argon ion laser was used (e.g. Huntley et al. 1985; Smith et al. 1990a, 1990b). As techniques developed, more convenient light sources, with regard to stability, lifetime and cost, became available. Systems have been

described where the stimulation is provided by light filtered from a halogen lamp (Bøtter-Jensen and Duller, 1992; Bortolot, 1997) or from a xenon arc lamp (Bortolot, 1997). Galloway (1993, 1994), Galloway et al. (1997) and Bortolot (2000) report on stimulation units based on green light from light emitting diodes (LED's). In this work, use was made of powerful blue (470 nm) LED's developed by Bøtter-Jensen and co-workers (1999a, 1999b, 2003b). The set-up will be outlined in Section 2.3, as well as in Chapter 4. Comprehensive reviews of the various optical stimulation sources have been presented most recently by Bøtter-Jensen et al. (2003a, 2003b).

2.2. Emission by quartz

As the colour (or wavelength) of the emitted luminescent signal is characteristic for the luminescence centre (see Chapter 1), emission spectra carry information about these recombination centres. Knowledge of luminescence emissions also helps to select the most appropriate detection window for dating, as different emissions might have different characteristics with regard to stability, bleachability or dose-response. Some signals are also characteristic of a certain mineral, and selection of an appropriate wavelength may therefore favour the contribution of one mineral with respect to another.

Whereas there are only a few studies concerned with quartz OSL stimulation spectra, there are even less reports on emission spectra from quartz OSL. Up to now, the only information available is that published by Huntley et al. (1991; the same data are presented in Huntley et al., 1996). Using 647 nm stimulation at room temperature, they found a single emission band centred at 365 nm (Figure 2.2), which confirmed the preliminary findings of Huntley et al. (1989). Similar spectra were obtained with green (514.5 nm) light stimulation.

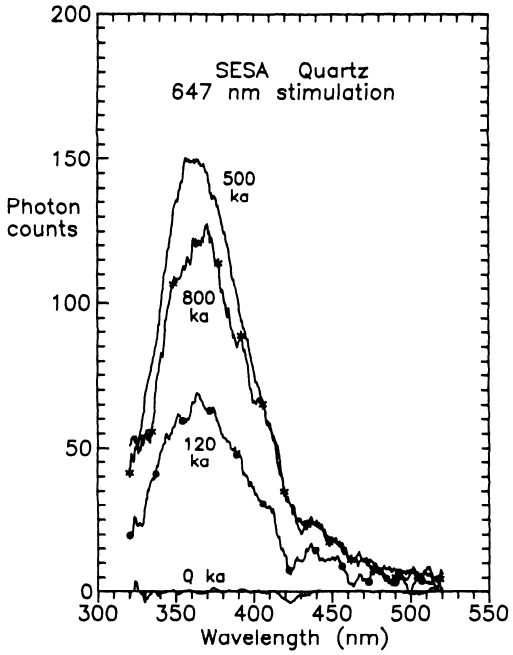

Figure 2.2: OSL emission spectrum of quartz (from Huntley et al. 1991). The data were obtained using 647 nm stimulation, but similar spectra were obtained using 514.5 nm. The quartz grains were extracted from dunes of various ages from south-east South Australia (see Huntley et al., 1993).

TL emission spectra, on the other hand, have been collected by a number of authors and summaries have been presented e.g. by McKeever (1985), Prescott et al. (1995), Krbetschek et al. (1997) and, most recently, by Bøtter-Jensen et al. (2003a). With respect to their use in luminescence dating, the three main quartz TL emission bands are at 360-440 nm (UV-blue), at 460-500 nm (blue-green) and at 600-650 nm (orange-red).

In their study of an Australian sedimentary quartz, Franklin et al. (1995) concluded "that the quartz TL peak at 305-325°C and the peaks at 95-110°C, 150-180°C and 200-220°C, which all emit at wavelengths below 430 nm, form a family, the electron traps of which all feed the same luminescence centre using the conduction band for electron transport." Based on their similarity in emission wavelength, the quartz OSL emission is thought to originate from the same recombination centres as those from which these TL peaks arise. As can be seen from Table 2.1, the emission wavelengths are indeed similar (note that the emission peak shifts to longer wavelengths as the temperature is raised), and are consistent with the OSL emission centred at 365 nm at room temperature. It remains to be

confirmed however, if the OSL emission wavelength also increases with increasing temperature.

Temperature (°C)	Wavelength (nm)
22	365
95-110	376
150-180	392
200-220	410
305-325	430

Table 2.1: Emission wavelengths of the "family" of TL peaks at ~100, 180, 220 and 305°C (Franklin et al., 1995). The emission peak at room temperature is for OSL, and was obtained by Huntley et al. (1991; see Figure 2.2).

The probable luminescence centre giving rise to the OSL emission has been identified by Yang and McKeever (1990a, b) as the $[H_3O_4]^\circ$ centre (these are silicon vacancies, occupied by 3 hydrogen atoms and a trapped hole, the latter being denoted by the superscript °). Using ESR (electron spin resonance) and TL, they were able to show that two point defects are responsible for the TL signal at ~100°C, namely $[AlO_4]^\circ$ and $[H_3O_4]^\circ$. However, only the $[H_3O_4]^\circ$ centre yields emission at 380 nm, comparable to the OSL emission (Figure 2.2 and Table 2.1), from which is deduced that it is the most likely recombination centre.

2.3. Measuring the OSL from quartz

To avoid detecting the stimulation light without a significant attenuation of the 365 nm luminescence to be measured, the wavelengths must be sufficiently separated from each other. Also, the stimulation wavelength must be longer than the one from the desired luminescence, to avoid the use of signals originating from traps that are not relevant to dating (Aitken, 1998; see also Chapter 1). On the other hand, the stimulating light must remain sufficiently energetic for the stimulation to be efficient.

A set-up of the possible wavelength windows for stimulating and detecting OSL from quartz – more specifically, the one used in this work – is shown in Figure 2.3. The stimulation is achieved by blue diodes emitting at 470 nm (Bøtter-Jensen et al., 1999a, 1999b, 2003b) and the resulting quartz OSL is detected through a Hoya U-340 UV filter. A Schott GG 420 optical filter removes the tail of the diode emission extending to shorter wavelengths. The Hoya U-340 filter also has a red transmission window (not indicated in the figure) and consequently the long wavelength tail in the blue diode emission spectrum could contribute to the measured luminescence. This problem is solved by using metal oxide coated U-340 filters (Bøtter-Jensen et al., 1999a), or, as was the case in this work, by using filters of a sufficient thickness (e.g. 7.5 mm) to ensure a complete attenuation of this disturbing component. Figure 2.3 also includes the data from Table 2.1 to illustrate that the U-340 filter is suited for measuring the OSL at room temperature, but that with increasing measurement temperature, the shift in emission wavelength causes a progressive loss in detection.

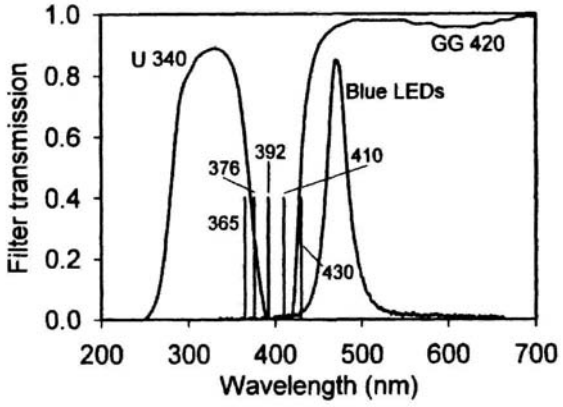

Figure 2.3: Characteristics of OSL emission and TL emission (see Table 2.1) and stimulation and detection windows (redrawn from Bøtter-Jensen et al., 1999b by Wintle and Murray, 2000).

2.4. The quartz shine-down curve

When measuring an optically stimulated luminescence signal, the emitted luminescence is recorded as a function of stimulation time. The resulting plot is called a 'shine-down' curve. An example of a shine-down curve obtained for one of the quartz samples investigated in this work is shown in Figure 2.4.

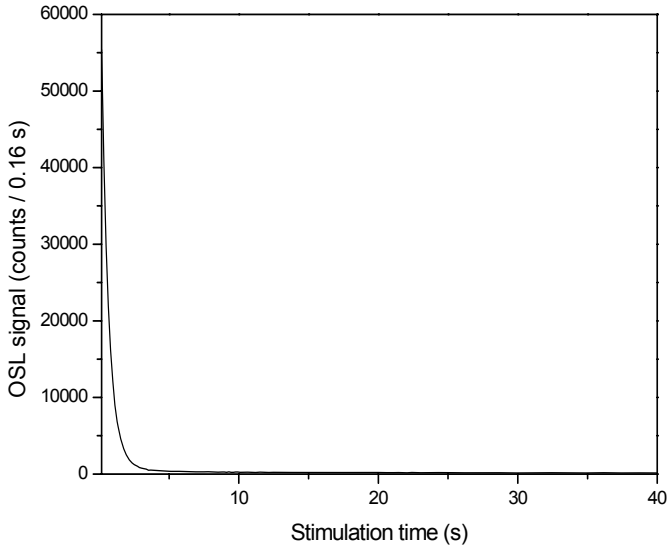

Figure 2.4: Example of a shine-down curve – the measured luminescence as a function of stimulation time.

The observed signal can be seen to decay with time. The commonly accepted explanation for this decay is that the number of trapped electrons is progressively depleted during stimulation. When the stimulation is for a long enough period, all the light-sensitive traps will be emptied. The total luminescence recorded (the area beneath the shine-down curve, or 'light-sum') is proportional to the number of electrons that was trapped (and hence to the accumulated dose). Because the probability of a photon interacting with a trapped electron is proportional to the total number of trapped electrons present, this is also true for a short exposure to stimulation light. The latter is called a 'short-shine' and involves consequently the sampling of only a fraction of the total population of charge trapped.

The OSL signal is usually recorded at a constant stimulation power, i.e. the rate at which the stimulating photons arrive is kept constant. As was previously mentioned in Chapter 1, the rate of electron eviction, and hence the decay rate of the shine-down, is dependent on the stimulation power. This dependency is illustrated in Figure 2.5. The dashed curve represents the luminescence measured at half of the stimulation power used to measure the solid curve. It is clear that doubling the stimulation power initially leads to doubling of the measured signal, and that the signal decays more rapidly. The light-sum is the same for both curves.

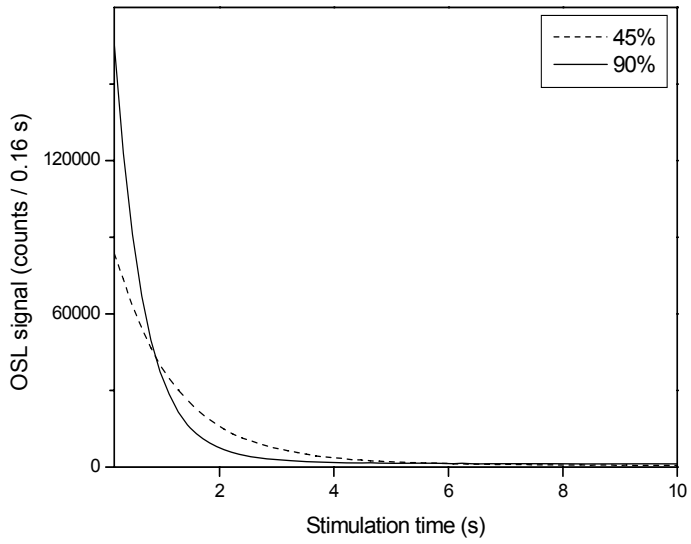

Figure 2.5: Influence of the stimulation power on the quartz shine-down curve. The stimulation light power used to record the shine-downs, expressed as percentage of the maximum power that is possible, is indicated in the upper right corner. The quartz grains were extracted from a fluvial sand that was investigated in this work (Grubbenvorst, lab code G10). The measurements were carried out at 125°C, after sensitising and stabilising the signal through repeated irradiation (~29 Gy) and heating (to 500°C) cycles.

Furthermore, there is a dependence on sample temperature. At low temperatures (~20°C), the eviction rate increases at about 1% per °C (Aitken, 1998). This is due to thermal assistance (see Section 2.1) and the effect is illustrated in Figure 2.6. It can be seen that stimulation at higher temperature results in an initially higher light output, and a steeper decay of the signal with time. There is however a competing process called "thermal quenching", which causes the efficiency of luminescence centres (i.e. their ability to emit a photon when an electron arrives) to decrease when the sample temperature is raised (Chen and McKeever, 1997, p. 74-76; Wintle, 1975). Due to this process the total light-sum is less for the shine-down recorded at the higher temperature. A shift to higher emission wavelengths can also cause the total measured luminescence to decrease (see Figure 2.3).

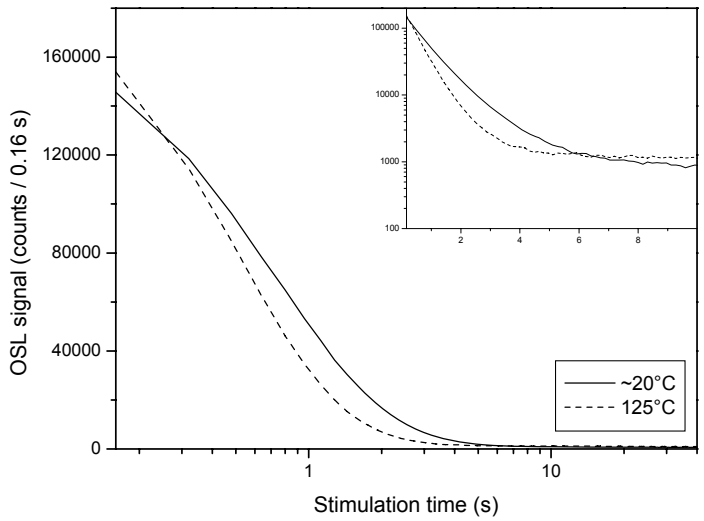

Figure 2.6: Influence of the measurement temperature on the shine-down curve. The quartz is the same as in Figure 2.5. Note that, for visualisation purposes, the intensity and stimulation time are shown on a linear and on a logarithmic axis, respectively, while in the inset the scales are inversed.

Stimulating with a high power and at an elevated temperature has the immediate practical advantage that the background becomes less important. This is especially relevant for measuring so-called "dim" samples. These are samples with a low light output either because they are insensitive, or because they are young. Due to the temperature dependence and the difficulty of maintaining a constant room temperature, working at an elevated temperature also improves the reproducibility of the measurements. There is, however, another reason why stimulating at higher temperatures proves to be advantageous, as discussed below.

Assuming that the loss of trapped electrons per unit of time (expressed as percentage of those remaining) remains constant throughout the shine-down, the number remaining is expected to decrease exponentially. The process is exactly the same as the one describing radioactive decay and can be expressed by:

$$\left(-\frac{dN}{dt}\right) = \lambda N \tag{2.1}$$

where N is the number of electrons remaining in the traps at time t and λ is a decay constant describing the probability that an electron will escape from the traps. The solution of this equation is:

$$N = N_0 e^{-\lambda t} \tag{2.2}$$

with N_0 the number of trapped electrons at t=0.

The OSL emitted per unit of time is proportional to the rate at which electrons are evicted from their traps, namely λN. The luminescence output consequently can be described as:

$$L = L_0 e^{-\lambda t} \tag{2.3}$$

with L_0 the value of L at t=0.

Consequently, assuming that the luminescence intensity is only determined by the rate of electrons escaping from traps*, one would expect the OSL curve to decay exponentially. However, the decay of the actually observed OSL signal is typically slower than exponential. This is illustrated in Figure 2.7, where the first 15 s of a shine-down is shown (note the logarithmic scale). The solid line represents the measured OSL signal. The dashed line shows what the measured OSL signal would look like if its decay could be truly characterised by a single exponentially decaying function.

* This implies that the change in the probability of an evicted electron giving rise to a luminescence photon (meaning the degree to which available luminescence centres are used up during the stimulation) and the probability of electrons being retrapped must be small.

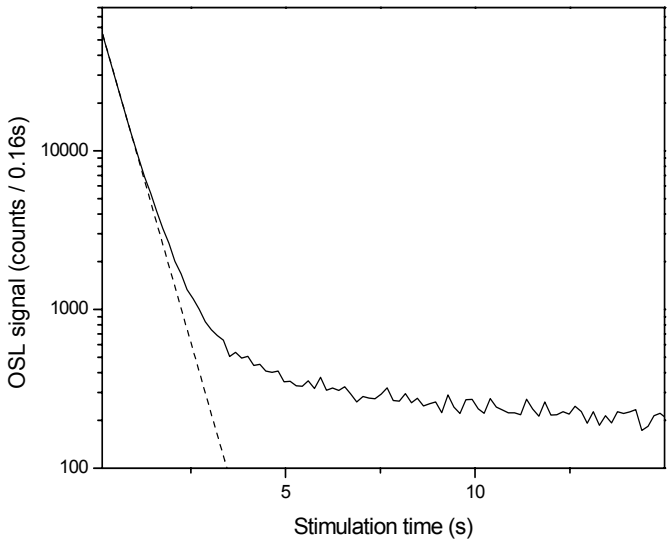

Figure 2.7: OSL signal (logarithmic scale) as a function of stimulation time (linear scale). The shine-down measured is shown as the solid line. The dashed curve shows what a single exponentially decaying signal would look like, having the same depletion rate as during the first 1 s of stimulation. The signal is the natural OSL signal from sample G7 (Grubbenvorst) and was measured at 125°C after a preheat of 10 s at 240°C, using the blue diodes for stimulation.

The slower-than-exponential decay can be explained by a number of causes (Aitken, 1998):

1) two or more traps are contributing to the observed OSL signal. These traps have different eviction probabilities and hence different depletion rates. In other words: the signal consists of different components. It is not necessary that each of these components then decays exponentially, as other processes (see e.g. #2 or #3) might still be operative;
2) some of the evicted electrons get trapped again in other OSL traps, instead of recombining directly. They are evicted later on, together with electrons released for the first time, as the stimulation process continues;
3) instead of being retrapped in the OSL traps, the electrons can get trapped temporarily in other traps. Subsequently they can be thermally evicted and give rise to a delayed signal;
4) the probability that an electron produces a photon changes during the stimulation (= the luminescence efficiency changes). This can be due to the retrapping of

charge in one way or another (see e.g. #2 and #3) or to a limited availability of luminescence centres. With respect to the latter possibility, it can be mentioned that McKeever and Morris (1994) and McKeever (1994, see also McKeever, 1991) describe the results obtained from a computer simulation of the bleaching of TL and the production of OSL during optical stimulation. In the model used for the simulation, the radiative recombination centers are depleted during optical stimulation. The simulated OSL signal decays rapidly at first, but has a long tail such that the overall decay is not exponential, which is in agreement with experimental observations. Wintle and Murray (1997), however, later found McKeever's model insufficient to explain their experimental observations.

A number of authors have shown that there is charge traffic between the OSL trap and other traps that temporarily store the electrons (possibility #3). More specifically, it has been demonstrated that electrons can be transferred both in and out of the quartz 110°C TL peak during optical stimulation (e.g. Bailey 1997; Wintle and Murray, 1997; Murray and Wintle, 1998). Figure 2.8 demonstrates this transfer of electrons (from the trap associated with the 325°C TL peak; see section 2.10) into the trap associated with the 110°C TL peak during the stimulation of an OSL signal. The 'no bleach' glow curve refers to the TL regenerated in a portion of (previously annealed) quartz grains by a beta dose of ~29 Gy. The second glow curve ('after bleach') was obtained in the same way, but the sample was first exposed to blue diode light (which releases an OSL signal) before the TL was recorded. Comparison of the two glow curves shows that the exposure to light caused a loss in TL at around 300°C and induced a new peak at about 100°C. This effect is known as photo-transferred TL.

This recycling of electrons in and out of traps would give rise to second-order effects. Murray and Wintle (1998) unambiguously identified the effect of the 110°C TL peak on the shape of the OSL decay curve, while Bøtter-Jensen et al. (1999b) identified the OSL component arising from the 110°C trap using the linear modulation technique. To remove the effect of retrapping, Wintle and Murray (1997) and Murray and Wintle (1998) therefore suggested to perform the measurements at or near an elevated temperature of 100°C.

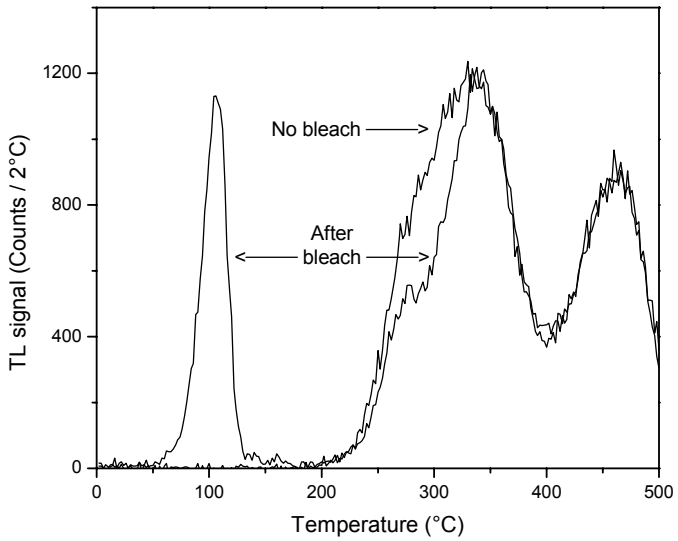

Figure 2.8: Illustration of photo-transfer in quartz. The quartz grains were first put through a repeated cycle of irradiation and heating to obtain a stable and reproducible luminescence signal. The sample was then given a regenerative beta dose (~29Gy), preheated for 10s at 240°C and measured, yielding the 'no bleach' TL glow curve. The measurement was then repeated, but before the TL was recorded the sample was first exposed to light (40s blue diode light at room temperature). Due to the exposure to light, electrons were evicted from deeper traps (at ~300-325°C) and were subsequently trapped again in more shallow traps (at ~110°C). The 110°C peak in the glow curve that is recorded after the illumination (or bleaching) is termed photo-transferred TL (PTTL). It is worth mentioning that this phenomenon can be exploited for dating pottery (e.g. Bailiff et al., 1977) as well as sediments (e.g. Wallner et al., 1990; Murray, 1996a). The quartz grains were extracted from a fluvial sand from the Netherlands (Grubbenvorst, lab code G10).

Wintle and Murray (2000) summarize all the above-mentioned effects to arrive at optimum measurement conditions for quartz OSL. Seeking a compromise between the increase in decay rate due to removal of the effect of the 110°C TL peak and thermal assistance and the decrease in OSL due to a probable shift of the emission peak to longer wavelengths with increasing temperature and thermal quenching, they conclude that measuring the OSL at or around 125°C gives a rapidly decaying luminescence signal, optimised for signal intensity.

2.5. Quartz OSL components

Although performing the measurements at an elevated temperature removes the possibility of retrapping in the 110°C peak, and consequently simplifies the interpretation of the decay curve, the decay remains slower-than-exponential. Smith and Rhodes (1994), e.g., observed the OSL signal at an elevated temperature of 220°C and found that the decay could still not be characterised by a single exponential. The shine-down curve shown in Figure 2.7 was recorded at 125°C and illustrates this observation. It can be seen that the decay remains more complicated than a single exponential even though the elevated measurement temperature removes the charge transfer effects involving the 110°C TL peak.

This observation led Smith and Rhodes (1994) to suggest that the signal has its origin in charge released from more than one trapping site, each with a different susceptibility to the optical stimulation (possibility #1 in the previous section). They demonstrated that the OSL signal could be broken down into three exponential components, which they termed "fast", "medium" and "slow", according to their decay throughout the stimulation. The fast component is the most light-sensitive and hence the most rapidly depleted component, followed by the medium and then the slow one. Bailey et al. (1997) confirmed the existence of these components and further investigated their properties with regard to thermal stability and dose response characteristics. Subsequent studies showed the quartz OSL signal to be composed of even more components. Jain et al. (2003) and Singarayer and Bailey (2003) recently identified up to 7 distinct components in the quartz OSL signal, although not all components were found to be present in all investigated samples.

Deconvolution of a decay curve is clearly not straightforward. The underlying components are poorly resolved, and the curve fitting used to separate them from each other is rather complex. Bulur (1996) introduced an alternative technique for measuring the OSL, which allows an easier discrimination between the various OSL components. In this technique, which is called linear modulation (LM), the excitation power is increased linearly from zero to a maximum value during the measurement. The most easily stimulated OSL is consequently measured first, while progressively harder to bleach components come out later. The individual OSL components from different traps are better separated as a function of time and a plot of the LM-OSL as a function of time shows peaks, instead of the monotonic decay that is obtained when measuring at a

constant power. Each peak corresponds to a different component. The situation is comparable to a TL glow curve, where the luminescence is recorded as the temperature is raised. The technique has been used in a number of studies dealing with the quartz OSL and component characterisation, amongst which those already mentioned by Jain et al. (2003) and Singarayer and Bailey (2003). Other relevant studies using LM-OSL include those by Agersnap Larsen et al. (2000), Bulur et al. (2000, 2001, 2002), Kuhns et al. (2000), Poolton et al. (2000), Schilles et al. (2001) and Choi et al. (2003a, b). It can be noted that Bulur (2000) presented a mathematical expression to transform the OSL decay curves obtained at a constant stimulation light intensity into LM-OSL curves. A more detailed discussion of this technique falls beyond the scope of this thesis. Nevertheless, it is worth mentioning here that in the course of the optical dating work described in subsequent chapters, the OSL from several samples was also investigated using the linear modulation technique. In the present context, it suffices to lift out one example from this dataset to illustrate the presence of different components in the OSL signal from quartz. Figure 2.9 shows an LM-OSL curve obtained for quartz grains extracted from a Dutch Holocene drift sand sample. In the given example, four distinct components can be recognised: a fast (peak 1), a medium (peak 2) and two slow (peaks 3 and 4) components.

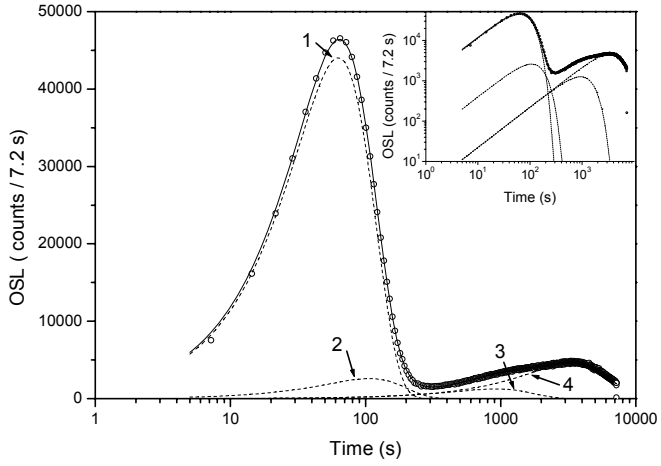

Figure 2.9: Regenerated LM-OSL from quartz extracted from a Holocene drift sand sample (Defensiedijk-I, lab code W3). The sample was first sensitised through repeated irradiation and heating cycles until a stable and reproducible signal was obtained. It was then given a regenerative dose of about 20 Gy and preheated for 10s at 240°C. The LM-OSL was subsequently measured at 125°C for 7200 s. The various components are indicated by the arrows and were obtained by curve fitting (dashed lines). A linear sum of these components gives the solid line, and approximated the measured LM-OSL data (open circles) successfully. The inset shows the same data on a log-log scale.

The characteristics of the various OSL components (thermal stability, signal growth, etc.) have been studied e.g. by Bulur et al. (2000), Jain et al. (2003) and Singarayer and Bailey (2003), and were found to be quite different. To give an example, some of the results by Singarayer and Bailey (2003) are reproduced in Figure 2.10. The growth of the luminescence with dose for five distinct quartz OSL components is shown (such curves are termed 'growth-curves' or 'dose-response curves'; see also Chapter 3). The dose-response characteristics of the various components are clearly different. One of the slow components (S3) especially appears to saturate at much higher doses. Singarayer and Bailey (2003) further suggest that this component also has a significant thermal stability, which might make it suitable for dating samples beyond the 100-200 ka limit that is usually accepted for quartz (see Chapter 1).

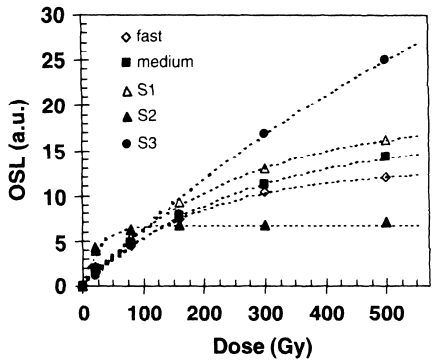

Figure 2.10: Growth of luminescence as a function of dose for several quartz OSL components (from Singarayer and Bailey, 2003). The different components were obtained using the linear modulation technique. S1, S2 and S3 refer to the slow components. The quartz was extracted from a Moroccan dune sand.

2.6. Signal stability

As outlined in Chapter 1, it is obviously necessary to use a signal that is stable over the time span that is being dated. Table 2.2 summarises some reported values for trap parameters and corresponding calculated lifetimes for quartz. Some values reported for the parameters of the electron trap associated with the 325°C TL peak are included in the table as well, to illustrate their similarity with the values obtained for the OSL signal. This is one of the pieces of evidence supporting the hypothesis that both signals originate from the same trapped charge population (see Section 2.10).

The uncertainties associated with the lifetimes are usually large, which might explain, beside sensitivity changes (see Section 2.7), some of the differences between the lifetimes obtained by various authors. It can also not be excluded that some differences arise due to the fact that different components of the OSL signal, or different combinations of them, were considered in these studies. Using the linear modulation technique, Singarayer and Bailey (2003) were able to carry out more detailed investigations on the thermal stability of the different components of the OSL signal. They found that the different components exhibited different thermal stabilities, with the so-called fast, medium and S1 component (and possibly also the S3 component; see section 2.5 and Figure 2.10) being sufficiently stable for dating sediments on Quaternary timescales. For the fast component, for instance, they found a lifetime of 310 Ma at 20°C, which is comparable to the estimates given in Table 2.2. On the whole, however, it can be concluded that the parts of the quartz OSL signal that are nowadays usually employed for dating, are sufficiently stable to permit dating over the entire time range of the Quaternary, with an upper limit determined by signal saturation, rather than thermal fading.

Signal	E (eV)	s (s^{-1})	$\tau_{20°C}$ (a)	Reference
OSL	1.84	$2 * 10^{15}$	$6 * 10^{8}$	Smith et al. (1990a)
OSL	1.65	$2.7 * 10^{13}$	$2.8 * 10^{7}$	Huntley et al. (1996)†
OSL	1.59	$2.8 * 10^{12}$	$2.1 * 10^{7}$	Spooner and Questiaux (2000)
OSL	1.66	$1 * 10^{13}$	$1.1 * 10^{8}$	Murray and Wintle (1999a)‡
325°C TL	1.69	$1 * 10^{14}$	$3.0 * 10^{7}$	Wintle (1975)
325°C TL	1.60	$5.7 * 10^{12}$	$1.7 * 10^{7}$	Spooner and Questiaux (2000)

Table 2.2: Some reported values of trap parameters E (trap depth) and s (frequency factor), and calculated lifetimes at 20°C for quartz. All values were obtained using isothermal decay methods. The table is by no means exhaustive. †: In their experiments, Huntley et al. (1996) identified four traps; the data tabulated here are those for the trap with the largest contribution to the total initial luminescence. ‡: Murray and Wintle (1999a) found three OSL components; the values given in the table are for the major component of the initial OSL decay in both natural and laboratory irradiated samples, after sensitivity correction. It can be added that only the values obtained by Murray and Wintle (1999a) are corrected for sensitivity changes occurring during the measurements (see Section 2.7).

2.7. Sensitivity changes

The sensitivity is defined as the luminescence produced per unit of dose. It has been known for a long time that this is not a constant property but can change from one measurement cycle to another. A change in sensitivity means in practice that upon reuse of the same portion of quartz grains, its properties will have changed in such a way, that a different OSL signal will result, even if they receive the same treatment every time they are reused. This is illustrated in Figure 2.9. Although each measurement cycle was carried out in exactly the same way, it is clear that, in this case, the sensitivity first decreases with progressive measurement cycles, before levelling off to an approximately constant value after 5 measurement cycles.

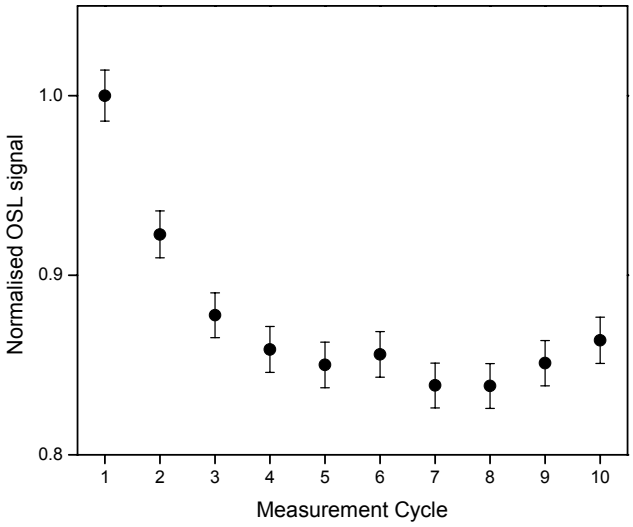

Figure 2.9: Illustration of the change in sensitivity (OSL per unit of dose) with reuse. The quartz grains were extracted from a coversand sample from Ossendrecht (lab code OS-C). After the natural signal was removed, the aliquot was put through a repeated identical cycle of irradiation (~11 Gy), preheat (10 s at 160°C) and OSL measurement (40 s 470 nm at 125°C). The signals are normalised to the OSL response obtained in the first measurement cycle.

Sensitivity changes such as shown in Figure 2.9 are primarily caused by the heat treatment (of a certain duration and stringency) that is applied to the samples after irradiation (in nature or the laboratory) and before the OSL measurement. As mentioned in Chapter 1, this treatment is called ‘preheating’ and it will be discussed more elaborately in the following chapter.

The occurrence of these sensitivity changes in quartz is well documented in literature, and this effect has been studied extensively over the last few years (e.g. Murray and Roberts, 1998; Wintle and Murray, 1999; Murray and Wintle, 1999b; Armitage et al., 2000; Chen and Li, 2000; Murray and Wintle, 2000a; Vartanian et al., 2000). One of the major insights gained is that the sensitivity change is different for the naturally acquired OSL and the artificial OSL arising from laboratory irradiation (Wintle and Murray, 1998, 1999). This means, for instance, that the same heat treatment can lead to the measurement of a different OSL signal for a natural sample compared to the OSL that would be measured for a sample that had been given a laboratory dose of exactly the same size as the natural dose. This different behaviour is illustrated in Figure 2.10 (from Wintle and Murray, 1998). The figure shows the response of the 110°C TL peak, which can be used as a sensitivity monitor of the OSL signal (see Chapter 3), to a small test dose given immediately after two aliquots were heated for 10 s at the indicated temperature. The two aliquots were identical (from the same sample), except that one was irradiated in nature (open circles), while the other was first bleached and subsequently irradiated in the laboratory (solid circles). The sensitivity change is clearly much larger for the laboratory-irradiated aliquot than for one irradiated in nature (up to ~300% compared to ~30%, respectively).

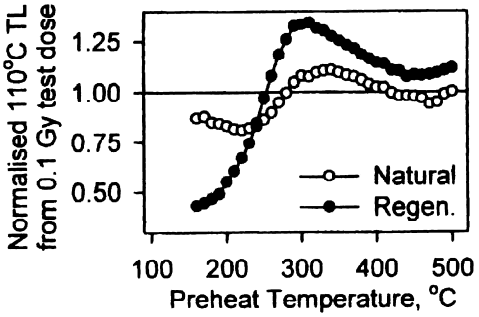

Figure 2.10: Sensitivity changes during preheating observed for a natural aliquot and one that received a laboratory dose after its signal was optically removed (from Wintle and Murray, 1998). The aliquots were heated to the temperature indicated, held there for 10s and cooled. Subsequently the 110°C TL response to a small test dose was measured. The data have been normalised to a value of 1 assigned to the natural aliquot after heating to 500°C. The responses of natural (open symbols) and artificially irradiated (solid symbols) quartz grains are only the same at a preheat of 10s at 240°C; otherwise the responses to the same preheat are clearly different.

As will be outlined in Chapter 3, a comparison between the natural OSL signal and OSL signals induced in the laboratory is one of the very things needed to arrive at an optical date. Figure 2.10 clearly illustrates that, for such a comparison to make sense, the effects of sensitivity change and the different behaviour of natural and artificial OSL signals must be taken into account.

There are two ways to accomplish this. One possibility is to equalise the sensitivity of both naturally and laboratory irradiated samples. This is possible, at least in principle, by using a heat treatment. As is clear from Figure 2.10, however, finding the appropriate preheat conditions is not straightforward. Furthermore, as the sensitisation depends on both temperature and duration of the storage in the lab and the environment (Wintle and Murray, 1999), the correct heat treatment is likely to differ from sample to sample. A better and more straightforward approach would be to measure the sensitivity appropriate to each OSL signal, and to make allowance for any differences. Such a procedure not only corrects for the difference in behaviour of the natural and regenerated OSL signals (Figure 2.10), but also for sensitivity changes between subsequent regeneration cycles (Figure 2.9). The OSL sensitivity can best be monitored using the OSL response to a small test dose that is given after every OSL measurement (Murray and Wintle, 2000a). This will be explained more detailed in the following chapter, but the idea can already be understood by looking at Figure 2.11. An aliquot of quartz grains was put through a repeated and identical cycle of irradiation, preheat and OSL measurement after the natural signal had been removed, exactly as was the case in Figure 2.9. The absolute intensities of measured OSL signals are now shown as solid squares on the left hand figure. The decrease in sensitivity with progressive measurement cycle can again be seen. Additionally, after each measurement cycle was completed, the OSL response to a small test dose was now measured as well. These signals are shown as the solid diamonds on the left hand figure (note that the intensities are multiplied by a factor of 3), and give a true representation of the luminescence sensitivity of the OSL signal recorded during the immediately preceding measurement cycle. A correction can then be made for the sensitivity changes by dividing the OSL signals by the corresponding test dose OSL signals. If the sensitivity correction is working properly, all the normalised sensitivity corrected signals should now lie on a straight line (because they are induced by the same laboratory dose), which, as is shown in the right hand figure, is indeed the case. The open symbols represent the signals

associated with the natural signal. The sensitivity corrected natural OSL signal (open circle) is slightly lower than the corrected regenerated circles. This is owing to the fact that the regenerative dose employed in the experiment was slightly higher than the natural dose.

Knowledge of the influence of thermal treatments (both in nature and in the laboratory) on the luminescence efficiency has revolutionised optical dating technology over the last few years. It can finally be pointed out, however, that an exact mechanism explaining sensitivity changes in quartz remains to be established. Some relevant studies of this matter are those by Zimmerman (1971), Aitken (1998), Wintle and Murray (1999), Chen and Li (2000), Vartanian et al. (2000) and Bailey (2001, 2002).

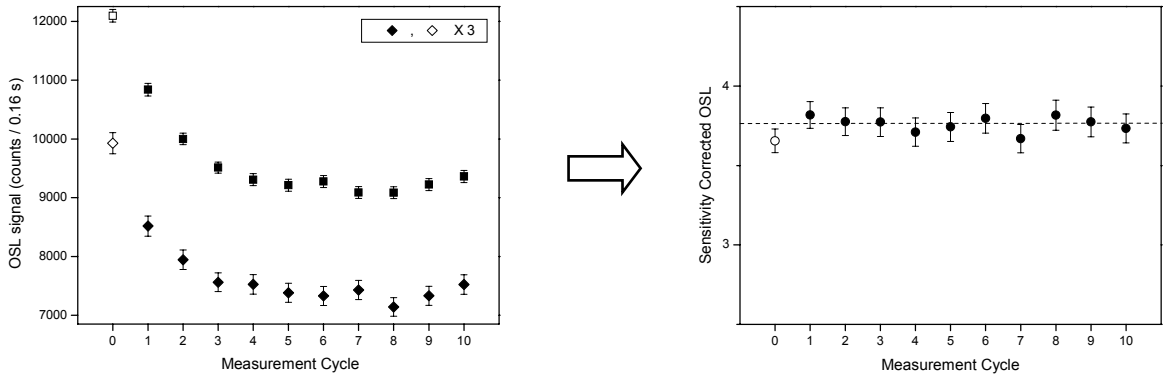

Figure 2.11: Illustration of monitoring the sensitivity change by the use of the OSL response to a small test dose given after every OSL measurement. The sample is the same as in Figure 2.10. After the natural signal was removed, the aliquot was put through a repeated identical cycle of irradiation (~11 Gy), preheat (10 s at 160°C) and OSL measurement (40 s 470 nm at 125°C). After each principal OSL measurement, a small test dose (~2.4 Gy) was administered and the corresponding OSL response recorded (after a 160°C cut heat; see Chapter 3). Shown in the graph on the left are the absolute intensities of the main OSL signals (squares) and test dose OSL signals (diamonds; note that for clarity, these values have been multiplied by three). The change in sensitivity is clear, and is closely followed by the test dose signals. The signals appropriate to the natural OSL signal are represented by the open symbols. The right hand figure shows the result when allowance is made for the sensitivity change, which is accomplished by normalising each OSL measurement to its appropriate sensitivity. The effectiveness is clearly illustrated by the fact that all points now lie on the dashed line representing the average. Note that the natural data-point falls slightly under the line, as the naturally accumulated dose in the quartz grains of this aliquot was a slightly lower than the dose of ~11Gy used in the repeat cycles.

2.8. Intrinsic luminescence characteristics

The majority of luminescence analyses that have been carried out in the past used a signal stimulated from aliquots containing many quartz grains (of the order of 1000). Investigations of the luminescence emitted by single grains appeared in the literature from time to time, but their technical complexity and laborious nature imposed serious limitations on such analyses. Recent developments in instrumentation (see e.g. Duller et al., 1999a, 1999b and Bøtter-Jensen et al., 2003b) have now made it possible to measure the luminescence of many hundreds, or even thousands, single grains of quartz in a practical and rapid way. Although this is a rather recent (but rapidly expanding) area of luminescence research, it has already led to a wealth of interesting information. The overall conclusion to be drawn from these studies is that each quartz grain may exhibit distinct luminescence characteristics. This obviously has implications for the interpretation of a combined luminescence signal that is obtained from many quartz grains at once. In the following, a short summary is presented of what is known about the OSL signal from single grains of quartz. The variability in radiation dose that each grain has received is not included in this discussion and will be dealt with later, as this is usually attributed to factors external to the grain rather than being related to its intrinsic luminescence properties.

2.8.1. Specific luminescence

It has been known already for some time that, for a given dose, not all quartz grains emit the same amount of luminescence. This has been shown for TL (Benkö, 1983; Huntley et al., 1993; McFee and Tite, 1994, 1998) as well as for OSL (Murray and Roberts, 1997; Duller et al., 2000; Adamiec, 2000; McCoy et al., 2000; Jacobs et al., 2003a). An example illustrating the variability in TL yield and in individual glow peaks for individual quartz grains extracted from an Australian sand dune is shown in Figure 2.12. The figure is taken from Huntley et al. (1993) and confirmed their deduction that only a small fraction of the grains contributes to the luminescence as measured from an aliquot containing about 10000 grains. They also point out that a small fraction of the grains is super-bright.

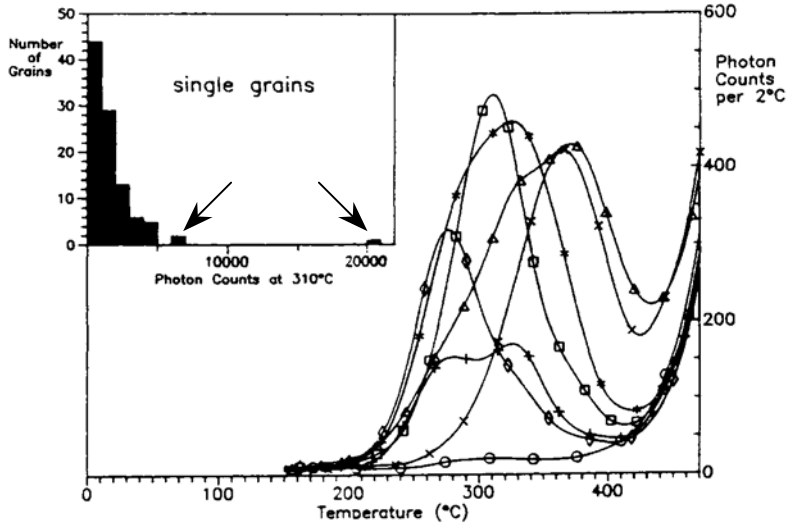

Figure 2.12: Glow curves for some individual quartz grains, illustrating the wide variability (modified from Huntley et al., 1993). The quartz grains were extracted from an Australian dune sand. The inset shows the distribution of photon counts for 100 grains and demonstrates the presence of a small fraction of super-bright grains (indicated by the arrows).

Using single-grain luminescence equipment, Duller et al. (2000) measured the OSL from a large number of individual quartz grains from seven samples. Their results are shown in Figure 2.13, from which it is clear that in reality each sample consists of a heterogeneous collection of grains. For a sample in which all the grains would emit the same luminescence, a straight diagonal line would be found. The study demonstrated furthermore that the proportion of the grains from which a significant OSL signal can be observed varies from one sample to another, and that in extreme cases, 95% of the total light-sum emitted can originate from only about 5% of all the grains measured. Jacobs et al. (2003a) recently investigated the variability in signal intensity for single quartz grains extracted from three coastal sand dunes from South Africa. For all three samples they found that only 10% of the grains gave rise to 90-95% of the total light-sum. It is perhaps worth mentioning that recent investigations by Duller et al. (2003) indicate that feldspars seem to be more uniform in their luminescence intensity than quartz.

The above clearly illustrates the extreme non-uniformity in luminescence brightness exhibited by different quartz grains. As only very few grains contribute to the measured luminescence, it can consequently be expected that some of this variability will also be

seen when different sub-samples consisting of many hundreds of grains are being measured.

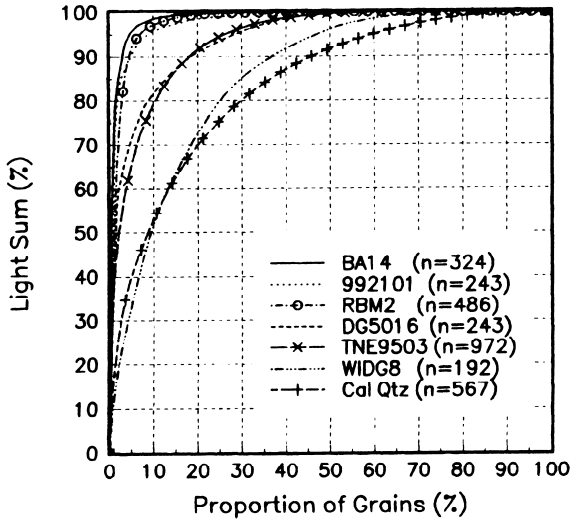

Figure 2.13: Distribution of OSL signal intensity from single grains (from Duller et al., 2000). Data are plotted as the percentage of the total light sum that originates from the specified proportion of the grains. The data for 7 samples are shown and the total number of grains (n) that was measured from each sample is shown in parentheses. The samples with codes WIDG8, BA14, RBM2 and TNE9503 are aeolian, DG5016 is alluvial and 992101 is a frost-wedge cast. The sample indicated by "Cal Qtz" refers to an annealed and artificially beta-dosed sedimentary quartz sample. For all samples, with the exception of the calibration quartz (Cal Qtz), the natural OSL signal was measured. It can be pointed out that the distributions for samples 992101 and RBM2 approximately overlap.

2.8.2. Components

Bulur et al. (2002) investigated the LM-OSL signal from single grains of quartz. They not only observed a great variation in brightness, but also in number of components underlying the LM-OSL signal. They could identify three types of quartz grains, those showing only an easy-to-bleach component, those with only a hard-to-bleach component, and those exhibiting both components. As was pointed out by Jain et al. (2003), it is interesting to note that for these single grains only up to three components have been identified, while in studies on multiple grains (see Section 2.5), up to seven components have been found.

2.8.3. Signal growth

Murray and Roberts (1997) were the first to suggest that the dose-response curves for individual quartz grains may be different. Although their observations might have been biased by sensitivity changes, they were later confirmed. In a study of individual quartz grains from Australian sedimentary deposits, Yoshida et al. (2000) observed that some grains (so-called "supergrains") were highly luminescent and saturated at high doses. They concluded that these properties could be used to their advantage for obtaining optical ages up to 1 Ma. Roberts et al. (1999; see Figure 2.14) and Duller et al. (2000) observed variations in dose-response characteristics for single grains as well, and also suggested that this variation might be used to advantage by selecting only those grains with high dose saturation characteristics in order to extend the age range over which quartz can be used. A considerable variation in the radiation dose at which the OSL signal from individual grains became saturated was observed also by Jacobs et al. (2003a).

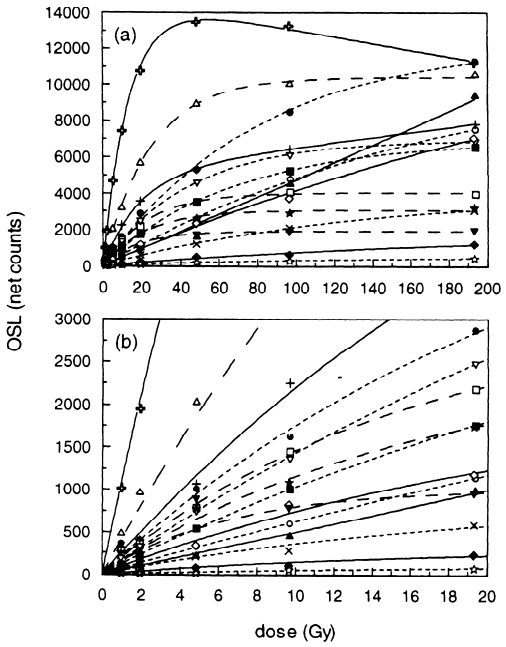

Figure 2.14: Variability in dose response characteristics for 15 single quartz grains as observed by Roberts et al. (1999) in their optical dating study of the Jinmium rock shelter in northern Australia. Full growth curves up to 200 Gy are shown in (a), while the region up to 20 Gy is enlarged in (b).

The implication of these results was already identified by Murray and Roberts (1997): "The results imply that the shape of a multiple-grain growth curve is not an intrinsic dose-response characteristic of the quartz under investigation but, rather, is the arithmetic sum of many different growth curve shapes." A wide range of growth curve shapes from multiple-grain aliquots has been reported in the literature, varying from linear to exponential, combinations of these, and shapes that could only be approximated by polynomial functions. The results summarised above, however, obviously place these findings and the resulting interpretations in a new light.
It is finally worth mentioning that Murray (2000) shows that the variations in growth curve shape can also be observed for single-aliquots consisting of about 7000 quartz grains.

2.9. Resetting of the quartz OSL signal

The aim of optical dating is to determine the time of deposition of the investigated sediment. For this to hold, the pre-sedimentation signal should have been completely removed during transport of the sediment grains. Otherwise, the true age will be overestimated. Some considerations with regard to the bleaching behaviour of quartz are therefore appropriate.

A first dataset of interest is that presented by Spooner (1994b). He investigated how efficient different wavelengths are in removing the OSL (514.5 nm) signal of quartz and his results are shown in Figure 2.15.
The figure clearly shows a dramatic wavelength dependence. Between 400 and 500 nm the bleaching efficiency (which is inversely proportional to the energy required to obtain a certain OSL reduction) decreases by a factor of about 10. Combining this with the spectrum of sunlight at sea-level, which sharply rises from about 330 nm to a maximum extending from about 500 to 700 nm before deceasing again (Figure 2.16), suggests that the region 330-500 nm is most important for bleaching. Figure 2.15 also illustrates how inefficient longer wavelengths are in removing the OSL from quartz (see Section 2.1).
Also included in Figure 2.15 are the data from Spooner et al. (1988) concerning the bleaching of the quartz 325°C TL peak. It is obvious that the bleaching behaviour is similar, which is taken as a piece of evidence for both signals to represent one and the same trap population (see Section 2.1).

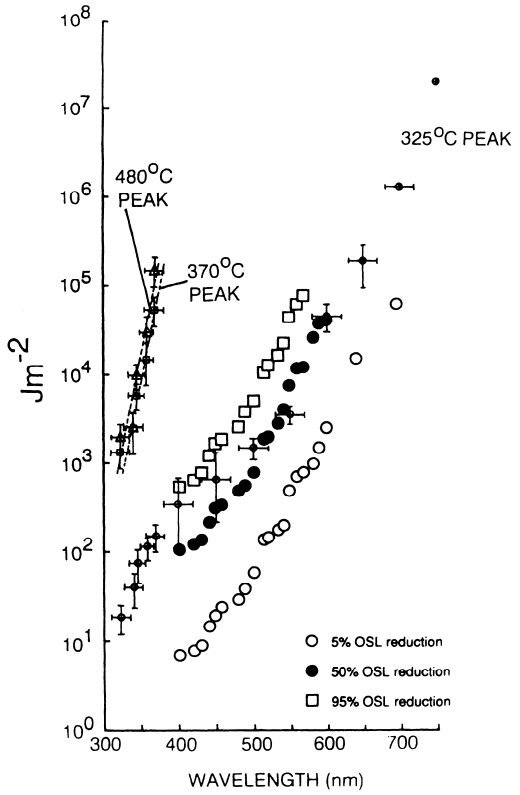

Figure 2.15: The energy required at certain wavelengths to reduce the 514.5 nm-stimulated quartz OSL to the given levels (from Spooner, 1994b). The dataset from Spooner et al. (1988, their Figure 3) concerning the bleaching response of the quartz 325°C (complete removal), 370°C and 480°C (80% reduction) TL peaks is included. The samples were from northern Australia (see the original references for details).

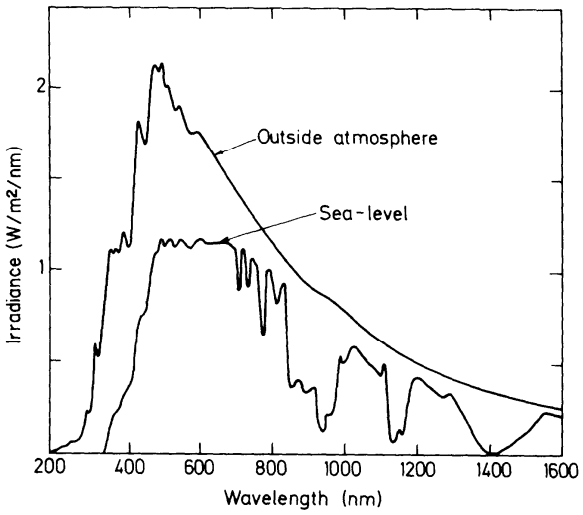

Figure 2.16: Spectrum of sunlight outside the atmosphere and at sea-level with the sun 60° below zenith. The figure is adapted from Aitken (1998), who modified it from the Oriel Solar Simulator handbook and is based on work by M.P. Thekaekara. The vertical scale gives the energy per unit wavelength interval received per unit time by unit area of a horizontal surface facing upwards.

Godfrey-Smith et al. (1988) presented the most complete dataset up till now concerning the bleaching of the natural OSL signal from quartz by sunlight. On bright days in May to August (spring/summer), they exposed portions of quartz grains to natural sunlight for varying durations and measured the luminescence signals. Their results are shown in Figure 2.17. The solid circles indicate the quartz OSL signals. It can be seen from this figure that the quartz OSL signal is rapidly reduced to a negligible level; after 10 s of sunlight exposure it is only about 1% of the initial value. The effect of sunlight exposure on the OSL signal from feldspar is also shown. Clearly, the feldspar OSL is not as rapidly nor as completely reduced compared to the quartz OSL signal (note that this applies to the signal stimulated by 514.5 nm light). Godfrey-Smith et al. (1988) also repeated this experiment on an overcast day (in September), with a light intensity of 10% of that during the previous experiment. They found that even in the absence of this direct sunlight, the quartz OSL signal was completely removed, albeit at a 10 times slower rate.

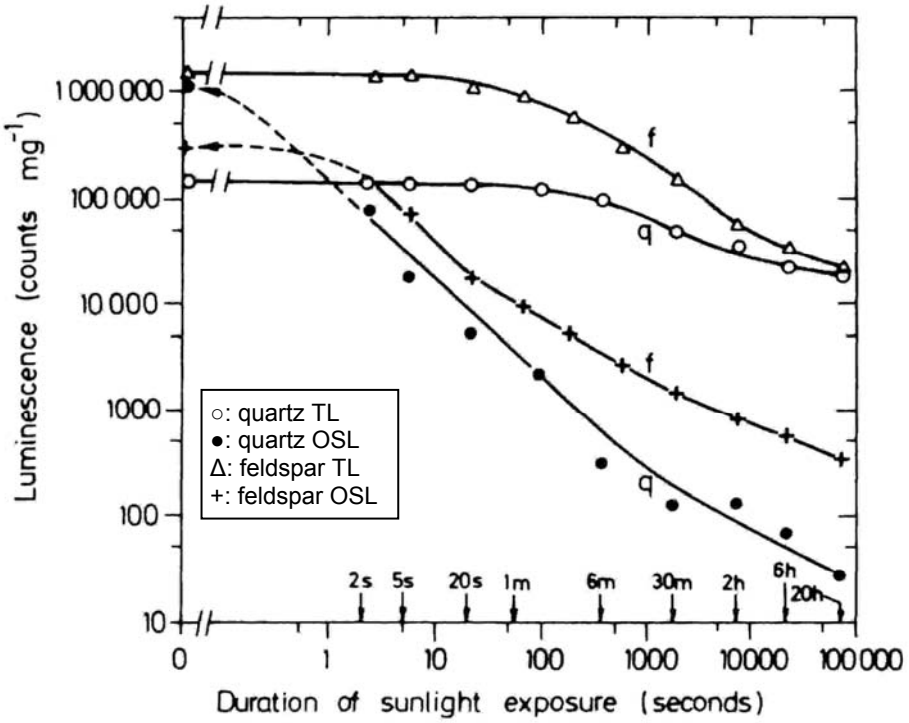

Figure 2.17: Effect of sunlight exposure on the luminescence (OSL and TL) signal from quartz and feldspars (from Godfrey-Smith et al., 1988). The quartz grains were extracted from a sand from south-east South Australia that was deposited ~500 ka ago, while the feldspar extract was from a Canadian sand deposited ~70 ka ago. The TL for quartz was for a well-defined peak at 320-330°C, and for feldspar at 310-320°C; these were obtained using a 5°C s^{-1} heating rate, and a detection filter with a maximum transmission wavelength at 410 nm. The optical signal was obtained during the first second of stimulation with green (514 nm) light; the detection window was centred on 380 nm.

For comparison, Figure 2.17 also shows the bleaching behaviour of the quartz TL signal (open circles). It can be seen that the OSL signal is reduced much faster and to a much lower level than the TL signal and that a substantial TL signal remains present even after 20 hours of sunlight exposure. This is because in TL, a glow curve is measured which usually includes contributions from several types of traps. Some of these traps are light sensitive and can be bleached, while others are not. However, when stimulating with heat, all electron traps are emptied. This means that there will always remain some unbleachable residual signal, arising from the light insensitive traps, even for a sample that has been exposed recently. The effect of bleaching on the TL glow curve is illustrated in Figure 2.18. The difference between the glow curves with and without exposure to light corresponds to the light sensitive region of the glow curve. In the example given here this is around 300°C, which is consistent with the presumption that the electron traps associated with this region are also the source traps for the OSL (see Section 2.10).

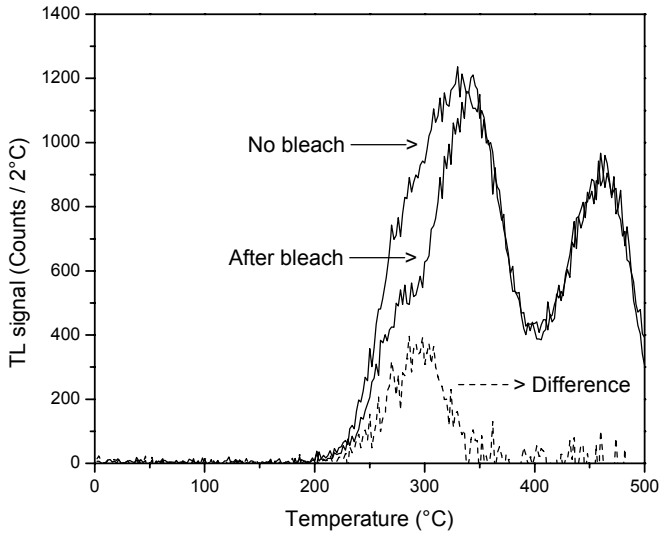

Figure 2.18: The effect of bleaching on the TL glow curve. The curves were recorded at a heating rate of 5°C s^{-1} and detected through a 7.5 mm thick Hoya U-340 filter. The measurements were carried out on the same sample as in Figure 2.5. The signal was first sensitised and stabilised through repeated cycles of irradiation (~14.5 Gy) and heating (to 500°C). The sample was subsequently given a ~29 Gy dose and preheated for 10 s at 240°C prior to the measurement. Bleaching was carried out for 40 s at 125°C using blue (470 nm) light. The dotted curve shows the difference between the two measured TL glow curves (difference = no OSL bleach – OSL bleach).

On the contrary, in OSL only the electrons accumulated in the light sensitive, easily bleachable traps are measured, i.e. those traps that are most likely to have been emptied during transport and deposition. In OSL no unbleachable residual is left because the traps that are not sensitive to light simply do not give rise to an OSL signal or, in other words, the light insensitive traps are simply not measured.

With regard to sediment dating, Figure 2.17 clearly illustrates the advantage of OSL over TL. The absence of a residual signal allows the dating of very young samples, while the sensitivity of the OSL signal to light allows sediments from a variety of depositional environments with less efficient bleaching conditions to be dated. The efficiency by which the luminescence signal is set to zero is of critical importance. The data from Spooner (1994b) and Godfrey-Smith et al. (1988) clearly show that the setting to zero is dependent on the intensity, the spectrum and the duration of the exposure. It is perhaps worth pointing out that the exact quantitative behaviour shown in the figures is likely to differ from sample to sample. The general observations and trends, however, are expected to hold. Therefore, it can be concluded from the above data that shorter wavelengths are more efficient in bleaching but that an extended exposure to longer wavelengths can also bleach the signal.

As outlined above, the region between 330 and 500 nm will be most important for sunlight bleaching at sea-level. The light spectrum is, however, severely altered and attenuated under water due to suspended solid particles and chlorophyll-bearing organisms, a situation consequently much subjected to natural variability. Nevertheless, to have an idea of what underwater bleaching conditions look like, some of the data from Berger (1990) are reproduced in Figure 2.19. It is clearly illustrated by this figure that with increasing depth the less energetic and less efficient wavelength regions centred on the green and yellow will become progressively more important. In general, Berger (1990) found blue- and red-attenuated underwater light spectra, having maxima near 580 nm.

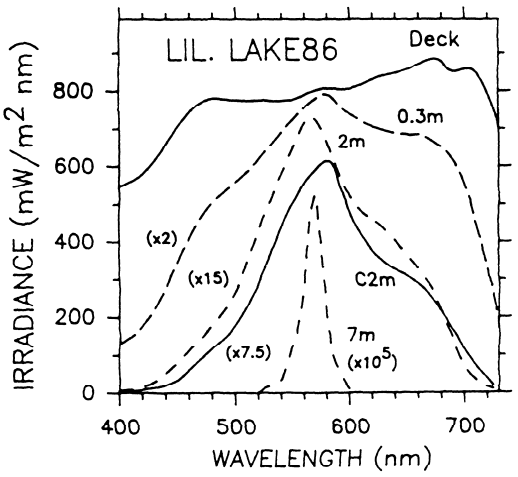

Figure 2.19: Underwater spectra at various depths in Lillooet Lake, British Columbia, Canada (from Berger, 1990). The curve C2m refers to the spectrum at a depth of 2m at a second measurement site. The irradiance is the radiant power (i.e. the rate of flow of electromagnetic energy) incident per unit area upon a surface.

Although the OSL signal is removed quite rapidly (in any case more rapidly and efficiently than the TL signal), circumstances may occur in which the light exposure was not sufficient for the pre-depositional OSL signal to be completely removed. This is especially true for water-laid sediments. If the signal is incompletely removed, the sample is said to be partially bleached and this leads to an overestimation of the age. Partial bleaching of quartz grains has been frequently reported in literature and Murray and Olley (1999) and Wallinga (2002a) presented comprehensive overviews on this matter. Partial bleaching will be further discussed in Chapter 3.

2.10. The relationship between OSL and TL of quartz

It was already pointed out in Chapter 1 that the precise mechanisms by which luminescence is produced are poorly understood. Several attempts have been made in the literature to formulate models that explain the luminescence behaviour of quartz. This issue is not covered here and reference is therefore made to Bailey (2001, 2002) and the literature quoted therein. However, as it is the purpose of this work to switch from TL to optical dating, it is perhaps relevant to consider one aspect of the quartz OSL production mechanism into a somewhat greater detail, namely the source of electrons giving rise to this signal and how these are related to the TL signal. Further justification of the following

lies in its relevance to the experimental procedure of preheating that will be discussed in Chapter 3.

It was already suggested during the initial trials of optical dating, that the 325°C TL peak and the OSL signal of quartz are related to each other (Smith et al., 1986, 1990a). This was based on the observation that after the quartz had been optically stimulated, the 325°C TL peak was reduced. The 325°C TL peak had also previously been found to bleach rapidly compared to other quartz TL peaks (Spooner et al., 1988), and is therefore referred to as the rapidly bleaching peak (Franklin and Hornyak, 1990). Spooner (1994b), Smith and Rhodes (1994) and Kaylor et al. (1995) reported on measurements that further suggest that both the OSL and this rapidly bleaching TL signal actually originate from the same electron traps. From these and subsequent studies, several strong pieces of evidence have emerged that support the hypothesis of this close relationship. These can be summarised as follows (Wintle and Murray, 2000).

The combined data of Spooner (1994b) and Spooner et al. (1988) show the similarity in bleaching behaviour of the 325°C TL peak and the OSL signal (Figure 2.15). Spooner (1994b) also conducted a series of measurements to examine quantitatively the hypothesised equivalence of the 325°C TL peak source population with that giving rise to the OSL signal. His data demonstrate that the OSL light-sums clearly overlap with the light-sums of the 325°C TL peak, any differences being mainly attributed to thermal quenching. Wintle and Murray (1997) further investigated the relationship between quartz OSL and TL. They found, for instance, a loss in TL from a peak centred around 310°C after optical stimulation (see e.g. Figure 2.18). Wintle and Murray (1997) furthermore found a good correlation between this loss in TL and the ‘gain’ in OSL resulting from optical stimulation. In a subsequent study, Wintle and Murray (1998) found that if the temperature is increased from 280°C to 330°C, the OSL is rapidly reduced to a negligibly low-level. This is expected if the electrons giving rise to an OSL signal originate from traps that are being emptied at a temperature of about 325°C and hence give rise to this peak in a TL glow curve. Finally, the OSL signal and the 325°C TL peak exhibit comparable physical properties as trap depth and lifetime (see Table 2.2).

This combined evidence clearly suggests that the same trapped charge is being sampled during optical stimulation as is giving rise to the 325°C TL peak. It can perhaps be recalled that, based on the similarity in emission wavelengths (Section 2.2, Table 2.1), the charge released from these traps also appears to recombine in the same luminescence centre.

– CHAPTER 3 –

THE OPTICAL DATING METHOD

3.1. The age equation

In luminescence dating, the age is obtained from the following equation:

$$\text{Age} = \frac{\text{Burial Dose}}{\text{Annual Dose}} \tag{3.1}$$

The burial dose is the energy absorbed from nuclear radiation by the sedimentary mineral grains since they were last exposed to sunlight. As it is a combined dose, resulting from exposure to α, β and γ (and cosmic) radiation, it is not possible to determine this burial dose (or palaeodose) directly. Therefore it is determined as an equivalent dose, which is the artificial laboratory α, β or γ dose necessary to induce a luminescence signal in the minerals that is of exactly the same magnitude as their natural signal. Equivalent doses are usually determined using beta radiation, as was also the case in this work. The burial dose is consequently determined as a beta equivalent dose. The unit of absorbed dose is the Gray (symbol: Gy) and is defined as 1 Joule per kg.
The equivalent dose is obtained using luminescence signals (Section 3.2), from:

$$\text{Equivalent Dose} = \frac{\text{Natural Luminescence Signal}}{\text{Luminescence Sensitivity}} \tag{3.2}$$

in which the luminescence sensitivity (photons/Gy) is the measure for the amount of luminescence resulting from the absorption of a given dose.

The annual dose, on the other hand, refers to the radiation energy that is annually absorbed per unit of mass and consequently it has the unit of Gy a^{-1}. It is usually derived from the measurement of the radiation emitted by the naturally occurring radioisotopes or from a determination of their concentration (Section 3.3).

3.2. The equivalent dose

3.2.1. Techniques for equivalent dose determination

All the techniques used to determine the equivalent dose all be reduced to two basic types: additive-dose and regenerative-dose. In both cases it is necessary to measure the natural OSL signal, as well as the OSL sensitivity that characterises the growth of the luminescence signal with dose. There are, however, many intricacies involved.
When this work was started in 1998-1999, a very rapid technique development was going on an international scale. Different measurement protocols, procedures and technical developments seemed to spring up like mushrooms. Obviously, it was not really clear to a luminescence dating novice, who at that time was trying to catch up with 15 years of scientific development, which procedure would have the highest probability of providing a reliable D_e for the sediments that were to be dated.
In the following sections, therefore, an overview of the different D_e determination techniques is presented, including those that have not been actually applied in this work. It can be an aid to those who are trying to find their way through all the complex and vast amount of literature that is available on the subject. Some illustrative applications of the techniques will be cited as well. The single-aliquot techniques, and especially those that have been developed for quartz, will be discussed in more detail because of their direct relevance to a major part of the dating work carried out in this thesis. For the same reason, the section dealing with the single-aliquot regenerative-dose protocol is more comprehensive. Reviews on techniques for D_e determination and on their practical application are also available in the open literature and include those by Berger (1995), Duller (1995, 1996), Wintle (1997), Prescott and Robertson (1997), Aitken (1998), Stokes (1999), Murray (2000)**,** Wallinga (2002a) and Bøtter-Jensen et al. (2003a).

3.2.1.1. Multiple-aliquot techniques

The protocols belonging to this category of techniques all require the use of many sub-samples or ‘aliquots’. Conceptually, they are the same techniques as used in TL dating (see e.g. Aitken, 1985 or Vancraeynest, 1998).

Disadvantages of these techniques include the large number of aliquots (and hence the amount of sample) that is required, and the need for normalization measurements to allow for aliquot-to-aliquot differences in luminescence sensitivity. Furthermore, they are time-consuming for the analyst as well as with regard to instrument time. As many aliquots are used to characterize only one sensitivity and one equivalent dose, the underlying assumption in the multiple-aliquot approaches is that for all aliquots these characteristics are indeed identical. From the discussion presented in Section 2.8, it is clear that this is an oversimplification. Every quartz grain can be quite different with regard to brightness and shape of the dose-response curve. It will be shown in Section 3.2.3, that also the starting point and amount of dose accumulation during burial can differ between individual quartz grains. Normalization procedures and increasing the size of the aliquots (i.e. increasing the amount of quartz grains in each sub-sample) can average some of these differences. Although this improves the measurement precision, the resulting D_e is, however, not necessarily also more accurate (see Section 3.2.3).
Despite these disadvantages and the availability of superior measurement protocols (see Section 3.2.1.2), multiple-aliquot techniques are still commonly used for equivalent dose determination (see e.g. Quickert et al., 2003; Thomas et al., 2003; Van den haute et al., 2003).

3.2.1.1.1. The **m**ultiple-**a**liquot **a**dditive-**d**ose technique (MAAD)

In this approach, a number of aliquots is prepared and divided in groups. From one group, the natural OSL signal is measured. The other groups are given known and different radiation doses on top of their natural dose, using a calibrated source in the laboratory. All the aliquots are subsequently preheated (see Section 3.2.2) and measured. A plot of the measured luminescence intensity as a function of the added dose yields the dose-response or growth-curve. The unknown dose is obtained by extrapolation of this growth-curve to zero luminescence intensity (Figure 3.1).
As the MAAD technique involves extrapolation, the result depends quite strongly on the choice of the mathematical function (linear, exponential, polynomial,…) that is used for describing the growth of the signal with dose. This is especially problematic for cases where the extrapolation is to be made over a large dose-span, where the growth is not

linear and/or where there is a large scatter between the data points. This drawback is circumvented using the regeneration method.

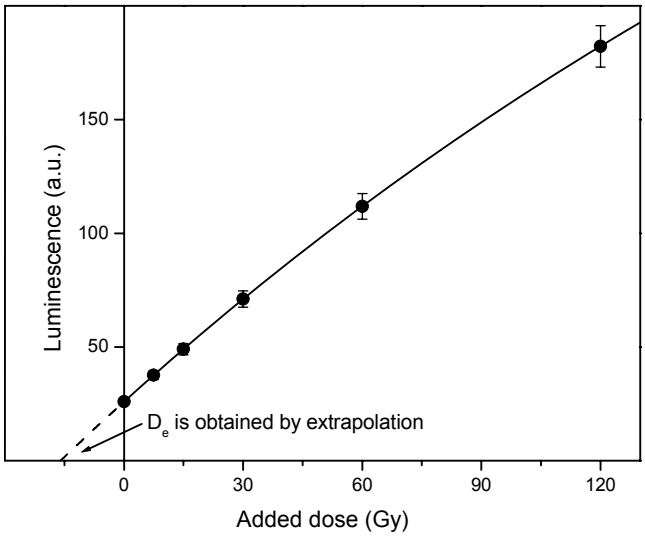

Figure 3.1: Schematic representation of the multiple-aliquot additive-dose technique for equivalent dose determination. Each data-point represents the average of a group of aliquots, which received an additional laboratory dose on top of the naturally accumulated dose. A function is fitted to these data (solid line), and is extrapolated to zero luminescence intensity to obtain the equivalent dose.

3.2.1.1.2. The **m**ultiple-**a**liquot **r**egenerative-**d**ose technique (MARD)

In this method, all groups of aliquots, with the exception of the group reserved to measure the natural signal, are first bleached to remove the naturally acquired luminescence signal. Subsequently, they receive different and known regenerative beta doses. Following a preheat, the natural and regenerated OSL signals are measured. The regeneration doses are chosen in such a way that the resulting luminescence signals encompass the natural signal. This allows determining the equivalent dose by interpolation **(**Figure 3.2), which has the advantage that uncertainties owing to the choice of the fitting function are reduced.

The most important disadvantage of this technique is that the bleaching, dosing and heating can change the luminescence properties of the mineral grains. More specifically, a change in sensitivity (luminescence per unit of dose) can occur between measurement of the natural OSL and measurement of the regenerated OSL. This has been observed in TL (e.g. Wintle, 1985; Bowall et al. 1987; Rendell and Townsend, 1988; Zhou and Wintle,

1994**)**, as well as in OSL dating studies (e.g. Rhodes, 1988; Li and Wintle, 1991, 1992; Richardson, 1994; Stokes, 1994; Jungner and Bøtter-Jensen, 1994) using feldspars, quartz or a mixture of minerals. Bleached and regenerated grains can have become more sensitive, for instance, and will emit more luminescence for the same dose as the natural ones. The growth-curve will consequently become steeper and the equivalent dose will be underestimated. This is illustrated in Figure 3.2. The occurrence of sensitivity changes can be recognised by comparing the slope of the regenerated growth-curve with that of the additive-dose growth-curve.

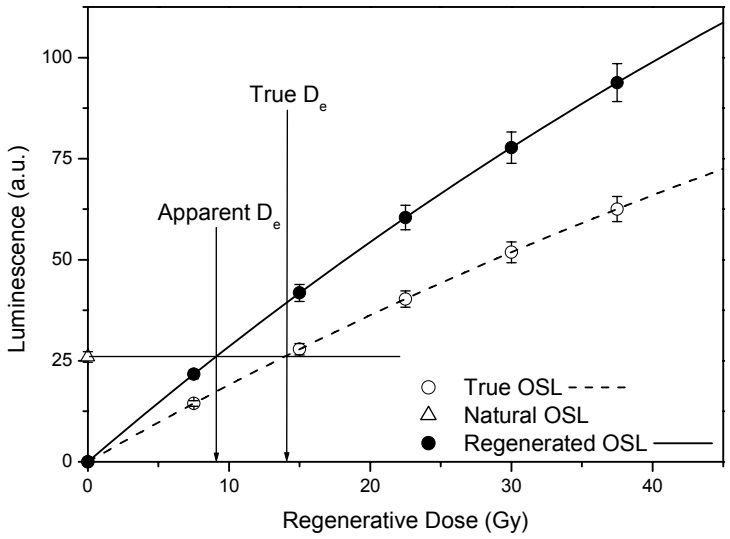

Figure 3.2: Schematic representation of the multiple-aliquot regenerative-dose technique for equivalent dose determination. Each data-point (circles) represents the average of a group of aliquots, which received a laboratory dose after the naturally acquired luminescence signal had been removed by bleaching. The solid circles represent the measured luminescence signals; the open circles the true signals that would have been measured had there been no increase in sensitivity due to the bleaching, dosing and heating. The apparent D_e is determined by interpolation of the natural signal (open triangle) on the growth-curve and is, in the absence of sensitivity changes, equal to the true D_e.

3.2.1.1.3. The "Australian slide" technique

In an attempt to circumvent the disadvantages of both the additive and regenerative-dose techniques, a hybrid technique was developed, known as the "Australian slide" technique (Prescott et al., 1993). It is especially suited for samples approaching saturation where uncertainties involved in the extrapolation of the additive-dose growth-curve are large. In

the slide technique, the equivalent dose is determined as the amount of displacement along the dose axis that is necessary to bring the regenerative-dose and the additive-dose growth-curves into coincidence (Figure 3.3). In this way, the regenerative-dose curve is used as a pattern for the missing (i.e. extrapolated) part of the additive-dose growth-curve. In the analysis program written by D.J. Huntley*, both sets of data-points are tested to see if they do indeed define a single growth-curve, i.e. whether or not the regenerated data are affected by sensitivity changes is checked. If desired, a sensitivity change can be corrected for.

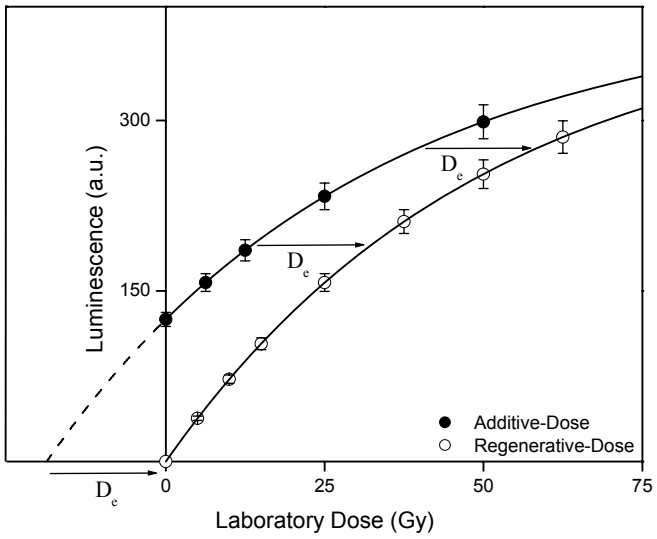

Figure 3.3: Simplified and ideal illustration of the slide technique for equivalent dose determination (modified from Prescott et al., 1993). The two growth-curves (additive and regenerative-dose) are identical except for a horizontal dose shift. In a fitting procedure, the additive-dose dataset is shifted to the right in order to obtain an optimum fit of both datasets to a single function. The D_e is then obtained as the amount of dose that the additive-dose set needs to be shifted.

The slide technique has been applied in TL dating studies of quartz from a sequence of stranded beach dunes in south-east South Australia by Huntley et al. (1993, 1994) and Huntley and Prescott (2001). A satisfactory agreement between the TL ages and the expected ages up to ~700ka was found. An interesting approach, and one of the few applications of the technique in optical dating, was by Feathers and Migliorini (2001). In their study of sediments associated with bone harpoon points (found in Katanda, East Africa), they used single-aliquot short-shine analysis (following Duller, 1995; see the

* Additional information is available at http://www.sfu.ca/physics/research/research/workarea/huntley/

following section), employing both additive-dose and regeneration approaches. These data were then processed using the "Australian slide" technique to determine the D_e.
In general, however, the technique does not seem to have been widely adopted. This is somewhat surprising as, prior to the widespread use of single-aliquot protocols, many laboratories routinely employed both the MAAD and MARD techniques. The "Australian slide" technique simply combines both these datasets – requiring no additional experimental efforts – to arrive at an improved estimate of the D_e. To those dating practitioners still using the multiple-aliquot approaches, the technique can in our opinion only be recommended. It is a robust procedure for analysing multiple-aliquot data and places more confidence in the results obtained (or at least in the way they are evaluated).
It can finally be noted that approaches similar to the "Australian slide" technique, but not as robust, were also suggested by Valladas and Gillot (1978), Readhead (1988) and Sanzelle et al. (1993), to name a few.

3.2.1.1.4. The **s**ingle-**a**liquot **r**egeneration and **a**dded-dose technique (SARA)

To overcome the problem of sensitivity changes in a regeneration-based approach, Mejdahl and Bøtter-Jensen (1994) designed the so-called SARA (**s**ingle **a**liquot **r**egeneration and **a**dded dose) protocol for dating heated archaeological materials. Murray (1996a, b) subsequently modified the protocol for application to unheated young sedimentary materials. The measurement sequence appropriate for dating sediments is outlined in Table 3.1.

Step	Aliquot 1	Aliquot 2	Aliquot 3	Aliquot 4	Aliquot 5	Aliquot 6	etc.
1: Add dose	$B_0 = 0$		B_1		B_2		
2: Preheat	10 s at 160-300°C						
3: Observe	L_N		L_1		L_2		
4: Add dose	$B_{0,\,ra} < D_e$	$B_{0,\,rb} > D_e$	$B_{1,\,ra} < (B_1 + D_e)$	$B_{1,\,rb} > (B_1 + D_e)$	$B_{2,\,ra} < (B_2 + D_e)$	$B_{2,\,rb} > (B_2 + D_e)$	
5: Preheat	10 s at 160-300°C						
6: Observe	$L_{N,\,ra}$	$L_{N,\,rb}$	$L_{1,\,ra}$	$L_{1,\,rb}$	$L_{2,\,ra}$	$L_{2,\,rb}$	
7: Calculate	C_N		C_1		C_2		
Plot calculated doses as function of B (Step 1) to obtain D_e							

Table 3.1: Generalised SARA measurement sequence, modified for application to sediments.

In a first step, different doses (B_0, B_1, …) are added to groups of two aliquots containing their natural signal. After a preheat, the resulting OSL signals are measured (L_N, L_1, …). Contrary to the additive-dose approach, the complete shine-downs are now recorded, meaning that each measurement completely removes the signal. Subsequently, a regenerative dose is given to one aliquot of the group, which is slightly lower than the sum of the dose added in the first step and the estimated D_e. The second aliquot receives a regenerative dose that is slightly higher. The aliquots are preheated again and the regenerated signals are measured. By plotting the measured luminescence signals versus the regenerative dose for each aliquot, the calculated doses C_N, C_1, … can be obtained as is shown in Figure 3.4.

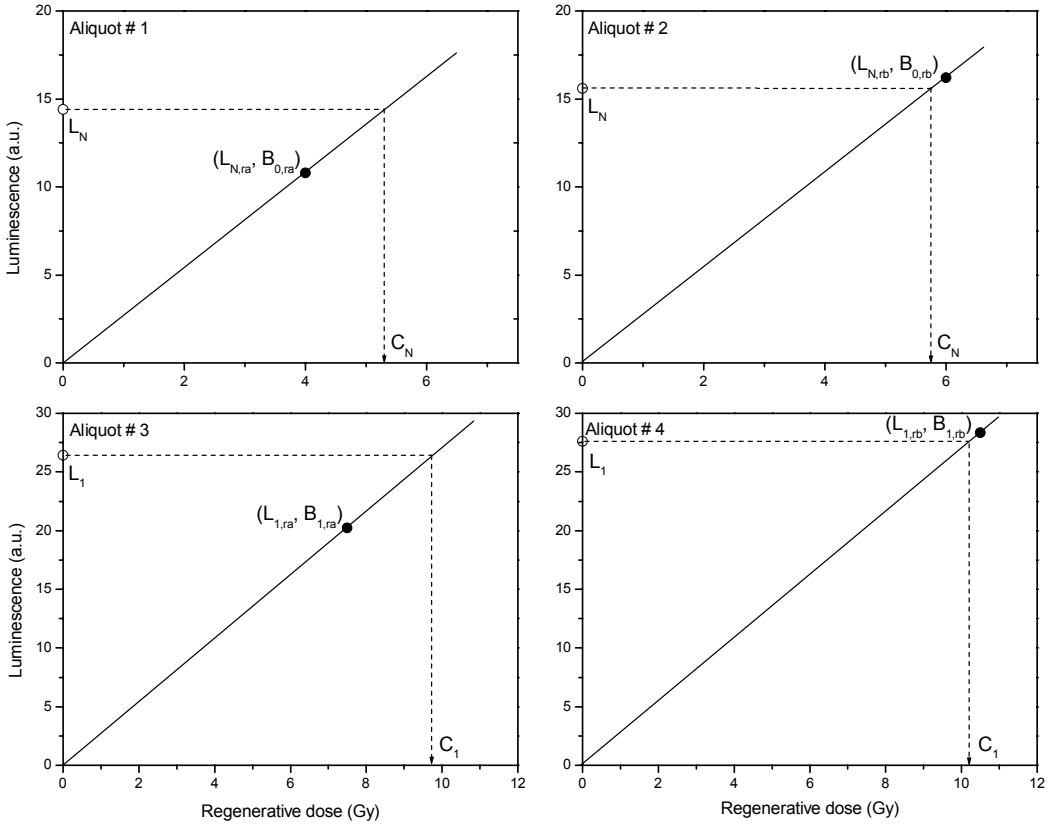

Figure 3.4: Modified interpolation procedure to allow application of the SARA protocol to unheated sediments (Murray 1996a, b). Aliquots #1 and #2 contain the natural dose, while aliquots #3 and #4 received a laboratory dose on top of the natural dose before all measurements were carried out. After measurement of these initial signals, known regenerative doses are added and the corresponding signals are measured again. The regeneration doses are chosen in such a way that they bracket the average unknown dose, i.e. one aliquot receives a lower dose than expected, and the other receives a higher. For each aliquot, a calculated dose is then obtained by inter- or extrapolation of the initial OSL signal (open circles) on the solid lines fitted through the origin and the regenerated data-point (solid circles). L: luminescence signal; B: dose; the subscript "r" refers to the regenerated data-point; C: calculated dose.

The calculated doses will be different from the true total dose in the quartz grains due to sensitivity changes. Assuming, however, that the sensitivity changes are independent of the dose (i.e. the changes cause a fixed percentage in increase or decrease of the measured signal from all aliquots), plotting of these apparent doses against the doses added in step 1 will yield the correct dose after extrapolation. This is shown in Figure 3.5. That sensitivity changes did occur can be seen from the difference between the extrapolated D_e (5 Gy) and the mean of the calculated dose values at zero added dose (~5.6 Gy).

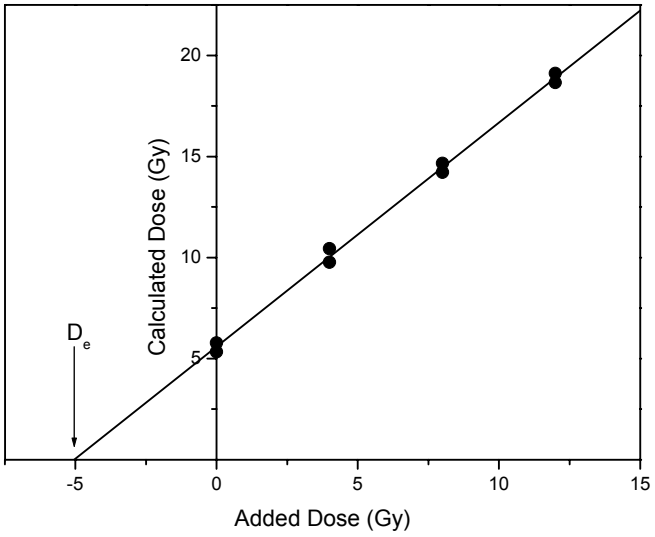

Figure 3.5: The calculated doses obtained as outlined in Figure 3.4 are plotted against the dose added to the naturally accumulated dose before all the measurements were carried out. The best estimate of the calculated dose for each group is obtained by taking the mean of the values derived from the two aliquots. By extrapolation, the true D_e can be obtained. That sensitivity changes have occurred can be seen from the fact that the D_e (5 Gy) is different from the average calculated dose at zero added dose (~5.6 Gy).

The important restriction in the protocol is that the sensitivity changes must be the same for all aliquots, regardless of the beta doses added initially in step 1. Mejdahl and Bøtter-Jensen (1997) give a simple procedure to test the dose independency of the sensitivity changes, and which can be used as a means to accept or reject a sample from the analysis. McKeever et al. (1997) presented computer simulations suggesting that the sensitivity changes are only weakly dependent on the added dose, lending support to the validity of the SARA technique.

As is illustrated in Figure 3.4, the calculated dose is obtained by proportion: the signal is assumed to grow linearly from its origin, and the calculated dose is then obtained by simply multiplying the regenerative dose (step 4 in Table 3.1) by the ratio of the natural (step 3) to the regenerated (step 6) luminescence signal. For this assumption to hold, it is required that the natural and regenerated luminescence signals are matched as closely as possible. Indeed, if the growth of the signal with dose is in reality non-linear, instead of linear, significant errors will be introduced if the light levels are not closely matched. This means, in practice, that some prior knowledge of the true D_e is required from the analyst, so that an appropriate regenerative dose can be applied. To overcome this problem, Duller et al. (1999c) developed a fully automated variant of the SARA technique in which the measurement system intelligently selects the necessary radiation doses within a suite of analyses.

The SARA technique has been applied to quartz extracted from heated archaeological samples as well as sediments. Mejdahl and Bøtter-Jensen (1997), e.g., showed a good agreement between SARA-based ages and TL ages, for sediments up to about 90 ka. Murray (1996b) used his version of the SARA protocol to study the influence of the preheat temperature on the equivalent dose. This had never been attempted before because of the enormous amount of labour required when doing this with the conventional multiple-aliquot protocols. Using a simplified version of Murray's (1996a, b) modified SARA protocol*, Murray et al. (1995) also presented the first quartz equivalent dose distributions (see Section 3.2.3.1).

It can finally be pointed out that although "single-aliquot" is in its name, the protocol is in fact a multiple-aliquot protocol, albeit an elegant one. Despite its interesting features, the SARA technique does not seem to have been widely adopted. The importance of the protocol, however, lies in the fact that, for the first time, a measurement procedure was developed that could cope with sensitivity changes.

* Murray et al. (1995) used only aliquot#1 and #2 in Table 3.1 to obtain an estimate of the D_e (because of the scatter in their OSL data which they attributed to partial bleaching). Their equivalent doses are consequently actually calculated doses, but they are estimated not to be more than about ± 10% off the true D_e values.

3.2.1.2. Single-aliquot techniques

Single-aliquot techniques are distinguished by the fact that all the measurements that are necessary to obtain an equivalent dose are carried out on 1 aliquot (at least in principle). Consequently, they offer a multitude of advantages compared to multiple-aliquot techniques:

- there is no need for normalization between aliquots;
- a single D_e can be determined with a high precision;
- less sample is required (in principle, even a single grain of quartz suffices);
- the D_e determination is relatively rapid, and can be completely automated;
- multiple estimates of the D_e can therefore be made and consequently external errors can be calculated (random errors, by examining the scatter in the many dose estimates)*;
- they allow an efficient investigation of the influence of different measuring parameters, as well as the intrinsic luminescence behaviour.

3.2.1.2.1. The **s**ingle-**a**liquot **a**dditive-**d**ose technique (SAAD)

When they introduced the optical dating method, Huntley et al. (1985) already noticed that, by stimulating for only a very short time, a measurable luminescence signal could be obtained without significantly depleting the total signal stored in the mineral grains. Consequently, they suggested that it should be possible to measure all the OSL signals necessary for an equivalent dose determination using only a single aliquot. In 1991, the first workable single-aliquot protocol was developed for potassium feldspars and using IRSL signals (Duller, 1991). The measurement sequence commences with a preheat, after which the aliquot is stimulated for only a very short time (a so-called "short-shine" of ~ 0.1 s) to obtain the natural signal. Subsequently, a dose is added, the aliquot is preheated

* In standard multiple-aliquot procedures, usually only one estimate of the D_e is obtained. The uncertainty on this value is then internal, i.e. derived from the mathematical fit to the data, and is consequently strongly dependent on the exact method of error analysis.

and the resulting signal is measured again using a short-shine. By repeating this measurement cycle, an additive-dose growth-curve is built up from which the unknown dose can be determined by extrapolation. Short-shines are used as to ensure that the accumulated signal is not significantly depleted. The dosing in this measurement sequence is thus cumulative, meaning that a measured signal results from all the previously administered doses, and not only from the last dose that was added. However, the preheating and the short shining do actually cause some small loss of signal. Duller (1991) estimated these losses by using a second natural aliquot that receives no additional dosing but is subjected to repeated preheating and short-shine measurements. These data can then be used to correct the raw luminescence data, as outlined by Duller (1991, 1994a, 1995). The protocol is consequently not really a single-aliquot protocol, as a minimum of two aliquots is required. Galloway (1996) later on refined Duller's protocol for feldspars to a true single-aliquot technique, by performing the measurements that characterise the signal depletion on the same aliquot, namely immediately after its additive-dose growth curve had been constructed. He also showed that the decay could be described by the mathematical function $f(n) = 1 - a \ln(n)$, where $f(n)$ is the fraction of initial signal remaining, a is a constant and n is the number of measurement cycles. Although this technique, being truly single-aliquot, should offer advantages, it does not seem, however, to have found wide acceptance.

Murray et al. (1997) were the first to devise a single-aliquot protocol for sedimentary quartz. In essence, it is similar to Galloway's (1996) modified protocol for feldspar. The difference lies in the fact that, for quartz, Murray et al. (1997) found the decay of OSL during a repeated preheat and short-shine cycle to be well approximated by an exponential decay, with a decay constant insensitive to the dose. These observations led them to present an additive-dose protocol requiring only one aliquot for the estimation of the equivalent dose. It can be noted that Liritzis et al. (1997) independently developed a very similar protocol for D_e-determination and successfully applied it to quartz extracted from ceramics.

The measurement sequence proposed by Murray et al. (1997) is outlined in Table 3.2.

Step	Treatment	Observed
1	Give Dose D_i	-
2	Preheat (10 s at 160-300°C)	-
3	Stimulate (e.g. 0.1 s at 125°C)	L_i
4	Go back to step 1 until enough growth curve data points	-
5	Preheat (10 s at 160-300°C)	-
6	Stimulate (e.g. 0.1 s at 125°C)	$L_{c,i}$
7	Go back to step 5 until enough correction curve data points	-

Table 3.2: Measurement sequence of the single-aliquot additive-dose protocol (Murray et al., 1997).

In steps 1 to 4, all the measurements are carried out that are necessary to characterise the growth of the signal with the dose. In steps 5 to 7 these measurements are repeated on the same aliquot, but without adding any further dose. The data obtained in these measurements are subsequently fitted to an exponentially decaying function, yielding a decay constant that can be used to correct the "raw" additive-dose signals. The accuracy of the correction is confirmed by applying it also to the measurements that were carried out to characterize the decay of the signal due to the repeated preheats and short-shines. After correction, these should lie on a straight horizontal line. The technique is illustrated in Figure 3.6.

Murray et al. (1997) tested their protocol on sedimentary quartz samples from 11 Australian sites, yielding results in good agreement with those from multiple-aliquot additive-dose protocols. They also found, however, that the protocol could not be applied to two other quartz samples, as these did not show the exponential decay. The SAAD protocol has subsequently been used in a number of other studies, such as those by Rich et al. (1999), Strickertsson and Murray (1999), Hong and Galloway (2000) and Hong et al. (2000), to name a few. A notable application was that by Murray and Roberts (1997). They used the protocol for determining the dose accumulated in individual grains of quartz, yielding optical ages in good agreement with independent age control. Their study is perhaps most important because of its demonstration, for the first time, of the variability in the luminescence behaviour as well as in the D_e between single grains of quartz.

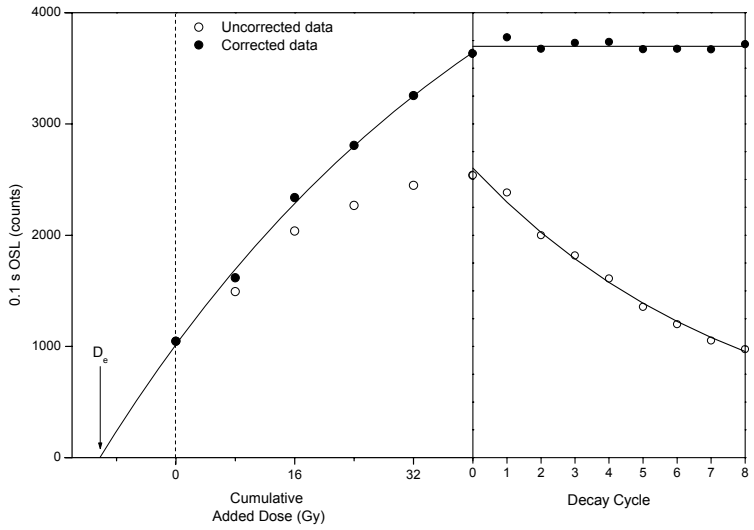

Figure 3.6: The single-aliquot additive-dose technique for equivalent dose determination. The measurements are carried out following the sequence outlined in Table 3.2 (open symbols). After the measurements that are necessary to construct the growth-curve are completed, preheating and measuring is continued without further dosing. The loss of signal is due to the preheating and the short-shine measurement itself. It is well represented by a single exponentially decaying function of which the decay constant can then be used for correcting the raw data and obtaining the true growth-curve (solid circles). Extrapolation of the growth-curve to zero intensity yields the D_e. If the correction works properly, the corrected decay data should lie on a straight line.

3.2.1.2.2. The **s**ingle-**a**liquot **r**egenerative-dose technique (SAR)

The fact that some samples had failed the SAAD approach (Murray et al., 1997; see Section 3.2.1.2.1.) led Murray and Roberts (1998) to investigate the potential of a true single-aliquot regenerative-dose protocol. As mentioned before, many workers dismissed the regenerative-dose approach because of sensitivity changes, and although SARA takes these changes into account, it still requires a theoretical minimum of two aliquots.

The starting point for the investigations by Murray and Roberts (1998) were the previously reported observations of the close relationship between the sensitivity changes in the OSL signal and the 110°C TL peak in quartz. This correspondence had been noted e.g. by Aitken and Smith (1988), Stoneham and Stokes (1991), Stokes (1994) and Wintle and Murray (1997, 1998), and led to the suggestion that the correlation provided a potential method for correcting for the sensitivity changes. Figure 3.7 illustrates this correlation.

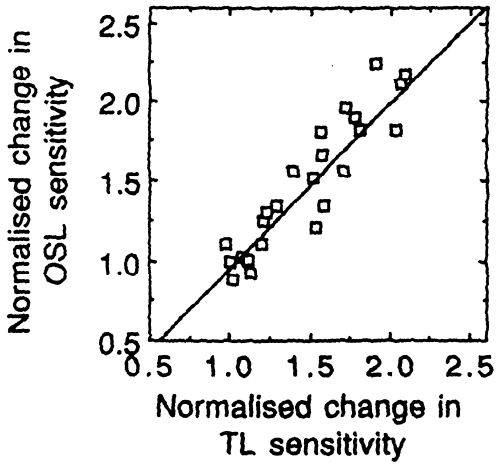

Figure 3.7: Relationship between the change in OSL and 110°C TL sensitivity in quartz (from Stoneham and Stokes, 1991). The scales have been normalised to unity for the average sensitivity of naturally irradiated aliquots; reference is made to the original paper for experimental details.

Murray and Roberts (1998) confirmed that the sensitivity changes of the 110°C TL peak correlate with those of the OSL signal, and demonstrated that it is possible to use this correlation to correct both natural and regenerated OSL signals for the effects of sensitivity change. Further investigations also indicated that preheating is the main cause for the sensitivity changes occurring in a repeated regeneration cycle. These observations led directly to the development of the first single-aliquot regenerative-dose protocol.

The measurement sequence starts with a preheat, followed by the measurement of the natural signal. Subsequently, the aliquot is given a regenerative dose and is preheated during which the 110°C TL peak is recorded. The measurement sequence consists further of repeating this cycle: OSL-measurement – irradiation – preheating. Preheating is for 10 s at a temperature in between 160 and 300°C. The regenerative dose is kept constant throughout the whole experiment and is chosen to match the natural dose as closely as possible. Because the sensitivity change occurs during the preheat, the 110°C TL signal relates to the immediately preceding OSL signal. In other words, the 110°C TL sensitivity signal associated with the natural OSL measurement is measured during the preheating of the first regenerative dose, the 110°C TL sensitivity signal associated with the first regenerated signal is measured during the preheating of the second regenerative dose, and so on. Several cycles of irradiation, preheating and OSL measurement are necessary to establish the relation between the OSL signal and the TL signal because this relation, although linear, does not necessarily pass through the origin. In the plot of OSL against

110°C TL, a straight line is then fitted through the regenerated data, which is extrapolated to the 110°C TL sensitivity associated with the natural OSL signal. From this, the natural luminescence signal can be predicted that would correspond to an equivalent dose equal to the regenerative dose. The true D_e is then simply obtained by multiplying the regenerative dose with the ratio of the observed natural OSL signal to the predicted OSL. The procedure is illustrated in Figure 3.8.

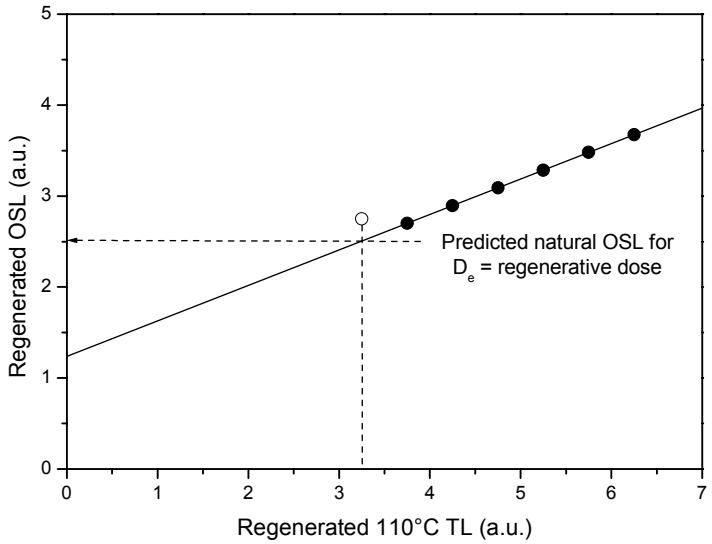

Figure 3.8: Schematic representation of the first single-aliquot regenerative-dose protocol for equivalent dose determination (Murray and Roberts, 1998). An aliquot of quartz grains is first preheated before the natural OSL signal is measured. The complete shine-down is recorded, meaning that the complete signal is erased by this measurement. Subsequently, the aliquot is given a regenerative dose and preheated during which the 110°C TL peak is recorded. The measurement sequence consists further of repeating this OSL-measurement – irradiation – preheating cycle. The solid circles plotted in the figure represent the regenerated signals, the open symbol the natural signal. A straight line is fitted to the regenerated data, and is extrapolated to the 110°C TL sensitivity associated with the natural OSL signal. From this the natural signal can be predicted that would correspond to a D_e equal to the regenerative dose. The true D_e is then obtained by multiplying the regenerative dose with the ratio measured / predicted natural OSL. The figure illustrates the linear relationship between the regenerated 110°C TL and OSL signals, but also that it does not go through the origin. This exemplifies the need for the repeated regeneration cycles.

Murray and Roberts (1998) applied their protocol to 13 samples from 9 Australian sites, finding an excellent agreement between the D_e's so obtained and those obtained with multiple and single-aliquot additive-dose protocols. This time, no samples were found to be unsuited for analysis. Murray and Roberts (1997) furthermore applied the protocol to

single grains of quartz extracted from an Australian aeolian deposit of a known age. The D_e's obtained were in good agreement with those obtained via the single-aliquot additive-dose protocol, and those obtained via multiple-grain single-aliquot and multiple-aliquot protocols. The optical ages were also in good agreement with radiocarbon and thermoluminescence ages. A remarkable application of the single-aliquot regenerative-dose technique was by Roberts et al. (1997). They used this technique (as well as the MAAD and SAAD techniques) to determine the age of quartz extracted from mud-wasp nests overlying prehistoric rock paintings in northern Australia. By doing so, they were able to estimate a minimum age for the paintings.

Since this first single-aliquot regenerative-dose protocol was suggested, there have been rapid further developments. Nevertheless, it was important because it focussed the attention on the possibility of explicitly measuring and correcting for sensitivity changes, while remaining a truly single-aliquot approach.

A second version of the protocol followed up the suggestion by Murray and Roberts (1998) of using the OSL response to test doses for monitoring sensitivity changes. This was based on their observations of the absence of a significant transfer of charge with preheating (so-called "thermal transfer", see section 3.2.2) and of the direct proportionality (a linear relationship passing approximately through the origin) between the OSL signal resulting from a small test dose given after the measurement of the natural or regenerated signal and this preceding OSL signal. The latter means that the relationship between the OSL test dose signal and the regenerated OSL may be defined using only one regeneration point; there is no need to repeat the regeneration cycles many times. The good correlation between the test dose OSL signals and regenerated OSL signals is illustrated in Figure 3.9. The D_e can then be calculated by multiplying the regenerative dose by the ratio of the natural to regenerated OSL signal, each signal being normalised to its corresponding test dose signals. As was previously pointed out, this approach implicitly assumes that the signal has grown linearly with dose up to the level of the natural signal. To avoid systematic errors, this implies that the regenerative dose should be a close match to the naturally accumulated dose. It can be noted that the same applies to the first single-aliquot regenerative-dose protocol.

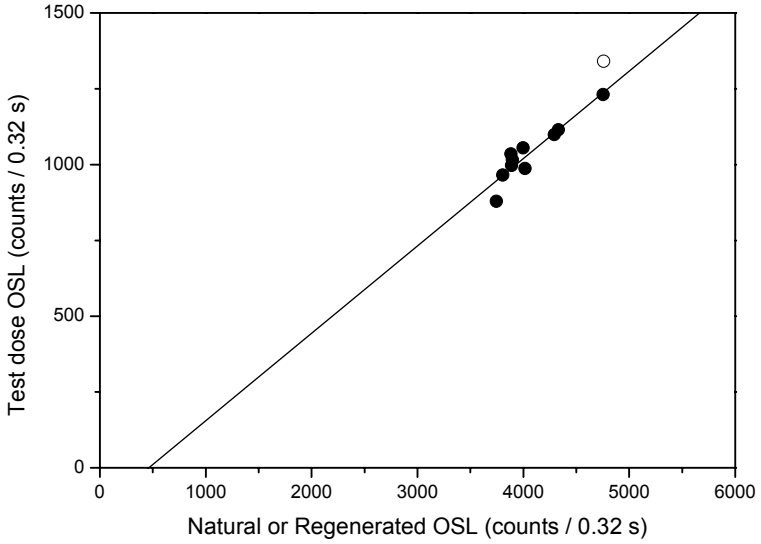

Figure 3.9: Relationship between the test dose OSL and the natural and regenerated OSL signals. The sample was preheated (10 s at 180°C) before its natural signal was recorded (40 s at 125°C using blue diodes). It was then given a test dose, followed by preheating (to 160°C) and measurement of the OSL response to the test dose. These data are plotted as the open circle. The aliquot was subsequently given a regenerative dose (~11Gy), followed by preheating and measurement of the regenerated OSL. The test dose OSL was measured again as before. This regeneration cycle was repeated 10 times in total and these data are plotted as the solid circles. The regenerative dose and test dose were kept constant throughout the experiment. The solid line is a fit to the regenerated data. The spread in the data is owing to sensitivity changes occurring during the repeated measurement cycles. The y-axis intercept is –130 ± 160, so it can be concluded that there is no evidence that the test dose and regeneration signals do not vary in direct proportion to each other. The natural datapoint lies somewhat off the solid line because the regenerative dose did not exactly match the D_e. The data are for a sample that was investigated in this work (Ossendrecht, lab code OS-C). Plots illustrating this correlation can also be found in Murray and Roberts (1998, Fig. 2 d-f), Murray and Mejdahl (1999, Fig. 2 iv-vi), Murray and Wintle (2000, Fig. 1) and Armitage et al. (2000, Fig. 3).

This second simplified single-aliquot regenerative-dose technique was successfully tested on heated quartz extracted from potsherds, burnt stones and bricks (Murray and Mejdahl, 1999) and unheated sedimentary quartz [Roberts et al, 1998a, 1998b, 1999 (see also Galbraith et al., 1999); Strickertson and Murray, 1999]. Zander et al. (2000) applied the simplified protocol to coarse grains of quartz extracted from six loess samples from a section in the Czech Republic. Their quartz samples showed a non-linear growth of OSL with dose and to avoid introducing systematic uncertainties by poorly matching light-levels, they used an automated iterative procedure originating from Duller et al.'s (1999) automated SARA procedure (see Section 3.2.1.1.4). The luminescence ages so obtained were found to be superior to those obtained with the quartz multiple-aliquot TL and OSL data. The single-aliquot ages were further in reasonable agreement with the ages

determined using the multiple-aliquot IRSL technique applied to polymineral fine-grains, and consistent with the (limited) geological evidence.

Using OSL signals from test doses to correct for sensitivity changes, Murray and Wintle (2000a) took this approach further to what is nowadays considered as the standard protocol for determining the accumulated dose in quartz grains, and is known as "the SAR protocol". Murray and Wintle (2000a) suggested that, as only one regeneration cycle is necessary to establish the relationship between the OSL test dose signal and the regenerated OSL signal, there is no practical impediment to repeat this cycle of regeneration and test dose measurements, using now a different regenerative dose in each cycle. By doing so, the complete growth of the luminescence signal with dose can be characterised, while the OSL responses to a fixed test dose can be used to correct for sensitivity changes. As in this manner sensitivity-corrected growth-curves can be constructed over a wide dose range, no prior knowledge of the D_e is required. The generalised measurement sequence proposed by Murray and Wintle (2000a) is outlined in Table 3.3.

Step	Treatment	Observed
1	Give Dose D_i	
2	Preheat (10 s at 160-300°C)	
3	Stimulate: 40 s at 125°C	L_i
4	Give Test dose D_t	
5	Preheat: ramp to 160°C **(to T < preheat step 2)**	
6	Stimulate: 40 s at 125°C	T_i
7	**Stimulate: 40 s at T > preheat step 2**	
8	Go back to Step 1	

Table 3.3: Generalised SAR measurement sequence (Murray and Wintle, 2000a). For the sake of completion, the modifications to the original protocol recently suggested by Murray and Wintle (2003) are included in bold; these are for dealing with samples exhibiting an ultra-fast OSL component (between brackets in step 5) and/or high levels of recuperation (step 7).

The measurement procedure starts with the measurement of the natural OSL signal, after the aliquot has been preheated ($D_{i=1}$ = 0 Gy). A test dose is then given, followed by another preheat and the measurement of the OSL response to the test dose. The test dose preheat is meant to empty shallow traps (such as that associated with the 110°C TL peak),

but is kept as low as possible to ensure that no additional sensitivity changes take place. This measurement cycle is then repeated after a regenerative dose is given, as many times as desired. Various regeneration doses can be used throughout the experiment but the test dose is kept constant. The OSL test dose responses monitor the sensitivity changes occurring during the measurement sequence and allow correcting for them. Figure 3.10 illustrates this measurement sequence, using a sample investigated in this work. In figure 3.10(a) the measured OSL signals and corresponding test dose OSL signals are shown as solid and open circles, respectively. The natural signal and its corresponding test dose OSL signal are indicated by the solid and open squares, respectively. The test dose responses illustrate how the sensitivity changes throughout the measurement sequence (about a factor of 1.8 in the given example). By dividing the regenerated OSL signals by the corresponding test dose signals, a normalised growth-curve is obtained, corrected for sensitivity changes. This is shown in Figure 3.10(b) by the solid circles. The equivalent dose is obtained by interpolation of the sensitivity-corrected natural OSL signal (solid square) on the corrected growth-curve.

If the sensitivity correction is working properly, a second measurement of the response to a dose equal to one that had previously been administered, should give an indistinguishable result. Therefore, such a repeat measurement is incorporated in the measurement sequence. In the given example, the first (and lowest) regenerative dose was repeated. This OSL signal and the associated OSL test dose response are indicated in Figure 3.10(a) by the solid and open diamonds, respectively. After correction, this response is indistinguishable from the earlier measurement of the same regenerative dose, as can be seen in Figure 3.10(b) by the open diamond overlying the first regenerative dose point of the growth-curve. The ratio of these two corrected regenerated OSL signals is called the “recycling ratio” and should ideally be unity. The deviation of the recycling ratio from unity can be used as a criterion for acceptance or rejection of aliquots.

A second important test is to check whether the dose-response curve starts indeed at the origin. This is accomplished by measuring the response to a zero regenerative dose. Although one would expect this to give a zero signal, in practice a small signal is observed. This “recuperation” of the signal is associated with charge-transfer effects during the preheating, and will be discussed in Section 3.2.2. The regenerated zero dose signal is shown as a solid triangle in Figure 3.10(a), the corresponding test dose signal as an open one. The corrected zero dose signal is shown as an open triangle in Figure 3.10(b) and is ~1% of the corrected natural signal. It can therefore be concluded that, in the given example, recuperation is negligible and the growth-curve shown in Figure 3.10 (b) does indeed pass through the origin. The amount of recuperation can also be used as a criterion for acceptance or rejection of a result.

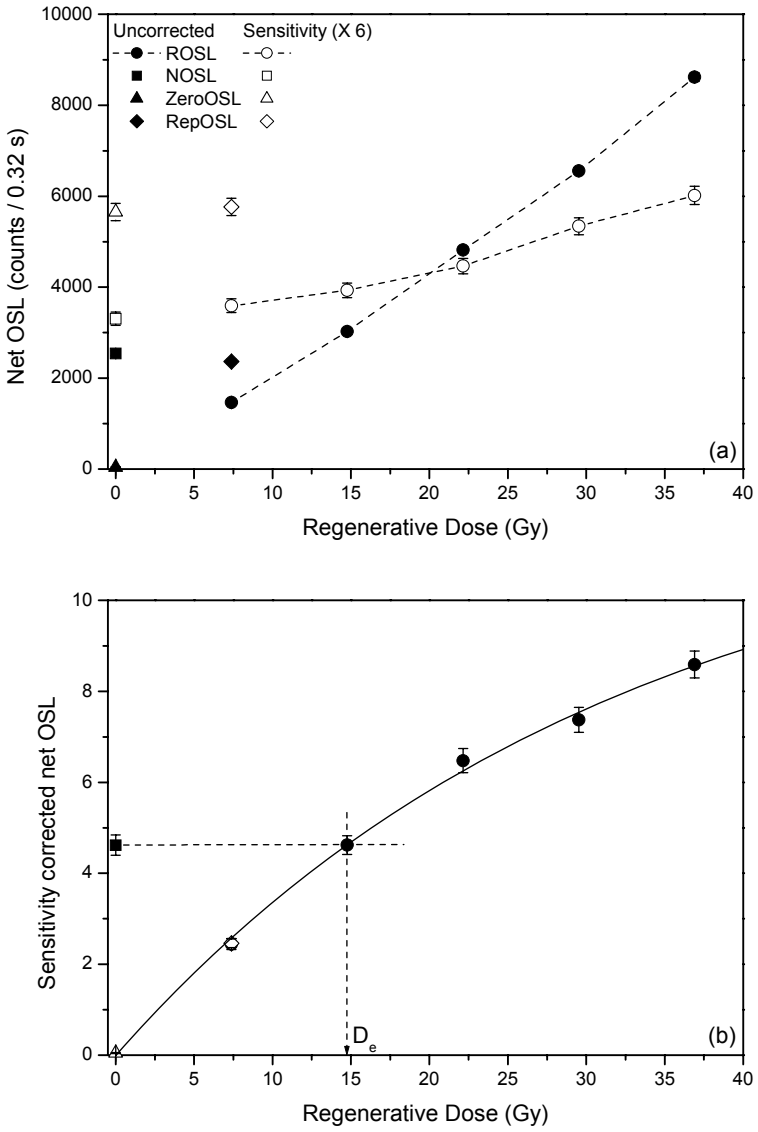

Figure 3.10: (a) Regenerated growth-curve for a single aliquot of quartz grains, obtained using the Murray and Wintle (2000a) SAR measurement sequence outlined in Table 3.3. After a preheat (10 s at 240°C), the natural OSL signal was measured (solid square, NOSL). Subsequently a small test dose was administered (~2.5 Gy), and the sample was heated to 160°C before measuring the OSL response to this test dose (open square). Then, the sample was put through repeated regeneration cycles. Note that throughout the entire measurement sequence, the only varying parameter is the regenerative dose; all other parameters (test dose, preheat,…) are kept constant. Plotted in the figure are the regenerated OSL signals (solid symbols) and corresponding test dose OSL signals (open symbols) versus the regenerative dose. For clarity, the test-dose responses have been multiplied by six. The signals associated with the zero dose and with the repeated measurement of the first regeneration dose are also included (diamond and triangle symbols, respectively). (b) The main OSL signals are divided through their corresponding test dose OSL signals and the resulting ratio's are plotted against the regenerative dose. The D_e is obtained by interpolation of the corrected natural OSL signal on the sensitivity corrected growth curve. The solid line represents a single saturating exponential fit to the regenerated data. The data shown are for quartz extracted from an aeolian sample from the Netherlands (Grubbenvorst, lab code G9).

The stimulation time mentioned in Table 3.3 is dependent on the stimulating light intensity. For the stimulation configuration used in this work (see Section 2.3 and Chapter 4), the OSL signal has decayed to a negligible level after 40s of stimulation. Although the complete shine-down is recorded in this way, it must be pointed out that only the initial OSL signal is actually used for D_e determination. This is to ensure that only the most readily bleachable component of the OSL is used, that most likely to have been completely reset in the past. Use of solely the initial signal also avoids possible complicating effects on the D_e determination by interference of the other OSL components, which exhibit different luminescence characteristics (see Section 2.5).

Another reason for using only the initial OSL signal is that even after a prolonged stimulation, some small signal in excess of the instrumental background will be observed. It arises from the presence of a very slowly bleaching OSL component. A complete removal of this signal by optical stimulation would take too long to be practical in routine measurements. To eliminate this component (and the instrumental background), the luminescence at the end of the natural and regenerated signals is subtracted from the initial OSL signals. The contribution of the slowly bleaching component to the OSL signal varies throughout the shine-down (as it slowly decreases with stimulation), and can vary from one measurement cycle to another. By using only the initial OSL signal, it is clear that the contribution of this "background", and any uncertainty associated with it, is minimised.

The slow component obviously delivers a more important contribution to the test dose signals, as these are usually weaker (induced by a relatively small dose). As the test doses are low, the majority of the slowly bleaching component underlying the test dose signal will consequently find its origin in the previous large natural or regenerated dose. Therefore, to obtain a net initial test dose signal, a background is subtracted that is evaluated from the end of the stimulation of the previous natural or regenerated signal.

A more detailed discussion on the selection of the OSL signal for D_e determination, and of appropriate background subtraction, can be found in Banerjee et al. (1999) and Murray and Wintle (2000a).

When they introduced the protocol, Murray and Wintle (2000a) also extensively investigated to what extent the choice of the measurement parameters (preheat

temperature, size of the test-dose, stimulation temperature, and test-dose preheat temperature) might influence the equivalent dose. They found the D_e estimates to be very insensitive to the exact measurement conditions. Although in the meantime this has been proven not to be a general conclusion for quartz samples, it is a very strong (and unique) feature of the protocol that the influence of any given measurement parameter on the D_e determination can be easily investigated.

Banerjee et al. (2000) further demonstrated the remarkable degree to which the SAR protocol can deal with sensitivity changes. They applied the protocol to determine the dose in quartz extracted from fired bricks that had been exposed to enhanced levels of ionising radiation as a result of the Chernobyl nuclear accident. They examined the response of one particular aliquot after three different treatments. First, they constructed a growth curve for the natural (untreated) aliquot. They subsequently reset this aliquot by exposure to light, and constructed a second growth curve. The same aliquot was finally zeroed once more by heating to 500°C and was reused to regenerate a third growth curve. The dosing, bleaching and heating had a considerable effect on the luminescence response. After sensitivity correction, however, the dose-response curves were found to be indistinguishable.

Because of its robust nature and the high precision it offers for equivalent dose determination, many laboratories have very rapidly adopted the SAR protocol. Although only a few years have passed since it was described by Murray and Wintle (2000a), it has already been applied for dating sediments from a wide range of depositional environments and age. The number of quartz-based applications is simply too large to be cited here. The SAR protocol has also been used to investigate the OSL properties of other dosimeters, such as feldspars (Wallinga et al., 2000a, 2000b; Strickertsson et al., 2001), salt (Bailey et al. 2000) and household chemicals such as washing powder, for instance (Thomsen et al., 2002). In a modified form, the protocol has been applied to polymineral fine grains extracted from loess from southern Germany (Banerjee et al., 2001a), China (Roberts and Wintle, 2001) and Belgium (Buylaert et al., 2003), and even to the polymineral fine grains extracted from a Martian soil simulant sample (Banerjee et al., 2002). Finally, it can be added that the principles of the technique have also been shown to apply to TL (Murray

and Wintle, 2000b) and Linearly Modulated OSL (LM-OSL; e.g. Singarayer and Bailey, 2003) signals.

Optical dating has been revolutionised by the introduction of the SAR technique. At the time of writing, it is indisputably the technique of choice for determining the quartz equivalent dose. Besides the unprecedented precision that can be achieved, SAR applied to quartz also seems to provide accurate ages. Convincing evidence for this latter has recently been presented by Murray and Olley (2002). They compiled both published and unpublished SAR quartz ages for which some independent age control exists and found, in general, an excellent agreement between the OSL and the independent ages. This comparison is shown in Figure 3.11. It should be pointed out, however, that the success of the protocol is more limited when it is applied to dosimeters other than quartz.

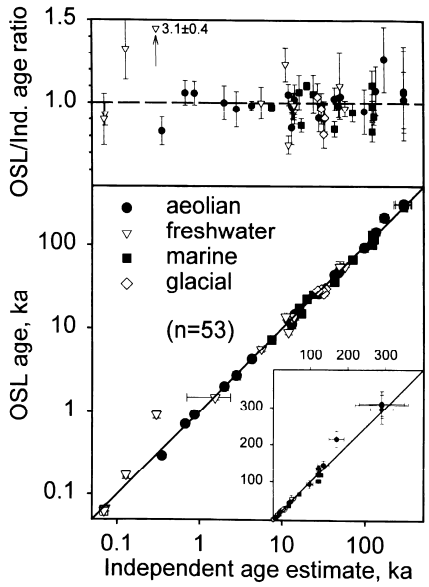

Figure 3.11: Comparison of quartz-based OSL ages obtained using SAR, with independent ages (from Murray and Olley, 2002). Note the logarithmic axes; the inset shows the same age data using linear axes. The OSL to independent age ratios are shown in the top part of the figure. It is clear that there is no evidence for any systematic difference over the entire age range. Omitting the freshwater result at 3.1 ± 0.4 ka, Murray and Olley (2002) found the average ratio of the OSL to independent ages to be 0.984 ± 0.016 (unweighted; weighted: 0.978 ± 0.009). Although the results are clearly encouraging, Murray and Olley (2002) point out that 5 out of the 53 results lie more than 3 standard deviations from unity. The age of 3.1 ± 0.4 ka is in error owing to partial bleaching; the significant deviation from unity for the remaining four ages is attributed to an underestimation of the uncertainties in the ratios.

3.2.2. Preheating and thermal transfer

3.2.2.1. Preheating

After an irradiation (whether in nature or in the laboratory) and before the OSL signal is recorded, usually some heat treatment is applied to the sample. This is the so-called "preheat" that was already mentioned in preceding sections. Several reasons have been formulated in the literature as to the need for preheating (Aitken, 1998):

1) When a sample is irradiated both deep and shallow (i.e. stable and unstable, respectively) electron traps are filled. The shallow traps will not contribute to the natural OSL signal, as they are too unstable to retain a significant amount of electrons over the time span that is being dated (thermal fading; see section 1.3). If the OSL signal would be recorded immediately after irradiation in the laboratory, however, these shallow traps may contribute to the measured artificial luminescence signal, if they are light sensitive and their luminescence lies in the detection wavelength region. Consequently the D_e would be underestimated. To avoid this, it is necessary to remove the unstable luminescence, which can be accomplished by preheating.
2) As outlined above, the shallow traps will not contribute directly to the measured natural OSL signal. However, they might do so indirectly, and regardless of whether these traps are light-sensitive or not. Indeed, some of the electrons released during thermal fading can get caught in deeper traps, including those that lead to the OSL signal. In nature, this process will have taken place to a degree depending on the stability (lifetime) of the traps and the exact burial conditions. This transfer process, however, will not have happened for the samples irradiated in the laboratory. Therefore, it is necessary to heat both the naturally and laboratory irradiated aliquots in such a way that ultimately the transfer contributions to all the OSL signals are equalised. If no heat treatment would be applied, the D_e would be overestimated.
3) A third reason why preheating is necessary, is on account of sensitivity changes. It has been shown that the luminescence efficiency (or sensitivity) of quartz is

strongly dependent on the exact conditions of its previous treatment. Consequently, the luminescence response of the quartz to natural and laboratory doses will be different (see Section 2.7, Figure 2.10). The purpose of preheating is then to equalize the effects, i.e. to make sure the probability that a recombining electron will produce luminescence is the same for the natural and the artificial laboratory doses. Otherwise an erroneous D_e will be obtained. Huntley et al. (1996), for instance, used a thermal treatment to avoid radiation quenching of luminescence sensitivity in quartz due to competition during the shine-down. Radiation quenching is the phenomenon in which an additional laboratory dose actually leads to a reduction of the subsequently measured luminescence. Huntley et al.'s (1996) interpretation of this radiation quenching is that the laboratory dose activates a recombination centre that competes with the one responsible for the OSL. The centres are also activated by the natural dose, but a thermal process on a timescale less than the age of the sample deactivates them again. A laboratory heat treatment is then necessary to deactivate the centres that were activated by the artificial dosing.

In the early days of optical dating, and for a long time thereafter, the main reasons for preheating were thought to be #1 and #2 of the above list, i.e. the removal of unstable components, and the equalisation of transferred charge contributions to natural and artificial signals. In this respect, the use of a single and known mineral, such as quartz, was considered to be advantageous. It was then already recognised that the quartz OSL signal is dominated by the contribution from a single electron trap, namely that associated with the 325°C TL peak (see Section 2.10). Consequently, it was assumed that once a preheat regime could be identified capable of meeting the above-mentioned needs, it should be applicable to all quartz samples (see e.g. Smith et al., 1990b). Both short duration high temperature and long duration lower temperature preheats were proposed, such as 48 hr at 150°C (Wolfe et al. 1995), 16 h at 160°C (Stokes, 1992), 5 min at 220°C (Smith et al., 1986; Rhodes, 1988) and 1 min at 240°C (Franklin et al. 1995), all supposed to have the same effect. The main reason as to why the different recipes were suggested, seems to be related to experimental convenience. For instance, if no automated measurement system is available, long duration low preheat temperatures are more

reproducible. If, on the other hand, the measurements are carried out using completely automated facilities, a short duration high temperature preheat is more convenient.

After some time, however, it was found that different preheats may result in different equivalent doses. This resulted in a considerable debate over the most appropriate heat treatment. The most notorious disagreement about preheat regime was probably between Roberts et al. (1993, 1994b, 1994c) and Stokes and Gaylord (1994; Stokes, 1996a, b). Roberts et al. found a significant underestimation of the D_e when long preheats of 16 h at 160°C were used and advocated the use of the 5 min 220°C preheat. Stokes, however, presented an extensive intercomparison using samples collected from a range of depositional environments and of varied provenance and age, finding no disagreement between the two procedures.

It had been suggested for many years that the effect of preheating on the D_e should be examined routinely (Huntley et al., 1985; Aitken, 1992, 1994). This was common practice in TL dating, using the plateau test, but unfortunately, such a test is not available in optical dating. For the latter, the validity of a preheat can be established by means of the "preheat plateau test". In this test, a series of equivalent dose determinations is made, employing a preheat of different intensity for each determination. This can be accomplished by keeping the temperature constant and varying the duration, or vice versa. If the preheat is not intense enough, some variation of equivalent dose can be expected. The values level off into a plateau once adequate heat treatments are being reached. A valid preheat treatment is then one that yields a D_e in this "preheat plateau" region. Investigating the appropriateness of a preheat regime for each sample that is to be dated is obviously a very laborious task when multiple-aliquot protocols are used. As a consequence, not many workers actually went through this effort, but simply adopted one of the above mentioned recipes. With the development of single-aliquot protocols, it became much more feasible to investigate the effect of the preheat on the D_e.

Murray et al. (1997) used their single-aliquot additive-dose protocol (see section 3.2.1.2.1) to conduct preheat plateau tests for 5 samples. They used short (10s) preheats between 160°C and 300°C. For three samples, they observed higher D_e values at lower temperature preheats, the estimates levelling off into a plateau at more stringent preheats. In general, it was found that the older samples required higher preheats to reach a plateau. Their observations could be entirely explained in terms of thermal transfer. Murray et al. (1997;

see also Wintle and Murray, 1997) therefore concluded that the main effect of preheating is indeed the transfer of charge from lower temperature traps to the deep OSL trap.

The development and application of the single-aliquot regenerative-dose protocols, however, shed a whole new light on these observations. Murray and Roberts (1998) used the first version of this protocol (see Section 3.2.1.2.3) to investigate the dependence of D_e on preheat temperature. Employing the same heat treatments as Murray et al. (1997; i.e. 10s at 160°C-300°C) they now found no significant variation in D_e over the entire temperature range. Subsequently, Wintle and Murray (1999) unambiguously showed that any dependency of the D_e on the preheat temperature is removed, once the measurements are corrected for sensitivity changes. This is illustrated in Figure 3.12 (from Wintle and Murray, 1999) where the results are compared from two preheat plateau tests for the same sample. One test was carried out using the single-aliquot additive-dose protocol, the other using the single aliquot regenerative-dose protocol. It can be seen that the D_e's obtained via the two techniques agree well at higher preheat temperatures, but that at lower preheat temperatures the SAAD values are significantly higher. If thermal transfer (reason #2 for preheating) had indeed been the true explanation for the higher SAAD values, as was previously thought, the same trend should have been observed using the regenerative-dose protocol. This is clearly not the case. Many workers have since then presented plots of equivalent dose versus preheat temperature (so-called "preheat plateau" plots). All of them found that, once sensitivity changes have been corrected for, the equivalent dose is effectively insensitive to the preheat temperature employed (e.g. Murray and Olley, 1999; Murray and Wintle, 2000a; Banerjee et al., 2001b; Murray and Clemmensen, 2001).

These observations can probably be understood best when turning back to Chapter 2.7. There it was shown (Figure 2.10; from Wintle and Murray, 1998) that the responses to the same preheat and dose of a naturally and an artificially irradiated aliquot can be different. This clearly explains why different D_e values will be obtained upon the use of different preheat temperatures, if these different sensitivities are not taken into account. If, on the other hand, they are explicitly measured and corrected for, as is done in the SAR protocol, D_e values become independent of the preheat conditions. There is no longer any evidence for transfer processes (reason #2 for preheating) playing an important role.

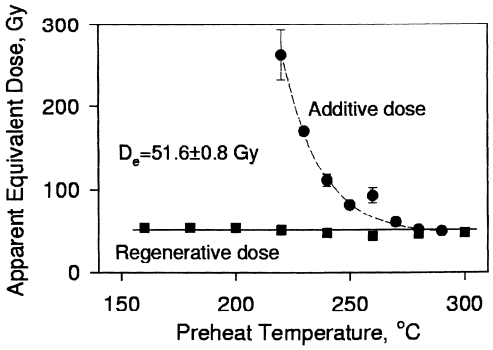

Figure 3.12: Comparison of D_e values obtained via the single-aliquot additive-dose protocol by Murray et al. (1997) and via the single-aliquot regenerative-dose protocol (by Murray and Roberts, 1998) as a function of the preheat temperature (from Wintle and Murray, 1999). Each datapoint represents the average of three determinations. The data are for quartz grains extracted from a sand-apron in the north of West Australia (laboratory code: WIDG8). For full details, the reader is referred to the original papers.

3.2.2.2. Unwanted thermal transfer

At this point, some further discussion is appropriate of thermally transferred charge processes as besides the supposed "wanted" charge transfer, preheating can also cause two other types of "unwanted" thermal transfer. Whereas the previously discussed transfer concerned electrons that resulted from irradiation in nature during burial and in the laboratory (the charge populations directly relevant for dating), the following concerns the movement of electrons that were already present in the quartz grains before the resetting event, as a result of their prior exposure to irradiation. These effects result in a contamination of the measured luminescence with a component that does not relate to the event being dated. Consequently they can be considered as "unwanted" effects of the preheating and some discussion of these additional effects is justified, as contrasting views concerning their importance have been put forward in the literature.

The two types of "unwanted" thermal transfer are termed (according to Aitken, 1998): "basic transfer" and "recuperation", and they are distinguished from each other by the mechanism by which they operate. It can be mentioned that the term "thermal transfer" is more comprehensive, referring to any transfer of charge that is thermally assisted.

"Basic transfer" is due to electrons that were already present in light-insensitive and thermally stable traps before the zeroing event. These traps are consequently not emptied during the bleaching and are sufficiently deep for thermal fading to be negligible. Due to

these properties, the traps are likely to be well populated. Although the traps are quite stable, preheating is able to remove some of the electrons from them. Some fraction of these released electrons can subsequently get trapped in the OSL trap. Obviously, the amount of transfer depends on the actual depth of the trap. It is possible that a first preheat removes all the charge; if the trap is more stable, only a small fraction is transferred during each preheat.

"Recuperation", on the other hand, is due to electrons stored in the OSL (thus light-sensitive) traps themselves. During the zeroing event, some of these electrons will get trapped in relatively light-insensitive and thermally stable traps. The traps are not so deep, however, as preheating can cause the electrons to be transferred back into the OSL traps. If the traps are shallow enough, transfer can occur during storage as well. Recuperation is consequently actually a double transfer effect: first a photo-transfer occurs during bleaching, which is then followed by a thermal transfer during the preheat.

The effect of both types of unwanted thermal transfer is the same: due to the preheat, a sample of zero age will not give a zero luminescence signal. In other words, thermal transfer leads to an overestimation of the equivalent dose, and hence the age. The effect becomes important when a significant proportion of the total electrons in the OSL trap results from thermal transfer.

Several authors have reported on the disturbing effects of basic transfer and recuperation, and reference is made to Aitken (1998) and Banerjee (2000) for overviews on these experimental observations. At the time of writing, however, it seems that the general concern that has arisen from these observations should be seriously moderated. Indeed, the presence of an unwanted thermally transferred contribution to the OSL signal should be reflected in an increase of the D_e with preheat temperature. As was mentioned above, a large number of authors have found the equivalent dose in both young and old samples to be effectively independent of preheat temperatures ranging from 160°C to 300°C, once the measurements had been corrected for sensitivity changes (Figure 3.12 illustrates this). Some additional evidence for recuperation can be gained from the zero dose point in a SAR measurement sequence (see Section 3.2.1.2.3). Again, once the correction for sensitivity changes has been made, the degree of recuperation is reduced to negligible levels (see e.g. Figure 3.10 and the above-mentioned literature). These observations

strongly suggest that most of the previously reported observations on significant thermal transfer effects were actually caused by sensitivity changes that were not corrected for. However, as also pointed out by Banerjee (2000), this is not a general conclusion applicable to all quartz samples. For some young sediments (deposited sometime during the last few hundred years) an increase in D_e estimates with preheat temperature has indeed been observed (see e.g. Figure 3.13, from Bailey et al. 2001). More recently, in a study of young coastal dunes from the Netherlands, Ballarini et al. (2003) found the D_e to be independent of preheat temperatures below 200°C. A rising trend in D_e was observed for more stringent preheats. Similar observations have also been made by Murray and Clemmensen (2001) and Hilgers (2004). In all these studies the SAR protocol was used for D_e determination, which corrects for sensitivity changes, and so the increases could convincingly be attributed to thermal transfer.

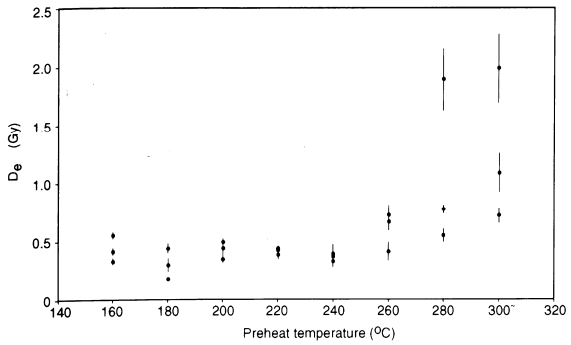

Figure 3.13: Illustration of a SAR preheat plateau test for a young (0.31 ± 0.09 ka) quartz sample extracted from a dune field in North Wales (UK; modified from Bailey et al., 2001). There is a clear increase in D_e values at preheat temperatures exceeding 240°C, suggesting the contribution of an "unwanted" thermally transferred component to the dose estimates.

From the whole of investigations and recent findings reported over the last few years in the literature, it can generally be concluded that the overall significance of any thermal transfer process, whether "wanted" or "not", seems more limited than previously thought. Nevertheless, thermal transfer can be important for some young samples and lead to significant equivalent dose overestimates. In practice, however, this does not impose any real problems, as the effect can be readily identified from a SAR-based D_e versus preheat

temperature plot and is easily overcome by simply using a lower preheat temperature chosen from the plateau region.

Finally, it is perhaps worth illustrating the role that the observation of the absence of a significant thermal transfer of charge played in the development of the SAR protocol (Section 3.2.1.2.3). Murray and Roberts (1998) used the regenerated 110°C TL signal instead of an OSL signal induced by a test dose for fear of incomplete preheating of the test dose. Indeed, a test dose is usually not preheated to a high temperature to avoid inducing additional sensitivity changes. This means that the "wanted" transfer of the charge induced by the test dose could be incomplete. It is then brought to completion during the subsequent high temperature preheat of the regenerative dose. Consequently, some fraction of the test dose could indirectly contribute to the regenerated signals, and systematically upset the accuracy of the D_e determination. However, Murray and Roberts' (1998) subsequent observation that the sensitivity corrected D_e estimates were relatively independent of the preheat, suggested that thermal transfer of electrons into the OSL trap is not as important. This opened up the possibility of using OSL responses to test doses to directly measure and correct for sensitivity changes, an important observation leading ultimately to the development of the improved SAR protocol by Murray and Wintle (2000a).

3.2.3. Equivalent Dose Variability

With the introduction of single-aliquot dating techniques it became easily possible to obtain many equivalent dose estimates for a single sample. As already stated at the beginning of section 3.2.1.2, this allows the examination of the random variability in D_e. Apart from such a scatter in D_e being caused by measurement or analytical uncertainties, a real spread in the absorbed energy from grain to grain can find its origin in several causes that relate to heterogeneity in the degree of resetting of the OSL signal in the past (i.e. partial bleaching), heterogeneity in the dosimetry or mixing of sedimentary grains of different age by natural processes.

3.2.3.1. Partial bleaching

If the sediment grains receive insufficient light exposure before their deposition, the resetting of their OSL signal will be incomplete. Some residual signal remains that contributes to the natural OSL signal and, consequently, causes the equivalent dose, and hence the age, to be an overestimate. Such a situation of incomplete resetting is called "partial bleaching". It can arise because the exposure to light was either simply too short, or because the wavelength of the light was inefficient in removing the previously accumulated luminescence signal (see Section 2.9). Partial bleaching, therefore, is an important limiting factor in the application of luminescence dating to non-aeolian deposits.

Two views or models for describing the zeroing process have been put forward (Duller, 1994b; Duller et al., 1995), which resulted in the classification of sediments into two types, 'A' and 'B'.

Type 'A' sediments are those in which all the grains have been equally bleached during transport and deposition. In other words, this model assumes a homogeneous light exposure during the resetting event, in which all grains are exposed to the same amount of daylight whether sufficient or not to reset the OSL signal completely. If there is partial bleaching, it is the same for all the grains. For these sediments, multiple D_e determinations would then be very reproducible, but wrong.

Type 'B' sediments are those that contain a mixture of grains that were exposed to daylight for different periods of time. In this case, the exposure to light is heterogeneous. Some grains will be completely reset, for instance, while others will contain a residual signal varying in magnitude from grain to grain. If multiple D_e determinations would then be carried out using grains from these sediments, a certain degree of scatter in the results would be expected.

The development of single-aliquot protocols made it possible to explicitly investigate these two models of resetting. Olley et al. (1998), for instance, used the simplified SARA protocol of Murray et al. (1995) to investigate the distribution of doses in recently transported fluvial and aeolian sediments. They used "small" aliquots containing only about 60 to 100 quartz grains in order to accentuate any heterogeneity. In other words, if the heterogeneous partial resetting model is applicable, the use of small aliquots will

increase the observed scatter. If the resetting was “homogeneous”, on the other hand, all aliquots should give the same answer, within analytical uncertainties, regardless of the scale of analysis. The results obtained by Olley et al. (1998) are reproduced in Figure 3.14. For the fluvial samples, it can be clearly seen that not all aliquots have been completely reset and, furthermore, that the residual dose is certainly not the same for all aliquots. The aeolian sand (Figure 3.14c), on the other hand, seems to consist mostly of completely reset grains. Nevertheless, some grains contain a measurable higher equivalent dose. The histograms clearly illustrate that signal resetting is heterogeneous in the fluvial environment. In the wind-blown environment, the light-exposure is also heterogeneous, but sufficient to result in a more complete resetting of the OSL signal in all the grains.
Other workers have produced similar equivalent dose distributions, either using small aliquots or single grains (Murray et al., 1995; Olley et al., 1999; Duller et al., 2000; Lepper et al., 2000; Spencer et al., 2003). All these studies demonstrated that the ‘homogeneous resetting model’ does not represent physical reality. From the evidence that has been published in the literature, Muray and Olley (1999) concluded that at the time of deposition sediments fall into one of two categories: either they have had sufficient light exposure to fully reset all the grains, or they are heterogeneously reset and the grains exhibit a range of residual doses. Such a resetting process is in keeping with intuition, where one would think of the natural transport and deposition process of sediments as being a random and turbulent one.

It can finally be pointed out that a special case of partial bleaching is the effect of “unwanted” thermal transfer. As was outlined previously (Section 3.2.2) these effects find their origin in charge that was not removed during the zeroing event, either because the charge was located in light-insensitive traps, or because it was transferred from light-sensitive to light-insensitive “shelter” traps instead of recombining with holes. During the preheat, the charge will be transferred back into the main OSL trap and lead to an increased natural OSL signal and hence to an overestimation of the age. If the amount of thermal transfer is different from grain to grain, it will lead to an additional scatter in the equivalent dose distribution. Although the existence of such a process is not denied, it has been argued in section 3.2.2 that, in general, it has only a limited impact on an equivalent dose determination.

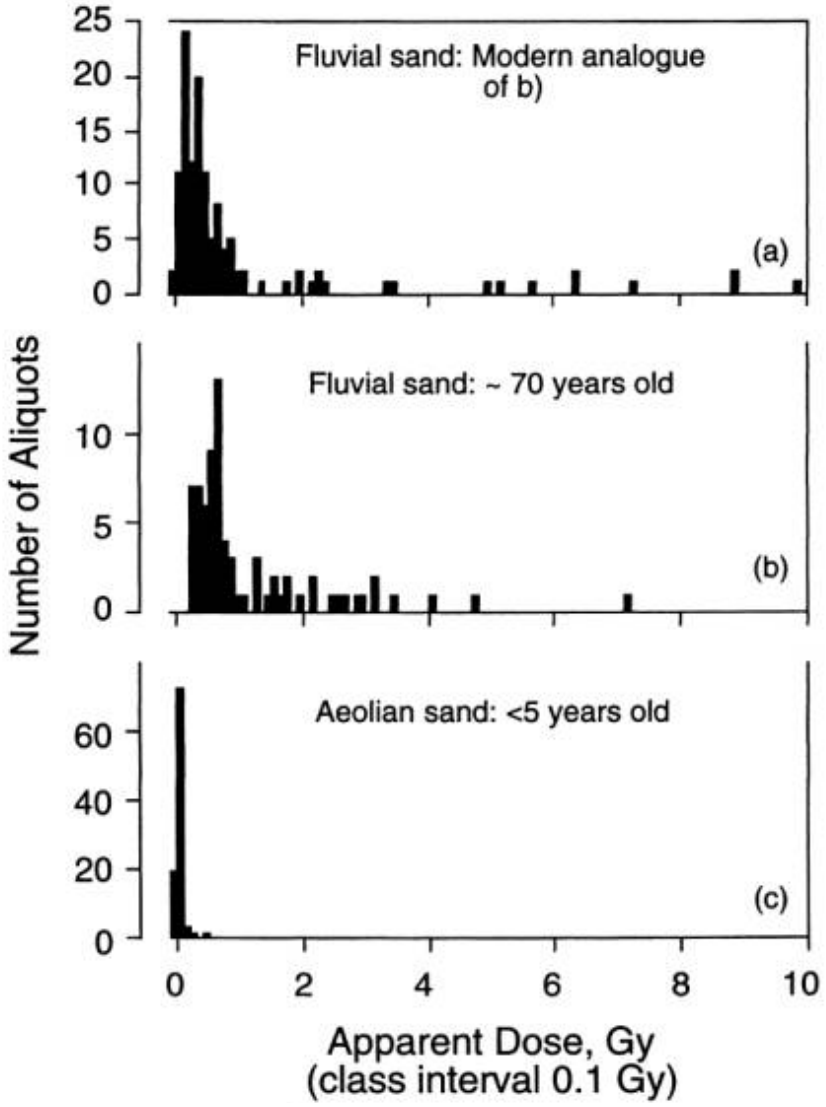

Figure 3.14: Apparent dose distributions obtained using aliquots containing between 60 and 100 grains. The figure is adapted from Murray and Olley (1999) who modified it from the original histograms by Olley et al. (1998). The simplified SARA protocol of Murray et al. (1995) was used to obtain the apparent doses (or "calculated" doses; see Section 3.2.1.2.2). (a) Apparent doses from 116 small aliquots of quartz grains extracted from a recent fluvial sand deposit from Australia. The sample is the modern analogue of the fluvial sand sample used to construct the dose distribution in (b). This second sample was deposited during a flood event that is known to have occurred in 1925. The apparent dose distribution was determined using 78 small aliquots. (c) Apparent doses in 96 small aliquots of quartz grains extracted from a modern aeolian dune sand from Australia. From geomorphic evidence, this sand was known to be less than 5 years old.

3.2.3.2. Microdosimetry

Microdosimetric variations are variations in annual dose on a very small scale. In such a situation, the individual sedimentary grains are exposed to different fluxes of radiation and consequently this will be reflected as a scatter in equivalent doses. Microdosimetric variations are mainly related to beta radiation. Inhomogeneities in the gamma radiation field are negligible due to the long penetration scale of gamma radiation in sediment. Equally unimportant are small-scale variations in the external alpha radiation field, as their contribution to the dose received by coarse quartz grains is removed by etching (see Section 3.3.7).

Variations in microdosimetry as a source for equivalent dose variability have been argued for by Murray and Roberts (1997), for instance. In their study of single grains extracted from a well-bleached deposit, they found an unexpected wide scatter in equivalent doses. They considered various possibilities (such as anomalous fading, thermal transfer, reworking of the sediment and non-linearity of the growth curve) but concluded that heterogeneity in external beta dosimetry was the most likely. The deposit they investigated was not only composed of aeolian material, but also for a significant percentage of carbonate. Quartz surrounded by the carbonate would then receive a much lower beta dose than grains surrounded by purely aeolian material, while other grains would receive a beta dose somewhere in between these extremes. Kalchgruber et al. (2003) mixed single grains of the highly sensitive Al_2O_3:C phosphor with loess sediment (from Nussloch in SW-Germany) and subsequently determined the doses absorbed by these grains. They observed a broad scatter in D_e values, which could partly be attributed to dose-rate inhomogeneities in the loess sediment, most likely arising from its high carbonate content. Through numerical (Monte Carlo) modelling, followed by some experimental validation (using single Al_2O_3:C grains, and laboratory mixtures), Nathan et al. (2003) were able to demonstrate that a heterogeneity in the beta radiation environment may indeed significantly influence the degree and manner to which D_e values are scattered.

In studies actually involving the luminescence dating of sediments (such as the one by Murray and Roberts, 1997), however, the possibility of microdosimetric variations as an additional source of scatter is often neglected, or it is called upon if no other obvious

cause can be found to explain an observed scatter. An interesting comment was recently made by Rieser and Smith (2003), who inverted conventional reasoning and concluded that partial bleaching is a rare event, and that the primary cause for scatter in most dose distributions is an inhomogeneous radiation field. This conclusion was based on their observation that the shape of dose distributions matches a log-normal behaviour. They applied their model to a large number of previously published (including those shown in Figure 3.14) and newly obtained dose distributions, with an impressive degree of success. They argue that if partial bleaching is indeed a truly random and highly unequal process, every distribution would be expected to have a different shape. Rieser and Smith (2003; Rieser, private communcication) suggest that the variations arise from the presence of radioactive "hot spots", i.e. minerals with a high radioactivity (such as zircon) that are dispersed through the sediment and disturb the homogeneity of the radiation field. This seems to be confirmed by their observations of wide distributions for sand-sized grains that were expected to have been well bleached in the past, and of narrow distributions if these coarse grains were embedded in a fine-grained matrix. Unfortunately, Rieser and Smith (2003) do not present any direct mineralogical or radioactivity data to support their hypotheses.

It appears that the effects of small-scale variations in annual dose are still not sufficiently quantified, and are worthy of consideration when dealing with scattered equivalent dose values. Furthermore, although by microdosimetric variations, external variations in the beta dosimetry are usually meant, internal variations in the alpha dose rate, i.e. in the alpha radioactivity contained within each quartz grain, might perhaps be relevant as well (see Section 3.3.8).

3.2.3.3. Post-depositional mixing

Another effect that can give rise to a D_e variability in a single sample is the mixing of sedimentary grains of a different age, after the depositional event. That such situations can occur was clearly illustrated by Roberts et al. (1998b) in their optical dating study of sediments deposited in the Jinmium rock shelter in northern Australia. In this case, the age of an aeolian deposit was overestimated due to contamination by older (unbleached) grains that had eroded from an overlying rock. Furthermore, they found intrusion by

younger grains from overlying layers caused by bioturbation processes. These can originate from burrowing animals (insects or mammals, such as wasps, rabbits or humans) or floral activity (roots growing into the ground), resulting in some mixing of grains from layers of different ages. These effects might be small, but with the improved precision made available by the single-aliquot techniques perhaps significant. Besides some oral communications at conferences and the recent paper by Bateman et al. (2003), not much work seems to have been undertaken to investigate the effects of these processes. Effects of bioturbation can be largely excluded if the original sedimentary structures have been preserved.

3.2.3.4. Analysis of equivalent dose variability

It is clear that any of the above-mentioned processes (partial bleaching, microdosimetric variations or post-depositional mixing) can have a detrimental effect on the accuracy of an optical age. Of these, partial bleaching has received the most attention in the literature and consequently the following overview is perforce also mostly in terms of incomplete resetting of the OSL signal.

The fact that partial bleaching is expected to lead to some degree of variability in the equivalent dose can be exploited to identify its presence. Analytical techniques in which the observed scatter in D_e values (obtained via multiple determinations) is examined and interpreted in some way are called "dose distribution" techniques (Section 3.2.3.4.1). A second class of techniques that have been developed are the "signal analysis" techniques, in which various parts of the OSL signals measured during the determination of a D_e are examined to find evidence for their partial bleaching (Section 3.2.3.4.2). Both types of techniques are, in principle, available for single- as well as multiple-aliquot procedures. Considering the complexity of heterogeneous signal-resetting (illustrated in Figure 3.14), however, makes it clear that any D_e determination technique that uses an average luminescence signal from a large number of grains is limited in its capability of identifying and dealing with partially bleached sediments. The capability of a technique for doing so, and consequently the probability of obtaining the true burial dose, increases with a decreasing aliquot size. It can be readily understood that any heterogeneity is averaged out to a lesser degree when employing single-aliquot protocols. In the following,

therefore, the attention will be focussed on those techniques that have been developed for (and via) single-aliquot protocols. The different techniques, their advantages and disadvantages will be summarised, and some illustrative examples from the literature will be included.

For the sake of completeness, it can be added that the different bleaching behaviour of different minerals, or of the TL and OSL signals can be exploited for the detection of partial bleaching as well. Reference is made to Aitken (1998) and Wallinga (2002a) and the literature they quote, for a more comprehensive treatise of these techniques.

3.2.3.4.1.Dose distribution methods

In the case of a sediment in which all the grains have been completely reset, multiple determinations of the equivalent dose are expected to give the same result, within analytical uncertainties. As was illustrated in Figure 3.14, partial bleaching will produce an additional scatter in the D_e values. It has therefore been suggested to quantify the scatter in D_e's by calculating the absolute and relative standard deviation and to define poorly bleached samples as those for which the values exceed 5 Gy and 10%, respectively (Clarke, 1996; Clarke et al., 1999). This approach obviously depends strongly on the degree of partial bleaching, as well as on the degree of averaging in each aliquot. The more luminescent grains an aliquot contains, the more the different doses absorbed by each of these grains will be averaged, and the more the scatter between aliquots is reduced. The concept of threshold values for the standard deviation is consequently not very robust.

In the first instance, it seems plausible to expect that an aliquot containing a higher dose will also yield a higher luminescence signal. Consequently, it has been put forward that the existence of a correlation between the two is an indication for partial bleaching. The idea was launched by Li (1994), followed by Clarke (1996), Clarke et al. (1999) and Colls (1999), to name a few. The latter further developed the approach and constructed standardised plots (mean = 0, SD = 1) of luminescence intensity versus equivalent dose (Figure 3.15). These plots allow a more easy visualisation of any correlation. To eliminate the subjectivity inherent to such an approach, Colls furthermore suggested to investigate the significance of any trend in the plot by using a t-test for establishing the statistical

significance of the resulting correlation coefficient. The interpretation of any of these plots is however not straightforward. Wallinga (2002b) concluded on the basis of computer simulations that the absence of a correlation between signal intensity and equivalent dose is not an indication that the sample was well bleached. Furthermore, as is also pointed out by Wallinga (2002a, b), these scatter plots implicitly assume that the luminescence sensitivity of the grains is relatively homogeneous. In other words, it is assumed that a grain with a higher dose, indeed gives a higher signal. However, it was shown in section 2.8.1 that, at least for quartz, there is an extreme non-uniformity in luminescence sensitivity.

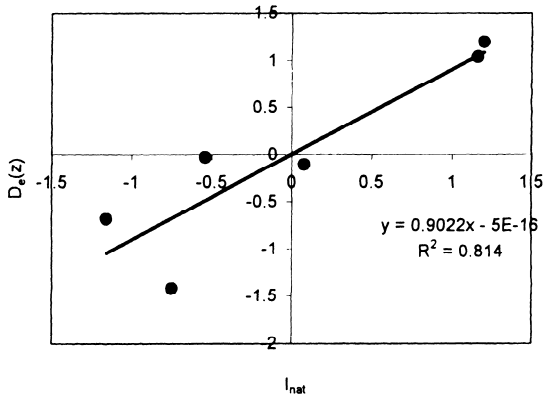

Figure 3.15: Plot of standardised equivalent dose versus signal intensity (from Rich and Stokes, 2001). The solid line is a least-squares linear fit to the data. The statistical significance of the so obtained correlation coefficient (R^2) is established by the use of a t-test (Colls, 1999).

Another way to visualise and interpret the results from multiple D_e determinations, is to plot the D_e's in a histogram, as in Figure 3.14. From the shape of this distribution, some conclusions can be drawn concerning partial bleaching. Indeed, for a well-bleached sample, D_e values are expected to cluster tightly and symmetrically around a mean value as the observed scatter should arise from counting statistics only. Partial bleaching is expected to disturb this symmetry, stretching out the distribution to higher D_e values. Other than this, partial bleaching is, however, not expected to lead to a distribution of a certain shape, as the resetting process is completely random and variable. The observation of an asymmetric equivalent dose distribution is consequently an indication for incompletely reset grains present in the sediment. Selecting only those aliquots from this

distribution that yield the lowest D_e values, will offer the highest probability at obtaining an accurate age (see e.g. Olley et al., 1998, 1999).

A drawback of the graphical representation and subsequent analysis of the results using histograms is that the uncertainty associated with each equivalent dose is not taken into account. Especially when only a small number of quartz grains is present in each aliquot, the observed OSL intensities may vary considerably (see Section 2.8.1). Consequently, the precision by which the individual equivalent doses are determined varies accordingly and this might lead to erroneous interpretation of the histograms.

A graphical representation especially suited for comparing several estimates which have different precisions is the so-called "radial plot" (Galbraith, 1988, 1990, 1994). The plot takes into account that the aliquots vary in OSL intensity, and hence yield D_e's of varying precision. In this plot (Figure 3.16, from Galbraith et al., 1999), the individual equivalent doses are represented by the circles. The value of an equivalent dose measured for an aliquot can be read off by drawing a line from the origin of the y-axis through the circle until the line intersects with the right hand circular scale. The x-axis represents the precision (calculated as the inverse of the standard error on $\log D_e$); it may also be expressed as relative standard error (in %). The precision by which an individual D_e has been obtained, can consequently be read off from the intersection with the x-axis by a vertical line drawn through the data-point in question. Points on any straight line radiating from the origin have the same D_e, but can bear a different uncertainty. The y-axis plots the standardised estimate of $\log D_e$. These are calculated as the $\log(D_e$ minus a reference value) divided by the standard error of $\log D_e$. The reference value employed is usually the weighted average for all aliquots, but any other arbitrary reference value (such as another equivalent dose estimate) can be used as well. Reference is made to the original papers by Galbraith for further details on the construction of a radial plot.

An interesting feature of a radial plot is that it sorts the data along the x-axis according their precision; the further to the right a data-point is plotted, the more precisely its value has been determined. It is especially useful that equivalent doses that are statistically consistent at the 2s level are easily recognized, as these will fall within a band extending ± 2 units vertically around a common radial line. This band is indicated by the dotted lines in Figure 3.16. As a consequence, the band allows an easy identification of whether a

spread in doses is caused by a lack in measurement precision or by an additional source of uncertainty (such as partial bleaching).

Radial plots were originally developed by Galbraith for fission track dating. Roberts et al. (1998a, 1998b, 1999) and Galbraith et al. (1999) were the first to introduce the plot in the luminescence dating methodology and since then it has been used to interpret single-aliquot and single-grain OSL data in a quite a number of studies, such as those by Baran et al. (2003), Feathers (2003), Jacobs et al. (2003a, b) Thomsen et al. (2003) and Yoshida et al. (2003).

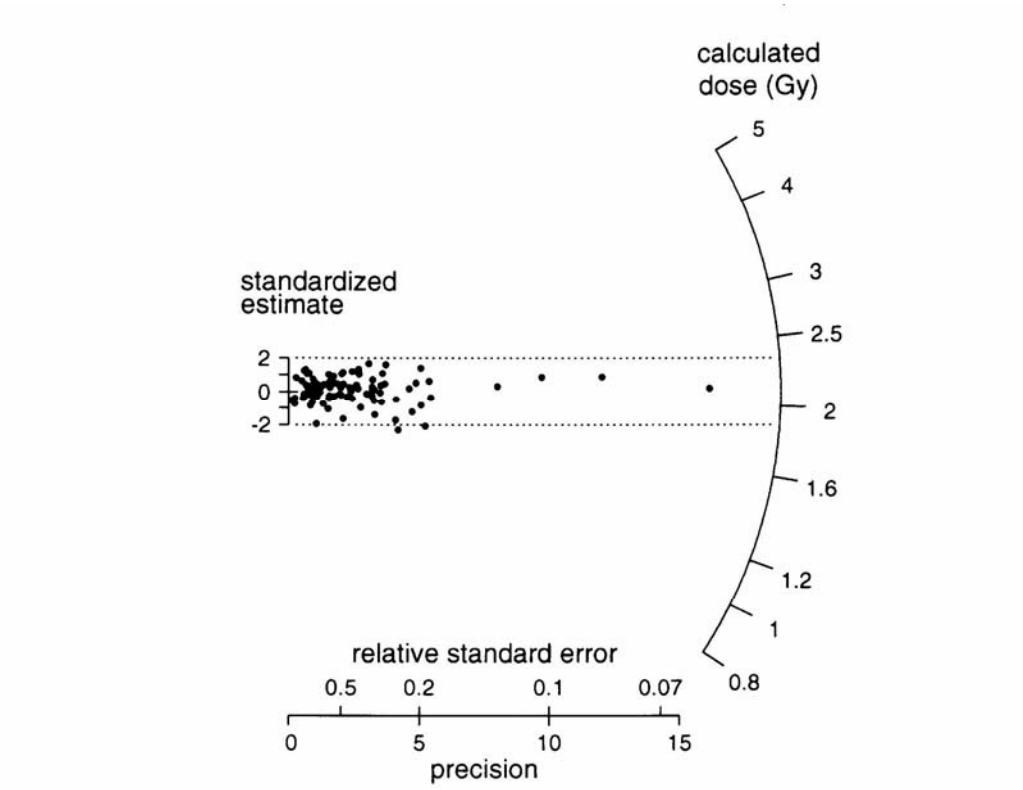

Figure 3.16: Example of a radial plot (figure 7 from Galbraith et al., 1999). The data are from a dose recycling experiment (applied dose 2.1Gy) for 95 single grains of quartz from a sample of the Jinmium rock shelter in northern Australia (laboratory code: COOR 2/2). The dotted lines delineate a band of ± 2 units on the y-axis, centred at the applied dose. As the grains had been completely bleached before the known dose was administered, it is expected that 95% of the data-points should be consistent with the known dose within 2s. From the 95 grains analysed, 93 indeed fall within the 2s band.

Although the radial plot provides a graphical means for comparing several estimates having different precisions, it should in the first instance be regarded as a visualisation tool; it shows if an apparent outlier was measured with adequate precision. A precise luminescent measurement is, however, no guarantee for an accurate result. Imagine, for

instance, a grain containing a large residual dose because it had not been zeroed at all. Neglecting, for the sake of reasoning, grain intrinsic variations, then it is likely that the D_e-determination for this grain will be more precise than for a grain that had been reset completely. The most precise measurement, however, will in this case also be the most inaccurate. That there is not always a link between precision and accuracy is something very important that should be born in mind. Methods of analysis that do use this link, as for instance, those using a precision weighted mean, can lead to a precise age that does not necessarily refer to the event of interest that we are trying to date, namely the date of deposition.

In analytical techniques using histograms or radial plots, the interpretations and conclusions might be influenced by the uncertainties associated with the D_e measurement itself. This led Lepper (2001) and Lepper et al. (2000) to develop a technique in which the experimental error is first deconvolved from the measured D_e distribution to arrive at the true distribution arising from sedimentary processes only. Once the effect of experimental uncertainties is removed, the obtained distribution should more accurately represent the true dose distribution and hence allow a more accurate D_e determination. The idea is schematically shown in Figure 3.17. The edge at the lower D_e value end of the 'true' distribution arises because the luminescence signal cannot have been reset to less than zero. Consequently, this "leading edge" value should correspond to the true D_e. From this starting point, the true dose distribution can be stretched towards higher D_e values due to various degrees of partial bleaching of the mineral grains in the sediment. The distribution will rise more sharply from the starting point as more grains had been completely reset. The sharpness of the leading edge therefore gives an idea on how likely this D_e is indeed accurately representing the true burial D_e. If for example most grains were partially reset, a distinct leading edge will not be observed due to the heterogeneity of the resetting process. In such a situation, the D_e derived from the leading edge bears a large uncertainty, as there is not much confidence in its accuracy since it is possibly derived from partially bleached grains as well. The technique further provides an objective and unambiguous way for plotting the deconvoluted distributions, selecting an age representative D_e from dose distributions and obtaining its corresponding uncertainty. The techniques developed by Lepper (2001) and Lepper et al. (2000) are important, not so

much because it should be the best possible approach, but because, as the authors state, at least it is an objective one. The computer codes necessary for deconvolving the distributions are quite complex, however, which (for as far as known to us) unfortunately has prevented the implementation of this technique by any luminescence laboratory other than the one of Lepper et al. (2000).

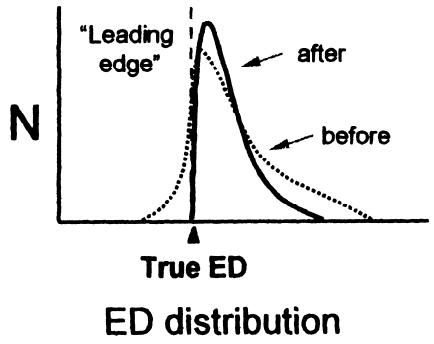

Figure 3.17: Illustration of the D_e distribution deconvolution concept (from Lepper et al., 2000). The dashed line represents the measured D_e distribution; the solid line depicts the deconvolved distribution after the effect of experimental uncertainties is removed. The sharp edge on the low D_e side is termed the leading edge, and should reflect the true burial dose. It originates from the fact that the luminescence signal in the grains cannot have been reset to a value less than zero. The sharpness of the edge is postulated to give some confidence for the "leading edge" D_e to accurately represent the true burial D_e; a sample strongly suffering from incomplete resetting should indeed have a broader distribution with less grains being complete reset, and hence should display a less pronounced edge effect.

For the application of the above methods, a large amount of data is required. Fuchs and Lang (2001) suggested a procedure that can be used to smaller datasets. In their procedure, the D_e's are ranked from low to high values. Starting from the lowest two D_e's, a mean and standard deviation is calculated. Subsequently, this is repeated for the lowest three D_e's, the lowest four D_e's, and so on, until the standard deviation reaches a value of 4%. The resulting mean equivalent dose is then chosen for age calculation. The 4% was the uncertainty obtained upon the determination of the dose in quartz samples that had been completely bleached and given a known gamma dose. It is consequently a measure for the precision that can be attained in ideal conditions, i.e. if the dataset would not be influenced by partial bleaching.

It can be concluded that dose distribution methods provide useful insights into the bleaching process that a sample has been subjected to, and that some methods can successfully be used for the detection and overcoming the effects of partial bleaching. It is worth pointing out, however, that all procedures of analysis relying on the observation and interpretation of scatter are strongly dependent on the scale of analysis (number of luminescent grains in an aliquot). An aliquot is, in analytical terms, a poorly defined and quite irreproducible quantity. Aliquots composed of as few grains as is practically possible (ideally one grain only) are best suited for this type of analysis and allow interpretations not to be significantly influenced by the effect of averaging the equivalent dose within each aliquot. If evidence for partial bleaching is found, one should not overlook the possibility that even the lowest D_e that was obtained might still be an overestimate. Furthermore, it must be realized that the precision by which the individual equivalent doses are measured (and the shape of the individual growth curves), can also influence the shape of a distribution.

As dose distribution techniques are in essence simply based on the analysis of a spread in the results, they do not allow differentiating between the possible causes of the observed scatter. Whereas it is possible to recognize post-depositional mixing from sedimentological evidence or field evidence, this is less straightforward for microdosimetric variations. The influence of these variations might prove to be insignificant, but until this is actually empirically substantiated it would seem prudent to keep in mind this possibility as an additional source of scatter.

3.2.3.4.2.Signal analysis methods

Methods belonging to this category make use of the fact that the quartz OSL signal consists of different components (see Section 2.5), of which some are easier to bleach than others. The initial OSL signal observed in a shine-down curve (the so-called fast component) is thought to be associated with the electron traps that are most sensitive to light, while the luminescence observed in later stimulation time intervals (the slow OSL components) is coming from progressively less light-sensitive traps. Comparison of the D_e calculated from the initial OSL signal with the D_e's calculated from later stimulation time intervals should then allow the identification of partial bleaching. A plot of equivalent

dose versus stimulation time is called a $D_e(t)$-plot. If it is flat, then it is inferred that the sample was adequately bleached at the time of deposition; if the D_e increases with stimulation time, the bleaching was incomplete.

It was already suggested by Huntley et al. (1985) that this approach might give information on the completeness of bleaching at deposition. However, when applied to multiple-aliquot protocols, the technique has not met expectations. Roberts et al. (1994a), for instance, reported a rising plot for a sample that was convincingly believed to have been well bleached (the TL-based equivalent doses formed a plateau over the 270 to 430°C region, i.e. both the easy 325°C as the hard-to-bleach 375°C TL trap yielded the same result). Perkins and Rhodes (1994) and Wood (1994), on the other hand, observed decreasing $D_e(t)$ plots. Bailey (2000) later showed both theoretically and empirically the unsuitability of the procedure for multiple-aliquot data. On the other hand, the laboratory-based investigations by Bailey (2003a,b) indicated a more promising potential of $D_e(t)$-plots for the detection of partial bleaching, when the SAR protocol is used for equivalent dose determination. He first showed that well bleached samples give flat plots, while incompletely bleached samples give rising plots. Bailey et al. (2003) subsequently tested the technique on modern sediments from various depositional environments. The results from this study confirmed the positive laboratory findings as both complete and incompletely reset samples were correctly identified. Figure 3.18 shows the principle of the SAR-based $D_e(t)$-technique.

A more refined technique would be to really extract the different individual OSL components, so as to avoid their overlap and consequently the masking of partial bleaching effects. This was explored by e.g. by Agersnap Larsen et al. (2000) who showed that using the linear modulation technique (see Section 2.5), it is possible to recognise incomplete bleaching of the different OSL components. Their experiments were conducted under controlled laboratory conditions, and were supported by computer simulations, so their observations still need to be confirmed on natural samples. The fitting procedures that are required for extracting the different components are furthermore quite complex and time consuming, which might in practice prevent routine use of the technique they suggested.

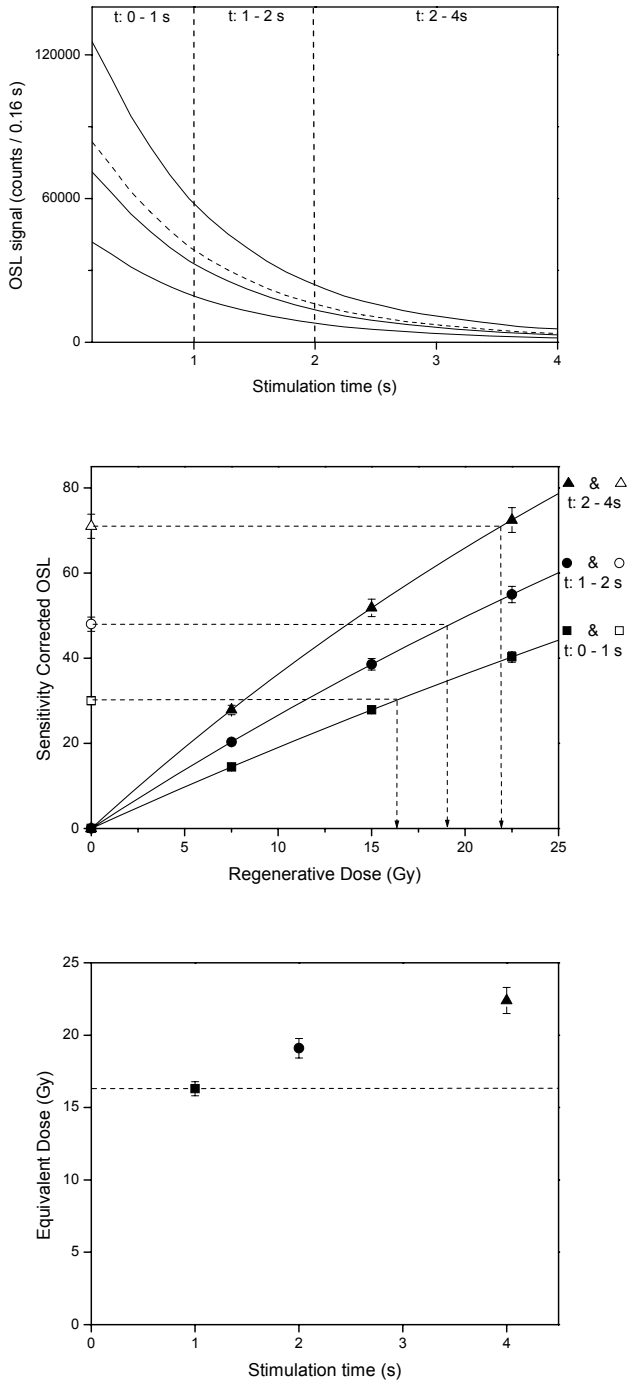

Figure 3.18: Illustration of the SAR-based $D_e(t)$-technique. The shine-down curves of the natural (dashed) and regenerated (solid) OSL signals are subdivided in different time intervals. For each interval the growth-curve is constructed, from which the corresponding natural signal is then interpolated to obtain the equivalent dose. By looking for a variation in equivalent dose with stimulation time, differential bleaching of the different OSL components can be recognized. In the given example, a rise in $D_e(t)$ can be observed, suggesting that the OSL signal was incompletely reset prior to burial.

The use of methods which are based on signal analysis are potentially more powerful for detecting incomplete resetting, as they are able to distinguish the effects of partial bleaching from the effects of microdosimetric (or other) variations. Indeed, if a scatter in D_e's is observed while the $D_e(t)$ plots are flat, the source of the variation is obviously not caused by incomplete resetting. Furthermore, the technique can be applied to each aliquot that has been measured, yielding information on the accuracy of each individual D_e. It can be concluded, therefore, that these signal analysis methods, especially the SAR $D_e(t)$ technique, are promising and powerful tools for analyzing the observed variability in equivalent doses.

More experimental work is still necessary, however, to fully establish its applicability. Although the D_e (t) method worked extremely well for their samples, Bailey et al. (2003) acknowledge that it is not expected to do so under all circumstances and they address potential complicating factors. For instance, for the technique to work, it obviously requires a differential bleaching of the different components under a given illumination spectrum. This has been found to be the case in fluvial environments, where the light spectrum is more restricted to longer wavelengths, but not in daylight (aeolian) conditions (Singarayer and Bailey, 2004). This is not a serious restriction, however, as bleaching conditions for windblown samples are most likely to have been adequate for complete resetting of the signal. Potentially more upsetting is the fact that the different OSL components do not all seem to exhibit suitable characteristics (such as an adequate thermal stability and a negligible recuperation, for instance) required for an accurate equivalent dose determination (Jain et al., 2003; Singarayer and Bailey, 2003). In particular, it is now known that at least one of the medium/slow components is thermally unstable. This would give rise to falling $D_e(t)$ plots in well-bleached samples, and thus to potentially flat $D_e(t)$ plots in some poorly-bleached samples. Finally, it is worth pointing out that, although the $D_e(t)$-technique might enable the identification of partial bleaching of other components relative to the fast component and hence provide information on the general bleaching conditions, it gives no information on the degree to which the fast component itself (the initial OSL) has been reset in the past. This is important, as it is usually only this initial part of the OSL signal that is actually employed in a SAR-based equivalent dose determination (see Section 3.2.1.2.3).

3.3. The annual dose

3.3.1. Natural Radioactivity

The annual dose refers to the rate at which the mineral grains in a sediment absorb energy from the surrounding flux of nuclear radiation. This radiation comes from the naturally occurring long-lived radionuclides ^{232}Th, ^{238}U, ^{235}U and their daughters, ^{40}K and ^{87}Rb, and from outer space.

The decay of these radionuclides is attended with the emission of alpha particles, beta particles and/or gamma rays, as is illustrated in Figures 3.19 to 3.22.

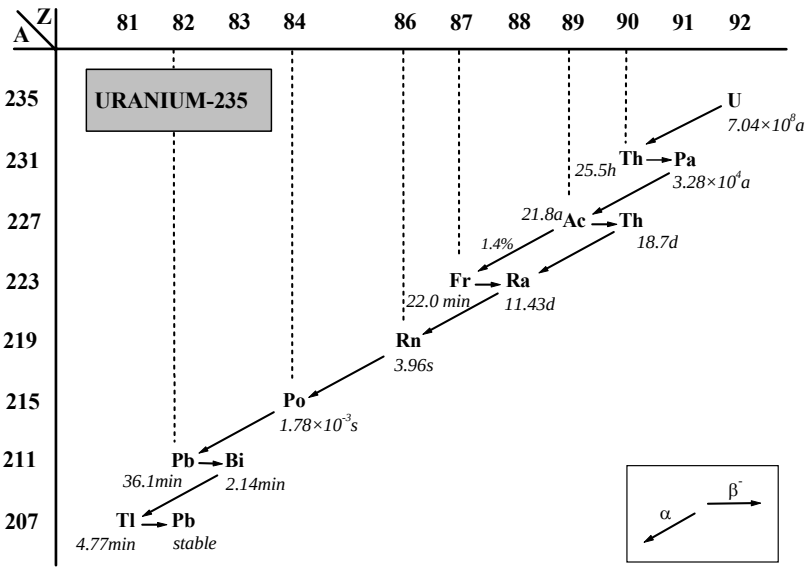

Figure 3.19: Decay scheme for the ^{235}U series (branchings with a probability of less than 1% are omitted). T½'s are from Isotope Explorer (ENSDF via Isotope Explorer; Chu et al., 1999).

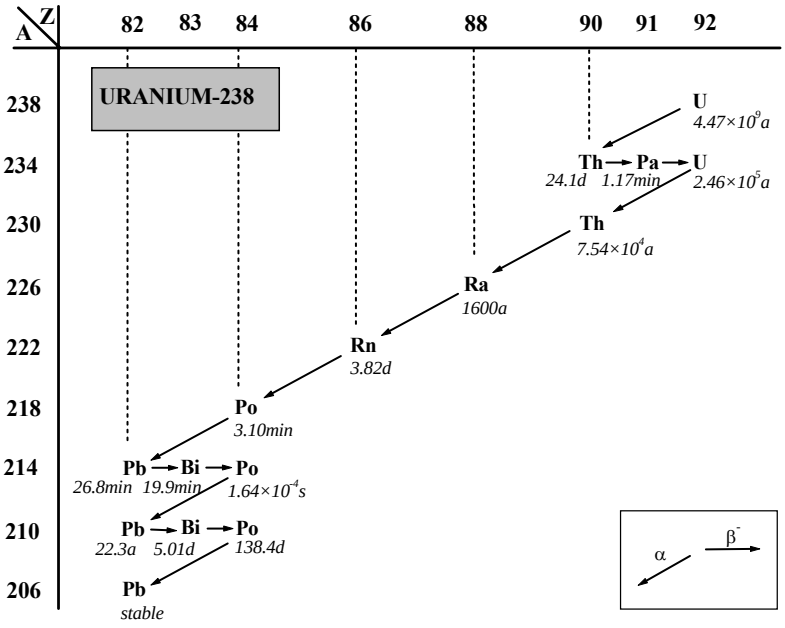

Figure 3.20: Decay scheme for the ^{238}U series (branchings with a probability of less than 1% are omitted). T½'s are from Isotope Explorer (ENSDF via Isotope Explorer; Chu et al., 1999).

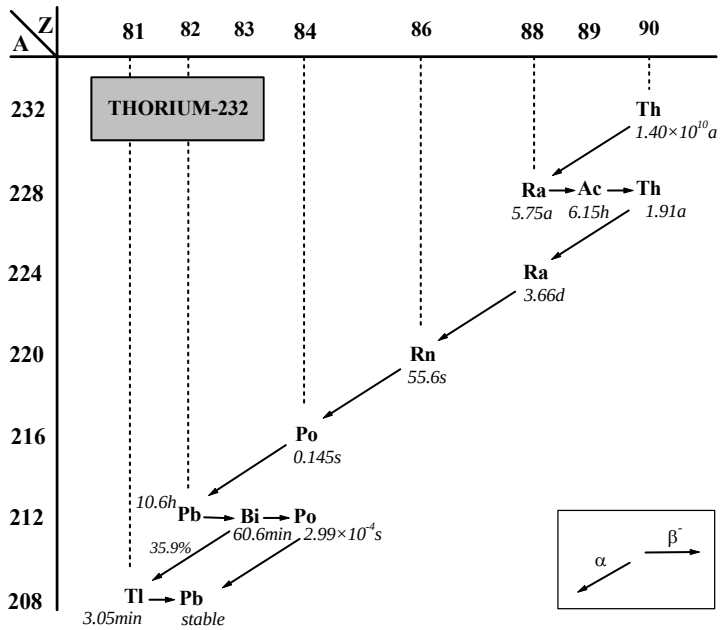

Figure 3.21: Decay scheme for the ^{232}Th series (branchings with a probability of less than 1% are omitted). T½'s are from Isotope Explorer (ENSDF via Isotope Explorer; Chu et al., 1999).

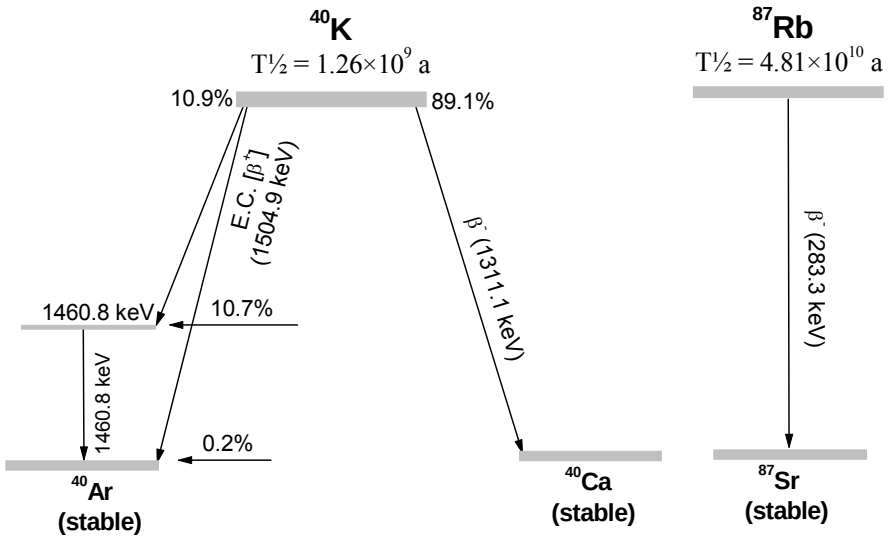

Figure 3.22: Decay schemes of ^{40}K and ^{87}Rb. The nuclear data are from Isotope Explorer (ENSDF via Isotope Explorer; Chu et al., 1999).

The different penetrating powers of these three types of radiation are very important with regard to luminescence dating. The short range of alpha and beta particles (of the order of 10^{-2} and 10^{0} mm, respectively) limits their contribution to the immediate location of the sample. Gamma rays, however, have a much higher penetrating power (~30–50 cm), and consequently a much larger volume of sediment provides the gamma dose to a sample. This means that the surroundings of the sample may play a significant role as well.

The different penetrating powers can be exploited to facilitate the dose-rate calculations, namely by selecting only a certain grain size fraction for the luminescence measurements. The fine-grain technique (Zimmerman, 1967, 1971) uses minerals with a grain size of 4-11 μm. These grains are small enough to ensure complete penetration by all three types of radiation. In the coarse-grain technique (Fleming, 1966, 1970; in pottery dating, this technique is referred to as the inclusion technique), the chosen grain size is typically around 100 μm. The outer layer of the grains can be etched away, so that the alpha contribution from external radioactivity is effectively removed (see Section 3.3.7). This leaves only contributions from gamma rays and a partly attenuated contribution from beta particles, as is illustrated in Figure 3.23. The quartz itself is assumed to be free of radioactivity.

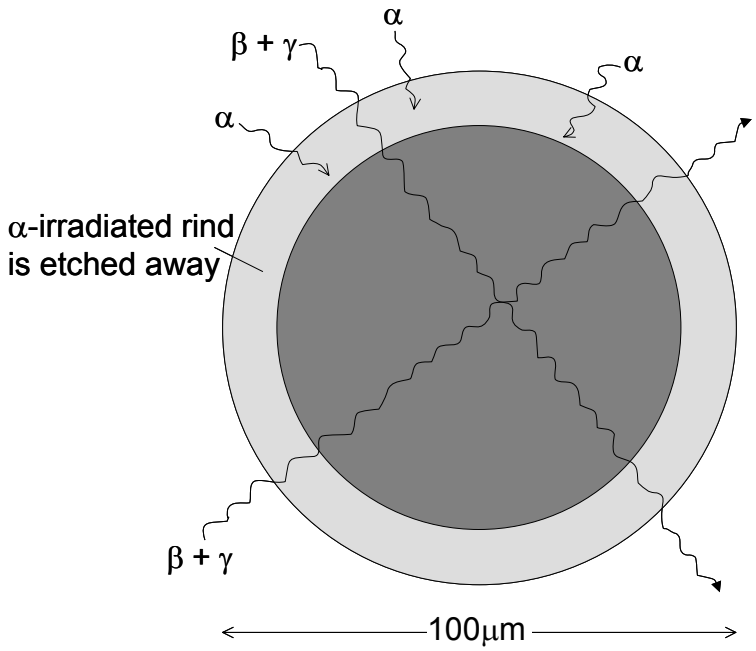

Figure 3.23: Schematic representation of the quartz coarse-grain technique. Grains of a size of about 100 μm are used. The quartz itself is assumed to be free of radioactivity. Due to their short range, alpha particles deliver their dose only to the outer layer of the grains (light grey shaded area). This layer can be removed by etching the grains with HF. As a consequence, the equivalent dose measured from these grains arises solely from their exposure to beta and gamma radiation (and cosmic rays), which have a much higher penetration power. The beta particles also experience some attenuation when passing through the grains, an effect which is accentuated by the etching process. This is taken into account when calculating the annual dose (Section 3.3.7).

3.3.2. Radioactive disequilibria

When considering the age equation (equation 3.1), it is clear that it rests on the assumption that the annual dose has remained constant over the time-span that is being dated. For this assumption to hold, it is necessary that the sample is located in a closed system from which no radionuclides are added or removed. The easiest example for such a situation is for a sample in a system that has remained closed long enough for the U and Th decay chains to have reached a situation of radioactive equilibrium. In such a case, the activity (number of disintegrations per unit of time) of each daughter is the same and equal to the parent activity. All the daughters from the U and Th decay chains will then contribute to a dose-rate that, owing to the very long half-life of the parent, remains effectively constant through time.

It is well documented, however, that certain processes can occur that disturb this equilibrium condition, by adding or removing a daughter. Such a situation is termed radioactive disequilibrium and examples in the context of luminescence dating have been given by Krbetschek et al. (1994), Prescott and Hutton (1995) and Olley et al. (1996), for instance.

Most common are disequilibria in the ^{238}U decay chain. A well-known example is the escape of gaseous ^{222}Rn. As a noble gas with a half-life of 3.82 days, it can easily diffuse through the sediment, especially if this is porous. Other types of disequilibrium involve ^{226}Ra (due to its solubility), ^{234}U (due to its weaker binding) and ^{210}Pb (which can be enriched in surface layers, due to the constant flux of ^{222}Rn from the earth's surface). Radioactive disequilibria in the ^{232}Th decay chain, on the other hand, are usually unimportant as the half-lives of the radionuclides that have a tendency for being mobile are relatively short. Disequilibria occurring in the ^{235}U decay chain are also unimportant, due to its low abundance and low contribution to the total dose rate.

In the case of a radioactive disequilibrium, the dose-rate will only have remained constant throughout the period that is to be dated if also the degree of disequilibrium has remained constant, or if it was only present for a negligibly small fraction of the entire burial period. In all other situations, the dose-rate will vary with time until the equilibrium condition is established again.

Whereas it is possible to measure individual radionuclide concentrations – and hence the degree of equilibrium – and to calculate variations in dose-rate in closed systems with time with a certain degree of confidence, it is not possible to predict when exactly in the past a disequilibrium came into existence. In luminescence dating, therefore, one simply has to make some assumption when the dose-rate is being determined. The two most common assumptions (Olley et al., 1996) are that the decay chains have always been in equilibrium, or that the dose-rate measured at present has prevailed throughout the entire burial period. The first assumption is implicitly made when only parent concentrations are being determined (e.g. using NAA or ICP-MS). The second assumption is implicitly made when the dose-rate is derived from measurements of only the parent (e.g. using NAA or ICP-MS), only the daughter (e.g. using field gamma spectrometry), or the mixed parent and daughter total radioactivity (e.g. using alpha counting, beta counting, or OSL dosimeters). Whatever assumption is being made, it is clearly desirable to be able to

recognize the presence of disequilibria, as this allows the accuracy of an age to be evaluated. This can be accomplished by high-resolution gamma spectrometry and/or alpha spectrometry.

3.3.3. Cosmic Radiation

Primary cosmic radiation comes from outer space and consists mostly of protons and alpha particles. By interaction with the atmosphere, secondary radiation results, of which the 'soft' electron component is absorbed by the upper half meter of sediment. Consequently, it is only the hard component of the cosmic radiation that is of interest in most luminescence dating. This hard component is composed mostly of muons. At sea level, it shows a weak dependency on latitude, the intensity rising by 7% on going from the equator to 40° latitude. At higher latitudes it remains practically constant. Only at a height of above a kilometre, the intensity rises appreciably with altitude, with a pronounced dependency on latitude. Prescott and Hutton (1994) further investigated how long-term variations in cosmic ray intensity can affect the dose-rate. They found that variations in the contribution of cosmic rays to the dose-rate due to geomagnetic dipole variations do not exceed about 3% at sea level for the past 80 ka and are not likely to be larger for earlier times. Furthermore, sites with geomagnetic latitudes above 35° are quasi insensitive to changes in the geomagnetic field. The effect is however larger at higher altitudes above sea level. In view of these rather small correction factors and the usually small contribution of cosmic rays to the total dose-rate, they concluded that correction for long-term variations is probably not necessary, with the exception for sites located at high altitudes near the equator.

The cosmic dose-rate is usually not measured directly. Expressions are available in the literature to calculate cosmic dose-rates at any depth below ground level (Prescott and Hutton, 1988; 1994), and at any altitude up to 5 km and at any geomagnetic latitude (Prescott and Stephan, 1982). Figure 3.24 illustrates how the cosmic dose-rate varies with depth below ground level and it can be seen that at a depth of 15 m it is already down to about 20% of its value at the surface. The cosmic dose-rates that can be read from the figure are quite representative for the sites investigated in this work. These sites are all situated in the southern Netherlands, at a height not much higher than sea level. As

explained above, the dependency of the cosmic dose-rate on small variations in the given coordinates is negligible; some deviation from the true values (a few percent, at most) might arise on account of slightly different packing densities.

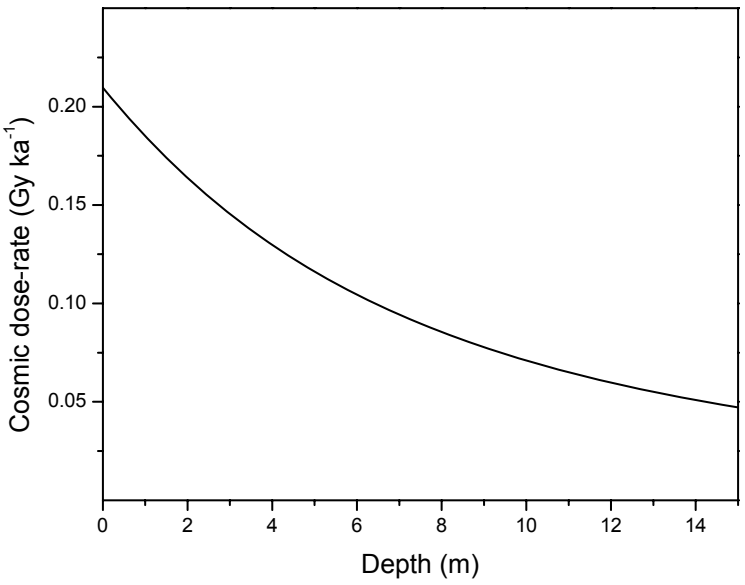

Figure 3.24: Dose-rate from cosmic rays as a function of the depth below the surface. The values were calculated using the formulas given by Prescott and Stephan (1982) and Prescott and Hutton (1994, expression 2), and apply to sites at a geomagnetic latitude of 53° and at a height of 25 m above sea level, for which the packing density of the sediment is 1.8 g cm^{-3}. The given cosmic dose-rates are representative for the sites investigated in this work.

Prescott and Hutton (1994) estimate the calculation of the cosmic dose-rate to be associated with 5% uncertainty. This is without any allowance being made for corrections in altitude and latitude. Also, as with any measurement, there are some uncertainties involved in the determination of the depth of the sample below the surface and of the packing density of the sediment. Furthermore, it is usually assumed in the calculations that the sample remained at the as-found depth during the entire burial period. This is obviously an oversimplification as each sediment was deposited at the surface and gets buried into deeper levels as time goes by. The situation becomes even more complex as the sedimentation not necessarily occurred at a constant rate, and furthermore may have been interrupted by erosional phases. Consequently, the cosmic ray dose-rate varied accordingly with time, and this in a rather unpredictable way. In this work, therefore, a

total uncertainty on the cosmic dose-rate of 15% was adopted. Fortunately, the contribution of cosmic radiation is usually a small (but non-negligible) percentage of the total dose-rate. When the total dose rate is low, however, a more careful evaluation of its contribution may be necessary, such as outlined by Munyikwa (2000).

3.3.4. Techniques for annual dose determination

Hossain (2003) recently presented an overview of the various analytical techniques that are available for the determination of the annual dose. He classified the techniques into two categories, according to whether they result in an indirect or a direct determination of the dose-rate.

Analysis techniques belonging to the first category (indirect determination) are neutron activation analysis (NAA), inductively coupled plasma mass spectrometry (ICP-MS), alpha-counting, beta-counting and gamma-spectrometry, to name a few. These techniques are termed indirect because they yield a radionuclide concentration (in mg/kg or Bq/kg) or a count-rate that subsequently needs to be evaluated in terms of energy absorbed per unit of mass and time (Gy/a). This "conversion" is accomplished by the use of tabulated factors (such as those by Adamiec and Aitken, 1998; see Chapter 4), which are based on measurements of the energy of emitted particles and radiations as published in nuclear data tables.

The annual dose can also be directly determined (i.e. directly in terms of Gy/a), by the use of highly sensitive luminescent dosimeters. The principle of such an evaluation is in essence the same as for an age determination. A luminescent phosphor is first reset and subsequently buried in the sediment. It is left there for some time during which it is exposed to the natural radioactivity and hence absorbs a certain dose. This absorbed dose can subsequently be determined using luminescence signals as outlined in Section 3.2. As it is exactly known when the dosimeter was buried, the annual dose can then simply be obtained by dividing the "equivalent dose" by this "age". The phosphor must be sufficiently sensitive to allow the measurements to be carried out on laboratory time-scales. An example of a suitable dosimeter is α-Al_2O_3:C

Each technique has its own merits, and in view of the possible presence of additional disturbing effects (such as sample inhomogeneity or radioactive disequilibrium), it is

therefore advantageous to use several techniques in combination. In this work, use was made of various techniques that allow an indirect determination of the dose-rate, namely alpha-counting, gamma-spectrometry and neutron activation analysis. Vancraeynest (1998) and Hossain (2003) already presented elaborate discussions on these techniques, and so there is little use in repeating this here. Relevant experimental details will be given in Chapter 4 and 5.

3.3.5.The effect of moisture

Water in the sediment pores absorbs part of the radiation that would otherwise reach the mineral grains. Using nuclear tables, Zimmerman (1971) calculated that, compared to silicates, the absorption coefficient of water is 50% higher for alpha radiation, 25 % higher for beta radiation and 14 % higher for gamma radiation. The values for beta and gamma radiation have been recalculated by Aitken and Xie (1990). They found slightly different values, especially for beta radiation, but as their analysis was incomplete, they recommended the further use of the Zimmerman values, awaiting more comprehensive computations.

In practice, the above means that the dose-rate in moist sediment is less than in dry sediment. Consequently, when the annual dose is derived from measurements on dried material, while it was wet in nature, this effect should be taken into account, or it leads to an underestimation of the age. It is important to realise that, although it is possible to determine the moisture content at the time of sampling quite accurately, it is the average moisture content over the whole burial span of the sediment that is relevant. As the moisture content can have fluctuated, for example owing to climatic change, seasonal changes or human activities, this means that measurements of natural ‘as-found’ moist material may need to be corrected as well. Uncertainty on how the water content may have varied is a fundamental limitation in the accuracy and precision attainable with the luminescence dating method (except in those cases of course where the sediment has always been dry or saturated). The saturation level, or porosity, fortunately sets an upper limit to the effect on the age. The porosity, denoted by the symbol W, is calculated as the ratio of the mass of water that the sample takes up at full saturation to the mass of the dry sample. For sediments, the saturation level ranges typically from 20 to 40%. Of course,

the question arises of how near to saturation the sample has been on the average over the entire burial span. It is usually assumed that in NW Europe the fraction F of saturation corresponding to the assumed average water content over the entire burial period is 0.8 ± 0.2. This value can be improved by a sedimentologist familiar with the site under study, which illustrates the need for a close cooperation between the dating and the field specialist.

If the dose-rates are obtained on dry material, the 'wet' dose-rates can be obtained by introducing the appropriate attenuation factors as follows:

$$D_{\alpha} = \frac{D_{\alpha,\,dry}}{1 + 1.50 \times W \times F} \tag{3.3}$$

$$D_{\beta} = \frac{D_{\beta,\,dry}}{1 + 1.25 \times W \times F} \tag{3.4}$$

$$D_{\gamma} = \frac{D_{\gamma,\,dry}}{1 + 1.14 \times W \times F} \tag{3.5}$$

3.3.6.Efficiency

Both beta and gamma radiation have the same efficiency in inducing luminescence, meaning that the same luminescence signal results when an identical beta or gamma dose is administered. The luminescence efficiency of alpha radiation, however, is lower by an order of magnitude. The reason for this lies in the heavily ionising nature of α-particles. The ionisation density they produce is so great that electron traps lying in the central track of the penetrating particles will get saturated. Compared to the more lightly ionising beta and gamma radiation, which have a larger penetration power and hence will cause an ionisation that is more evenly distributed over longer distances, a greater portion of the electrons that is created in the process of ionisation by alpha particles will go to waste. As a result, the luminescence resulting per unit of Gy that is absorbed will be substantially lower for alpha radiation, typically a factor in between 0.5 and 0.05 compared to beta or gamma radiation.

Because the equivalent dose is measured using beta radiation, allowance must be made for the relatively lower contribution from alpha particles. This can be accomplished by separately evaluating this contribution and, subsequently, by multiplying this by some experimentally determined efficiency factor that relates the luminescence caused by alpha irradiation to that caused by beta irradiation. Several approaches exist to express the lower effectiveness of alpha particles, such as the ε or k-value (Zimmerman, 1971, 1972), the a-value (Aitken and Bowman, 1975) and the b-value (Huntley et al., 1988).
In the quartz coarse-grain technique, the rather time-consuming task of determining the alpha-efficiency is avoided by simply physically removing any significant contribution of the alpha particles to the total dose (by etching, see Figure 3.23 and Section 3.3.7). As the quartz grains themselves are furthermore considered to be free of radioactivity, this leaves only the contributions from beta, gamma and cosmic radiation to be taken into account. However, if the quartz grains do contain a significant amount of uranium and thorium (see Section 3.3.8), and the external radioactivity is low, an evaluation of the effective internal alpha contribution to the annual dose may be desirable.

3.3.7.Attenuation and the effect of etching

In the fine-grain technique, grains are used that are small enough to ensure a full penetration by alpha and beta particles. Consequently, attenuation effects can be neglected when using this technique (see e.g. Vancraeynest, 1998). In the quartz coarse-grain technique, on the other hand, quartz grains of typically around 100 μm diameter are used and alpha and beta radiation will suffer from significant attenuation when passing through these grains. As the quartz grains themselves are approximately free of radioactivity, this attenuation causes the dose-rate to the quartz grains to be less than the dose-rate that is derived from the radioactivity of its surroundings. Etching causes a further reduction of the alpha and beta dose received by these grains. If the equivalent dose is determined using such quartz grains, this implies that an appropriate attenuated annual dose must be inserted in equation 3.1 to avoid an overestimation of the dose-rate (and hence an underestimation of the OSL age). Most of the research carried out on these issues dates back to the late seventies, and there is nothing substantial to be added to the overview presented by Aitken (1985, Appendix C, p. 252-263). However, as this work deals with

the first implementation of the quartz coarse-grain technique in our laboratory, the most important aspects are repeated in the following. It can be added that the attenuation of gamma rays is negligible as they have a penetration power of up to about 50 cm in sediment.

In the quartz coarse-grain technique, use is made of quartz grains with a diameter of typically about a 100 μm*. As the average range of the alpha particles emitted in the U and Th decay series is of the order of only 25 μm, alpha radiation will be severely attenuated when passing through the quartz grains. In fact, the inner cores of the quartz grains will have received a negligible alpha dose. Compared to a very small grain for which attenuation is negligible, therefore, the average alpha dose received by these larger quartz grains will be less. Figure 3.25 shows how the average alpha dose received by a quartz grain (expressed as the fraction of that received by an infinitesimally small grain) varies with its diameter. It can be seen that a 100 μm grain receives an alpha dose of only about 20% of that received by a grain that is small enough for attenuation to be negligible. For comparison, the right hand scale shows the much smaller attenuation experienced by the small grains (4-11 μm) used in the fine grain technique.
It must be remembered that the efficiency of alpha radiation for inducing luminescence is low (see Section 3.3.6.), and consequently, the effective contribution of alpha radiation to the observed luminescence emitted by a 100 μm quartz grain is in fact much less. This contribution is furthermore reduced to a negligible level by the etching process. Indeed, the sample preparation procedure for extracting coarse quartz grains from a sample involves a treatment with concentrated HF to remove the feldspathic minerals. Besides removing these feldspars, however, etching also affects the quartz grains, by removing their surface layer. This has the advantageous side-effect of removing the contribution from alpha radiation as well, as due to the short range of the alpha particles, the alpha dose is contained only into the outer layer of the quartz grains.

* Some studies use larger grain sizes, or a fraction in between fine (4-11 μm) and coarse (> 90 μm) grains. The choice of which fraction is used is usually dependent on the availability within the sample. Obviously, each chosen fraction requires an appropriate evaluation of attenuation effects.

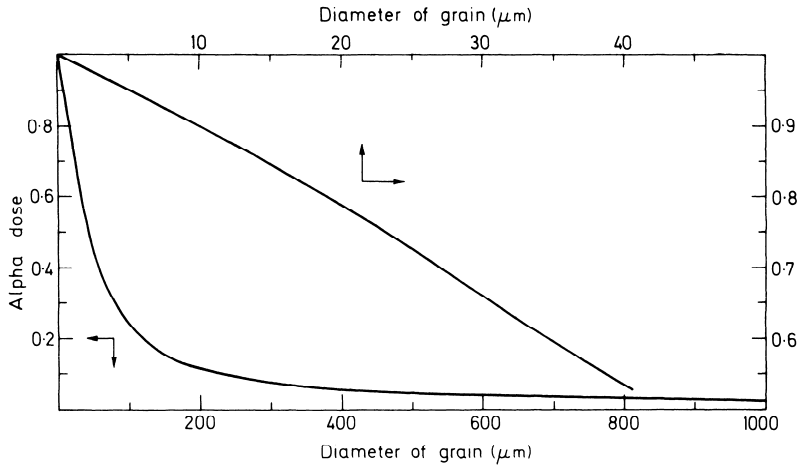

Figure 3.25: Average alpha dose for a quartz grain of the given diameter embedded in a matrix having equal thorium and uranium activities. The quartz grains themselves are assumed to be free of radioactivity. The alpha dose is expressed as a fraction of that experienced by an infinitesimally small grain, for which attenuation effects are negligible. The figure is from Aitken (1985) and is based on calculations by Bell (1980).

Figure 3.26 (a) illustrates the decrease of the alpha dose with depth into a spherical quartz grain and shows that is contained only in its outer layer (the alpha dose is expressed as a fraction of that received by an infinitesimally small grain). Curve (b) in Figure 3.26, shows how much of the alpha dose received by the quartz grain is removed by etching away a rind of the thickness indicated. Etching experiments using geological quartz indicate that a 60 min etch in 40% HF removes an outer layer of about 9 μm, when it is assumed that the etching process proceeds isotropically. According to Figure 3.26 (b), this will reduce about 60% of the alpha contribution. The alpha contribution to the total annual dose is however not only dependent on the effects of attenuation and etching, but also on the radionuclide composition (^{40}K emits solely beta particles and gamma rays) and the efficiency of alpha radiation in inducing luminescence. Bell (1979) considered how these factors affect the alpha contribution to the overall dose for a 100 μm quartz grain. He concluded that a 1 hour immersion in 40% HF renders the alpha contribution negligible for the majority of the samples that are likely to be encountered, and that any residual dose should not introduce an error of more than 5%.

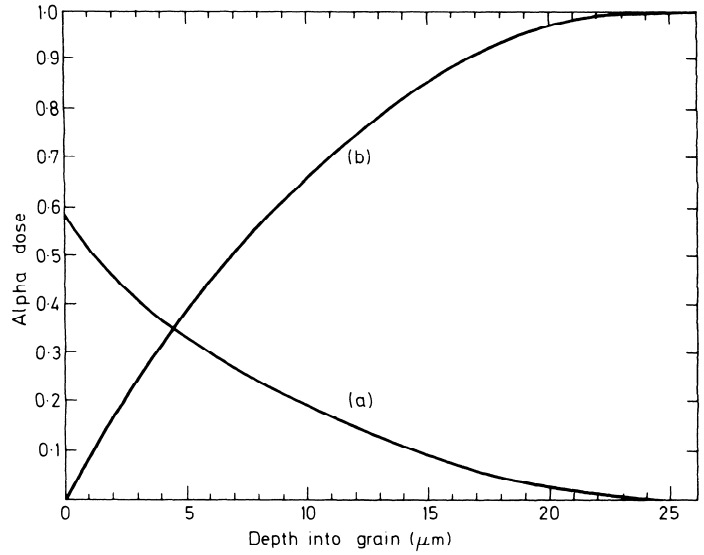

Figure 3.26: (a) Decrease of alpha dose with depth into a spherical quartz grain of diameter 100 μm that is embedded in a matrix having equal thorium and uranium activities. The alpha dose is expressed as a fraction of that received by an infinitesimally small grain for which attenuation effects are negligible. It can be noted that also at the surface this fraction is smaller than unity. This is because the alpha particles come from one side only and the grain itself is assumed to be radioactivity free. (b) Fraction of the overall alpha dose that is removed by etching away the outer layer of a quartz grain to the depth indicated. The figure is taken from Aitken (1985) and is based on calculations by Bell (1979).

Compared to alpha particles, beta particles have a much larger range. The beta dose will therefore undergo a less, but nevertheless non-negligible attenuation. Two aspects must be considered: the factor by which the dose to a larger grain is reduced in comparison to an infinitesimally small grain, and the factor by which that dose is reduced if a given thickness is removed by etching.

Both Bell (1979) and Mejdahl (1979) calculated the attenuation effect for unetched 100 μm quartz grains. The results from both authors are in good agreement. Mejdahl (1979) extended the calculations to grains having diameters in the range of 5 μm to 10 mm, and his results (up to 0.5 mm) are graphically represented in Figure 3.27.

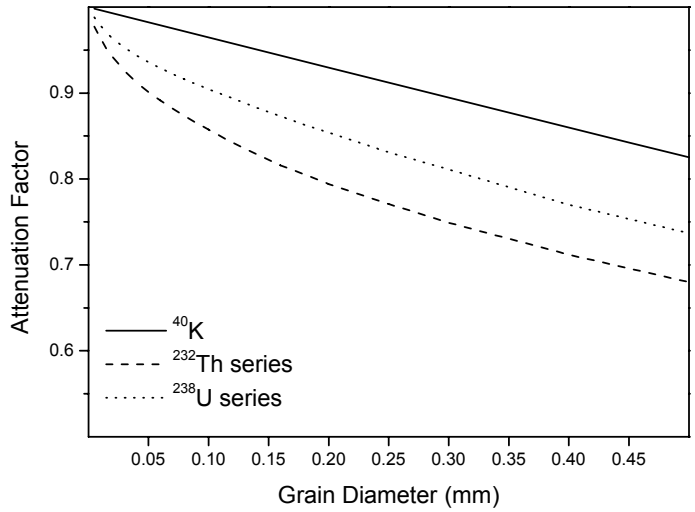

Figure 3.27: Attenuation of the beta dose in quartz grains. The figure is based on the results tabulated by Mejdahl (1979).

Due to a larger proportion of lower energy contributions, the attenuation is larger for the ^{232}Th series than for the ^{238}U series, in its turn larger than for ^{40}K. Consequently, a combined attenuation factor will be dependent on the relative abundance of radionuclides in a sample. The dependency is however weak, as is shown in Figure 3.28. For instance, the average attenuation factor is 0.921 for a 100 μm quartz grain embedded in a matrix containing 12 mg kg^{-1} Th, 3 mg kg^{-1} U and 1% K_2O. For a sample containing twice as much K_2O the value is 0.935, which is only 1.5% higher.

The effect of etching is a further reduction of the beta dose. Bell (1979) calculated that an etching depth of 9 μm reduces the beta dose from the thorium series by a factor 0.915 and that from the uranium series by a factor of 0.940, whereas the beta dose from ^{40}K undergoes a negligible dose reduction. Combining these factors with the attenuation factors yields an overall factor of 0.89 for the 1% K_2O composition and a factor of 0.91 for the 2% K_2O composition*; the difference between these two values is only about 2%.

* The calculations can be understood as follows. For the [12 mg kg^{-1} Th, 3 mg kg^{-1} U, 1% K_2O]-composition the relative beta dose-rates obtained by Mejdahl (1979) are 0.234, 0.300 and 0.466 for the Th series, U series and ^{40}K, respectively. These should be used as weight factors for calculating the combined attenuation factor from the data depicted in Figure 3.27, as well as for the combined etch factor. For instance, the combined etch factor for the given composition is obtained as 0.915*0.234 + 0.940*0.300 + 1*0.466 = 0.962. This value multiplied by the combined attenuation factor of 0.921 that is obtained via similar calculations, yields an overall factor of 0.89. The value of 0.91 for the 2% K_2O composition is obtained in the same way.

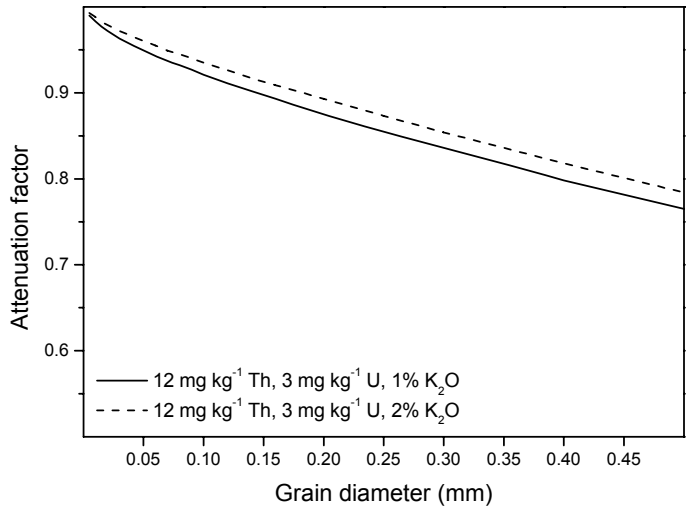

Figure 3.28: Attenuation factors for radioactivity-free quartz grains embedded in a matrix of the radioelements indicated in the figure.

The above calculations assume that the grain is spherical and that etching proceeds isotropically. That the assumption of isotropic etching might be an oversimplification was demonstrated by Bell and Zimmerman (1978). They show that etching proceeds more quickly for some quartz grains than for others, and that some grains even lose a substantial portion of their inner volume as etch tunnels may form through the grains. This obviously has consequences with regard to the efficiency by which the alpha dose (as well as the beta dose) is removed. Besides from this disturbing study, no other reports on the influence of etching can be found in the literature. However, as quartz is an anisotropic solid, it is expected to etch anisotropically.

Considering the uncertainties that seem to be associated with the etching process, it was therefore considered rather pointless to make detailed calculations of a combined attenuation factor. In this work, therefore, preference was given to the use of a single attenuation factor of 0.90 with an associated uncertainty of 5%, for 100 μm (on average) quartz grains that were etched for 40-60 minutes in 48% HF. These etching conditions proved to be sufficient to ensure a complete removal of the feldspars, while it should also be a reasonable compromise between the risks of incomplete removal of the alpha contribution on the one hand, and the formation of etch tunnels on the other hand. The same suggestions were made by Bell (1979) and Aitken (1985).

Finally, an alternative approach suggested by Valladas and Valladas (1982) deserves to be mentioned. These authors investigated how effective the etching is in removing the alpha dose contribution and they found that some contribution persisted even after a prolonged treatment with HF. Therefore, their suggestion was not to try to remove the alpha dose chemically, but to determine its contribution experimentally. They show that this can be accomplished by mounting the quartz grains as a monolayer in a cup that is shaken up and down during the irradiation in the laboratory. By doing so, an omnidirectional isotropic flux is ensured. The irradiation should be carried out with an artificial source that emits alpha particles of an energy equal to the effective average energy of those emitted in nature.

3.3.8.The contribution of ^{87}Rb

Up to now, no mention has been made of ^{87}Rb. This was because its contribution to the dose-rate can usually be neglected in quartz coarse-grain dating. This can be understood as follows. The rubidium content is usually not determined in luminescence dating and it is quite customary to assume a potassium to rubidium ratio of 200:1, an arbitrary choice that is within the range of ratios encountered in samples (Aitken, 1985; Adamiec and Aitken, 1998; it can be noted that this dates back to the work on pottery by Warren in 1978). Further, the energy of the beta particles emitted by ^{87}Rb is low and hence their attenuation high. Readhead (2002a) recently calculated an attenuation factor of 0.512 for 100 μm diameter grains. Taking the appropriate attenuation factors into account (i.e. 0.9 for ^{40}K and 0.5 for ^{87}Rb), and assuming the above-mentioned concentration ratio, leads to a K to Rb dose-rate ratio of about 100:1. The attenuation factor given by Readhead (2002a) does not take into account the effect of etching and so the actual ratio should be even higher. When considering that also U, Th and cosmic rays contribute to the total dose-rate, it is clear that the contribution from Rb can be safely ignored. In some specific cases (e.g. when using coarse-grained K-feldspars), however, it may be necessary to calculate the dose-rate from ^{87}Rb. Relevant references for such cases are Mejdahl (1987), Huntley and Hancock (2001) and Readhead (2002a, b).

3.3.9.Internal Radioactivity

So far, it has been assumed that any radioactivity is located outside the quartz grains and that the grains themselves are free of radioactivity. It is usually a good approximation to assume that the internal dose-rate is negligible in quartz grains, moreover since the alpha efficiency for quartz is low. Note that it is only the alpha activity that is relevant in this case, as the range of the beta particles and gamma rays is much larger than the size of the grains under consideration (~100 μm diameter). However, some reports are available in the literature of situations in which the internal radioactivity did make a non-negligible contribution to the total dose-rate.

Sutton and Zimmerman (1978), for instance, used alpha counting to determine the internal alpha activity in quartz extracted from four heated samples. They found uranium concentrations ranging from 0.8 to 3.1 mg kg^{-1}. The corresponding effective internal alpha contributions amounted to about 5%, on the average, of the total dose-rate and for two samples, the internal contribution was higher than that arising from cosmic rays. They furthermore showed that in some quartz grains, the radioactivity is heterogeneously distributed.

Mejdahl (1987) also reported values for U and Th concentrations in quartz grains. His dataset is unfortunately not very transparent, as results obtained on feldspars are included as well. The only exception to this are the results reproduced in Figure 3.28. Shown are the uranium contents in quartz extracted from 39 different samples from Scandinavia. For most samples the U content is below 0.5 mg kg^{-1}, only one of the investigated samples yielded a concentration higher than 1 mg kg^{-1}. It can be noted that no information is given on whether it concerns quartz extracted from sedimentary or heated archaeological materials. This might be relevant, as Mejdahl also notes that the U and Th contents in grains from archaeological samples are considerably higher than those in sediment samples.

Murray and Roberts (1997) determined the U and Th concentrations in eight sedimentary quartz grains using laser-ablation ICP-MS. Only two grains had localised concentrations in excess of the minimum detection limits of approximately 0.015 mg kg^{-1} U and 0.022 mg kg^{-1} Th. The highest concentrations they observed were 0.23 mg kg^{-1} U and 10.3 mg kg^{-1} Th.

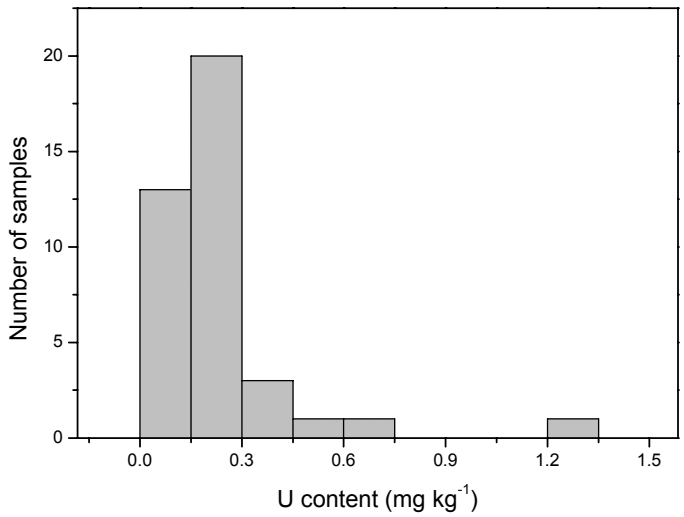

Figure 3.28: Uranium content in 39 quartz samples from Scandinavia (redrawn from Mejdahl, 1987). The concentrations were obtained via the delayed neutron counting technique.

It must be realised that the significance of a contribution from the internal alpha radioactivity in the quartz grains depends on the actual U and Th concentrations in the grains, the alpha efficiency and the external dose-rate. The observations reported above indicate that it may be worthwhile to check the level of internal radioactivity, especially when the external radioactivity is low. However, if this cannot be accomplished due to the lack of material, appropriate analysis techniques or instrument time, for instance, the better course of action is to introduce an additional estimated systematic uncertainty into the overall uncertainty calculation on a luminescence age. Finally, it is perhaps worth mentioning that Sutton and Zimmerman (1978) identified quartz grains containing several hundred mg kg^{-1} of uranium. Although this was observed for only some grains of the several hundreds investigated, it might bear some relevance to the optical dating of single grains, where it is not uncommon to measure several thousands of individual grains.

– CHAPTER 4 –

IMPLEMENTATION OF THE OPTICAL DATING METHOD:

a pilot study on the coversands from Ossendrecht

4.1. Introduction

This chapter describes the implementation of the optical dating method in the Ghent luminescence dating laboratory. It should be looked upon as the account of a pilot study, which had as the major objective to gain experience with various practical aspects of the method. As was outlined in Chapter 3, two quantities need to be determined to arrive at a luminescence age, namely the equivalent dose and the annual dose. Our study focuses entirely on the determination of the equivalent dose with OSL, which had not been done in our laboratory before. The annual dose formed the subject of a comprehensive study recently carried out by Hossain (2003). It was also discussed by Vancraeynest (1998).
The samples that we selected for our study come from a sequence of Late Pleniglacial to Late-glacial coversands exposed at the locality of Ossendrecht in the southwestern Netherlands. These sediments are aeolian and, for this reason, one can expect the OSL signal to have been effectively reset during transport and deposition. Furthermore, independent age information (radiocarbon and earlier luminescence dates) is available for the sediments, which should allow a validation, via the resulting optical ages, of the implemented dating procedures.

4.2. Geological setting*

The sediments to be dated were sampled in the Boudewijn sandpit, a large quarry to the east of the village of Ossendrecht, in the southern Netherlands (Province of Noord-Brabant). The location of the study area is shown in Figure 4.1.

* Adopted from Vandenberghe et al. (2004).

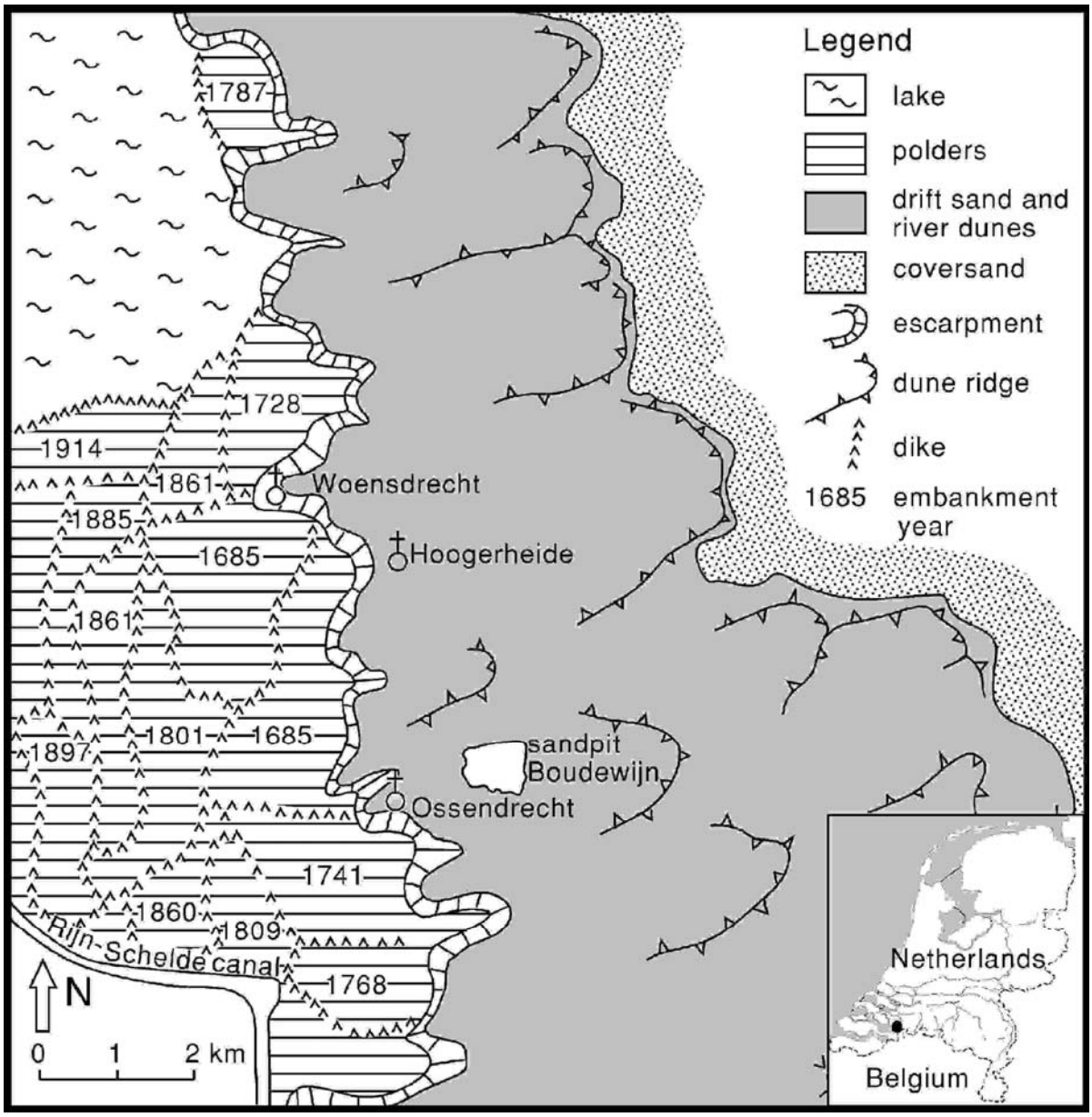

Figure 4.1: Location map and geomorphological setting of the investigated site. The figure was kindly provided by C. Kasse.

The village of Ossendrecht is situated near the limit between two geomorphological regions (Figure 4.1). The region to the east is the driftsand and river dune region, ca. 20 m above sea level. It consists mostly of Late Pleistocene and Holocene non-calcareous dune sands covered with pine forest. The region to the west is situated around sea level and consists of Late Holocene tidal flat and marsh deposits. The transition between the two landscapes is formed by an undulating north-south oriented escarpment, that has been shaped through Middle and Late Pleistocene fluvial erosion by the Scheldt river and

through ground-water seepage erosion at the foot of the escarpment (Kasse, 1988; Westerhoff and Dobma, 1995). Ossendrecht is situated in the sand region very near to the escarpment.

In the Boudewijn sandpit, the Late Pleistocene to Holocene aeolian sands immediately overlie Early Pleistocene tidal estuarine sediments (Kasse, 1988, 1990) (Figure 4.2). These Early Pleistocene deposits occur at an elevation of ca. 18 m above sea-level, dipping in a northerly direction towards the subsiding North Sea Basin. The lower tidal part of the exposed sediments is characteristic for western Noord-Brabant and northern Belgium. These sediments have been described by Kasse (1988, 1990). They belong to the Tegelen Formation of Late Tiglian age (ca. 1.7 – 2.0 Ma), which consists of fine to medium whitish sands with many thin clay layers, overlain by a clay bed of variable thickness (Figure 4.2). The sand and clay sequence has been formed in a gradually infilling tidal estuarine environment in a warm temperate climate with a high sea-level (Dricot, 1961; Kasse, 1988). The uppermost clay bed has a strong influence on the local hydrology, causing a perched water table and water saturated conditions in the sand units above.

The stratigraphy of the aeolian sands overlying the Tegelen Formation is more important to this study. The sands are also of international significance since similar aeolian units have been identified all over northwest and central Europe. In the sandpit they form the upper 8 m of sediment and lithostratigraphically they belong to two formations: the Upper-Pleistocene Twente Formation and the Holocene Kootwijk Formation. More detailed stratigraphic and sedimentological information is given by Kasse (1988) and Schwan (1991), respectively. Recently, georadar investigations of the aeolian units have been performed by Van Dam and Schlager (2000).

A thin gravel bed separates the Early Pleistocene Tegelen Formation from the overlying Twente Formation (Figure 4.2). The gravel (diameter of 2 mm to 5 cm) consists predominantly of well-rounded quartz and flint, and represents a major hiatus reflecting a phase of uplift in western Noord-Brabant during the Middle and Late Pleistocene. The gravel was concentrated as an erosional lag deposit truncating the top of the Tegelen Formation.

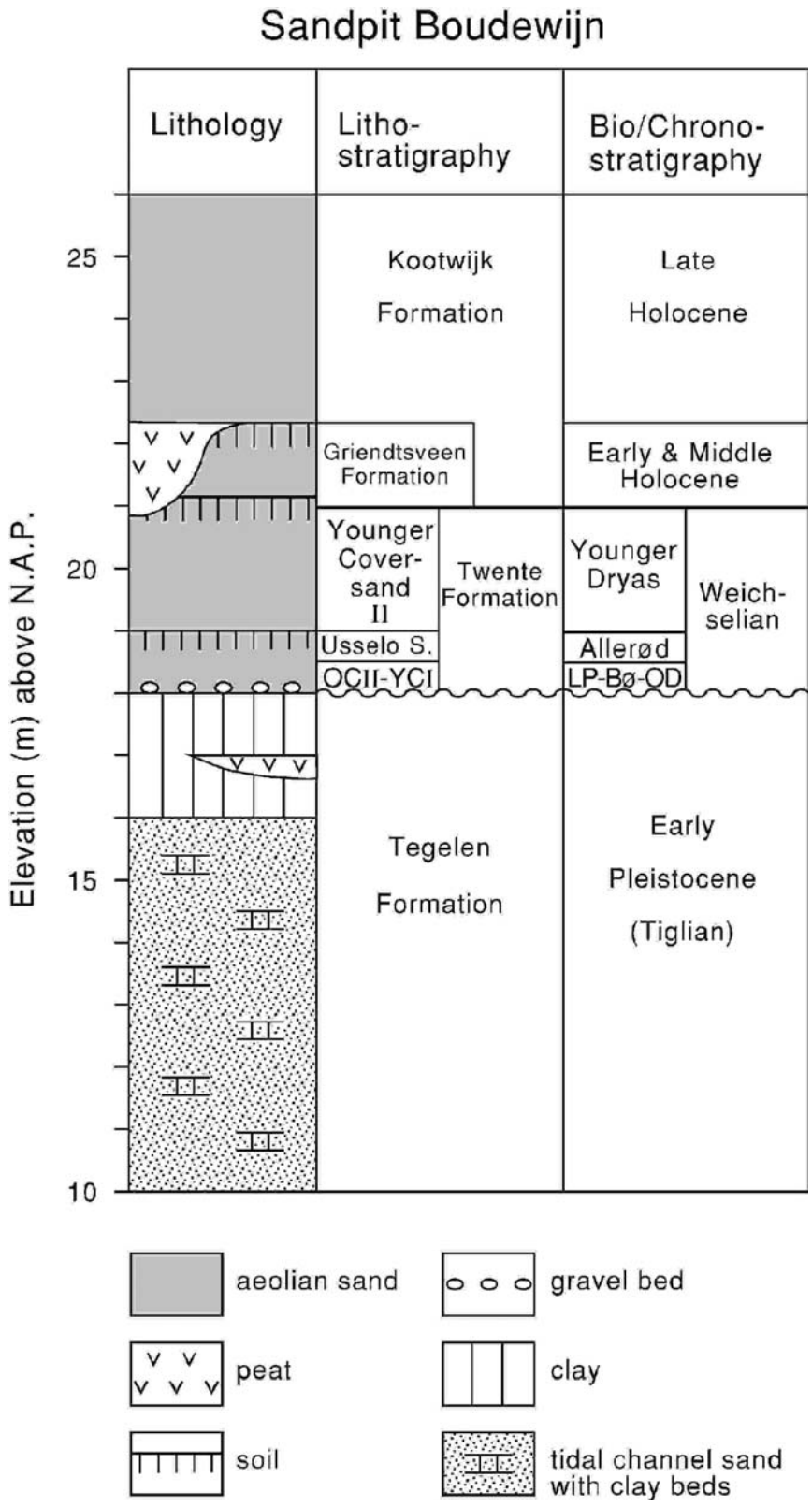

Figure 4.2: Litho- and chronostratigraphy of the Boudewijn sand pit: OCII-YCI, Older Coversand II-Younger Coversand I; LP-Bø-OD, Late Pleniglacial-Bølling-Older Dryas. The figure was kindly provided by C. Kasse.

The basal part of the aeolian sequence consists of horizontally laminated, loamy, fine sands [mean grain size 169 μm, n = 2 (n is the number of grain size analyses)*], locally disturbed by cryogenic deformation. The age of these sands is not well known. They represent Younger Coversand I (Early Late-glacial) and/or Older Coversand II (Weichselian Late Pleniglacial) sediments (a diagnostic horizon representing the Bølling interstadial is missing and hence a more precise chronostratigraphic position cannot be given). During this period, widespread aeolian deposition occurred over most of the Netherlands and surrounding regions and the landscape was covered by an aeolian blanket or sand sheet that was several meters thick (Koster, 1988; Kasse, 1997). The major phase of coversand deposition, leading to the formation of the so-called Older Coversand II and Younger Coversand I units, lasted until the start of the Late-glacial period, but regionally it continued into the Late-glacial (Van Geel et al., 1989; Kasse, 1999).

The sands are overlain by the Usselo Soil, which is a widespread marker horizon in the Late-glacial aeolian stratigraphy (Van der Hammen, 1951, 1971) and represents the Allerød interstadial. In the Boudewijn pit, the Usselo Soil consists of a humic Ah soil horizon ca. 10 cm thick, with some pedogenic bleaching underneath. Locally, it grades laterally into a peaty bed (Figure 4.2).

The Usselo Soil is overlain by aeolian sands representing the Younger Coversand II, supposed to be of Younger Dryas age (Figure 4.2). The deposition of these sands is generally ascribed to an effect of cooling and increased aridity, causing a decline of the vegetation cover and a change in river style from meandering to braided. Especially on higher and therefore drier interfluves, local deflation and accumulation occurred, and along river valleys, sand was deposited on the east banks indicating westerly winds (Kasse, 1999). In the Boudewijn exposure, the Younger Coversand II unit is prominent and consists of horizontally laminated and low-angle cross-bedded fine to medium sand (mean grain size 267 μm, n = 7). High-angle, dune slipface cross-bedding is rare. At the base, adhesion ripple cross-lamination is frequently observed, indicating a, at least periodically, high water table during deposition. Schwan (1991) concluded that a drying-up sequence is present in this aeolian succession.

The morphology of the undulating buried upper surface of the Younger Coversand II unit, marked by the well-developed Holocene humic podsol, further indicates that the sediments were deposited as low sand dunes not exceeding 5 m in height. The dunes are correlated with the extensive, generally 4 to 8 km wide, N-S trending river dune region extending to the east of Ossendrecht (Figure 4.1). This river dune zone is parallel to the

* The results from the grain size analyses were kindly provided by C. Kasse.

former Late-glacial Scheldt Valley that is present in the subsurface below the young Holocene polders. These dunes are therefore thought to have been blown out of the Scheldt Valley during the cold Younger Dryas stadial. Similar dunes have been described on the east bank of the Meuse valley (Kasse et al., 1995).
A humic-iron podsol has developed in the Younger Dryas dune sands. This soil in turn is overlain by a new sequence of drift sands assigned to the Kootwijk Formation. The grain size and sedimentary structures of the Kootwijk Formation resemble those of the Younger Coversands II (mean grain size 309 μm, n= 9). The present-day surface morphology in the vicinity of the sand pit indicates that the sands have been deposited in dunes up to 10 m high. Until a few years ago, only one podsol could be observed in the Boudewijn sandpit underlying the medieval drift sands. At the time of our investigations, two superposed podsols were exposed with an intercalated aeolian sand unit, indicating that at least two phases of drift sand accumulation and two phases of land surface stability and soil formation have occurred.

4.3. Independent age information

The stratigraphy of the late Quaternary deposits of the Netherlands is based largely on pollen analysis and ^{14}C age determinations of organic material (Van der Hammen, 1951, 1971; Van der Hammen et al., 1967; Zagwijn, 1964; Van Geel et al., 1989; Hoek, 1997). Because of the abundant organic material in both the Weichselian and Holocene sequences (as a result of widespread and frequent peat formation), ^{14}C dating of intercalated organic layers has been used intensively to derive the time of deposition of the Late Pleniglacial and Late-glacial aeolian sediments.
Our study was focused on the coversands directly above and below the Usselo Soil (see Section 4.4), and hence, the most important age information is undoubtedly yielded by this intercalated soil. As was mentioned in Section 4.2, the Usselo Soil is a very common soil in Late-glacial aeolian sequences of the Netherlands, and quite often it contains organic material (such as charcoal) that is suitable for ^{14}C-dating. Based on 23 ^{14}C dates on charcoal samples collected in several localities of The Netherlands, the age of the Usselo Soil is accepted to be ca. 13.1 ka (Hoek, 1997). It must be mentioned here that all the radiocarbon ages quoted in this discussion (as well as in Table 4.1, see further) were calibrated using the OxCal program (version 3.5; Bronk Ramsey, 1995, 1998) and are expressed in ka before AD 2000 (obtained by adding 50 years to the CalBP years). In the Boudewijn pit the Usselo Soil has been dated at 13.3 ± 0.3 ka (93.1% probability) by Schwan (1991). More recently, Vandenberghe et al. (2004) dated wood from the top of

this unit at 12.9 – 13.2 ka (89 % probability), which is slightly younger than the date obtained by Schwan (1991), but in perfect accordance with the accepted Allerød age of ca. 13 ka.

No radiocarbon ages are available for the sands underlying the Usselo Soil in the Boudewijn sandpit. Thus, it cannot be established whether they were deposited during the Older Dryas (ca. 14 ka) or during the Late Pleniglacial (≥ 15 ka).

Vandenberghe et al. (2004) also reported some new ^{14}C dates from the organic base of the Younger Coversand II unit, in order to establish the start of aeolian sedimentation following the Usselo Soil formation. They found an age of 12.4 – 13.0 ka (92 % probability), indicating that deposition of the Younger Coversands II started in the second part of the Younger Dryas. Their results were in accordance with previous findings by Bohncke et al. (1993), Kasse et al. (1995) and Isarin et al. (1997).

The final phase of Younger Coversand II deposition is not well dated because in most cases the aeolian dune sands are immediately overlain by the Holocene podsol (Figure 4.2). Locally, in former dune slacks, this podsol grades downwards into a peat layer, which has been dated by Schwan (1991) at 10.3 ± 0.1 ka (90.5% probability). Hence, deposition of the Younger Coversand II phase can be bracketed between ca. 12.7 and 10.3 ka. This demonstrates that aeolian deposition possibly occurred through the Younger Dryas to Holocene boundary.

Besides the radiocarbon dates, also some earlier luminescence dates are available for the same (i.e. exposed in Ossendrecht) and for stratigrapically equivalent deposits (i.e. exposed at other localities in the Netherlands). Table 4.1 presents an overview of the previously conducted luminescence dating research relevant to the present study. The most important ^{14}C-ages are included in the table as well.

The first luminescence dates were obtained using thermoluminescence and polymineral fine grains (Aitken et al., 1986) or coarse-grained feldspars (Dijkmans et al., 1988, 1992; Dijkmans and Wintle, 1991). The results, however, were not very encouraging as the dates generally were too young compared with the litho- and chronostratigraphical record. Optically stimulated luminescence together with the use of quartz, on the other hand, has been more successful. Smith et al. (1990b) and Stokes (1991) reported a good agreement with independent age control for the coversand deposits in the Dinkel Valley (Lutterzand). Recently, optical dating techniques were also applied successfully to the Late Weichselian aeolian sediments exposed in the type locality in the Dinkel valley in the eastern Netherlands (Bateman and Van Huissteden, 1999). Fink (2000) applied optical dating techniques to coversand samples from the Boudewijn sandpit in Ossendrecht, and obtained ages consistent with the available radiocarbon ages.

Bio- / Chrono-Stratigraphy	*Litho-stratigraphy*	*Age (ka)*								
		TL [a]	TL [b]	TL [c]	OSL [d]	OSL [e]	^{14}C calibrated age [f]	OSL [g]	OSL [h]	^{14}C calibrated age [i]
Younger Dryas	Younger Coversand II	7.6 ± 1.2		9.3 ± 1.0 8.1 ± 0.5 8.8 ± 0.5	7.2 ± 1.8 8.2 ± 1.7	11.4 ± 1.4		13.27 ± 0.9 11.72 ± 1.5	11.0 ± 1.7 15.1 ± 3.9 10.0 ± 1.5	12.4 - 13.0
Allerød	Usselo Layer						13.3 ± 0.3			12.9 - 13.2
Older Dryas	Younger Coversand I	⇑ 10.3 ± 2.3 ⇓	⇑ 11.4 ± 1.5 ⇓	6.2 ± 0.5 7.9 ± 0.4	⇑ 11.0 ± 2.5 10.6 ± 2.4 ⇓	⇑ 13.2 ± 2.4 ⇓		⇑ 17.55 ± 2.6 16.08 ± 1.9 13.90 ± 1.3 ⇓	⇑ 18.1 ± 2.9 ⇓	
Bølling	Lower Loamy Bed			6.9 ± 0.5						
Upper Pleniglacial	Older Coversand II			8.7 ± 0.5 9.2 ± 0.6						

Table 4.1: Summary of luminescence and ^{14}C dating research of Late Pleniglacial and Late-glacial sediments in The Netherlands. ^{14}C ages are expressed in ka before AD 2000 (see text for details). [a] Aitken et al. (1986), using polymineral fine grains. [b] Dijkmans et al. (1988) using potassium feldspar. [c] Dijkmans and Wintle (1991), using potassium feldspar. [d] Smith et al. (1990b), using quartz. [e] Stokes (1991) using quartz. [f] Schwan (1991). [g] Bateman and Van Huissteden (1999) using quartz. [h] Fink (2000) using quartz. [i] Vandenberghe et al. (2004).

4.4. Sampling and field measurements

Only a relatively small profile of about 2 m of sediment and the intercalated Usselo Soil was available at the time of the field work (Figure 4.3). The profile was cleaned by removing a few centimeters of the outermost sediment from the profile wall. Steel or plastic tubes were forced into the profile wall, dug out, capped and sealed using black plastic bags and tape. Three samples were taken above the Usselo Soil (OS-C, OS-4 and OS-B) and three below it (OS-A, OS-D and OS-2), at about 20 cm intervals. A detail of the profile showing the position of the samples is given in Figure 4.4. Two additional samples of sediment (one above and one below the Usselo Soil) were sealed in watertight plastic bags for determination of the natural moisture content. As part of the study by Hossain (2003) on the comparison and evaluation of methods for annual dose determination, four additional samples were taken from below the Usselo Soil. They were taken from the same location as the samples for luminescence analysis (S-A, S-D and S-2, equivalent to OS-A, OS-D and OS-2, respectively), and one additional sample (S-1) was taken about 20 cm beside the central sample (Figure 4.4)[*].

Field gamma-ray spectrometry was conducted at the location of sample OS-D. The experimental set-up is shown in Figure 4.5. Unfortunately, this spectrum got lost due to a failure in the power supply. Two spectra, however, were available from a previous visit to the sandpit. The exact position of these measurements in the profile cannot be shown, but it was in the same stratigraphic level (i.e. below the Usselo layer), at a position in the vicinity of sample OS-D.

[*] Samples S-A, S-D, S-2 and S-1 are denoted by Hossain (2003) as S2, SD, S3 and S1, respectively.

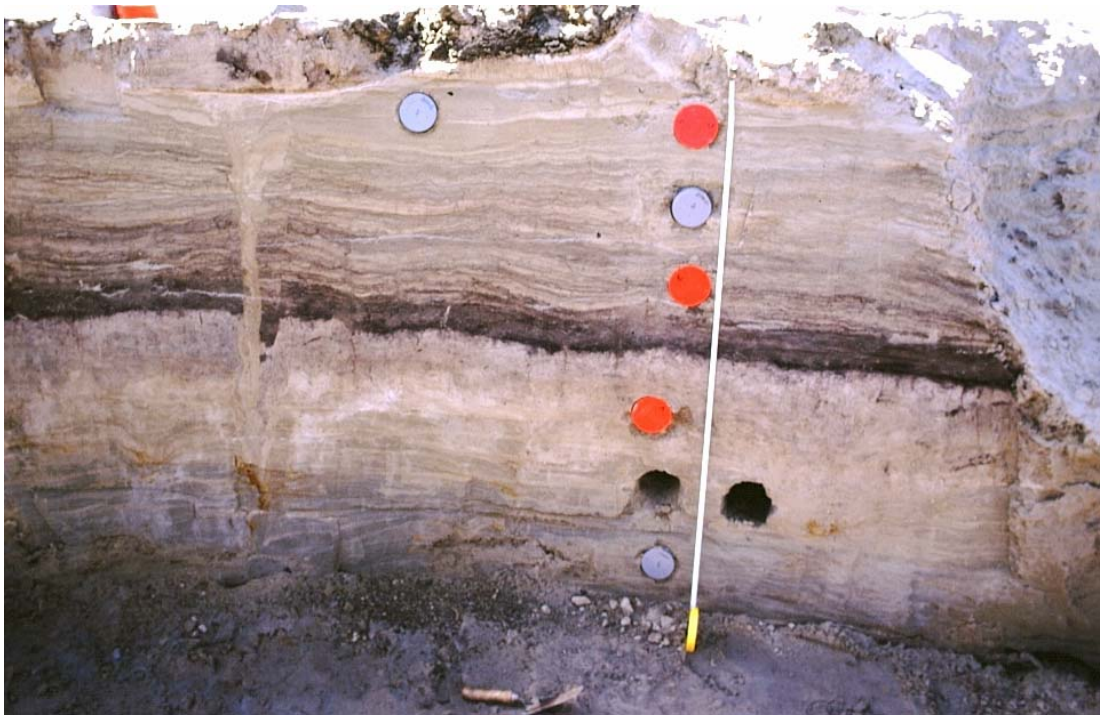

Figure 4.3: The sampled coversand profile in Ossendrecht. The total height of the profile is about 2 m. Three samples were taken above the Usselo Soil (the dark horizon halfway in the profile), and three below it.

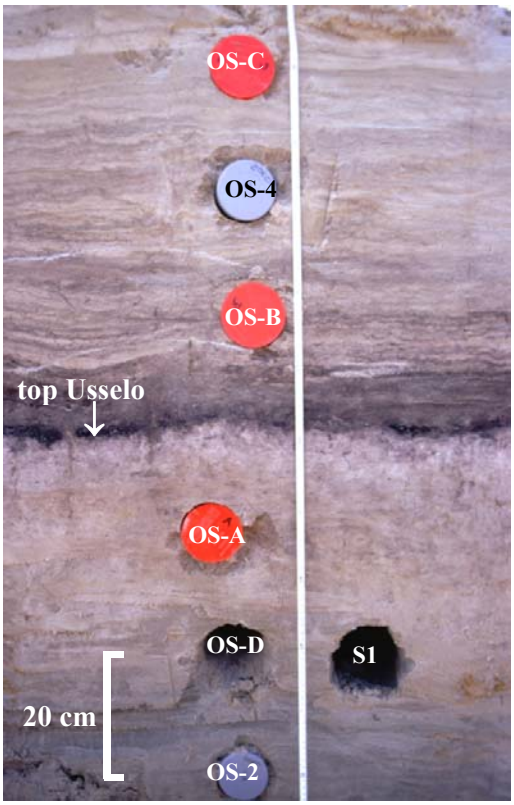

Figure 4.4: Detail of the profile, showing the location of the samples for luminescence dating and for annual dose determination. The arrow indicates the top of the Usselo Soil, which was radiocarbon dated by Vandenberghe et al. (2004; see Section 4.3).

Figure 4.5: Illustration of the experimental set-up for field gamma-ray spectrometry. The measurement was conducted at the location of sample OS-D (see also Figure 4.4).

4.5. Equivalent dose determination

4.5.1. Sample preparation

All the luminescence measurements were conducted on coarse (90-125 μm) quartz grains ("the quartz coarse-grain technique"; see e.g. Section 3.3.1). Conventional procedures (Stokes, 1992; Mejdahl and Christiansen, 1994; Lang et al., 1996; Mauz et al., 2002) were used to extract the quartz from the samples. For obvious reasons, all sample preparation was carried out under dim red or orange light conditions (Encapsulite R-10 or Ilford 902 safelights, respectively).

The samples first went through the pretreatment described by Vancraeynest (1998). From both ends of each sampling tube, the outer material (a slice of about 1 cm thick that had been exposed to sunlight during the sampling) was removed and retained for dosimetric purposes (see Section 4.6). Distilled water was added to the inner core and the pH of this mixture was measured. To remove organic material, the sediment was treated with H_2O_2, first with a 10% solution for about one hour and then with a 30% solution, which was left overnight on a magnetic stirrer to react. The peroxide mixture was subsequently decanted

and the sand was washed with distilled water. Carbonates were removed by adding diluted (10%) HCl (note that this treatment is not necessary if the pH at the start is lower than 3). After leaving the mixture again overnight on a magnetic stirrer, it was decanted and washed several times with distilled water.

Following this pretreatment, particles smaller than 50 μm were removed by wet sieving, while the fraction > 50 μm was dried in an oven at 50°C. From this fraction, the 90-125 μm grain size fraction was then isolated through dry sieving*. Non-magnetic crystalline grains were subsequently separated from the magnetic grains using a Franz magnetic-barrier separator. The resulting non-magnetic fraction was a mixture of quartz, feldspars and heavy minerals. These minerals have small differences in density and, therefore, can be isolated from each other by suspension in heavy liquids (Mejdahl and Winther-Nielsen, 1982; Mejdahl, 1985). Heavy liquids are solutions of varying density and can be prepared by mixing sodium polytungstate (a heavy inorganic salt: $Na_6[H_2W_{12}O_{40}].xH_2O$) with distilled water. The principle of the technique is outlined in Figure 4.6. First, the polymineral sample is suspended in a solution of 2.62 g cm^{-3}, and is left to spin in a centrifuge for some time. The fraction heavier than 2.62 g cm^{-3} contains the quartz and will sink to the bottom. This fraction is retained, washed and dried, and put at least one more time through this process to ensure the separation is as complete as possible. Subsequently, the mineral grains are suspended in a solution with a density of 2.75 g cm^{-3}. Heavy minerals such as zircons and apatite will sink, while a mixture of quartz and plagioclase feldspars will float on top. It is this floating fraction that is retained. After washing and drying, this last step is repeated once more.

In this manner, a mixture of quartz and plagioclase feldspars could be extracted from each sample. Due to their overlapping densities, it is not possible to further separate these two minerals from each other by means of heavy liquids. Therefore, after the density separation, the mixture of quartz and feldspars was etched for 1 hour (see Section 4.5.3) in 48% HF. The feldspars are chemically less resistant to HF and are consequently partly or completely dissolved. As mentioned previously in Section 3.3.7, the outer rinds of the quartz grains themselves are also removed during the etching. This has the advantage of

* Actually, sieving yielded the grain size fractions: <50 μm, 50-63 μm, 63-90 μm, 90-125 μm, 125-160 μm, 160-200 μm, 200-250 μm and >250 μm. All these fractions were stored. For most samples, only the 90-125 μm fraction was put through the complete purification process.

reducing the external alpha particle contribution to a negligible level. A 60 min wash with warm (ca. 50°C) dilute HCl was applied after etching to remove any precipitated fluorides. This was followed by several thorough washings with distilled water and drying in the oven at 50°C. Finally, the extract was sieved again using an 80 μm sieve to remove partially dissolved feldspars and quartz grains that had broken or become too small.

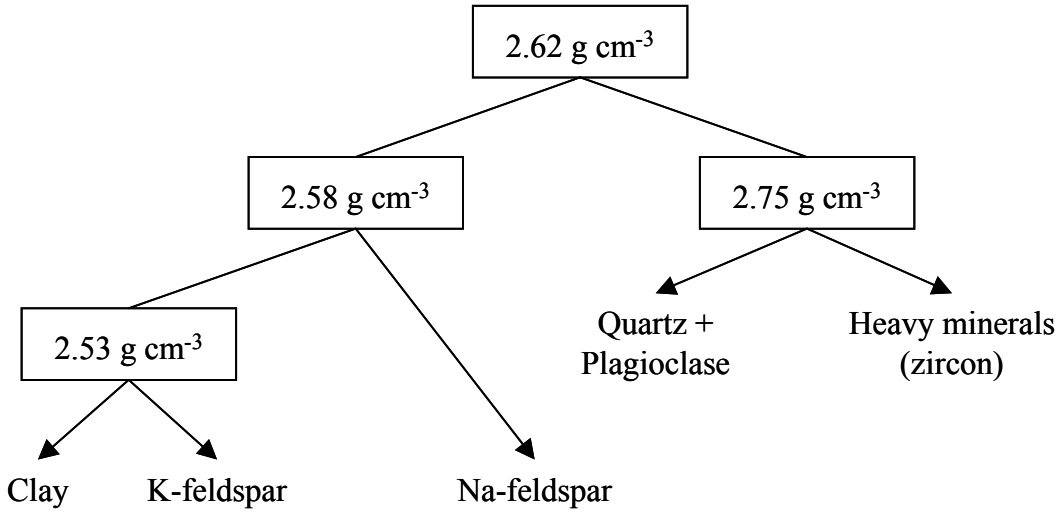

Figure 4.6: Flow-chart of density separation (after Mejdahl, 1985); the left branch indicates the floating fraction, the right the one that sinks.

It is perhaps worth mentioning that, instead of the density separation, a possibly more elegant procedure for separating quartz from feldspar grains is the so-called "flotation" technique (see e.g. Miallier et al., 1983). This technique consists of changing the surface properties of a specific mineral in such a way that gas bubbles can carry these mineral grains away from a mixed powder in suspension. Although the flotation technique is well established in the industry and exists already for decades, it still has not found its way to most luminescence laboratories. Nevertheless, the technique has certain advantages which lie in its simplicity and speed, the fact that it is cheap compared to heavy liquids (50 g of sodium polytungstate can cost as much as 50 Euro) and the fact that the quartz can be completely separated from all types of feldspar, making the etching a less critical step. Also, by combining the technique with heavy liquids (see Figure 4.6), it enables the isolation of the different types of feldspar minerals, including the plagioclases, which are otherwise dissolved by the HF treatment. The flotation technique appears to work

extremely well for sediments (M. Krbetschek, private communication), and although it was not actually employed in this work, it can be added that because of its attractive features, initial steps towards its implementation in our laboratory have already been undertaken.

4.5.2. Aliquot preparation and presentation

For measurement, the quartz grains are deposited on metal discs, of about 0.5 mm thick and 10 mm in diameter. For adherence, the discs are first coated with silicone oil using an aerosol spray (Rüsch silkospray). Two things should be born in mind when subsequently spreading the grains on the discs. Firstly, due to the fact that there is a distance between the beta irradiation source and the aliquot, the outer part of the aliquot receives a smaller dose than the center of the disc. This means in practice, that it is advantageous to limit the grains to the central area of the disc. Secondly, when using coarse grains, effects of build-up and attenuation will influence the dose received by the grains quite strongly. Reference is made to Aitken (1985) for a more detailed discussion on these issues. Here, it suffices to say that it is important to ensure that all the grains on every aliquot receive the same and reproducible dose. It can be readily understood that this situation will be disturbed by variations in sample thickness. Therefore, it is necessary that discs carry only a single layer (a so-called “monolayer”) of grains.

Throughout the initial stages of this work, i.e. for all the Ossendrecht samples, use was made of cup-like stainless steel discs. These discs had a diameter of 10 mm, and an elevated edge of 1 mm. Thus, only the central area (Ø = 8 mm) of the discs carried the quartz grains. The following recipe for making a monolayer sample was used. After spraying the discs with silicone oil, the quartz grains were poured through a funnel on the discs. The funnel was designed in such a way that, when placed on top of a disc, the grains could only fall on its central area (Ø = 8 mm). A fine grid inside the funnel ensured an even spreading of the grains. Finally, the discs were turned upside down and the surplus of grains was tapped off. Examination under a microscope confirmed that this resulted in a monolayer of grains evenly fixed on the center of the discs. A small metal plate with a tiny hole drilled in it served as spoon to scoop a (plus-minus) fixed amount of grains and to pour them through the funnel. Different spoons were made with holes of

varying size. In this way, aliquots containing varying amounts of grains (from ~ 0.5 to 5 mg) could be prepared.
After some practicing, quite reproducible aliquots could be prepared in this manner. However, the mounting of the grains (and the cleaning of the aliquots afterwards) was quite time consuming. Therefore, a less laborious technique (Aitken, 1985) for preparing the aliquots was used in the second stage of this work. This will be discussed in Section 5.2.4.2.

4.5.3. Sample purity

After sample preparation, a few "test" aliquots were prepared for checking the purity of the quartz extracts. This purity check was performed by looking for an infrared stimulated luminescence (IRSL) response at room temperature to a large regenerative β-dose (~ 5 - 10 times the estimated equivalent dose, D_e). As explained in Section 2.1, there is no luminescent signal to be expected when quartz is stimulated at room temperature with infrared light. The IRSL response induced by a large regenerative laboratory dose was preferred to the use of the natural IRSL signal, because the test is then more sensitive.
Small regenerated IRSL signals were observed for all samples, varying from 0.1% to about 8% of the corresponding quartz OSL (470 nm) signal (the latter was recorded immediately after the stimulation with infrared light). The samples had initially been etched for only 40 minutes with HF, and extending the duration of etching was tested to see if it could reduce the observed IRSL signal. After 1 hour (in total) of etching, the testing at random did not indicate a further decrease of the IRSL signal so this duration was considered as optimal and was applied to all samples (see Section 4.5.1). It is worth mentioning that the additional 20 min HF treatment resulted only in a relatively small further reduction of the observed IRSL signal (by a few percent, at most). No longer etching times were used for fear of damaging the quartz grains too much (see Section 3.3.7). The IRSL check was also performed on each aliquot, after all the principal measurements (e.g. for D_e-determination) were finished, to eliminate any aliquots with significant feldspar contamination from the analyses.

The question arises now as to which degree feldspar (or IRSL) contamination can be tolerated. Of course, ideally no IRSL signal should be observed. In practice, however, it is

not uncommon to observe an IRSL signal from a purified quartz extract. In view of all the effort that goes into the preparation of a sample, most workers therefore allow the IRSL/OSL ratio to reach an arbitrarily set upper limit, before an aliquot is rejected from the analysis (E. Bulur, private communication). Consequently, when the experiments were started on the Ossendrecht samples, it was concluded that the small regenerated IRSL signals could probably be safely neglected. After all the experiments were completed, however, a more objective insight into this matter could be gained. Indeed, as every D_e determination had been followed by the purity check outlined above, it became possible to really look for the effect of the presence and magnitude of any observed IRSL signal on the equivalent dose. To illustrate this, Figure 4.8 shows the results of 118 equivalent dose determinations for sample OS-D, plotted against the observed IRSL signals (expressed as a percentage of the corresponding OSL signals).

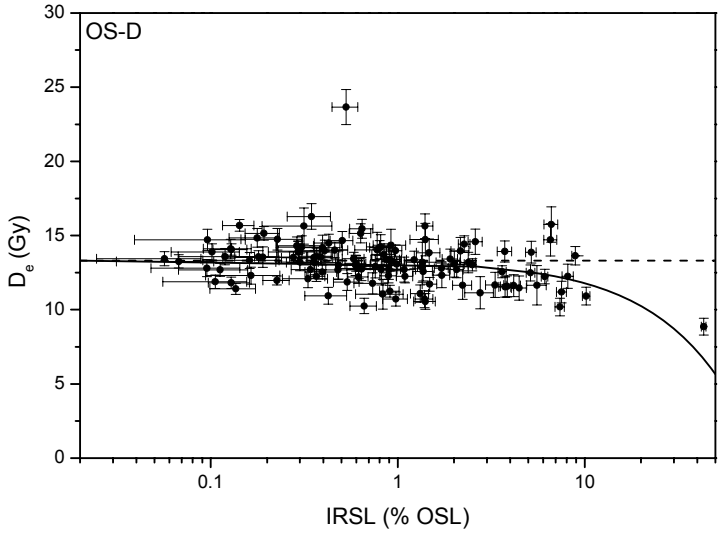

Figure 4.7: Results of 118 equivalent dose determinations plotted against the observed IRSL signals (expressed as a percentage of the corresponding OSL signals). The data are for sample OS-D. The error bars are derived from counting statistics, and represent 1s. A linear regression was performed on the data (solid line), ignoring both the high IRSL point and the high D_e point. The dashed line is meant as an eye guide and represents what would have been observed if there had been no dependency of the D_e on the IRSL/OSL ratio.

For all aliquots, clearly some sensitivity to the infrared stimulation was observed and one aliquot even yielded an IRSL signal much higher than 10% of the corresponding OSL signal. A similar picture was obtained for the other samples.

A weak but clear tendency is visible in Figure 4.7 for the dose to decrease as the IR stimulated OSL increases. A linear regression was performed on the data (ignoring both the high IRSL point and the high D_e point), yielding a value of -0.15 ± 0.06 (1s) for the slope of the fitted line (solid line in Figure 4.7). An IRSL "contamination" of 10% would hence correspond to an underestimation of the true D_e by 1.5 ± 0.6 Gy. When looking at the spread in D_e-results for IRSL/OSL ratios ≤ 1% and taking analytical uncertainties into account, this can be considered as acceptable.

For the other Ossendrecht samples, the dose depression with increasing IRSL contamination was similar or even less, and the whole of observations points at a certain degree of flexibility concerning the amount of feldspar (or IRSL) contamination that can be allowed. Based on the data exemplified by Figure 4.7, a threshold of ≤ 10 % for the ratio of the regenerated IRSL signal to the corresponding OSL signal was set. If the "test" aliquots passed this criterion (and they all did), the sample preparation procedure was considered as adequate. The IRSL check was also performed on each aliquot that was measured, to ensure they all passed the acceptance/rejection criterion. In hindsight, therefore, it can be concluded that a less stringent 40 min HF etch would probably have sufficed for these samples, especially as the additional 20 minutes of etching did not substantially reduce the observed IRSL signal. The 40 min etch with 48% HF was therefore routinely employed in the investigations that followed this pilot study (see Chapter 5).

4.5.4. Measurement and irradiation facilities

All measurements were performed using either a Risø TL/OSL-DA-12 or TL/OSL-DA-15 reader. Both systems allow fully automated measurement sequences to be run for quartz, feldspar or polymineral samples. The Risø TL/OSL-DA-12 reader is the same as was earlier described and employed by Vancraeynest (1998). However, in view of the present work, the system was modified and upgraded, and the following description refers to its configuration at the time of writing. In May 2003, the new TL/OSL-DA-15 reader was installed in our laboratory.

The basic features of both readers are the same and are illustrated in Figure 4.8. In essence, the reader consists of a sample chamber that is light tight and holds a turntable in

which the aliquots can be placed. The turntable places the aliquots above a lift mechanism that raises the samples into measurement position. On top of the lift mechanism, a heater element is mounted, which allows a reproducible heating of the aliquots (for preheating, measuring OSL at an elevated temperature, or recording thermoluminescence). The emitted luminescence signals are optically filtered and detected using a photomultiplier (PM-) tube. In this work, all signals passed through a 7.5 mm thick Hoya U-340 filter (see Section 2.3) and were detected using a bialkali EMI 9235QA (TL/OSL-DA-12) or 9235QB (TL/OSL-DA-15) PM-tube. Both tubes have a pure quartz window and a maximum detection efficiency peaking around 400 nm, which makes them very suitable for detecting the 365 nm emission from quartz. The background (dark current) of the tubes was measured before each experiment and was found to be typically around 30 counts per second at room temperature. If this would be required, such as for the measurement of very low light-levels, this background can be further reduced by removing the beta sources (see below) from the readers. It is perhaps worth mentioning that in the control box of the TL/OSL-DA-12, a divider is set to electronically divide the number of counts detected by the photomultiplier by two. This means in practice that the number of counts registered is only half of those really emitted by the sample. If desired, this setting can be readily changed.

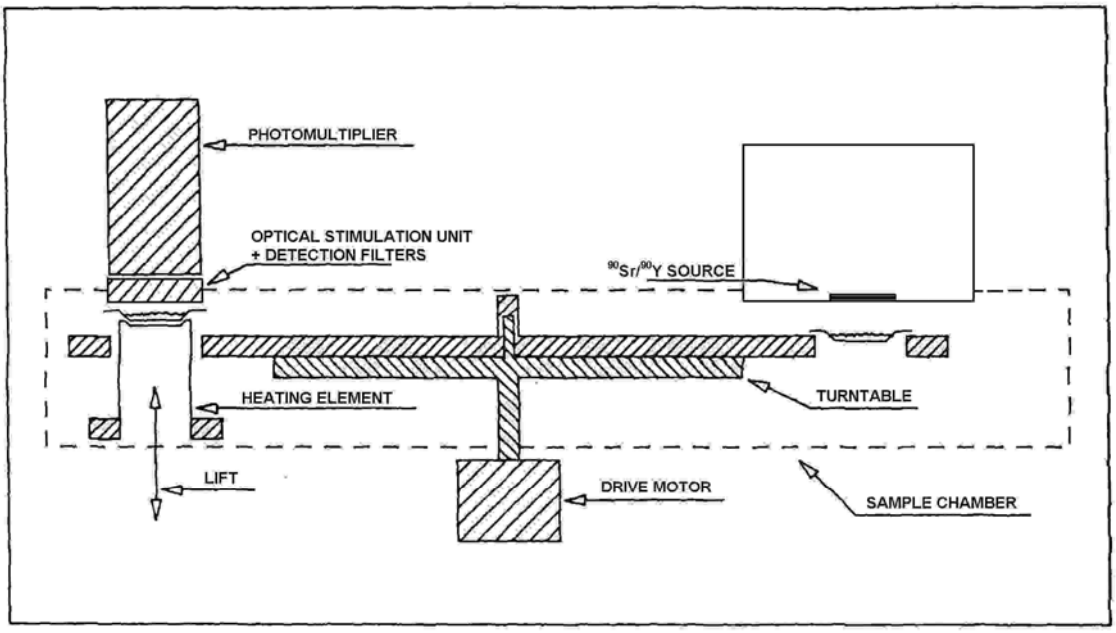

Figure 4.8: Schematic representation of the Risø luminescence reader (modified from Bøtter-Jensen, 1988).

The optical stimulation sources (and the detection filter) are mounted in between the PM-tube and the sample chamber (see Figures 4.8 and 4.9).

For the optical stimulation of feldspars and polymineral fine grains, the Risø TL/OSL-DA-12 reader is equipped with an infrared laser diode emitting at 830 nm (Bøtter-Jensen and Murray, 1999). An array of 42 blue LEDs (light emitting diodes), having a peak emission at 470 nm, provides the stimulation source for quartz *(*Bøtter-Jensen et al., 1999b*)*. The blue diodes are grouped in six clusters, each cluster consisting of 7 diodes. The whole is arranged concentrically around the position of the sample, as is illustrated in Figure 4.9.

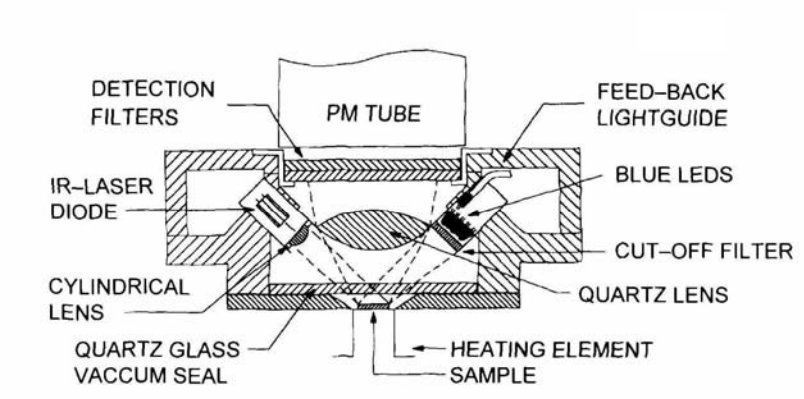

Figure 4.9: Schematic diagram of the combined blue LED and IR laser diode OSL unit (from Bøtter-Jensen et al., 2003a). The blue diode array is equipped with an optical feedback servo-system (indicated by "feed-back lightguide" in the figure) to ensure stability of the output power. Optimal stimulation and luminescence collection are optimized by the use of lenses. The emission from the blue diodes is filtered by a Schott GG-420 cut-off filter to avoid measuring the high-energy tail of the LED emission (see Section 2.3). The detection filter is a 7.5 mm thick Hoya U-340. The diagram is for the stimulation unit mounted on the TL/OSL-DA-12 reader. The experimental configuration of the unit on the TL/OSL-DA-15 reader is similar (see below). The difference lies in the fact that the infrared laser diode has been replaced with infrared LED's and that the unit consequently contains less blue diodes. As these latter are more powerful than those mounted in the TL/OSL-DA-12 unit, however, the blue stimulation power provided by both units is about the same.

The Risø TL/OSL-DA-15 system, on the other hand, is equipped with twenty-one powerful IR LEDs, emitting at 875 nm (Bøtter-Jensen et al., 2003b). Compared to the IR laser diode, these have the advantage of an increased lifetime and stability. For the stimulation of quartz, an array of 28 blue LEDs is incorporated in the unit. These blue diodes are of the latest type and provide > 40% more power than the ones mounted on the TL/OSL-DA-12 unit (Bøtter-Jensen et al., 2003b). Consequently, less diodes are

necessary to obtain approximately the same stimulation power. The diodes are placed in clusters (3 clusters of infrared LEDs and 4 clusters of blue LEDs, each cluster containing 7 diodes) in a ring around the sample, leading to a configuration similar to the one shown in Figure 4.9.
The wavelength characteristics of the stimulation and detection windows resulting from the given experimental configuration have already been shown in Figure 2.3.

On each reader, an irradiation unit containing a 40mCi $^{90}Sr/^{90}Y$ beta source is mounted*. At the start of the investigations, when only the TL/OSL-DA-12 reader was available, the source was mounted in an irradiator attachment that employed a shutter system. Later on, this system was replaced by a more newly developed design, in which the source is mounted in a rotating stainless steel wheel (Markey et al., 1997). Figure 4.10 illustrates the latter to a greater detail. The TL/OSL-DA-15 reader is equipped with the same irradiator attachment.

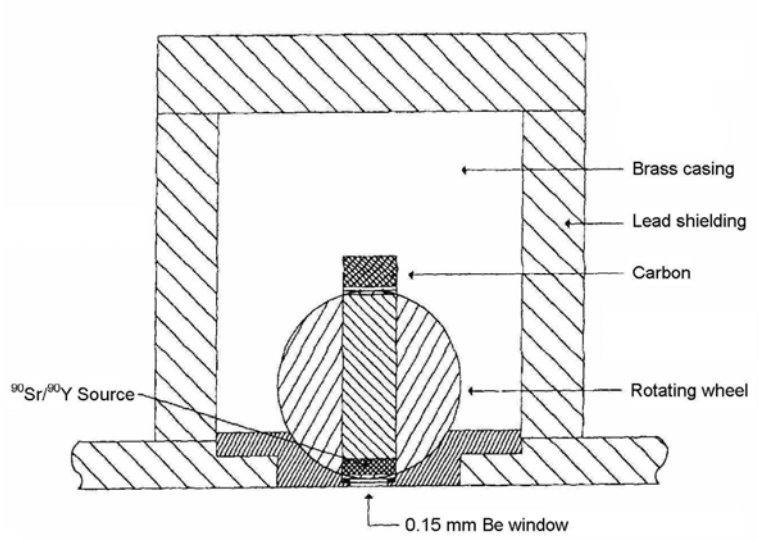

Figure 4.10: Cross section of the irradiation attachment (from Markey et al., 1997). The source is mounted in a rotating stainless steel wheel as shown. When not irradiating, the wheel is rotated 180° and the source points upwards (facing the carbon absorber). A pneumatic system (using pressurized air or N_2-gas) makes the wheel turn into the "open" irradiation position.

* The source in the irradiation unit mounted on the TL/OSL-DA-12 is a silver plaque source; the one on the TL/OSL-DA-15 is a ceramic-substrate source. In the silver plaque source, the activity is incorporated as a thin layer into the front surface of a silver plate. A thin silver protective screen covers the active face. In the ceramic-substrate source (the new generation of beta sources manufactured by Amersham International), the activity is deposited on the surface of the ceramic-substrate and is protected by a thin titanium layer. Spooner and Allsop (2000) found that both types of sources are suitable for luminescence applications.

During a measurement sequence, aliquots are sequentially moved between the measurement/heating position and the irradiation position (Figure 4.8). Upon irradiation, the active side of the source is turned towards an aliquot that is positioned exactly underneath the irradiation unit (see Figure 4.8). When the irradiation has finished, the wheel containing the source is rotated 180° and the source points upwards. The rotating of the wheel is accomplished by a pneumatic system.
The advantage of this irradiation system is that the source can be mounted much closer to the aliquots (as no intervening shutter is employed), providing as a result a much higher dose-rate (approximately by a factor of two when compared to the older irradiation configuration; see Section 4.5.6). When the irradiator is not in action, the samples also receive less background radiation, as the distance between source and aliquot is larger.

For more details on the equipment and its development throughout the years, reference is made to Bøtter-Jensen (1997) and Bøtter-Jensen et al. (2003a, 2003b), and the literature cited therein. Some recent and exciting developments in the field of OSL measurement technology worth mentioning are the single grain OSL attachment (which enables the practical measurement of individual OSL signals from large numbers of single grains; e.g. Duller et al., 1999, 2003), the radioluminescence attachment (to measure the prompt luminescence emitted during exposure to radiation; e.g. Poolton et al., 2001; Erfurt, 2003), and the mini X-ray generator (as an alternative to the radio-isotopic irradiation source; Hashimoto et al., 2002; Andersen et al., 2003).

4.5.5. Data collection and processing

The Windows-based program SEQUENCE EDITOR (Risø National Laboratory) was used to steer both readers through the so-called GENI-SYS (for the Risø TL/OSL-DA-12) or MINI-SYS (for the Risø TL/OSL-DA-15) computer. In this sequence editor, any measurement sequence can be created and subsequently directly run through Windows. The reader then carries out all the measurements full-automatically.
The program VIEW (authored by G.A.T. Duller) was used to view and export the recorded data. In this work, all data were further processed using either Microsoft Excel 2000 and/or Microcal Origin. It can be mentioned that user-friendly software is

commercially available, which has been specifically developed for processing luminescence data ("Analyst", authored by G.A.T. Duller). However, to gain a better insight into the data and on how these should be processed to arrive at an accurate equivalent dose, preference was given to homemade software and calculations "by hand". This working practice has the further advantage of avoiding "black-box" scenarios, but made the processing of the data a lot more time-consuming.

4.5.6. Calibration of the irradiation facilities

For a D_e determination to be accurate, the beta source dose rate (in Gy per unit of time) has to be known as precisely and accurately as possible. The dose that a sample receives from a beta source (Aitken, 1985) is strongly influenced by effects as build-up, backscattering and attenuation. Consequently, a whole variety of parameters (such as the distance between source and sample, the grain size and thickness of the sample, the substrate on which the grains are deposited) determine the effective calibration. This implies in practice that a beta source must be calibrated for any given irradiation geometry, and that this calibration is only valid for this precise configuration. For instance, if another substrate for carrying the quartz grains is used (say aluminium instead of stainless steel), if fine grains are used instead of coarse grains, or if the source is positioned closer to the sample, than it is necessary to carry out a new calibration.
The beta source calibration procedure consists of comparing the luminescence induced in a sample by a known dose (usually administered by a calibrated gamma source), with the luminescence induced in the same sample by a given duration of irradiation by the beta source of unknown strength. The sample used for calibration purposes in this work was the so-called "calibration quartz", provided by A.S. Murray (the Nordic Laboratory for Luminescence Dating, Risø, Denmark). This is a quartz sample extracted from a Scandinavian sedimentary deposit, that had been annealed to a high temperature to remove its accumulated luminescence signal and subsequently received a known gamma dose of, depending on the batch, 4.96 or 5 Gy. The calibration was performed using the SAR protocol (see Section 3.2.1.2.2, Table 3.3) and employing a preheat of 10s at 260°C, as was recommended by Murray.

Essentially, the measurement sequence for calibrating the source is identical to the one that would be used for a D_e determination. A growth curve is constructed in which sensitivity corrected OSL signals are plotted against the corresponding regenerative doses (Figure 4.11). The dose is now expressed in units of irradiation time, as at this point, the source strength is still unknown. By interpolation of the "natural" sensitivity corrected OSL signal on the growth curve, the duration of the beta irradiation that induces a signal equal to that induced by the known gamma dose can be derived. In such a way, the relation between irradiation time and delivered dose – in other words, the source strength – can be derived.

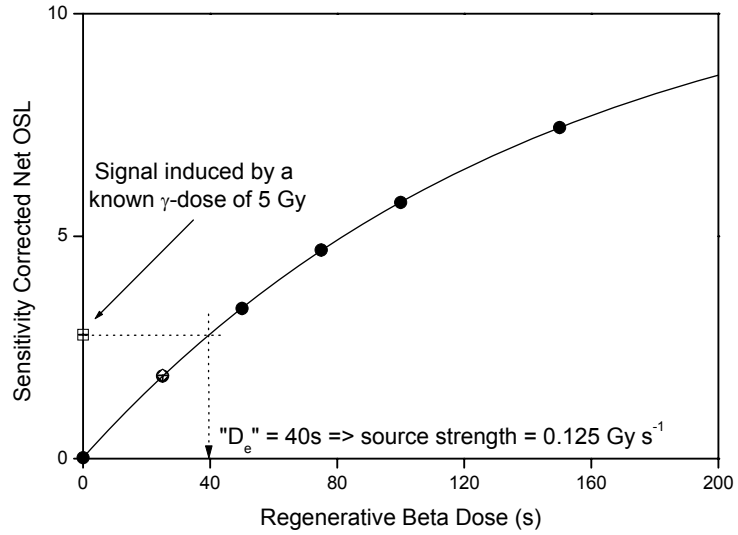

Figure 4.11: Illustration of the procedure for calibrating a beta source. A growth-curve was constructed for an aliquot of "calibration quartz" using the SAR protocol as outlined in Table 3.3. The solid circles represent the sensitivity corrected regenerated OSL signals. A repeat measurement was conducted of the lowest regenerative dose (the recycling point, indicated by the open diamond). These two measurements were found to be indistinguishable. The beta source strength is obtained by dividing the known calibration dose (5 Gy) by the beta irradiation time (40 s) that yields a sensitivity corrected luminescence signal equal in magnitude to the sensitivity corrected OSL signal induced by the known dose (indicated by the open square).

The sources mounted on each of the two Risø readers were calibrated by applying the calibration procedure outlined in the above to six aliquots of calibration quartz. This provided six independent estimates of the source strength and an associated external uncertainty.

Throughout this work, the measurement and irradiation facilities went through minor and major modifications (such as the replacement of the shutter-based irradiation unit by the unit shown in Figure 4.10). Also, as was already mentioned in Section 4.5.2, a different aliquot preparation technique was used in the second stage of the investigations, resulting in a different presentation of the quartz grains to the irradiation source. With each change in the precise conditions of the beta irradiation, the sources were calibrated accordingly. The source strengths corresponding to the current routinely used irradiation configurations are 0.086 Gy s^{-1} for the beta source mounted on the TL/OSL-DA-12 reader, and 0.125 Gy s^{-1} for the one mounted on the TL/OSL-DA-15 reader (reference date: 16/05/2002). These values apply to the irradiation of 90-125 μm quartz grains deposited on the inner 7 mm diameter of stainless steel discs (diameter = 9.7 mm, thickness = 0.5 mm). For comparison, the strength of the source in the TL/OSL-DA-12 shutter system to quartz in the aliquot presentation outlined in Section 4.5.3 was only 0.041 Gy s^{-1}.

In later experiments (see Section 5.2.4.3.4), it was required to confine the quartz grains to an area smaller than 7 mm. In these investigations, the quartz grains were spread over an area of 2 mm in diameter on the inner centre of the 9.7 mm diameter stainless steel discs. Because of the spatial variation in the dose an aliquot receives from a beta source, these "small" aliquots will, on average, receive a higher dose for the same irradiation duration. These measurements were only conducted using the TL/OSL-DA-15 reader and calibration for this small aliquot size yielded a beta source strength of about 2% higher than for the 7 mm diameter aliquots, admittedly hardly significant.

From the above-mentioned beta source strengths, the value at any given date can be calculated [$T_{½}(^{90}Sr)$ = 28.74a; from Isotope Explorer, Chu et al., 1999]. The better approach is, however, to repeat the calibration from time to time. This way of working allows to identify and to take into account any instrumental fluctuations, and this practice was also handled throughout this work. It is therefore recommended that the given source strengths are considered as indicative, rather than that future workers adopt them as set-in-stone values.

A total systematic uncertainty of 2% (1s) was adopted for the beta source calibration. This uncertainty finds its origin in the observed spread on the calibration measurements and uncertainties associated with the gamma irradiation. It is considerably smaller than the

value of 5% adopted in the work by Vancraeynest (1998). This is owing to the fact that in this work the calibration was based on a direct intercomparison with a calibrated gamma beam (instead of on an intercomparison between beta sources), as well as to the high precision by which equivalent doses can be determined with the SAR protocol.

4.5.7. Equivalent dose determination

It is clear from Chapter 3 that a multitude of measuring protocols is available for determining the equivalent dose. None of these have yet proven to be universally applicable. As a consequence, it is worthwhile to thoroughly investigate the applicability of a given technique for any new sediment that is to be dated using luminescence. In this study, three techniques were selected, namely the multiple-aliquot additive-dose technique (MAAD), the single-aliquot additive-dose (SAAD) technique and the single-aliquot regenerative-dose technique (SAR). At the time this work was started, these techniques seemed the most commonly applied ones, or seemed to hold the most promise for obtaining accurate equivalent doses. The principles of the three analytical protocols have already been outlined in Chapter 3.

4.5.7.1. D_e determination using the multiple-aliquot additive-dose (MAAD) technique

Multiple-aliquot additive-dose measurements were performed on samples OS-B and OS-D, using conventional procedures (Aitken, 1998; Lian and Huntley, 2001). To build up the dose-response curves, twenty-four aliquots were used, in groups of four. Doses were chosen using half, one, two, four and eight times the estimated D_e (based on Felix and Singhvi, 1997). After preheating for 5 min at 220ºC, the OSL was measured for 100 s at 125ºC. Another set of twenty-four aliquots provided the data to correct for thermal transfer (Galbraith et al., 1999; Lian and Huntley, 2001, and references therein). These natural aliquots received the same treatment as the set for the construction of the additive-dose growth curve, but were bleached for 100 s using the blue diodes before being preheated and measured. Normalization was by means of the OSL response to a small test dose (about 15 – 20 % of the estimated D_e) administered after each principal measurement was made, as recommended by Wintle and Murray (1999). This should correct for any

inter-aliquot differences in sensitivity (due to e.g. differences in sensitivity change, mass or number of bright grains on each aliquot), so that any observed scatter of the data points can be ascribed to the presence of a residual dose or an intrinsic difference between the aliquots in luminescence behavior. The first 0.4 s of the OSL signal was used to construct the growth curves, from which the background was subtracted, evaluated from the last 4 seconds. The sensitivity corrected data were further processed using the "Intercept Dose" program authored by D. J. Huntley. The additive-dose data were fitted to a single saturating exponential, the thermal transfer data to a straight line. The equivalent dose is obtained as the intersection of both extrapolated curves.

The multiple-aliquot additive-dose growth curve with correction for thermal transfer is shown in Figure 4.12a for sample OS-B and in Figure 4.12b for sample OS-D. The intercept correction is small (~ 2.5% of the corrected natural signal) and it is concluded that thermal transfer is insignificant for both samples. The resulting D_e's are 21.1 ± 3.6 Gy for OS-B and 17.1 ± 2.2 Gy for OS-D.

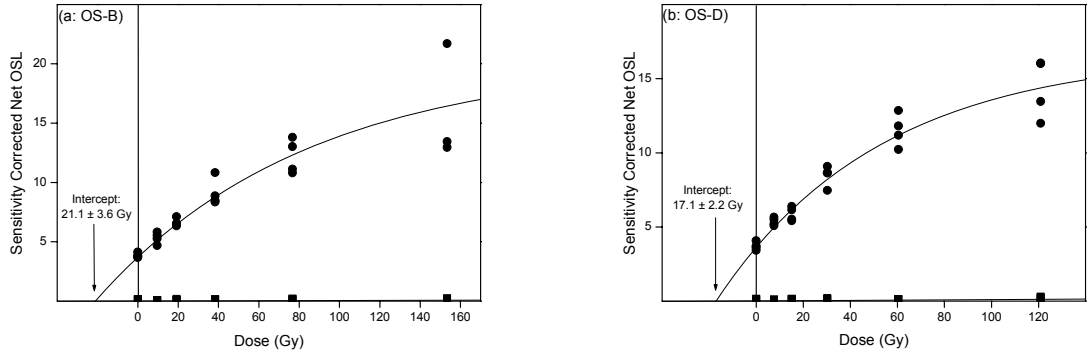

Figure 4.12: (a) Multiple-aliquot additive-dose growth curve with correction for thermal transfer for sample OS-B. The black circles represent the additive dose data; the squares are the thermal transfer data. (b) Same as in (a) but for sample OS-D.

4.5.7.2. D_e determination using the single-aliquot additive-dose (SAAD) technique

In the single-aliquot additive-dose approach (Murray et al., 1997; see Section 3.2.1.2.1.) a single aliquot is put through a repeating cycle of irradiation, preheating and short OSL measurement, to construct the additive-dose growth curve. Stokes et al. (2000) showed the

limited applicability of this protocol for a variety of samples, and cautioned against the use of it without prior testing the validity of the assumptions underlying the protocol.

The first test suggested by Stokes et al. (2000) deals with the constancy of the decay rate of the OSL signal due to the preheating and stimulation and was performed on samples OS-4, OS-D and OS-2. For each sample, eight groups of three aliquots were subjected to 15 cycles of preheating and stimulation. Each group received a different preheat, ranging from 160 to 300ºC, in 20ºC intervals. Stimulation was for 0.2 s at 125ºC using the blue diodes. Subsequently the discs were heated to 450ºC, cooled to room temperature and finally stimulated again to obtain an estimate for the background. Exponential functions were fitted to the complete decay and to the first five and the last five data points.

An example of the depletion of OSL due to the repeated preheating and optical stimulation is shown in Figure 4.13a. The R^2 values indicate a good fit to the full decay. When the decay terms derived from the first and last five cycles are compared, however, the decay term is seen to reduce drastically in the course of the experiment. In Figure 4.13b this comparison of decay terms is shown for sample OS-2 as a function of preheat temperature. The decrease is relatively independent of the preheat temperature up to about 260ºC, and is typically around 40%. The decay at a preheat temperature of 300°C is too thermally eroded to be of any use. The same observations were made for samples OS-D and OS-4 (Figures 4.13c and 4.13d, respectively). It is clear that a single exponential function is inappropriate to characterize the decay. The results can possibly be understood when taking into consideration that the quartz OSL signal consists of various components, each having different characteristics (e.g. Bailey et al., 1997 and Bulur et al., 2000; see Section 2.5). When constructing the single-aliquot additive-dose growth curve, the most easily stimulated component (the so-called fast component) is being preferentially sampled. While constructing the decay curve, however, no irradiation is administered and consequently this component is progressively eroded, while the other component(s) gain in importance. In view of this, it is even reasonable to expect that it will not be possible to describe the decay by a simple single exponential function, but rather by a sum of them. Preliminary investigations on the different OSL components of the Ossendrecht quartz will be reported in Vandenberghe et al. (in preparation).

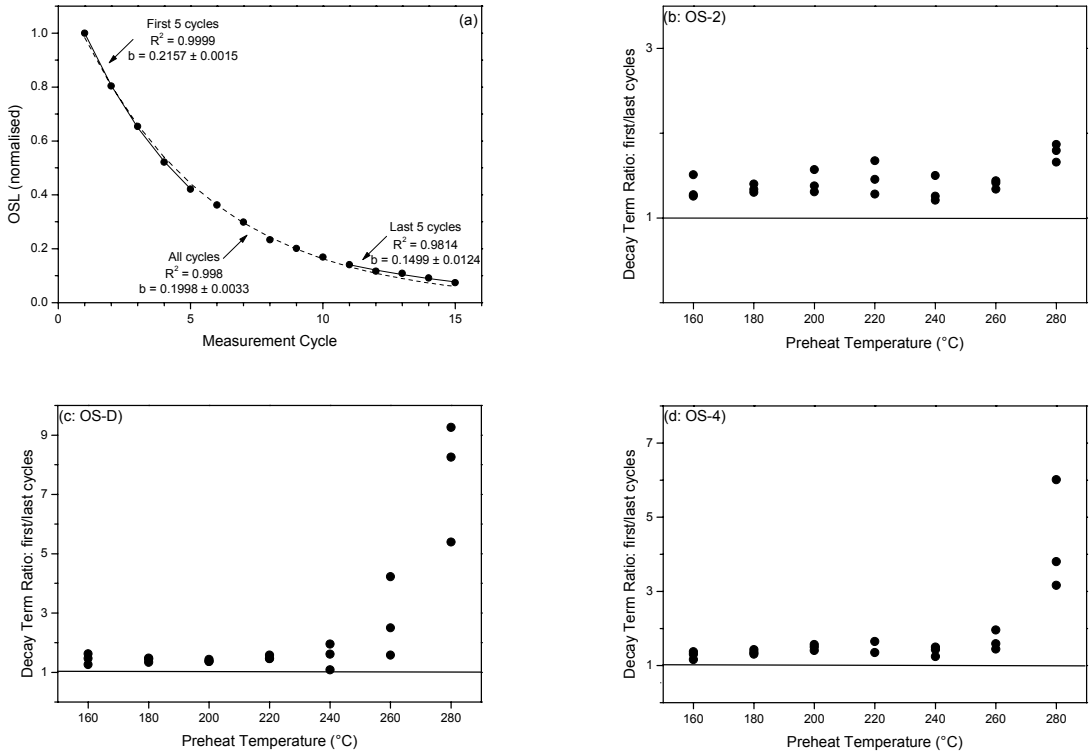

Figure 4.13: (a) Example of OSL depletion as a result of preheating and stimulation. Exponential functions $y = a \times e^{-b \times x}$ were fitted to the complete decay and to the first five and last five data points. (b) Comparison of the decay terms derived from the first and the last five measurement cycles as a function of the preheat temperature for sample OS-2. The solid line is meant as an eye guide and represents a ratio equal to unity. (c) and (d) Same as in (b) for samples OS-D and OS-4, respectively.

The second test suggested by Stokes et al. (2000) concerns the effect on the sensitivity by the repeated preheating and measuring. Five aliquots of samples OS-D and OS-4 received the same treatment as above but between each preheat and OSL measurement a test dose of about 0.5 Gy was administered and the 110ºC TL peak was recorded. The response to the test dose was also measured before the first preheat. A single preheat of 10 s at 240ºC was used.

The information obtained by the second test is shown in Figures 4.14a and 4.14b for an aliquot of sample OS-4 and OS-D, respectively. A slight rise in sensitivity is observed which could be due to an accumulation of dose by the repeated administration of the test doses (Stokes et al., 2000). For both samples, therefore, no real conclusions could be drawn concerning the constancy of the sensitivity during the experimental steps in the SAAD protocol.

However, because the protocol fails at least for one of the two test criteria, it was not considered further.

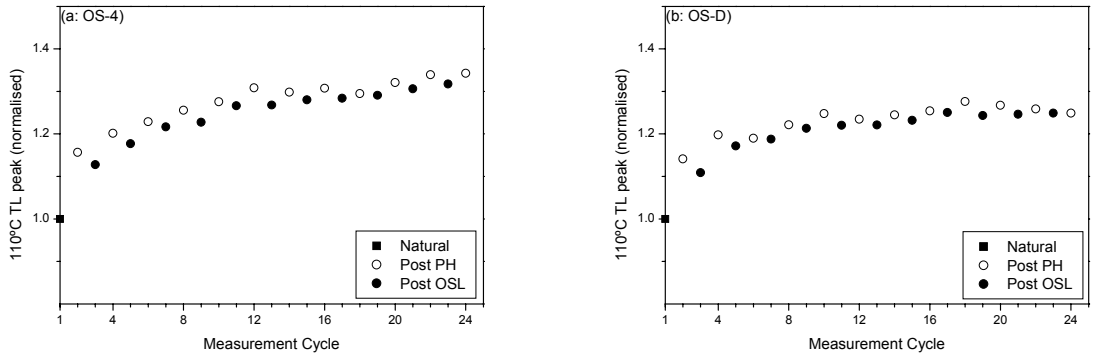

Figure 4.14: (a) Apparent sensitivity changes as a result of the preheating and stimulation as indicated by the 110°C TL peak (integrated from 48°C to 144°C, with the dark-count rate subtracted). The data are for an aliquot of quartz grains extracted from sample OS-4. (b) Same as in (a) but for sample OS-D.

4.5.7.3. D_e determination using the single-aliquot regenerative-dose (SAR) technique

The single-aliquot regenerative-dose (SAR) protocol was extensively described in Section 3.2.1.2.2. To recapitulate in short, the measurement procedure involves the measurement of the natural OSL signal, followed by the measurement of the response to various regeneration doses. After each measurement the OSL response to a test dose is measured. This is necessary because dosing, preheating and measuring can change the sensitivity of the sample. By dividing the regenerated OSL by the corresponding test-dose response, a "calibration curve" can be constructed, characterizing the growth of the signal with dose. From this curve the unknown dose (= D_e) can be deduced by interpolation of the corrected natural signal. A repeat measurement of the response to a dose equal to one that had previously been administered, is incorporated in the measurement sequence to see if the sensitivity correction is working properly. If all is well, the so-called recycling ratio should be unity. To check if the dose-response curve starts indeed at the origin, the response to a zero dose is measured as well. Ideally, this should give a zero signal, but in practice a small signal is observed due to recuperation.

All the experiments reported in the following were carried out according to the generalized SAR measurement sequence presented in Table 3.3 (i.e. SAR in its basic form, as originally proposed by Murray and Wintle, 2000a). Optical stimulation was for

40 s at 125ºC. The first 0.3 s were used for D_e evaluation after the background was subtracted based on the last 4 s. The same background as calculated for the natural and regenerated signals was used for the corresponding test dose signals. Preheating of the regenerative doses was for 10 s at a temperature in between 160°C and 300°C (see further). All the test dose preheats were in the form of a cut heat to 160°C, meaning that the aliquots were heated at a rate of 5°C s^{-1} to the given temperature and then immediately cooled again to room temperature. The growth curves were typically constructed using five regenerative doses of 0.5, 1, 1.5, 2, and 2.5 times the estimated D_e. The zero dose point and the recycling point (a repeat measurement of the lowest regenerative dose) were measured before the highest regenerative dose was administered. The measurement of this highest regenerative dose point was also preceded by an IRSL measurement (40s at room temperature) to trace any aliquots suffering from significant feldspar contamination (see Section 4.5.3). The D_e was determined by interpolation of the corrected natural signal on a single saturating exponential fitted to the regenerative dose points (including the zero dose point but not the recycling point).

The four natural aliquots that were used in the multiple-aliquot experiments (see Section 4.5.7.1) were also put through a complete single-aliquot regenerative-dose (SAR) sequence after the measurement of the natural signal and test dose response. These SAR measurements used the same experimental parameters as in the multiple-aliquot experiments, to allow a direct comparison of equivalent doses obtained via the two protocols (see Section 4.5.7.4).

For all samples, the influence of the preheat temperature on the equivalent dose was investigated first (the so-called “preheat plateau” test; see Section 3.2.2). Three aliquots were measured at each of eight different preheat temperatures (in the range of 160°C-300°C, in 20°C steps). The results are summarized in Figure 4.15*.

* It is impossible to include all the growth curves, as probably a few thousand of them were constructed throughout this entire work (Chapter 4 and 5). This illustrates one of the advantages of single-aliquot protocols, namely the rapidity of the D_e determination (see Section 3.2.1.2).

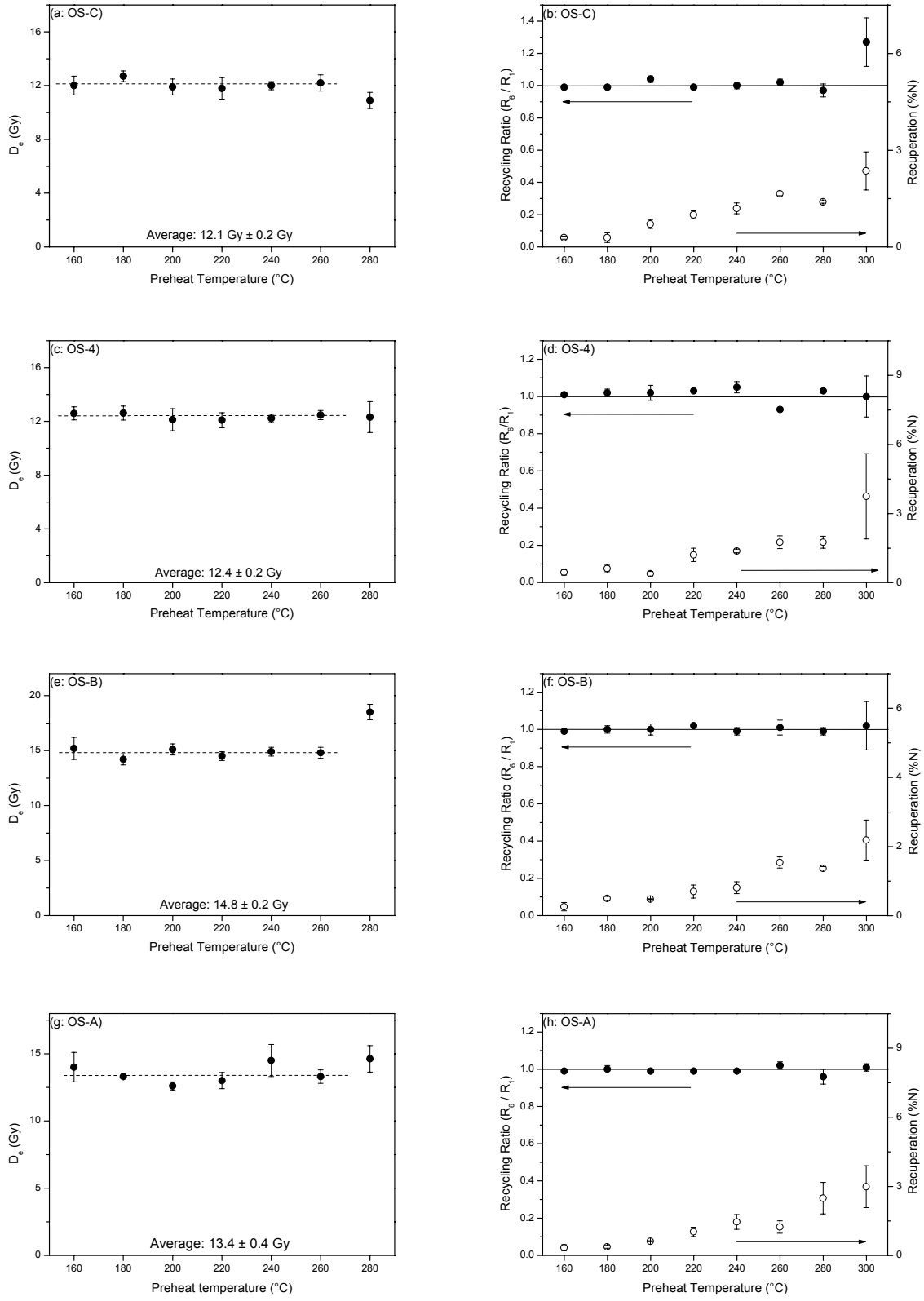

Figure 4.15: The figures on the left show the dependence of the equivalent dose (D_e) on the preheat temperature ('preheat plateau' tests) for the samples from Ossendrecht. Sample identification is given in the upper left corner of each figure. The dashed line represents the unweighted average over the 160-260°C region (continued on the next page).

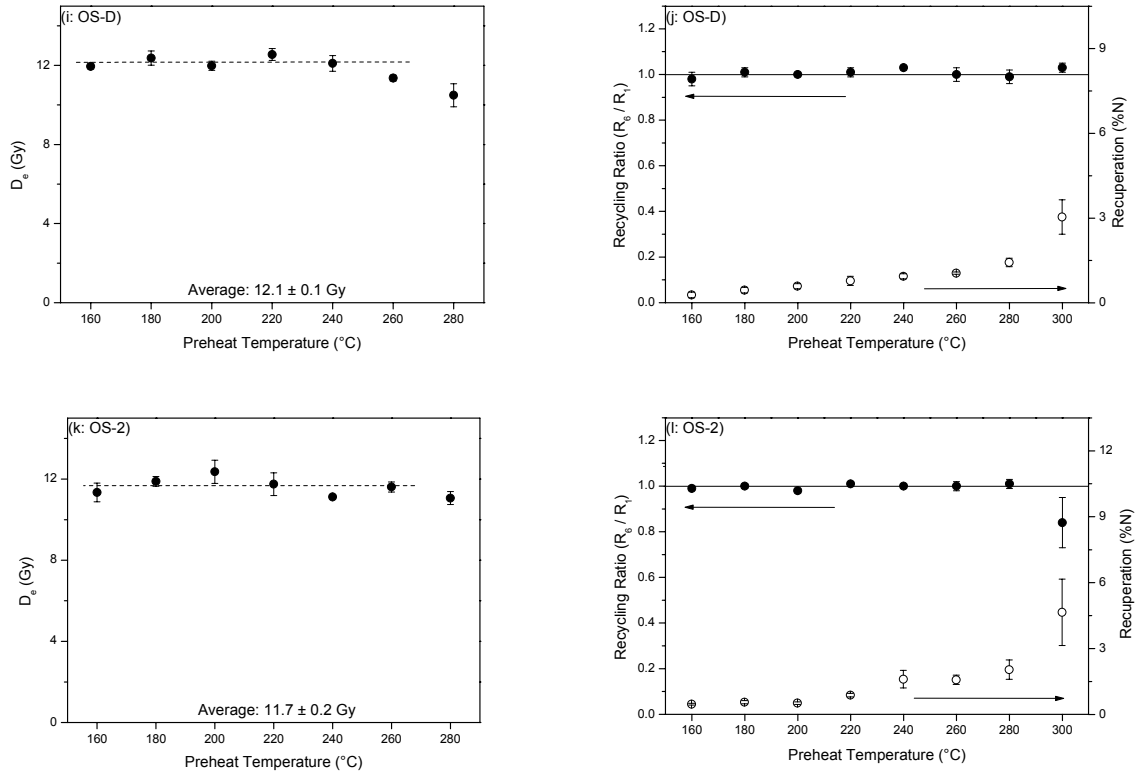

Figure 4.15 (continued): The figures on the right show the corresponding recycling ratios (solid circles, left hand axis) and recuperation (expressed as a percentage of the corrected natural OSL signal; open circles, right hand axis). The solid line (eye guide) represents a recycling ratio equal to unity. Each data point is the average of three aliquots; error bars are 1 standard error.

The preheat plateau tests indicate no detectable dependence of D_e on the preheat temperature up to temperatures of 260-280ºC. At higher temperatures the signal becomes too thermally eroded to be of any use. This lack of sensitivity of D_e to preheat temperature suggests that thermal transfer is unimportant for these samples (see Section 3.2.2). The corresponding recycling ratios and recuperation (expressed as a percentage of the corrected natural signal) as a function of preheat temperature are shown on the right hand side of each figure. The recycling ratios are approximately equal to unity across the whole 160-280°C temperature range. A slight increase of the recuperation with preheat temperature can be seen, but on the average it remains below 4.5%.

For three samples, OS-2, OS-D and OS-4, the dependency of the equivalent dose on the test dose size was also investigated. Three discs were used for each test dose size, the size

going up to 5-6 times the equivalent dose. A preheat temperature of 10s at 240°C was used, chosen from the preheat plateau region. The results are shown in Figure 4.16.

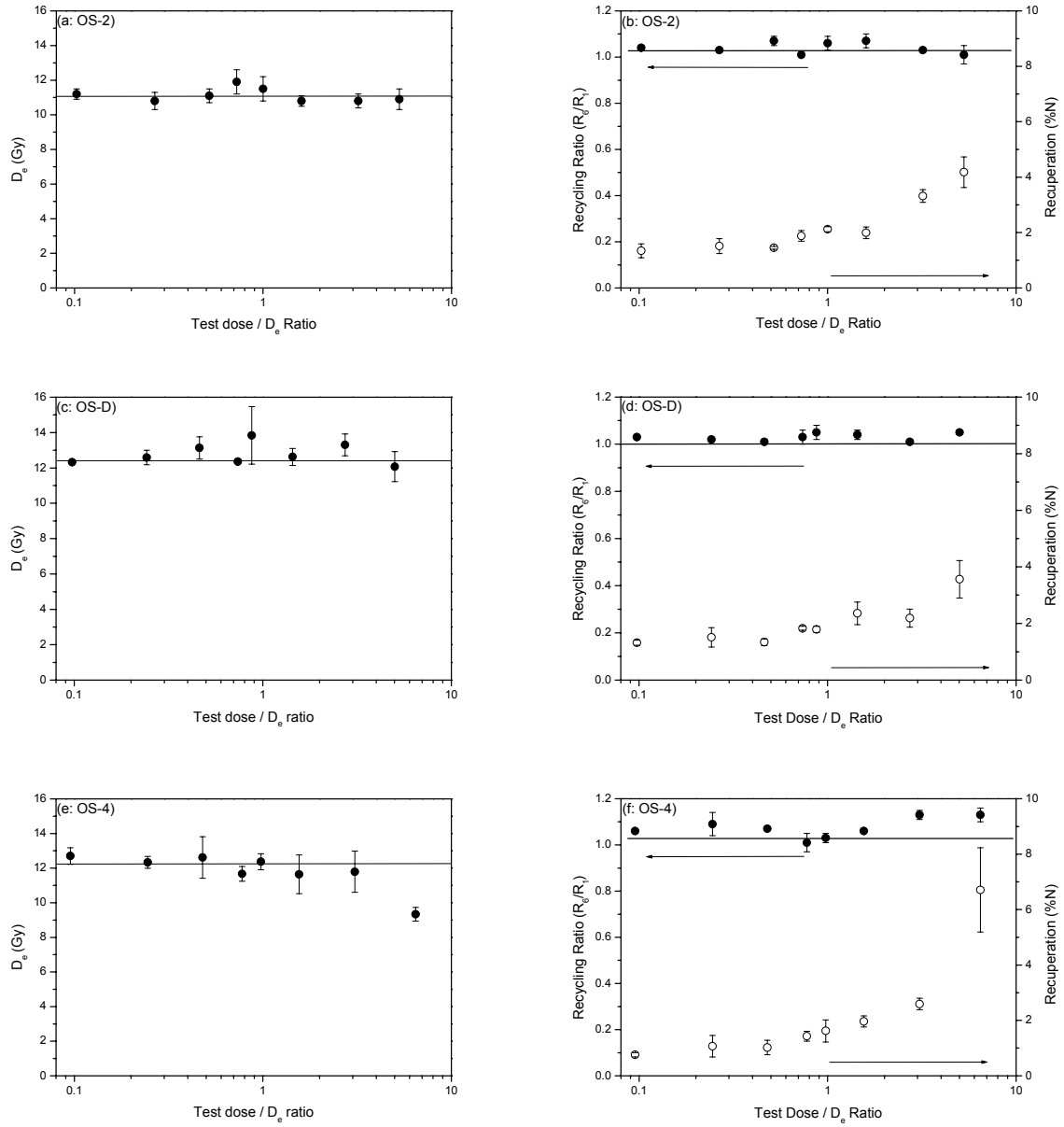

Figure 4.16: Shown on the left is the dependence of the D_e on the size of the test dose for samples OS-2, OS-D and OS-4. Sample identification is given in the upper left corner of each figure. Note that the test dose is expressed relative to the D_e, on a logarithmic axis. Shown on the right are the corresponding recycling ratios (solid circles) and recuperation (open circles). Each data point represents the average of three determinations; the error bars are 1 standard error.

For samples OS-2 (Figure 4.16a) and OS-D (Figure 4.16c) there seems to be no dependence on the size of the test dose. For sample OS-4 (Figure 4.16e), taken from above the Usselo Soil, the D_e is significantly lower at the highest value of the test dose. On the average, OS-2 and OS-D behaved better than OS-4 in terms of recycling ratios and recuperation. The recuperation observed for OS-4 at the highest test dose size was 6.7% on average, with an average recycling ratio of 1.13 ± 0.03, while for OS-D, for instance, the corresponding values were 3.6% and 1.05 ± 0.01, respectively. For all three samples, the recuperation can be seen to increase with test dose size (Figures 4.16b, 4.16d and 4.16f). This points at some thermal transfer of the charge inserted into shallow light-insensitive traps by the test dose, to the OSL trap during the high temperature preheat. The recuperation is small, however, and seems to produce no detectable effect on the D_e, with the exception of sample OS-4 at the highest values of the test dose. Nevertheless, as the relationship between recuperation and D_e is not well understood (Murray and Wintle, 2000a) and as also from the standpoint of measurement precision no high test doses were required, the test dose size was kept relatively low, i.e. at 15-20% of the estimated D_e.

The above datasets (Figures 4.15 and 4.16) illustrate the good behavior of the samples in the SAR protocol. The sensitivity correction appears to be working well (recycling ratios close to unity), and there is no evidence for significant thermal transfer effects. The observations also agree with previous findings concerning the insensitivity of the D_e on measurement parameters as preheat temperature and test dose size (see e.g. Murray and Wintle, 2000a).

However, Murray and Wintle (2003a) recently showed that the recycling ratio is not a particularly sensitive measure for the suitability of the SAR measurement protocol. Wallinga et al. (2000b) had already earlier made this observation, but for SAR applied to coarse-grain feldspar. Murray and Wintle (2003; see also Wallinga et al. 2000b) therefore suggested the use of so-called “dose recovery tests”. In such a test, the SAR protocol is used to measure a known laboratory dose that had been administered to an aliquot after optical bleaching at room temperature and prior to any thermal treatment. The applied laboratory dose mimics the natural dose, and any protocol that is used for equivalent dose determination should at least be able to determine (or “recover”) this known dose. Although the dose recovery test still does not give information on the accuracy by which

the naturally acquired dose can be determined, Murray and Wintle (2003) showed that it is more diagnostic than the recycling ratio for evaluating the applicability of a SAR procedure to a given sample. Dose recovery tests were therefore carried out for all the Ossendrecht samples.

For each sample, 24 aliquots were first bleached, using a single optical stimulation at room temperature employing the blue diodes for 100s. The aliquots were grouped in eight sets of three and each group received a different laboratory dose somewhere in between ~5 and ~40 Gy. This dose range comfortably brackets the natural dose. The SAR protocol was then applied as previously, using a preheat temperature of 10 s at 240°C (chosen from the preheat plateau region) and a test dose of about 15% of the given laboratory dose. The results are shown in Figure 4.17.

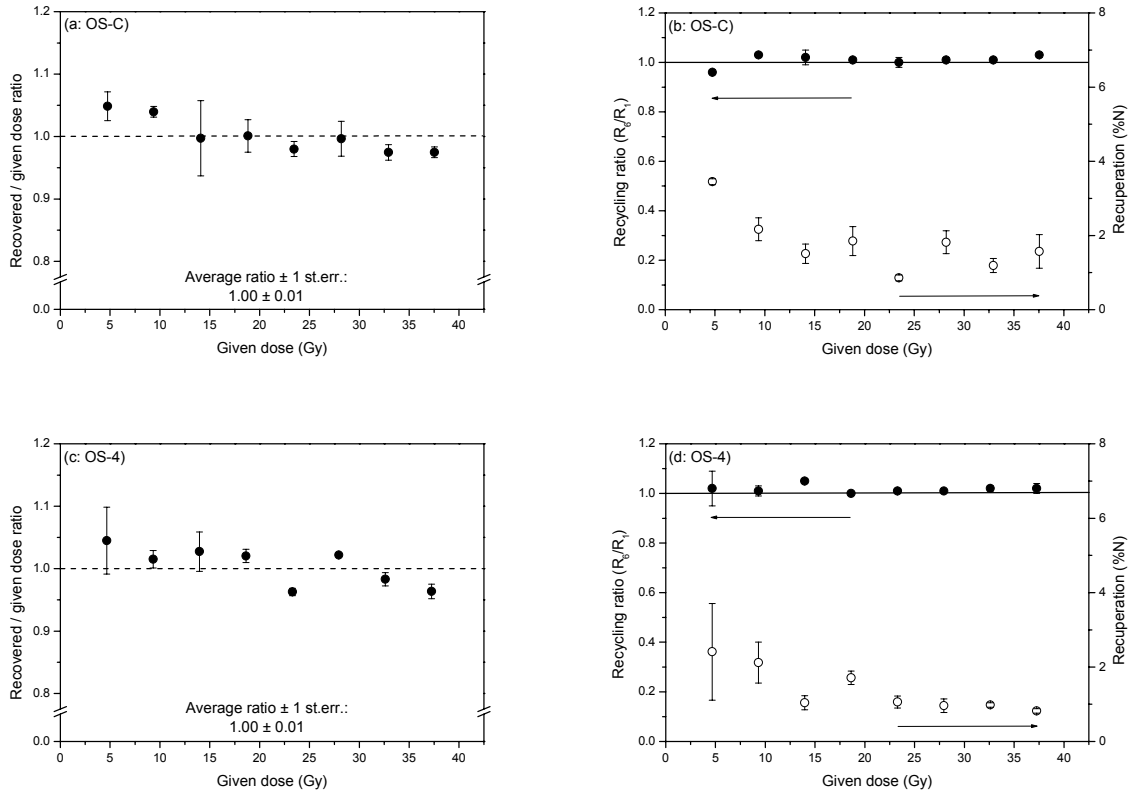

Figure 4.17: The figures on the left show the results of the dose-recovery tests for the samples from Ossendrecht. Sample identification is given in the upper left corner of each figure. The dotted line is an eye guide, representing a recovered to given dose ratio equal to unity (continued on the next page).

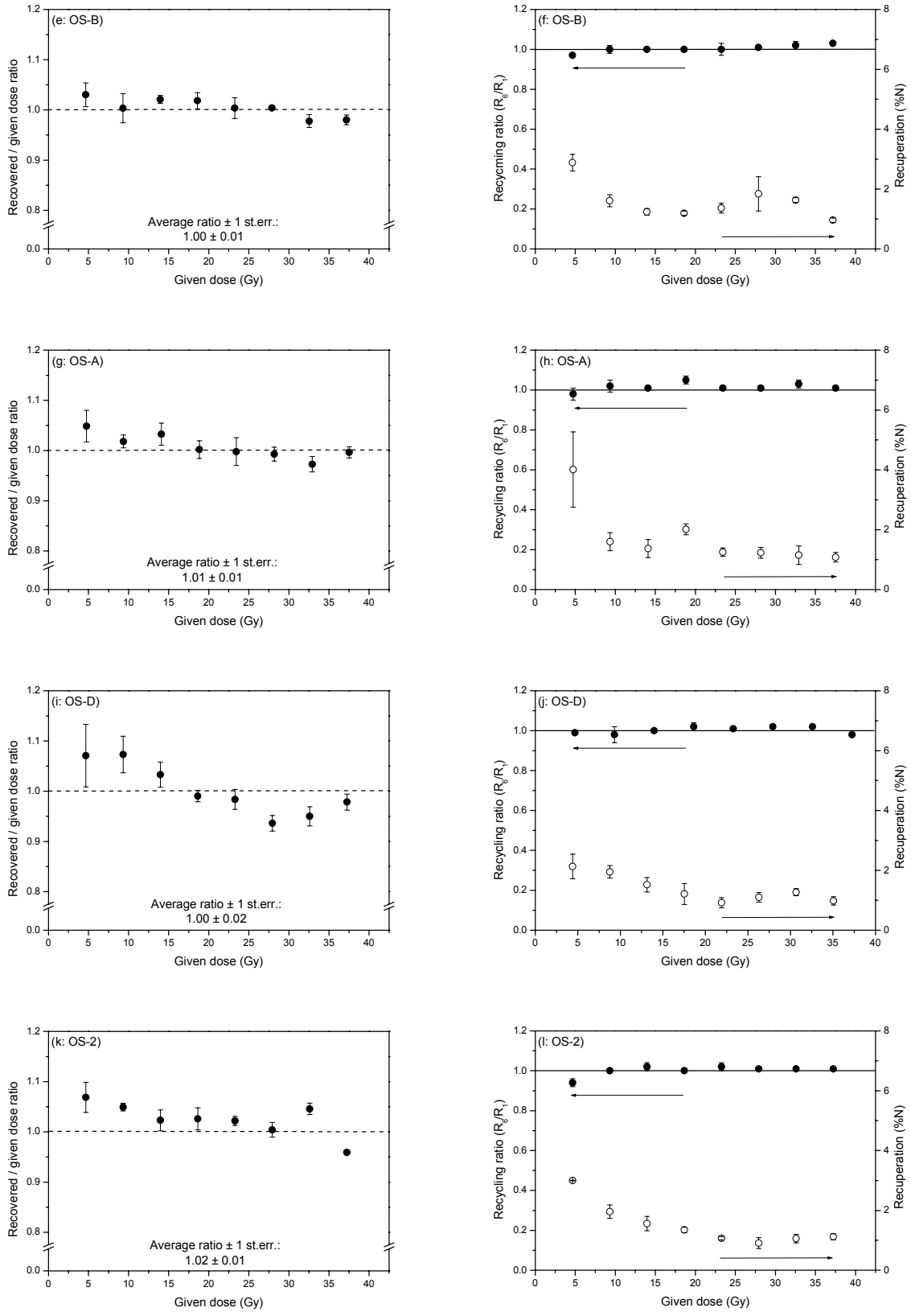

Figure 4.17 (continued): The figures on the right show the corresponding recycling ratios (solid circles) and recuperation (expressed as % of the corrected signal induced by the given dose; open circles). Each data point is the average of three measurements; the error bars represent 1 standard error.

There seems to be a systematic tendency of a small overestimation at lower given doses, and a small underestimation at higher doses. However, for all samples the given doses could be recovered to within 5%, and the overall ratios over the whole dose range are consistent with unity. It is concluded, therefore, that for these samples quite acceptable dose recoveries could be achieved. The recycling ratios and the recuperation (expressed as a percentage of the corrected "natural" signal) are also shown on the right hand side of each figure. All recycling ratios fall within the range 0.95-1.05, most of them being consistent with unity. The recuperation does not exceed 4% of the corresponding corrected "natural" signal induced by the lowest given dose; for higher given doses, it remains constant at a value of about 1 to 2%.
On the whole, the results from the dose recovery experiments suggest that the SAR protocol is applicable to the investigated samples. The ultimate validation lies in the comparison with the independent age information (see Section 4.7).

Finally, the implementation of the SAR technique in the Ghent laboratory was investigated, by setting up a small laboratory intercomparison in which a few samples were independently analysed by at least one other luminescence dating laboratory (Heidelberg and Risø) using the SAR protocol. The results are summarized in Table 4.2. Details on the HDS-# samples (which are samples of quartz extracted from Holocene sediments from the northeastern Peloponnese, Greece) can be found in Fuchs (2001). All D_e's are, within the analytical uncertainty, consistent with each other, but the observed standard deviations are rather large, preventing a more precise comparison. The fair overall agreement, however, does give some confidence in the implementation of the technique at our laboratory.

	Risø *(Gy)*	*Ghent* *(Gy)*	*Heidelberg* *(Gy)*
OS-2 (125-160 μm)	11.12 ± 0.34 (n = 18)	10.98 ± 0.25 (n = 18)	10.7 ± 0.64 (n = 11)
OS-D (125-160 μm)	11.77 ± 0.28 (n = 18)	12.62 ± 0.31 (n = 23) 12.88 ± 0.29 (n = 118)	11.0 ± 0.63 (n = 13)
OS-4 (90-125 μm)	-	12.36 ± 0.31 (n = 18) 12.83 ± 0.29 (n = 119)	11.8 ± 0.63 (n = 13)
HDS 1028	-	6.06 ± 0.16 (n = 24)	5.74 ± 0.24 (n = 25)
HDS 1031	-	2.93 ± 0.14 (n = 16)	3.27 ± 0.22 (n = 24)
HDS 1032	-	7.62 ± 0.18 (n = 30)	7.26 ± 0.30 (n = 26)

Table 4.2: Results of interlaboratory comparison. The number of aliquots that was used for determining the D_e is mentioned between brackets. Uncertainties are 1 standard error and include the uncertainty arising from beta source calibration. The D_e values based on n > 100 were obtained using small aliquots containing ~0.5-1 mg quartz grains. These experiments will be discussed in section 4.9.

4.5.7.4. Evaluation of the MAAD and SAR technique

For the reasons outlined in section 4.5.7.2, the SAAD protocol was excluded from the investigations and in the following, only the MAAD and SAR techniques for equivalent dose determination are compared and discussed.

As shown in Figure 4.12a, the additive-dose growth curve for OS-B shows a considerable scatter at the highest dose point. Upon screening for feldspar contamination, no significant IRSL sensitivity was observed. The presence of a residual dose in some of the grains due to incomplete bleaching in the past was thought not to be very likely. In such a case, one would expect a higher scatter for the natural and the lower dose points and a lower scatter for the higher dose points because of a reduction of the relative size of the residual dose when laboratory dose is added (Wintle et al., 1995). Nevertheless, a bright grain with a large residual dose (the grain might perhaps not have been bleached at all) could be present in an aliquot, and this might dominate the natural luminescence signal. Therefore,

to examine the source of the scatter more closely, the individual dose-response curves were constructed for these aliquots using the SAR protocol. The same experimental conditions were applied as in the multiple-aliquot measurements (preheat, stimulation time, test dose size). The result is shown in Figure 4.18a. A repeat measurement of the first regenerative dose was conducted. The recycling ratios were equal to unity within analytical uncertainty, indicating that the sensitivity correction is working. From Figure 4.18a it is clear that the observed scatter can be explained in terms of different dose-response characteristics for the three aliquots. Similar differences in growth curve characteristics, albeit less pronounced, were found for the natural aliquots (e.g. see Figure 4.18b for sample OS-D). These findings clearly illustrate that even for an aliquot containing thousands of quartz grains, not necessarily all the variations in intrinsic luminescence characteristics between the individual quartz grains (see Section 2.8) are averaged out. Murray (2000) reported on similar observations for a Scandinavian sedimentary sample.

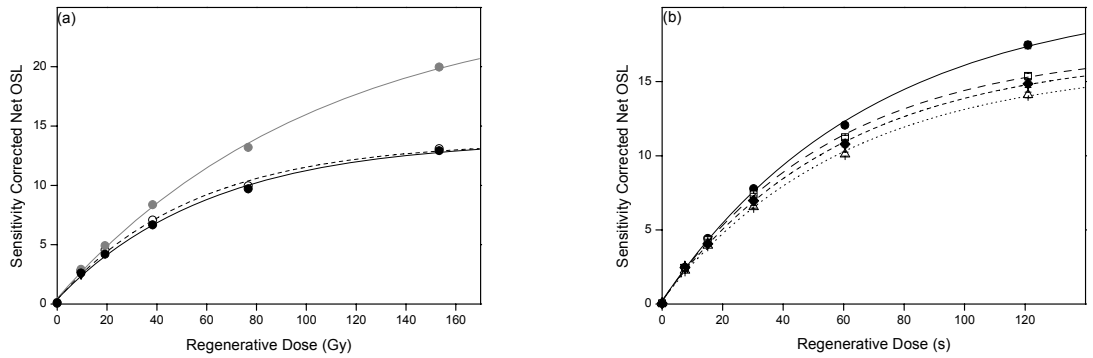

Figure 4.18 (a) Individual growth curves, constructed using the SAR protocol, for the three aliquots at the highest dose point of the multiple-aliquot additive-dose growth curve shown in Figure 4.12a (sample OS-B). (b) Same as in (a) but for the natural aliquots of the multiple-aliquot additive-dose growth curve shown in Figure 4.12b (sample OS-D).

The multiple-aliquot approach uses an average growth curve, composed of the sum of individual growth curves for each aliquot. The equivalent dose derived from it is then likely to be an average of the true D_e´s of the individual aliquots, as well as a mathematical artifact (owing to the fact that only a limited number of aliquots is measured), which could lead to the wrong answer. To allow a direct comparison between the MAAD and SAR protocol, the natural aliquots from the MAAD experiments were

also put through a complete SAR sequence, using the same experimental parameters. The D_e obtained with the multiple-aliquot approach (21.1 ± 3.6 Gy for OS-B and 17.1 ± 2.2 Gy for OS-D) is considered consistent with the average D_e obtained from the four natural aliquots using SAR (16.7 ± 0.4 Gy and 13.4 ± 0.2 Gy, for OS-B and OS-D, respectively; the uncertainties are the standard errors). Nevertheless, the underlying assumption in multiple-aliquot protocols is that all aliquots have identical luminescence characteristics, and identical resetting in the past (Murray and Olley, 1999). Because at least the first assumption is clearly false for one sample (and to a lesser degree for the second sample), the multiple-aliquot protocol was not further investigated.

The SAR-based D_e's for OS-B and OS-D calculated from the 160 – 260ºC plateau region [14.8 ± 0.2 Gy (n = 18) and 12.1 ± 0.1 Gy (n = 18), respectively] are significantly different from the values obtained from the four aliquots that were put through the SAR sequence after the MAAD measurements were performed (16.7 ± 0.4 Gy and 13.4 ± 0.2 Gy, for OS-B and OS-D, respectively). This discrepancy might arise from the different preheat conditions, but this remains to be further investigated (with the aid of dose recovery tests, for example). The MAAD values, on the other hand, are within 3s consistent with the D_e values based on the SAR preheat plateau region, although they show a tendency to be higher. The poor precision associated with the MAAD data (amounting to 40 – 50% on the 3s level) tends to might mask any systematic differences between the two techniques.

The generally good agreement of the observations on the SAR protocol with those described in literature, and the good behavior of the samples (recycling ratios close to unity, a negligible recuperation, and acceptable dose recovery), suggest that the protocol is applicable for the investigated deposits. Consequently, the D_e estimates obtained with this technique were used for age calculation (see Section 4.7).

4.6. Annual dose determination

Vancraeynest (1998), and more recently Hossain (2003), presented very detailed accounts and performance evaluations of the different methods for dose rate determination that are applied in the Ghent luminescence laboratory. In the following, therefore, only a brief

overview is given of the methods that were used in the present study, as well as some relevant experimental details.

Our study of the Ossendrecht section was carried out in close collaboration with Hossain, and some of the results have already been reported in his PhD thesis (namely those for samples S-1, S-2, S-A and S-D). As an annual dose is an essential part of an optical date, Hossain's results are included in the following, together with new results. This makes the whole chapter on the optical dating of the Ossendrecht coversands self-contained. Some minor differences between the calculated annual doses reported on in this work and those given in Hossain (2003) might be noted. This is owing to a different interpretation of the results and/or the use of a different set of conversion factors.

4.6.1. Gamma-ray spectrometry

4.6.1.1. Field NaI(Tl) gamma-ray spectrometry

Using this technique, the gamma-ray activity from naturally occurring radio-elements is measured at the sampling site by placing a NaI(Tl) detector in the auger hole from which the sample for OSL analysis was taken. Individual contributions from K (via ^{40}K, E_γ = 1460.8 keV), U (via ^{214}Bi, E_γ = 1764.5 keV) and Th (via ^{208}Tl, E_γ = 2614.4 keV) are obtained. The technique has the obvious advantage that the effect on the annual dose of any heterogeneity (such as rocks) surrounding the sample within a radius of 30-50 cm is taken into account.

Field gamma spectrometry was performed using our Canberra Portable Plus γ-spectrometry system, Model 1150. It is equipped with a 3 X 3 inch NaI(Tl) detector. The system was calibrated, in a relative way, by measurements in calibration blocks containing known amounts of K, U and Th. This procedure has been extensively outlined in Vancraeynest (1998) and Hossain (2003), and will receive some further attention in the following chapter. Throughout this work, use was made of the calibration measurements carried out in the Flossenburg granite block "Flossi", located at the Forschungstelle Archäeometrie (Max-Planck-Institut für Kernphysik) in Heidelberg, Germany. This "Heidelberg" calibration procedure was chosen for its simplicity, its better-defined uncertainty budget, the quasi-infiniteness of the granite block and because the "mixed"

calibration spectrum is more comparable to the natural spectrum. Rieser (1991) and Hossain and De Corte (1999) found an inhomogeneous distribution of K, U and Th in the block, but this is thought to introduce only a minor error compared to other sources of uncertainty arising from counting statistics and peak fitting (especially for U). This is supported by the good agreement that was previously found (Vancraynest, 1998; Hossain, 2003) between the results obtained via field measurements and via other analytical techniques.

As outlined in section 4.4, two measurements were performed at about the same stratigraphic level as OS-D and S-1. The collected spectra were analysed using Hypermet-PC (Fazekas et al., 1997), to obtain the net peak areas. The K, U and Th concentrations finally obtained are shown in Table 4.3.

	K (%)	U (mg kg^{-1})	Th (mg kg^{-1})
1^{st} measurement	0.530 ± 0.007	0.57 ± 0.04	2.09 ± 0.05
2^{nd} measurement	0.500 ± 0.005	0.63 ± 0.03	1.63 ± 0.04
Average	0.51 ± 0.01	0.60 ± 0.03	1.86 ± 0.23

Table 4.3: K, U and Th concentrations obtained via field gamma-ray spectrometry. Uncertainties on the individual results represent 1s and are from counting statistics only (this means that the systematic uncertainties associated with the measurements in the calibration block and with its specified radionuclide content are not included). Uncertainties on the averages are the largest of expected and observed uncertainties, and are 1s as well. The values have been corrected for the difference in composition and packing density between the sand and the granite calibration block following De Corte et al. (2003).

4.6.1.2. Low-background Ge gamma-ray spectrometry

The most important advantage of this technique is that it allows investigating the degree of radioactive equilibrium in the ^{238}U and ^{232}Th decay series in the samples. The high resolution of a HPGe detector and the low background that can be achieved when it is properly constructed and shielded, allows distinction between the several gamma-emitting daughters in these decay chains. From the measured daughter activities an equivalent U and Th concentration can be calculated. If the series are in equilibrium, the different daughters should yield equal parent concentrations, within statistical uncertainties. If not,

the chain is said to be in disequilibrium. As the daughters are identified, the position of the disequilibrium in the decay chain can be determined as well.

Reference is made to Hossain (2003) for an elaborate description of the apparatus, calibration, different measurement conditions and data processing procedures. Here only some relevant experimental details are summarised.

The extended-energy range HPGe detector "Bertha", was used for low-background gamma-ray spectrometry in the laboratory. All measurements were carried out on dried material (at 110°C, until constant weight). Enough material from the immediate surroundings of the dating samples OS-A, OS-D and OS-2 was collected (samples S-A, S-D and S-2, respectively; see Section 4.4), for the measurements to be carried out in a Marinelli geometry. A Marinelli measurement was also carried out for sample S-1, taken from the same stratigraphic level at a horizontal distance of about 20 cm from OS-D (and hence S-D). For all samples, with the exception of OS-4, the outer material that had been discarded from the sampling tubes (see Section 4.5.1) was also measured. These measurements were carried out in a "Bluecap" geometry (which is a simple plastic container with a screw-cap), because of the smaller amount of material available. The samples were sealed and stored for at least a month before being measured. The cylindrical samples were typically measured for about 4 weeks, following the recommendation by Hossain. The Marinelli beakers, on the other hand, were measured for two weeks. The spectra were processed using Hypermet-PC (Fazekas et al., 1997) to obtain the peak areas. Small corrections for different peak detection efficiency were made, based on effective solid angle calculation via the computer codes MARSANGLE (Jovanović et al., 1992) and SOLCOI (KAYZERO/SOLCOI version 5, 2003) for Marinelli and cylindrical geometry, respectively. For both measurement configurations, the system had been calibrated in a relative way using the well-characterised Volkegem loess as a secondary standard (Hossain, 2003; the Volkegem loess contains 1.784 ± 0.010 % K, 2.52 ± 0.02 mg kg^{-1} U and 10.22 ± 0.04 mg kg^{-1} Th; the uncertainties are 1 standard error).

The following daughter nuclides (and photo-peaks) of the ^{238}U decay series were considered: ^{234}Th (E_γ = 63.3 keV), ^{214}Pb (E_γ = 295.0 keV and 351.9 keV), ^{214}Bi (E_γ = 609.3

keV and 1764.5 keV) and ^{210}Pb (E_γ = 46.5 keV). For the Th decay series these were: ^{228}Ac (E_γ = 338.3 keV, 911.2 keV and 969.0 keV), ^{212}Pb (E_γ = 238.6 keV) and ^{208}Tl (E_γ = 583.2 keV and 2614.5 keV). The K concentration was obtained using the ^{40}K gamma line at 1460.8 keV. The gamma line from ^{214}Pb at 242.0 keV, as well as the line from ^{224}Ra at 241.0 keV, were omitted from the calculations because this doublet could not be reliably deconvoluted using the Hypermet-PC software.

The results for all measurements are shown in Figure 4.19 for U and Th, and in Figure 4.20 for K. It can be seen that for every sample, and in both the ^{238}U and the ^{232}Th decay series, the different daughter isotopes give quite consistent results. It is concluded that the decay series are in equilibrium. The results for K are self-explanatory. It can be noted that, compared to the other samples, sample OS-B yields a significantly higher K concentration. For this sample, also a distinctly higher U and Th concentration was found (Figure 4.19b).

Where a comparison is possible, some differences can be noted between the results obtained for the outer material of the OSL sample cylinders and those obtained for the surrounding Marinelli samples. The difference can amount to more than 20% (the U content of OS-2 versus that of S-2; Figures 4.19h and 4.19i, respectively) and does not seem to be systematic, being higher for one set of samples (OS-A versus S-A; Figures 4.19c and 4.19d, respectively) and lower for another (OS-D versus S-D; Figures 4.19e and 4.19f, respectively). This suggests that the observed discrepancies are not caused by a systematic error in the calibration or the calculation of the detection efficiencies for one of the two measurement geometries, but rather reflect a true difference in radionuclide content. Hence, the differences are interpreted as being caused by sample inhomogeneity.

As the Marinelli beaker contained about 1.5 kg of sample, any heterogeneity of the sample should be averaged out to a greater degree than for the “Bluecap”, which contained only about 70 g. Comparison of the Marinelli results for samples S-D and S-1, which were taken from the same horizontal level, indeed yield consistent U and Th results (Figures 4.19f and 4.19g, respectively). It can be noted, however, that their K concentrations differ by about 7%, which is small but nevertheless significant even at the 3s level (Figure 4.20).

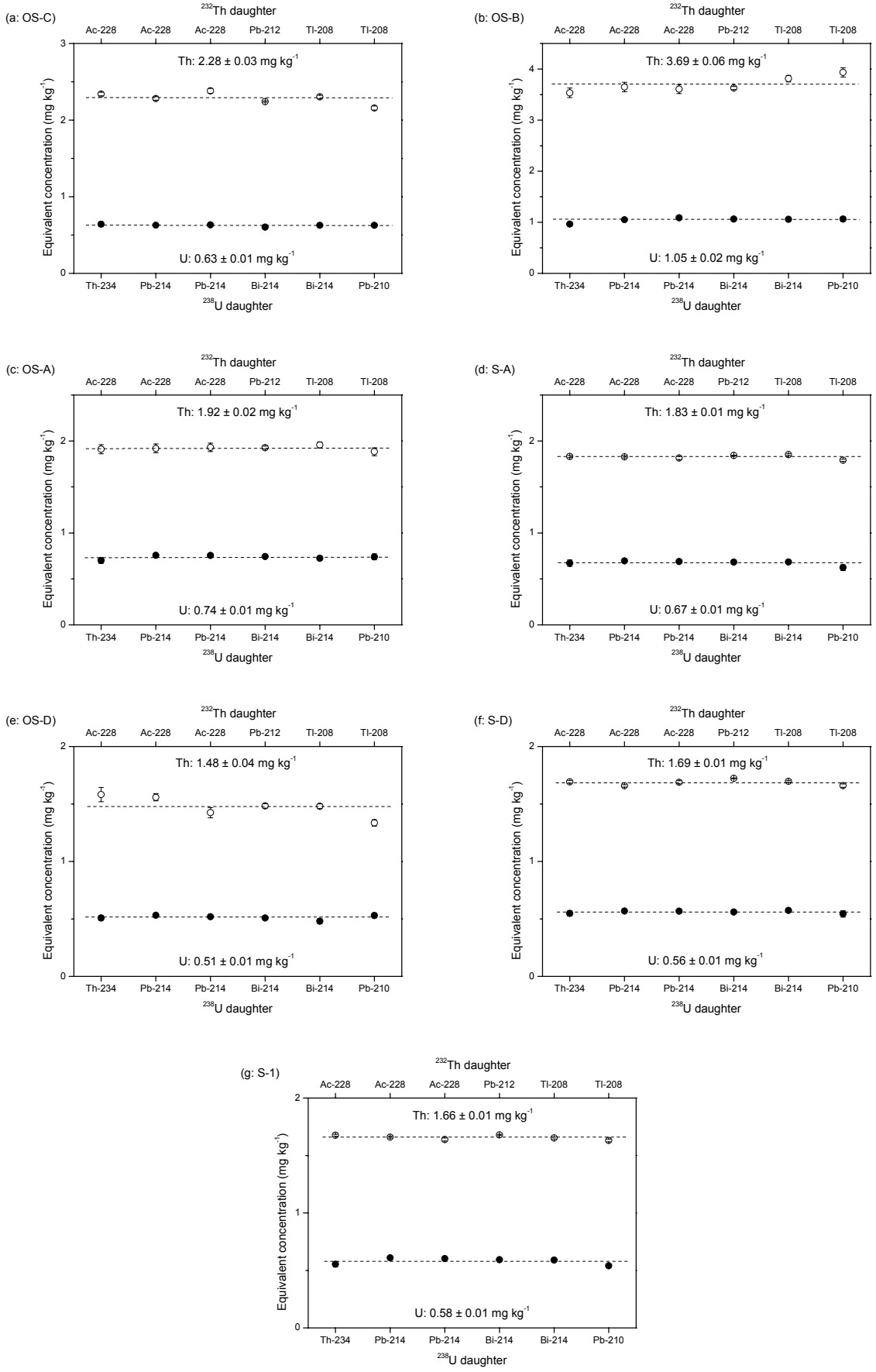

Figure 4.19: Results from low-level gamma spectrometry in the laboratory (continued on the next page).

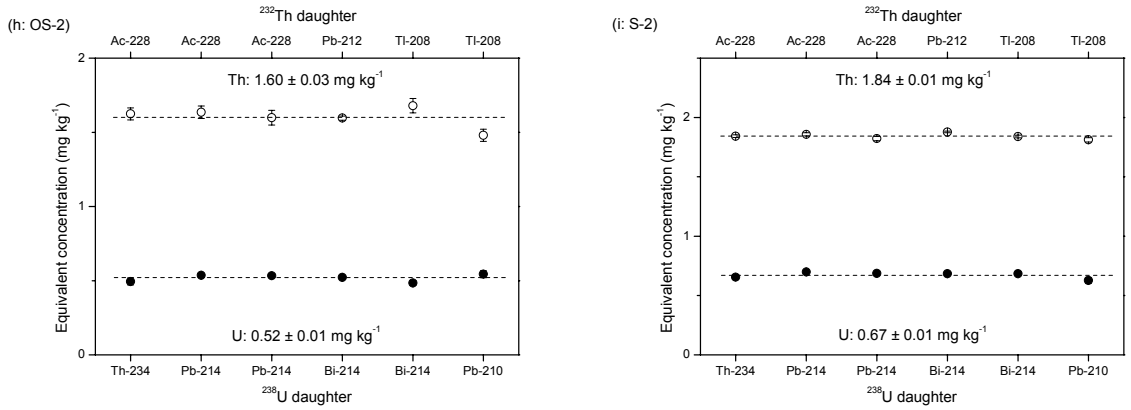

Figure 4.19 (continued): Equivalent U (solid circles) and Th (open circles) concentrations obtained via low-level gamma-ray spectrometry in the laboratory. The equivalent concentration is the concentration of U or Th that would be needed to give the observed activity of the daughters, if the series were in equilibrium. Sample identification is given in the upper left corner of each figure. The measurements for samples S-1, S-2, S-A and S-D (surrounding material) were carried out in a Marinelli geometry. For all other samples (the outer material that was discarded from the dating samples), the measurements were conducted in a cylindrical "Bluecap" geometry. The error bars are derived from the counting statistics only and represent 1s. The unweighted averages are indicated by the dashed line, and their values ± 1 standard error are given above (for Th) and below (for U) this line. The difference with the values reported by Hossain (2003) lies in the fact that the ^{214}Pb line (^{238}U-series) at 242.0 keV and the ^{224}Ra line (^{232}Th-series) at 241.0 keV line are omitted, as well as in the fact that, here, no systematic uncertainties are included.

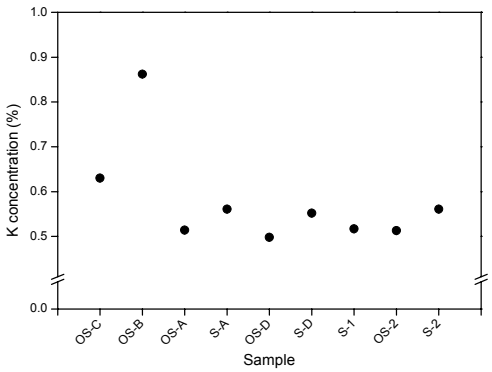

Figure 4.20: K concentrations obtained via low-level gamma spectrometry in the laboratory. The uncertainties represent 1s and are referring to the counting statistics on the net ^{40}K 1460.8 keV peak area only; it can be noted that the error bars are smaller than the symbols.

4.6.2. Neutron activation analysis

When a sample is irradiated with neutrons in a nuclear reactor, unstable radionuclides are formed. Upon decay, gamma radiation is emitted, which is characteristic for the elements

in the sample. Consequently, this allows their identification by gamma-ray spectrometry. The count-rate is then a measure of the concentration.

In this work, instrumental neutron activation analysis was used to determine the K, U and Th concentrations in most of the investigated sediments. The Rb content could be automatically obtained as well, but for the reasons outlined in Section 3.3.7, its contribution to the total annual dose was not taken into consideration. It is worth pointing out that, contrary to the gamma-ray spectrometry of natural samples, the concentrations of U and Th are now derived from the parents of the decay series, i.e. ^{238}U and ^{232}Th.

The k_0-method was used for standardization (De Corte, 2001a). The k_0-method has the advantage that it is a "standardless" method and that one does not have to deal with the individual nuclear constants (and their associated uncertainties and inconsistencies) as they are contained in experimentally determined k_0-factors. The total systematic uncertainty associated with the method is typically 3-4% in average experimental conditions (De Corte, 1987, 2001b; De Corte et al., 1987). This can be considered as a further advantage when comparing it to the systematic uncertainties associated with commercially available standards (certified or not) and other analysis techniques. At least for the k_0-method, all sources of uncertainty are known, as neither pains nor expense were spared in drawing up the uncertainty budget and in testing it with respect to accuracy and precision. The method furthermore has a proven adequate traceability (De Corte, 1987, 2001a).

About 100-200 gram of each sample was first pulverised (< 63 μm, either by ball milling, or by manually crushing in an agate mortar) to circumvent the problem of inhomogeneity encountered by Hossain (2003). From this material, at least two sub-samples of ~1 g each were retrieved for analysis. For samples OS-C, OS-A, OS-D and OS-2, purified quartz extracts were analysed as well, to get an idea of the internal radioactivity of the quartz grains (see Section 3.3.8). Due to the relatively small amount of purified quartz available in total, only 1 gram was taken for each sample, which was then subdivided into three smaller portions for analysis. The neutron irradiations were carried out in reactor "Thetis" of the Ghent University, for 7 hours in either channel 3 or 12. The certified Al-0.1%Au alloyed reference material (IRMM-530; Ingelbrecht et al., 1991) was used as comparator. After irradiation, the samples were measured on the calibrated HPGe detector "Amanda".

Spectrum analysis was performed with Hypermet-PC Version 5 (Fazekas et al., 1997) and concentrations were calculated using the PC-based software package KAYZERO/SOLCOI Version 5 (KAYZERO/SOLCOI, 2003). K was determined via the 1524.6 keV gamma line of ^{42}K, U via the 228.5 keV and 277.6 keV gamma lines of ^{239}Np, and Th via the 300.3 keV and 312.2 keV gamma lines of ^{233}Pa. More details on sample preparation, irradiation and measurement conditions, spectrum processing and concentration calculation procedures can be found in Hossain (2003).

All available results are summarised in Table 4.4. The uncertainties quoted are 1 standard error and are the largest of the observed and expected uncertainties. The number of sub-samples used (n), is given in a subscript between parentheses. The results for samples S-1, S-2, S-A and S-D are taken from Hossain (2003); the raw sample OS-2 was not analysed. Some differences can again be noted between the results obtained for the dating sample OS-A and those obtained for its surroundings (sample S-A). This is attributed to sample inhomogeneity. The results for OS-D, S-D and S-1, on the other hand, are quite consistent.

The results for the quartz extracts are shown in italics. Surprisingly, a significant portion of the U and Th seems to be contained within the quartz grains themselves. It must be pointed out that, under the given experimental measurement conditions (cf. Hossain, 2003), the analysis of such a small amount of material (each subsample contained about 0.3 g of quartz) might introduce a substantial systematic uncertainty in the calculation of the detection efficiency (10% or more; De Corte, private communication). Consequently, the absolute values of the concentrations given in italics in Table 4.4 might deviate from the true radionuclide contents correspondingly. Nevertheless, it is unquestionable that the purified quartz extracts do contain U and Th, as the induced activities could unambiguously be recognised in the recorded gamma spectra. A more detailed experimental study, with the purpose of obtaining more accurate information on the internal radioactivity in quartz grains, is being carried out at the time of writing. It can also be mentioned that, as far as annual dose calculation is concerned, the effective internal contribution is only small compared to that arising from the radioactivity external to the grains, and hence the associated uncertainty is largely diluted as well (see Sections 3.3.6-3.3.8).

Sample	K (%) *(mg kg^{-1})*	U (mg kg^{-1})	Th (mg kg^{-1})
OS-C	0.634 ± 0.006 $_{(2)}$	0.69 ± 0.01 $_{(2)}$	2.35 ± 0.05 $_{(2)}$
	79.7 ± 1.7 $_{(3)}$	*0.48 ± 0.01 $_{(3)}$*	*0.58 ± 0.01 $_{(3)}$*
OS-4	0.652 ± 0.026 $_{(2)}$	0.71 ± 0.02 $_{(2)}$	2.30 ± 0.07 $_{(2)}$
	n.a.	*n.a.*	*n.a.*
OS-B	0.839 ± 0.002 $_{(2)}$	1.09 ± 0.06 $_{(2)}$	3.69 ± 0.02 $_{(2)}$
	n.a.	*n.a.*	*n.a.*
OS-A	0.543 ± 0.005 $_{(3)}$	0.89 ± 0.02 $_{(3)}$	2.34 ± 0.07 $_{(3)}$
	106.4 ± 0.5 $_{(3)}$	*0.51 ± 0.01 $_{(3)}$*	*0.51 ± 0.01 $_{(3)}$*
S-A$^{(a)}$	0.558 ± 0.004 $_{(6)}$	0.70 ± 0.01 $_{(6)}$	1.91 ± 0.03 $_{(6)}$
OS-D	0.516 ± 0.004 $_{(2)}$	0.58 ± 0.01 $_{(3)}$	1.57 ± 0.03 $_{(3)}$
	33.47 ± 0.3 $_{(1)}$	*0.15 ± 0.01 $_{(1)}$*	*0.34 ± 0.01 $_{(1)}$*
S-D$^{(a)}$	0.496 ± 0.002 $_{(3)}$	0.58 ± 0.01 $_{(3)}$	1.66 ± 0.05 $_{(3)}$
S-1$^{(a)}$	0.507 ± 0.003 $_{(3)}$	0.56 ± 0.01 $_{(3)}$	1.58 ± 0.02 $_{(3)}$
OS-2	n.a.	n.a.	n.a.
	92.8 ± 2.6 $_{(3)}$	*0.26 ± 0.01 $_{(3)}$*	*0.34 ± 0.01 $_{(3)}$*
S-2$^{(a)}$	0.541 ± 0.009 $_{(3)}$	0.61 ± 0.01 $_{(3)}$	1.70 ± 0.04 $_{(3)}$

Table 4.4: K, U and Th concentrations obtained via k_0-NAA. The results for the purified quartz extracts are given in italics. Uncertainties represent 1s, the largest of the observed and the expected uncertainty being adopted. The number of analysis leading to the given averages is shown in the subscript between parentheses. The superscript (a) denotes results adopted from Hossain (2003).

4.6.3. Thick source alpha counting

The principle of alpha counting is based on the property of some materials (scintillators) to emit light (photons or scintillations) when they interact with ionising radiation. The photons are measured using a photomultiplier tube, leading eventually to the registration of a number of pulses per unit of time (count-rate) that is proportional to the activity of the sample. In the case of thick source alpha counting, alpha particles emitted by the U and Th

decay series are measured, making use of zinc sulphide as scintillator. From the measured count-rate, the annual dose can be calculated using conversion factors (see the Appendix). Use was made of an ELSEC (Littlemore Scientific) 7286 low-level α-counting system. Experimental set-up and calibration of the apparatus are described in Hossain (2003). For the underlying theory of thick source alpha counting reference is made to Turner et al. (1958) and Aitken (1985). Commercially available ZnS screens (Ø = 42 mm, from Littlemore Scientific) were used as scintillation screens.

Alpha counting was carried out for samples S-A, S-D, S-1 and S-2 by Hossain (2003); no other samples were measured. The measurements were carried out on about 1 g of dried (at 110°C, until constant weight) and pulverised (< 63 μm, using a ball-mill) material, that was spread out on the ZnS screens. As the most energetic alpha particles have only a range of about 50 μm, this means that the sample is presented as an infinitely thick source. Only one counting was performed, namely after the sample was sealed and stored for at least four weeks. More details on the sample preparation and measurement procedure can be found in Hossain (2003). The measured alpha count-rates he obtained are shown in Table 4.5*.

Sample	Measured alpha count-rate (counts per 10ks)
S-A	22.24 ± 0.47
S-D	18.63 ± 0.43
S-1	19.45 ± 0.40
S-2	21.31 ± 0.44

Table 4.5: Measured (sealed) alpha count-rates (counts per 10 ks) for samples S-A, S-D, S-1 and S-2. The data are from Hossain (2003).

4.6.4. Evaluation of the results

When making a comparison between methods, it is necessary to take the systematic uncertainties associated with each method into account. For k_0-NAA, this systematic

* Hossain (2003) gives no information on the pairs (see the Appendix) registered during this counting.

uncertainty is rather well defined to ~3.5% (De Corte, 2001b). For low-level gamma-ray spectrometry, an estimated total systematic uncertainty of 2.5% was adopted (1σ). This is based on the uncertainties on the K, U and Th concentrations in the standard, and an additional 2% for the calculation of the detection efficiencies (De Corte et al., 1987). The systematic uncertainties associated with the field measurements are estimated at ~4%, ~13% and ~8% for K, U and Th, respectively. This will be further discussed in Chapter 5. Following Vancraeynest (1998), a total uncertainty of 5% was adopted on the measured alpha count-rates (this incorporates the statistical uncertainty of ~1.5% and an estimated systematic uncertainty owing to differences in the efficiency of ZnS screens and the differences in sample properties).

The comparison between k_0-NAA and low-level gamma-ray spectrometry is shown in Figure 4.21. Note that the error bars represent 1s. As no disequilibria were detected in the decay series (see Figure 4.19), the U and Th concentrations adopted for low-level gamma-ray spectrometry are the averages calculated from all the daughter isotopes.

For K and Th (Figure 4.21a and 4.21c, respectively), the average ratio is consistent with unity within 1s; for U this is achieved within 2s (Figure 4.21b). The average ratios (indicated by the open circles in Figure 4.21) are 0.99 ± 0.02, 1.05 ± 0.03, 1.03 ± 0.03, for K, U and Th respectively. In general, it is therefore concluded that neutron activation analysis and low-level gamma-ray spectrometry in the laboratory yield consistent results. This is in agreement with the earlier findings by Hossain (2003) on a more limited data set. In the present work, the results obtained via both methods were consequently also used for the final annual dose calculation (see Section 4.7).

When looking at the comparisons for each sample and each element individually, the discrepancy between NAA and gamma-ray spectrometry is clearly the highest for sample OS-A (~20% for U and Th). For the other samples, any deviation from unity does not exceed 10%. As there is no clear indication for one of the two techniques yielding either systematically higher or lower results for none of the three elements, it is suggested that at least some of the differences can probably be explained in terms of sample inhomogeneity.

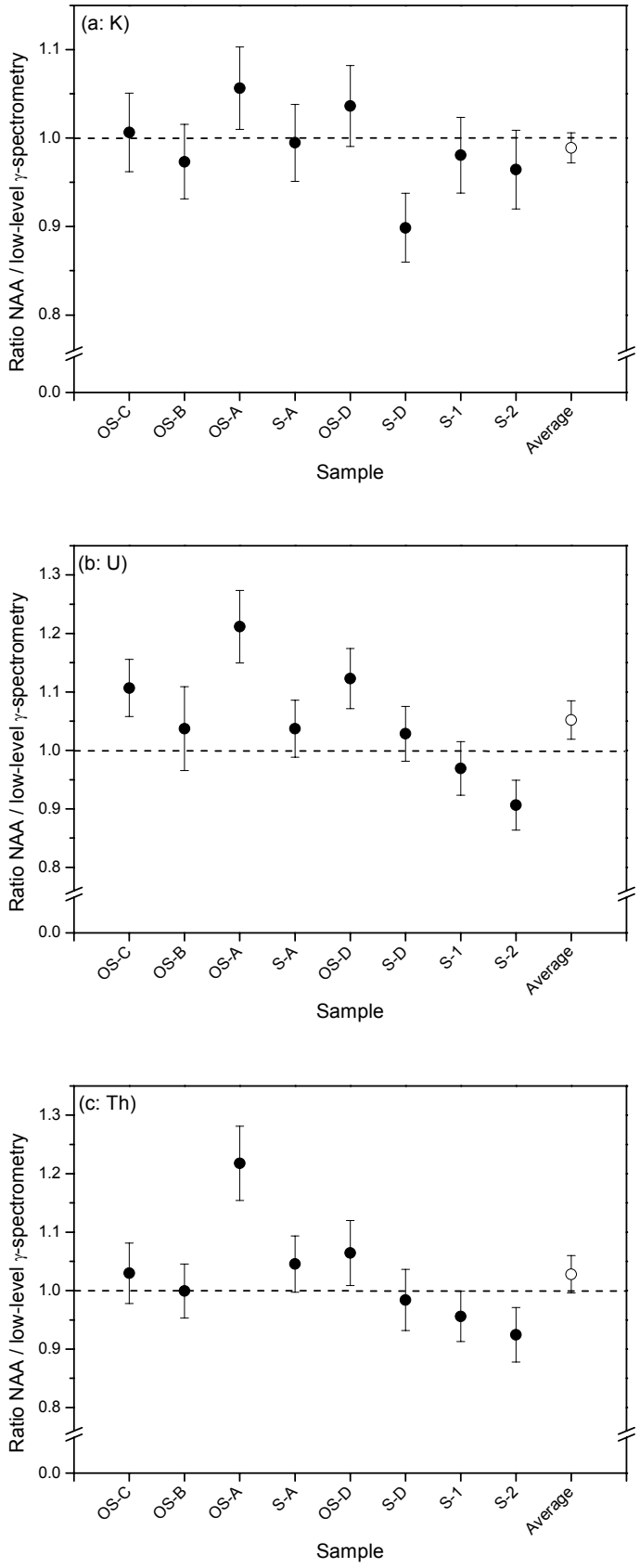

Figure 4.21: Comparison of the results obtained via k_0-NAA and low-level gamma-ray spectrometry in the laboratory for K (a), U (b) and Th (c). The error bars take systematic uncertainties into account, and represent 1s. The dashed line is meant as an eye guide and indicates a ratio equal to unity.

Figure 4.22 compares the results obtained via gamma-ray spectrometry in the field (i.e. the average of the two field measurements), with the average of the results obtained for samples OS-D, S-D and S-1 via low-level gamma-ray spectrometry and neutron activation analysis. Note that the values obtained via field gamma-ray spectrometry have been corrected for the difference in composition between the calibration block (granite) and the sand (De Corte et al., 2003). Error bars are 1s and include systematic uncertainties (for the average of NAA and low-level gamma-ray spectrometry, a systematic uncertainty of 3% was adopted).

For all three elements, the ratios are consistent with unity within 1s uncertainties (1.00 ± 0.06, 1.06 ± 0.15 and 1.16 ± 0.18, for K, U and Th, respectively). Unfortunately, these uncertainties are rather large. For U, this is due to the fact that the ^{214}Bi peak (at 1764.5 keV) in the field gamma-ray spectrum is tightly squeezed between other peaks, a spectral situation that seriously disturbs the reproducibility of the peak fitting (hence the large systematic uncertainty of ~13% associated with the U determination; see Chapter 5). For Th, on the other hand, the large uncertainty arises mainly from the large discrepancy between the results obtained via the two field measurements. As can be seen from Table 4.3, only the second measurement yields truly consistent values with those obtained for OS-D, S-1 and S-D via NAA and laboratory gamma-ray spectrometry. The exact location of where the field measurements were carried out is poorly documented, so it cannot be ruled out that that the measurements were actually performed at a different stratigraphic level. For this reason, it was decided to exclude the results obtained via the field measurements from the annual dose calulations.

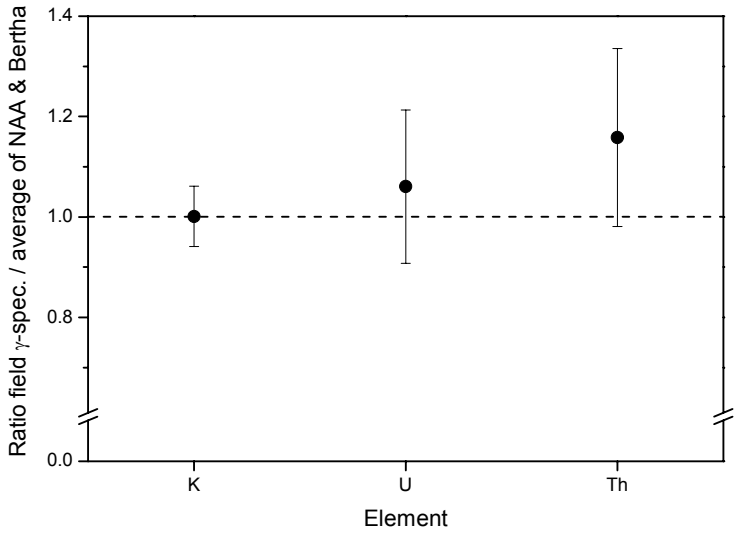

Figure 4.22: Comparison between the K, U and Th concentrations obtained via field gamma-ray spectrometry and the average concentrations obtained via NAA and low-level gamma-ray spectrometry in the laboratory (denoted by "Bertha"). Error bars represent 1s. The dashed line is meant as an eye guide and indicates a ratio equal to unity.

Finally, the measured alpha count-rates can be compared to those calculated from the average U and Th concentrations obtained via NAA and low-level gamma-ray spectrometry*. This comparison is shown in Figure 4.23. It can be seen that for the four samples, the individual ratios are consistent with unity within 2s. The overall average of 1.09 ± 0.03 (± 1s), nevertheless, indicates a systematic discrepancy. This might seem to contradict the conclusions of Hossain (private communication; 2003), who found an excellent agreement between measured and predicted count-rates. This difference, however, can be entirely subscribed to the use in this work of the more recent conversion factors by Adamiec and Aitken (1998), instead of those given by Aitken (1998) that were used by Hossain. As outlined in the Appendix, Adamiec and Aitken (1998) reported alpha range values that are about 6 to 7% lower than those given by Aitken (1998). This leads to corresponding differences in predicted count-rates, and consequently, to the discrepancy shown in Figure 4.23 that previously went undetected.

It is clear that the interpretation of the results is dependent on what set of nuclear data are used, a situation that is somewhat disturbing. Using the techniques employed in this work, however, conversion factors are indispensable for obtaining annual doses, and one simply has to rely on their accuracy. Throughout this work, it was assumed that the most recent

* The conversion factors that are necessary to convert concentrations into alpha count-rates are given in Table A.2.

values are more reliable, because they are based on more complete experimental data sets and improved calculation techniques. It is therefore concluded that the four Ossendrecht samples seem to suffer from a small degree of overcounting, which is why the results from alpha-counting were rejected for annual dose calculations. It can be pointed out that the observations are attributed to overcounting, rather than being related to sample inhomogeneity, because all four of the samples yield ratios higher than unity. If sample inhomogeneity effects would play a role, one would expect the ratios to be somewhat more scattered around the ideal value of unity.

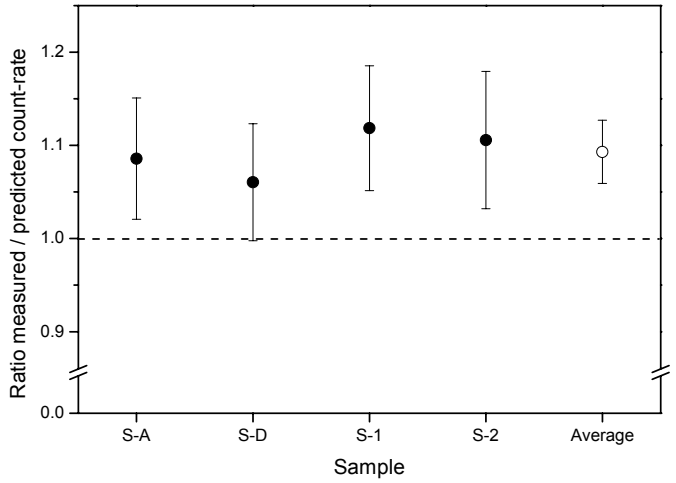

Figure 4.23: Comparison of measured and calculated (from the average U and Th concentrations obtained via NAA and low-level gamma-ray spectrometry) alpha count-rates. Error bars are 1s and include both random and systematic uncertainties. The dashed line at a ratio equal to unity is meant as an eye guide. The measured count-rates are those from Hossain (2003).

4.6.5. Conversion factors

The elemental K, U and Th concentrations can be converted to dose-rates using conversion factors. These are calculated from the energy carried by the emitted particles and radiations given in nuclear data tables. As these nuclear data are continuously refined, correspondingly updated conversion factors have been tabulated in the literature over the years. Reference is made to the paper by Adamiec and Aitken (1998) for a historical overview. In this work, use was made of the conversion factors derived by Adamiec and Aitken (1998) to convert concentrations to dose-rates (Table 4.6). They are based on the ENSDF* tables from the 22nd of June 1998.

* Evaluated Nuclear Structure Data File – a computer file of evaluated experimental nuclear structure data maintained by the National Nuclear Data Center, Brookhaven National Lab, for the International Nuclear Structure and Decay Data Network (file as of June 22, 1998).

	$\dot{D}_\beta$	$\dot{D}_\gamma$
Th	0.0273	0.0476
natural U*	0.146	0.113
K	0.782	0.243
Rb	0.019	-

Table 4.6: Conversion factors for the calculation of dose-rates (Gy ka^{-1}) from elemental concentrations of 1 mg kg^{-1} U or Th, 1% K and 50 mg kg^{-1} Rb (from Adamiec and Aitken, 1998). Note that for coarse-grain dating the alpha contribution from radioactivity external to the grains is made negligible by etching. *: abundance by weight ^{238}U: 99.29%, ^{235}U: 0.71%. The conversion factor for Rb is included for the sake of completeness; for the reasons outlined in Section 3.3.7, its contribution to the annual dose was neglected in this work.

Likewise, for the conversion of alpha count-rates to annual doses (or of concentrations to alpha count-rates), use is made of conversion factors. As the results from alpha counting were not used for annual dose calculation (see Section 4.6.4), it is of little use to mention them here. The values are given in the Appendix (Tables A.1 and A.2), where some aspects of alpha counting are considered to greater detail.

4.7. Age calculation, optical ages and discussion

Table 4.7 summarizes all the analytical data from Sections 4.5 and 4.6 that are relevant to the age and uncertainty calculation, and includes the final optical dates.

For annual dose calculation, the averages of the radionuclide concentrations obtained via gamma-ray spectrometry and k_0-NAA were used (see Section 4.6.4). It can be noted that the annual dose for sample OS-4 is derived from NAA solely, as for this sample no gamma-ray spectrometry was carried out. For the samples below the Usselo soil (OS-A, OS-D and OS-2) the results obtained for the immediately surrounding material (S-A, S-D and S-2, respectively) are included, while for OS-D the results from S-1 are taken into account as well. The observed uncertainty was adopted and the uncertainties quoted are 1 standard errors. The results for the etched quartz extracts (where available) are shown in italics. To estimate the internal contribution to the annual dose for samples OS-4 and OS-B, the average of the U, Th and K concentrations obtained for the etched quartz from the other samples was used, with an associated systematic uncertainty of 50% being adopted.

Note that in Table 4.7, all concentrations have been converted to specific activities (Bq kg^{-1}).

As outlined in Section 4.6.5., annual doses were calculated using the conversion factors of Adamiec and Aitken (1998). The systematic uncertainty associated with this conversion was estimated at 3% (Murray and Olley, 2002). The external beta dose-rate was corrected for the effect of attenuation and etching (see Section 3.3.7), and both the beta and gamma contributions were corrected for the effect of moisture (see Section 3.3.5.). Based on the fact that the impermeable clay bed of the Tegelen Formation causes water saturated conditions in the sand unit above, a value for $F = 0.9 \pm 0.1$ was assumed for this. The external dose rate given in Table 4.7 also includes the contribution from cosmic rays, which was calculated following Prescott and Hutton (1994), assuming an uncertainty of 15% (see Section 3.3.3.). As the different intercalated soils have been radiocarbon dated (see Section 4.3.), some information is available on the duration that each sample had been buried at a certain depth. This was exploited to calculate "time-weighted" average cosmic dose rates, yielding values of ~0.14 Gy ka^{-1}. An alpha efficiency factor of 0.04 ± 0.02 was assumed to calculate the internal alpha dose rate, based on the work by Rees-Jones and Tite (1997). To calculate the absorbed beta dose fractions, use was made of the data tabulated by Mejdahl (1979), with an associated uncertainty of 5% (Aitken, 1985). It is worthwhile mentioning that the internal dose rate in the etched quartz grains was not completely negligible, values between 3.2% (OS-D) and 7.5% (OS-A) of the external dose rate being found (Table 4.7).

The equivalent dose given in Table 4.7 represents the average D_e across the 160-260ºC region in the SAR D_e versus preheat temperature plot (Figure 4.15). The ages were then obtained according to equation 3.1, i.e. by dividing the equivalent dose by the total effective annual dose. Uncertainties on the luminescence ages were calculated following the error assessment system proposed by Aitken and Alldred (1972) and Aitken (1976), which is also summarized in Appendix B of Aitken (1985). In addition to the previously mentioned uncertainties, the uncertainty arising from the beta source calibration (~2 %, based on the uncertainty associated with the calibration measurements and the gamma-irradiation of the calibration quartz; see Section 4.5.6.) and the uncertainty associated with the concentration calibrations (estimated at ~ 3%; see also De Corte, 2001b; Murray and Olley, 2002) were included in the final age uncertainty. It can be seen from Table 4.7 that the systematic uncertainty is dominant in the overall uncertainty on the ages, which typically amounts to about 6.5% (1s). Within this uncertainty, all ages are stratigraphically consistent.

	natural U ($Bq\ kg^{-1}$)	^{232}Th ($Bq\ kg^{-1}$)	^{40}K ($Bq\ kg^{-1}$)	*W*	*External Dose rate* ($Gy\ ka^{-1}$)	*Internal Dose rate* ($mGy\ ka^{-1}$)	D_e (Gy)	*Age* (ka)	*Random uncertainty* (%)	*Systematic uncertainty* (%)	*Total Uncertainty*	
											(%)	(ka)
OS-C	8.52 ± 0.43 *6.19 ± 0.05*	9.42 ± 0.14 *2.34 ± 0.06*	191.2 ± 0.6 *2.41 ± 0.05*	0.205	0.901 ± 0.007	62.27 ± 0.03	12.1 ± 0.2	12.6	1.73	5.75	6.00	0.8
OS-4	9.12 ± 0.30 *n.a.*	9.31 ± 0.29 *n.a.*	197.2 ± 7.9 *n.a.*	0.205	0.921 ± 0.020	45.99 ± 0.40	12.4 ± 0.3	12.8	3.30	6.25	7.07	0.9
OS-B	13.77 ± 0.25 *n.a.*	14.99 ± 0.01 *n.a.*	257.3 ± 3.5 *n.a.*	0.205	1.227 ± 0.009	45.99 ± 0.31	14.8 ± 0.2	11.6	1.51	6.07	6.25	0.7
OS-A	9.68 ± 0.63 *6.53 ± 0.05*	8.11 ± 0.47 *2.05 ± 0.06*	164.6 ± 3.3 *3.22 ± 0.02*	0.199	0.837 ± 0.014	63.07 ± 0.04	13.4 ± 0.3	14.9	2.66	5.72	6.31	0.9
OS-D	7.25 ± 0.13 *6.19 ± 0.17*	6.52 ± 0.13 *2.34 ± 0.03*	155.6 ± 2.5 *2.41 ± 0.01*	0.199	0.749 ± 0.007	23.83 ± 0.01	12.1 ± 0.1	15.7	1.22	5.86	5.98	0.9
OS-2	7.75 ± 0.58 *3.35 ± 0.14*	6.97 ± 0.28 *1.38 ± 0.04*	162.8 ± 4.2 *2.96 ± 0.08*	0.199	0.779 ± 0.014	34.80 ± 0.05	11.7 ± 0.2	14.4	2.44	5.80	6.30	0.9

Table 4.7: Radionuclide concentrations used for dose rate evaluation (uncertainties are 1 standard error), W values, calculated dose rates, D_e values, ages, and random, systematic and total uncertainties. Radionuclide concentrations for the etched quartz extracts are shown in italics (n.a., not available). The uncertainties mentioned with the D_e values and the analytical data are random. See text for details on the different sources of uncertainty and their contributions. The total relative uncertainty on the age was obtained by quadratic summation of the random and the systematic components (see Aitken and Alldred, 1972; Aitken, 1976).

The obvious way to evaluate the accuracy of the SAR-OSL ages is to compare them with the calibrated radiocarbon dates quoted in Section 4.3 (it can be recalled that all ^{14}C and OSL ages are expressed in ka before AD 2000). The weighted mean* OSL age for the samples above the Usselo Layer is 12.2 ± 0.7 ka. This is consistent with the ^{14}C ages of ca. 12.7 and 10.3 ka that bracket the deposition of the Younger Coversand II phase.

The OSL age of all three samples from below the Usselo Soil are older than the radiocarbon age of this soil (13.1 ka), which is in accordance with geological expectation. Their average age (15.0 ± 0.9 ka) indicates that the sediments were deposited at the Late Pleniglacial to Late-glacial transition. Therefore, the dates do not allow us to decide whether the sediments belong to the Younger Coversand I or to the top of the Older Coversand II. It is consequently also not possible to decide whether Pleniglacial coversand deposition continued into the Lateglacial without a clear deposition break during the Bølling, as indicated by previous findings (Kasse, 1999), or not. This illustrates the limit on the time-resolution achievable with the techniques used in this work.

Table 4.1 also includes an overview of luminescence dating research relevant to the present study. For instance, Bateman and Van Huissteden (1999) obtained OSL ages on stratigraphically equivalent deposits exposed in the Dinkel valley (E Netherlands). They used both the multiple-aliquot additive-dose approach without correction for thermal transfer or sensitivity changes, and the single-aliquot additive-dose approach. The comparison between these results and those given in Table 4.7 suggests that any of the three protocols for optical dating may yield acceptable ages. From the present work alone, one would arrive at a different conclusion, having full confidence in the SAR protocol only. It must be pointed out, however, that for instance for the SAAD protocol, it is not yet known how sensitive the D_e actually is to the criteria suggested by Stokes et al. (2000).

---

* Weighted averages have been calculated according to $A = \frac{\sum A_i / \sigma_i^2}{\sum 1/\sigma_i^2}$, in which A_i denotes the age for the i^{th} sample, and σ_i its associated overall uncertainty. The standard error on this average is given by $\sigma^2 = \sigma_s^2 + \sigma_r^2$, where the systematic contribution is given by $\sigma_s = \frac{\sum (\sigma_i)_s / \sigma_i^2}{\sum 1/\sigma_i^2}$, with $\sigma_i^2 = (\sigma_i)_s^2 + (\sigma_i)_r^2$, and the random uncertainty is defined by $\sigma_r^2 = \frac{1}{\sum 1/(\sigma_i)_r^2}$; the subscripts s and r refer to the systematic and random contributions, respectively. Reference is made to Aitken and Alldred (1972) or Aitken (1985, Appendix B) for more information on this procedure.

Fink (2000) also applied the SAR protocol to samples from the Ossendrecht site, which allows probably the most direct comparison. He obtained ages with a somewhat larger uncertainty compared to ours, but within analytical uncertainties (1s) both datasets are in excellent agreement.

It is appropriate to make a final remark on the uncertainties quoted on the optical dates in Table 4.7. As with the experimental determination of any quantity, it is important to have a good understanding of the different sources of uncertainty involved, and of their magnitudes. As an illustration, a detailed uncertainty budget is presented in Table 4.8 for one of the samples that was dated (sample OS-D). The uncertainty budget yields information, for instance, on how efforts should be directed to improve the precision on an optical age. Table 4.8 illustrates clearly that the systematic uncertainties provide the dominant contributions to the overall uncertainty. This is owing to the very high analytical precision by which D_e's can be determined using SAR, and by which annual doses can be obtained using sophisticated analytical techniques as NAA and gamma-ray spectrometry.

Uncertainty arising from	***A***	***B***
D_e determination	0.80 %	
annual dose	0.91 %	
a-value		0.83%
Calibration (β-source, conc. measurements)		3.06%
various parameters (conversion and attenuation factors)		3.51%
cosmic ray dose-rate		2.73%
water content		2.10%
Total Type A (random)	1.22%	
Total Type B (systematic)		5.86%
Total	5.98%	

Table 4.8: Uncertainty budget for sample OS-D. The uncertainty calculation followed the system outlined by Aitken and Alldred (1972) and Aitken (1976), and used the uncertainties described in the above.

To improve the quality on an optical dating result, it would hence be necessary to eliminate or reduce some sources of systematic uncertainty. Using more conventional techniques, such as those employed in this study, the question now obviously arises to what extent this can be accomplished. In this context, it is our opinion that the uncertainty budget shown in Table 4.8 is, for the time being, probably as good as it can possibly get. Indeed, one will always be confronted with calibration of the concentration measurements, a conversion from concentration to dose rates, etc… Hence, one simply cannot eliminate the uncertainties associated with these operations. A reduction of their contribution to the overall uncertainty, on the other hand, requires further analytical developments, such as improved reference materials and a better knowledge of nuclear data. Therefore, until these are available, it is concluded that it is hard, if not impossible, to obtain optical ages with uncertainties of, say, better than 5 to 6 percent using a conventional experimental set-up. Smaller uncertainties would be unrealistic. From a practical point of view, the importance of Table 4.8 lies in the fact that it puts the capabilities of the optical dating method into a better perspective.

4.8. Further equivalent dose determination using SAR

In the course of the optical dating of the Ossendrecht sediments, the distribution of equivalent doses was also investigated. The prime motivation for these investigations was a simple empirical curiosity about the appearance of these distributions. Indeed, this type of investigation is usually carried out with more functional purposes, i.e. when there is concern on the degree of resetting in the past (such as, for instance, for fluvial sediments). Windblown sediments, however, are expected to have been exposed to sunlight long enough for the OSL signal to be fully reset before burial. Taking also the experimental effort into account that goes into the construction of equivalent dose distributions, there is consequently comparatively little information available in the literature on the spread in D_e that can be observed for this type of deposits. Furthermore, to our knowledge, no investigations into the D_e distribution have previously been carried out for quartz from aeolian sediments deposited in the Netherlands and Flanders.

If a large number of equivalent doses were determined for an aeolian sample, it is reasonable to expect a tight and symmetric dose distribution for an aeolian sample.

Indeed, in the assumption that it was completely reset during transport and deposition, all grains should more or less yield the same equivalent dose and the width of the distribution should be predominantly determined by the precision of the luminescence measurements. Olley et al. (1998; see also Figure 3.14) examined the dose distribution for quartz from a modern Australian aeolian sand dune. While the majority of the aliquots indeed yielded a zero dose, as expected, they also found a few incomplete reset grains. Lepper et al. (2000) examined Holocene aeolian quartz sands from central Oklahoma and also found narrow D_e distributions with little asymmetry. Cause for concern, however, was presented by Murray and Roberts (1997; see also Section 3.2.3.2.), who examined the D_e distribution of quartz grains extracted from an aeolian archaeological deposit from southern Australia. An unexpectedly broad distribution was found and heterogeneity in the external beta-dosimetry was the most likely explanation. Duller et al. (2000) also obtained a broader than expected dose distribution for quartz grains extracted from a aeolian dune sand from Tasmania and concluded that his might be related to bioturbation or microdosimetry.

In this work, the single-aliquot regenerative-dose protocol was applied to small aliquots (~ 0.5 – 1 mg) of quartz extracted from the aeolian sand samples from Ossendrecht to obtain the distribution of equivalent doses. As will be shown, the obtained distributions were, however, broader than could be expected. These observations raised the concern that the scatter had been introduced at some stage during the implementation of the optical dating procedures, which explains why the investigations on the possible causes of the broad dose distributions are reported on in this chapter.

4.8.1. Determination of the D_e distributions

Equivalent dose distributions were examined for samples OS-C, OS-4, OS-A and OS-D. To construct the D_e distributions, the SAR protocol (in the form as originally suggested by Murray and Wintle, 2000a; see Table 3.3) was applied to aliquots containing about 0.5 to 1 mg of quartz. The reason for decreasing the number of grains on each aliquot (in the previous experiments aliquots containing 3-5 mg of quartz were used) was to accentuate any heterogeneity. For each aliquot, a complete growth curve was constructed. As outlined in Section 3.2.1.2.2, this involved a measurement of the natural luminescence

signal and of the response to various regenerative doses, each of these measurements being immediately followed by that of the response to a fixed test dose. The response to a zero dose and to a recycling dose (i.e. the response to the same dose as had been administered in the first regenerative dose cycle) was measured as well. The preheat temperature used for all samples was 10 s at 240ºC, based on the D_e versus preheat temperature plots shown in Figure 4.15. In this way, 120 equivalent doses were determined for each sample.

Figure 4.24 shows a selection of the growth-curves obtained for sample OS-D, and illustrates the wide variability in dose-response (see Section 2.8.3). All the samples behaved acceptably in the SAR protocol, as indicated by recycling ratios within the 1.0 ± 0.1 interval and a recuperation, on the average, of about 1 % of the natural corrected OSL signal. This is consistent with the earlier findings reported in the previous sections.

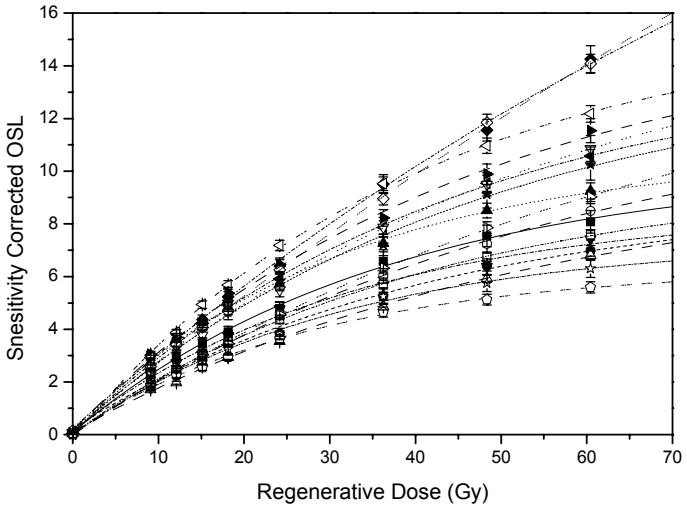

Figure 4.24: Some of the growth-curves obtained for sample OS-D, illustrating the variability in dose response.

The results of the D_e determinations are shown as histograms in Figures 4.25 (a) to (d), for samples OS-C, OS-4, OS-A and OS-D respectively. Of the 120 aliquots analysed for each sample, some had to be rejected because of a recycling ratio or IRSL/BLSL ratio exceeding a threshold set at 10%; the number of aliquots that was accepted is indicated in the upper left corner of each histogram. For all samples, it can be seen that the distribution is broad and Gaussian of shape, with a relative standard deviation of 11–12 %.

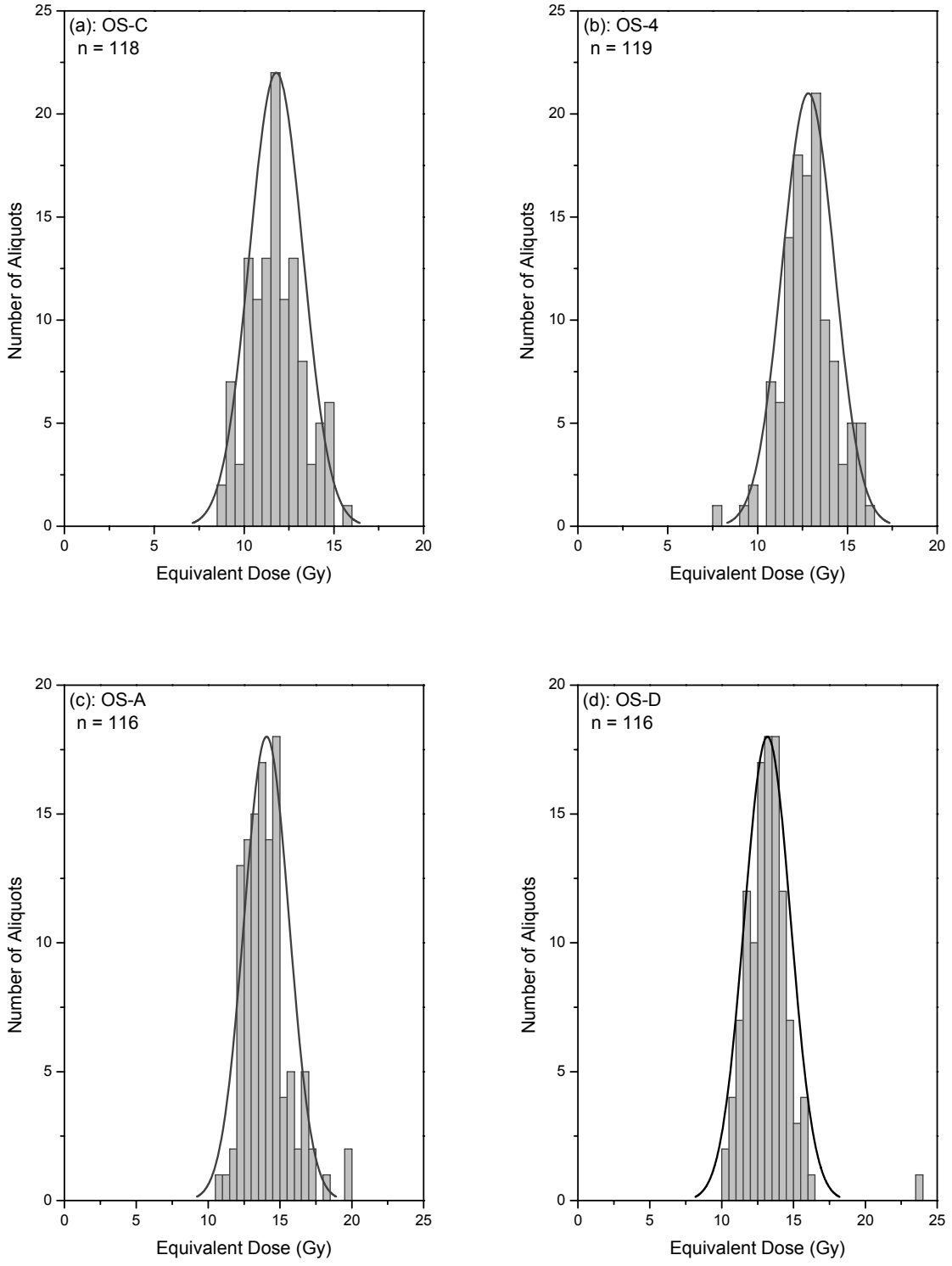

Figure 4.25: Dose distributions obtained for sample OS-C (a), OS-4 (b); OS-A (c) and OS-D (d). The total number of aliquots (n) is indicated in the upper left corner of each histogram. The normal distribution curve overlying the data is meant as an eye guide. The bin width that was used for plotting the data is 0.5 Gy, which corresponds, in general, to the uncertainty on each individual equivalent dose.

4.8.2. Investigations on the origin of the dose distributions

The uncertainty on the corrected natural OSL signals due to counting statistics is typically only about 4%, while the uncertainty on the D_e's arising from counting statistics is about 7%. Given also the fact that the samples are most likely to have been well bleached in the past, the broad distributions were therefore unexpected. The observations are all the more surprising since we are not dealing here with single grains, but with aliquots consisting of a few hundred grains. That this variation could be seen at this scale of analysis, as is also illustrated by the different shapes in dose-response curves (Figure 4.24), might indicate that only few grains contribute effectively to the measured luminescence signal. The distribution of signal intensity from single grains was investigated e.g. by Duller et al. (2000; see Section 2.8.1). They show that the fraction of grains that deliver about 95% of the total light sum can be as low as 5%. For such samples, multiple grain analyses would be dominated by these few grains. It has been shown in Section 4.5.7.4 (Figure 4.18) that for the samples from Ossendrecht, the variation is visible indeed, albeit to a lesser degree, even in larger aliquots of about 3 to 5 mg of quartz, composed of a few thousands of grains. The purpose of this study was, however, not to investigate how the distributions vary by reducing the scale of analysis (one can expect any heterogeneity to be accentuated), but rather to find an explanation for the variation as it was seen under the given measurement conditions. Three possible causes were investigated: scatter related to measurement procedures, partial bleaching and microdosimetric variations.

4.8.2.1. Experimental artefact?

The first concern was that the observed spread was due to an experimental error introduced at some stage during the measurement or data processing. To test the accuracy and precision of the measurement procedures, the recycling dose was treated as an unknown dose. The results for sample OS-D (similar results were obtained for the other three samples) are shown in Figure 4.26 as a radial plot (Galbraith, 1988; see Section 3.2.3.4.1). The known recycling dose was 9.1 Gy. It can be seen that the distribution obtained is now much narrower: 97% of the aliquots give the recycling dose within 2s (unweighted mean ± 1s = 9.3 ± 0.5 Gy). The uncertainty on the sensitivity corrected

recycled OSL signals due to counting statistics is about 4%, comparable to that for the natural dataset.

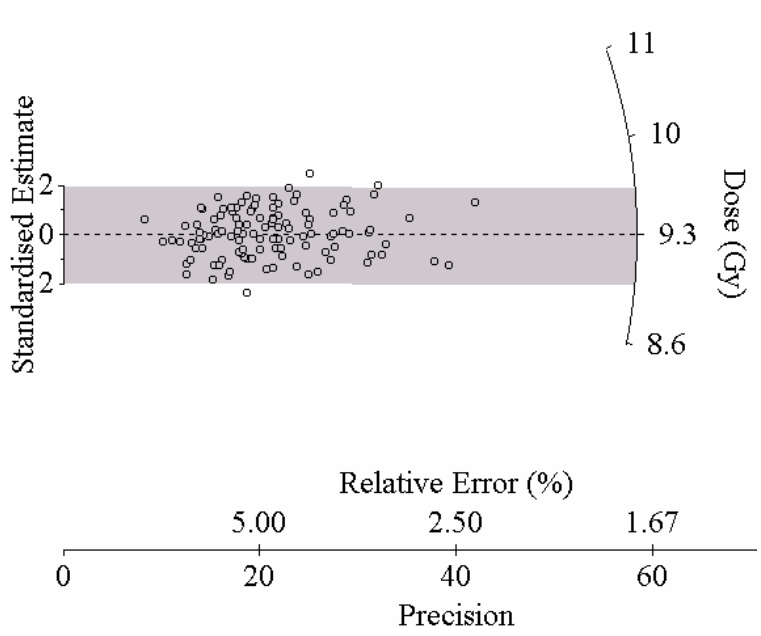

Figure 4.26: Radial plot of the D_e's obtained for 116 small aliquots of OS-D, when the recycling dose was treated as an unknown dose.

In a second experiment, the D_e distribution was reconstructed using heated (2 hrs at 500ºC, the efficiency of which was confirmed by the absence of a TL signal) and then gamma-dosed quartz, applying the same measurement conditions as for the natural sample. The sample used in this experiment was OS-D, as for this sample the largest amount of purified quartz was available. The given gamma dose was 11.7 Gy, close to its natural D_e of 12.1 Gy (see Table 4.7). The D_e results from 72 aliquots are shown in Figure 4.27 as a histogram to facilitate comparison with the natural data in Figure 4.25(d). The distribution is again much tighter, with an unweighted mean of 11.5 Gy and an RSD of 2.5%. The uncertainty arising from counting statistics is now reduced to ~ 1% due to an increased sensitivity caused by the heating.

In both experiments, use was made of heated material (either preheated in the recycling test, or heated before the gamma radiation). It was not investigated for previously unheated material how precisely a laboratory dose can be measured. The critical experiment, of measuring a 'perfect' natural dose can't be done, but a dose recovery experiment (see Section 4.5.7.3) would have been a more complete test to see if the unexplained extra uncertainty is related to measurement or analytical uncertainties. With

these reservations, and within the limits of the experiments described above, it can be concluded that the results from both experiments indicate that a true additional source of scatter is present in the natural data, which is not related to analytical or instrumental uncertainties.

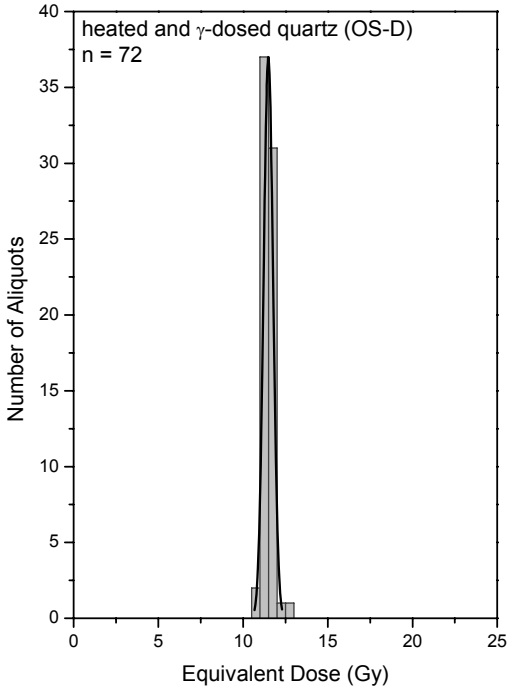

Figure 4.27: D_e's obtained for 72 small aliquots of heated and then gamma dosed quartz (from OS-D), presented as a histogram.

4.8.2.2. Partial bleaching?

A number of methods have been suggested in the literature to check for the presence of partial bleaching, most of them based on an analysis of the scatter seen in the luminescence data (e.g. Li, 1994; Murray et al., 1995; Clarke et al., 1999; Olley et al., 1998, 1999; see also the summary presented in Section 3.2.3.4.1). Colls (1999) suggested to construct standardized plots of D_e versus natural OSL intensity and to use a t-test to identify statistically significant relationships. The method was applied to the OS-D dataset, but no significant relationship could be established (Figure 4.28; $R^2 \approx 0.05$). The interpretation of these plots is, however, not straightforward. Wallinga (2002) concluded on the basis of computer simulations that the absence of such a correlation is not an

indication that the sample was well bleached. Besides, the use of these plots assumes that high D_e values are a priori associated with high natural OSL intensities. This is, however, an oversimplification as the specific luminescence originating from quartz grains has been found to be very heterogeneous (see Section 2.8.1). The usefulness of these plots is further limited because they do not allow differentiating between partial bleaching and microdosimetric effects.

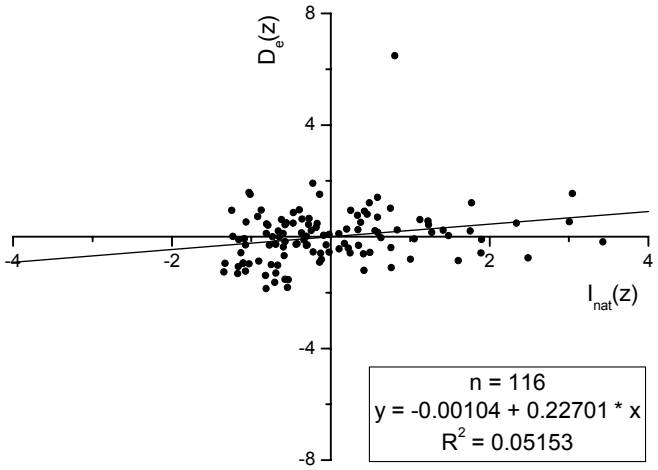

Figure 4.28: Plot of standardised D_e versus natural OSL intensity (following Colls, 1999) for the dataset shown in Figure 4.25(d).

The use of methods which are based on signal analyses are potentially more powerful tools for detecting and distinguishing between partial bleaching and microdosimetric effects. The applicability of $D_e(t)$ plots, as suggested by Bailey (2003a, b), was therefore investigated for the available dataset. As outlined previously in Section 3.2.3.4.2, the method uses the fact that the quartz OSL signal consists of different components (e.g. Bailey et al. 1997, Bulur et al. 2000) of which some are easier to bleach than others. Comparison of the D_e calculated from the initial OSL signal (which is most sensitive to light) with the D_e's calculated from later stimulation time intervals (which are more difficult to bleach), should then allow the identification of partial bleaching.

Using samples OS-D and OS-4, fully bleached and partially bleached samples were tested to see if they give flat and rising $D_e(t)$ plots, respectively. For each sample, a set of 24 aliquots was bleached for 40 s at 125ºC using the blue diodes at full power. They then received a dose of about 11 Gy, a preheat of 10 s at 240ºC and were subsequently, in sets

of three aliquots, partially bleached at room temperature and with a reduced power of the diodes. Each set was bleached for a different duration ranging from 0 to 30 s. Finally, the D_e was determined using the SAR protocol. It is worth mentioning that during these SAR measurements the stimulation power of the blue diodes was not decreased to obtain a higher resolution, as this had also not been the case during the measurements of the natural D_e distribution. The results are shown in Figures 4.29(a) and 4.29(d) for samples OS-D and OS-4, respectively. Upon partial bleaching, a rise in the plot clearly can be observed, the rise being more pronounced when the partial bleaching time increases. The open symbols in the figures represent the so-called replacement points (Bailey, 2003a), which are here the recycling points treated as an unknown signal. These should yield a flat $D_e(t)$ plot, since they were fully bleached in the preceding measurement cycle.

It was next tested (again using samples OS-D and OS-4) if the changes are preserved following further irradiation. For each sample, a second set of 24 aliquots was given the same treatment as in the first experiment, but received, after the partial bleach, a preheat of 10 s at 240ºC and an additional beta-dose of ~11 Gy to simulate the post-depositional irradiation. The results are shown in Figure 4.29(b) and 4.29(e) for samples OS-D and OS-4, respectively. The changes are indeed preserved after further irradiation, albeit to a lesser degree due to a dilution of the residual dose. Again, flat plots are observed for the replacement points.

These findings indicate that the method is applicable to the investigated samples, to a degree depending on the predepositional dose, the spectrum (Singarayer and Bailey, 2004) and the extent of bleaching in the past, and the signal intensity. No rising plots however were observed for the natural aliquots. This is illustrated in Figure 4.29(c) for an aliquot of OS-D and in Figure 4.29(f) for an aliquot of OS-4; both aliquots yielded a D_e higher than the overall average D_e calculated from all aliquots. The dip in the $D_e(t)$ plot of the natural aliquot at longer stimulation times is probably due to the interference of one of the slow components in the OSL signal of quartz (R. Bailey, private communication). The presence of such a complicating factor suggests that, despite the positive findings from the laboratory simulations, the usefulness of the SAR $D_e(t)$ technique for identifying partial bleaching in these samples is rather limited. This matter will be further discussed in Section 5.5.3.4.

Although the ability of the $D_e(t)$ method to identify partial bleaching is at its "worst' for windblown sediments (based on the findings by Singarayer and Bailey, 2004), it is precisely this windblown nature of the investigated sediments, combined with the good

agreement between the OSL and the independent age information (see Section 4.7), which makes partial bleaching unlikely. It was therefore investigated if small-scale variations in annual dose could offer an explanation for the observed scatter.

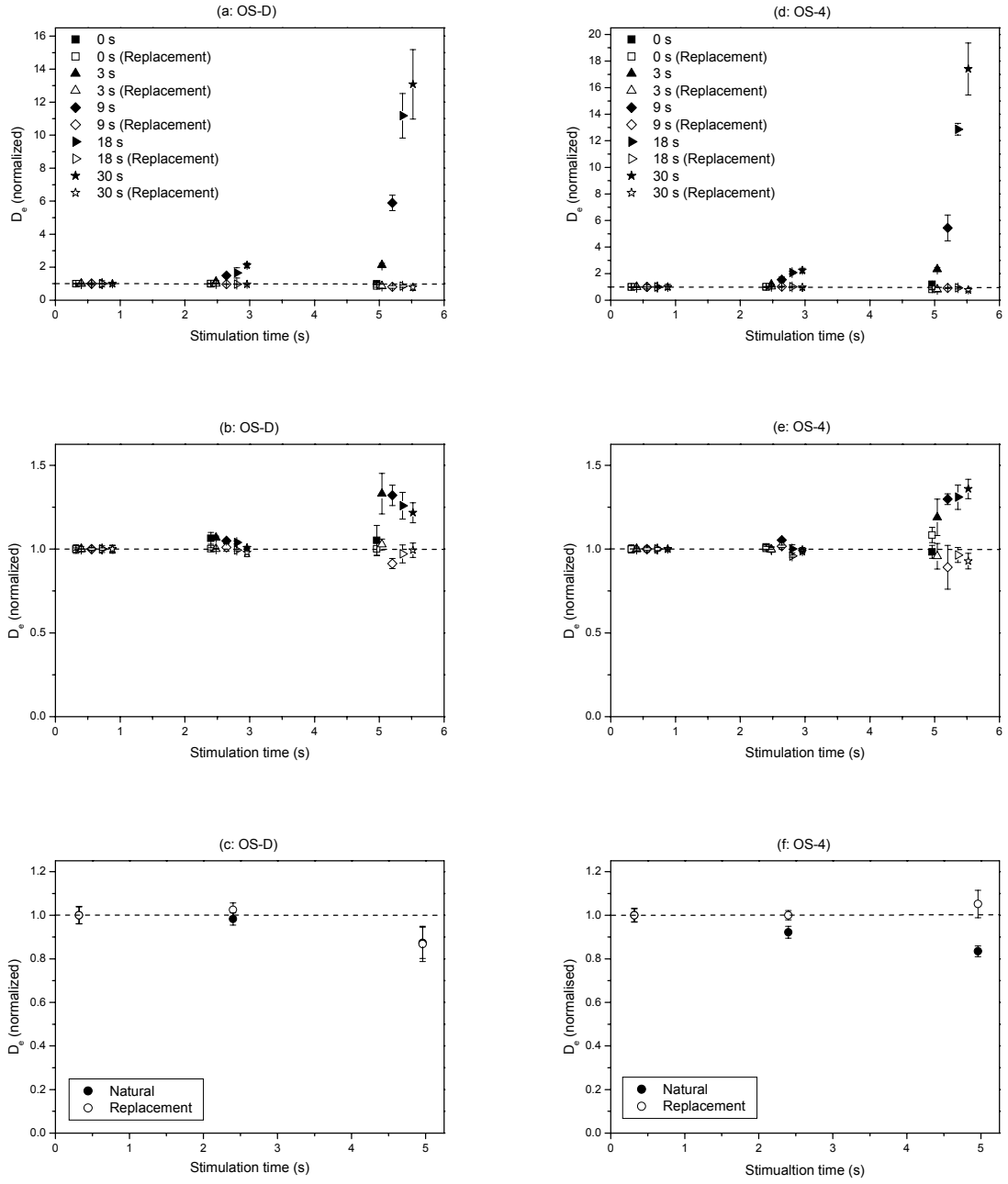

Figure 4.29: Test of the applicability of the SAR $D_e(t)$ technique on the investigated sediments: (a) $D_e(t)$ plots for aliquots of sample OS-D that were fully bleached, beta-dosed (~11 Gy) and partially bleached; the symbols are explained in the text. (b) Same as in (a), but after the partial bleach the aliquots received an additional irradiation (~11 Gy) to simulate the post-depositional irradiation. (c) Application of the SAR $D_e(t)$ technique to the natural aliquot of OS-D yielding the highest equivalent dose in Figure 4.25. (d) and (e) Same as in (a) and (b) but for sample OS-4. (f) Same as in (c) but for an aliquot of OS-4 yielding an above average D_e (~15.5) Gy.

4.8.2.3. Variations in microdosimetry?

The possibility of a heterogeneous distribution of radionuclides throughout the sediment profile was investigated using NAA of small amounts (0.5 – 1 g) of sediment. Experimental details on the analyses are the same as described in Section 4.6.2 (see also Hossain, 2003), with the exception that now the samples had not been pulverised. As was already discussed in Section 4.6.2, NAA of small amounts (~300 mg) of etched quartz was also performed for some of the samples.

The obtained K, U and Th concentrations are shown in Figures 4.30(a), (b) and (c), respectively. The results for S-A, S-D, S-1 and S-2 are taken from Hossain (2003). The graphs include the NAA results for U and Th obtained by Fink (2000), who applied OSL dating to the same sequence at Ossendrecht. The figures clearly show a large scatter in the results obtained for each sample, and between the different samples. The individual results have been normalized to an overall average calculated from all the results from all samples (indicated by the dashed line), to allow a more clear visualization of the variations. The random uncertainty introduced by the method of analysis itself is estimated at ~ 3%, based on a consideration of various possible sources such as weighing, flux gradients, an inhomogeneous distribution of Au in the Al-Au monitors, positioning of the sample on the detector, efficiency evaluation, counting statistics and gamma-peak fitting. This confirms that the observed scatter really reflects radioisotope heterogeneity and not an inherent difficulty with the method. In fact, the observation of such a heterogeneity was the reason why Hossain (2003) suggested pulverizing and homogenizing a large amount of sample before analysis, a procedure which was also adopted in this work (see Section 4.6.2).

The results for the etched quartz, where available, have been shown in Table 4.4 and indicate that a considerable amount of U and Th is present in the quartz grains themselves. Important here is that the internal contribution is not negligible, and can amount to 7% of the total dose rate.

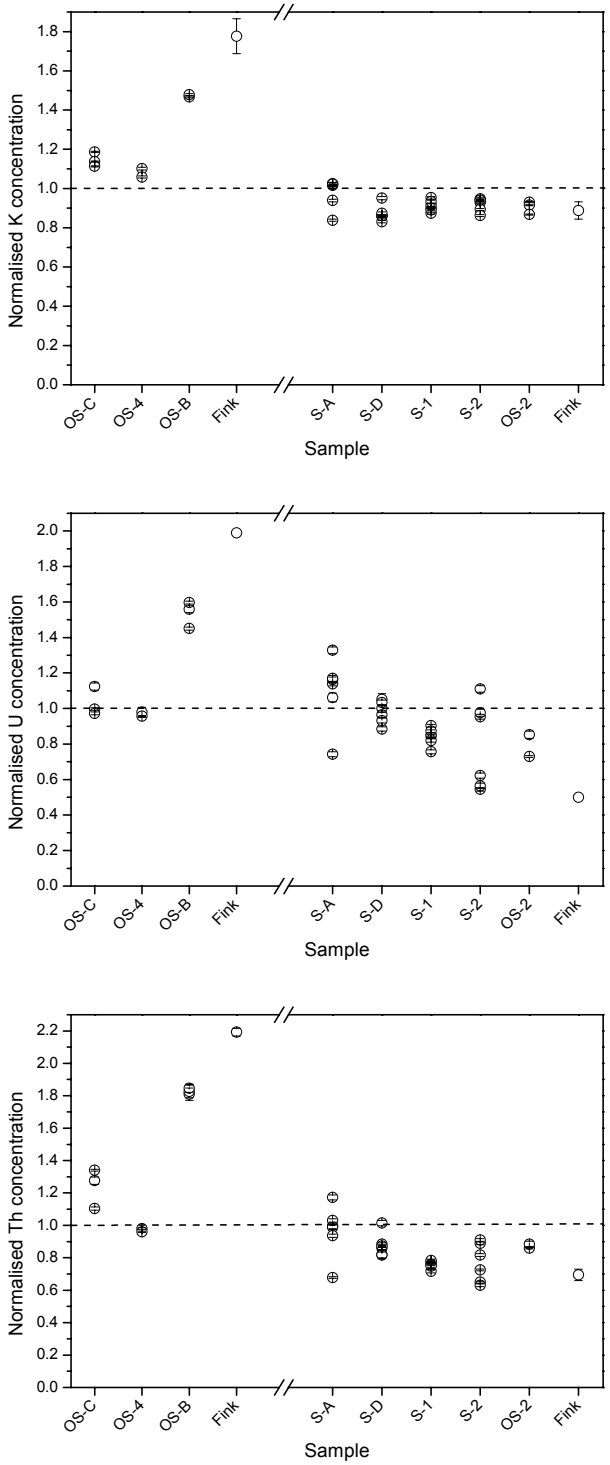

Figure 4.30: (a) K concentration obtained for all samples of the investigated sedimentary profile at Ossendrecht, as obtained by k_0-NAA of small amounts of sediment. The results are normalised to the overall average for visualisation purposes. The error bars represent 1s and are derived from counting statistics for K; for U and Th the largest of the observed and expected uncertainty was adopted. The break in the X-axis schematically represents the intercalated Usselo Soil. (b) Same as in (a) but for U, and in (c) for Th. Included in (a), (b) and (c) are the NAA results obtained by Fink (2000) on the same deposits. The uncertainties he gives for U vary between 8 and 25%.

4.8.3. Discussion

When the SAR protocol was applied to small aliquots of quartz extracted from the aeolian coversands from Ossendrecht, unexpectedly broad D_e distributions were found. These observations raised concerns as to the "goodness" of the implemented working practices. However, experiments in which the sample was artificially reset and dosed, showed that the scatter could not be due to any measurement related uncertainties. Although partial bleaching was not thought to be a very likely cause, because of the windblown nature of the deposit, this possibility was nevertheless investigated using the SAR $D_e(t)$ technique. After proving the technique to be able to identify artificially partially bleached samples, it was applied to the natural dataset. No evidence for partial bleaching was found. The possibility of small-scale variations in radioactivity was considered next. The presence of feldspar inclusions in the quartz grains could give rise to a locally significant beta dose from ^{40}K decay. However, no significant IRSL signals were observed, and aliquots yielding an IRSL/BLSL ratio higher than 10 % (3 out of 120 investigated) were rejected from the analyses. Heterogeneity in microdosimetry due to small-scale variations in water content is considered to be unlikely as well, given the fact that an immediately underlying clay bed causes water-saturated conditions in the sediment unit above, from which sample OS-D was extracted. It can be mentioned that no radioactive disequilibrium was discovered throughout the sedimentary unit (see Section 4.6.1.2). In this work, no experiments on single grains were conducted, so that no evidence can be presented to rule out grain-to-grain variations in internal radioactivity [as done by Murray and Roberts (1997) for an Australian aeolian sand]. However, it must be noted that the internal dose rate is not negligible (varying from 3.2 to 7.3% of the total dose rate). It is possible that detrital grains of chert, which have higher U and Th contents, are present in the sediment (Kasse C., private communication). Preliminary microscopic investigations of the etched quartz did not support this, but further examinations are needed to confirm their absence also from coarse grain size fractions. Coatings around the quartz grains could cause a heterogeneous attenuation of incoming radiation, which might be a further source of scatter. If the coatings contain some radioactivity, the dose rate estimated from the etched quartz grains would be an underestimate. At this point however, it remains to be established whether or not coatings are present, and further and more comprehensive work

is planned. Further thought is also given to the possible role of the fine fraction (silt and clay), which is certainly present in the samples under consideration. This fine fraction can act as a "surrogate" coating by resting in the pores between and very close to the quartz grains (Kasse C., private communication). As far as external variations in microdosimetry are concerned, a large spread was found in U and Th concentrations, as determined by NAA of several samples from the coversand unit. This indicates that the radionuclides are heterogeneously distributed throughout the sediment profile, a variation that is already visible at the 1 g level (the scale of analysis).

It is therefore concluded that differences in radioactivity on a very small scale are the most likely explanation for the observed D_e distribution. To establish whether external or internal variations in microdosimetry are the dominant factor, more investigations are necessary.

The effect on the age of the sample(s) investigated here is difficult to quantify, but is thought to be minor, given the good agreement between the optical and calibrated radiocarbon ages (See Section 4.7). Apparently the scale of analyses (sampling, D_e and annual dose determination) was large enough to average out any effects. In general however, as there is currently a tendency of reducing the scale of analyses (e.g. D_e determination on single grains and ICP-MS for radionuclide determination), the effects of a non-uniform beta-microdosimetry may become more important.

4.9. Conclusions

The implementation of the optical dating method in our laboratory involved an investigation of the applicability of three different techniques to determine the quartz equivalent dose (the multiple-aliquot additive-dose, the single-aliquot additive-dose and the single-aliquot regenerative-dose protocol). The quartz was extracted from a sequence of Upper-Pleniglacial to Late-glacial coversands exposed at the locality of Ossendrecht in the southwestern Netherlands. This site was chosen because of its windblown origin and because a number of radiocarbon dates are available that provide independent age control.

For each D_e determination technique to work for a given type of sediment, it is necessary that it fulfills the criteria on which it is based. From investigations of these underlying assumptions for each technique, it can be concluded that the single-aliquot regenerative-

dose protocol performs best. Furthermore, a small laboratory intercomparison on SAR D_e determination yielded an acceptable overall agreement, which gives confidence in the implementation of the technique and the results obtained. No specific methodological investigations were carried out with respect to the annual dose determination. Neutron activation analysis and low-level gamma-spectrometry in routine experimental conditions yielded results in acceptable agreement. The results obtained via field-gamma spectrometry and alpha counting, on the other hand, were interpreted as less reliable and were therefore not used for the age calculations.

A fair to good agreement was found between the SAR-based ages and the optical ages previously obtained on the same and equivalent deposits by other authors. Nevertheless, from all the data presented in the above, it is concluded that SAR is the technique of choice. From the good agreement between the SAR-based ages and the ^{14}C ages, it can be concluded that SAR also yields accurate results, which confirms previous findings (Murray and Olley, 2002; see also Figure 3.11) concerning the accuracy and robustness of this protocol. The distribution of equivalent doses in some of the samples was investigated explicitly, by applying SAR to small aliquots of quartz grains. This resulted in an unexpectedly wide spread in the data. A series of investigations was then conducted as to the origin of these D_e distributions, which indicated that small-scale variations in the annual dose are probably the main cause.

– CHAPTER 5 –

APPLICATION OF THE OPTICAL DATING METHOD

IN A CASE-STUDY:

the Late Pleniglacial coversands of Grubbenvorst

5.1. Introduction

The following chapter describes the application of the optical dating method to sandy sediments deposited between ~ 10 and 30 ka ago. The samples were taken from a site in the southern Netherlands, close to the village of Grubbenvorst.

In the Grubbenvorst sand pit, the exposed sequence of sediments bears witness to the landscape evolution in the southeastern Netherlands between the Last Glacial Maximum and the early Holocene, i.e. a time span encompassing the transition from very cold-climate conditions to the start of climatic amelioration. The sediments represent a quasi-complete record of these very important climatic fluctuations and the site is therefore considered as important for the stratigraphy of the southern Netherlands. Because of the scarcity of datable organic material, the age information is mainly based on correlation using palaeoclimate indicators and stratigraphic markers.

The good results obtained for the Ossendrecht samples (Chapter 4) indicated that optical dating could indeed provide accurate ages for sands. Therefore, to improve the chronology of the Grubbenvorst site and to provide the southern Netherlands with a well-dated locality, optical dating was also applied to these sediments.

5.2. Geological setting

The village of Grubbenvorst is located north of Venlo (in the southern Netherlands), on the Late Pleniglacial terrace at the western side of the Meuse valley (Figure 5.1). The sediments to be dated were sampled in a large quarry situated in the south of

Grubbenvorst (Figure 5.2). In the sandpit, a sequence of sediments is exposed comparable to the classic succession observed in the Dinkel Valley. The latter is well documented (see e.g. Van der Hammen and Wijmstra, 1971; Van Huissteden et al., 2000, 2001) and has been the subject of a number of TL and OSL dating studies (Dijkmans and Wintle, 1991; Bateman and Van Huissteden, 1999).

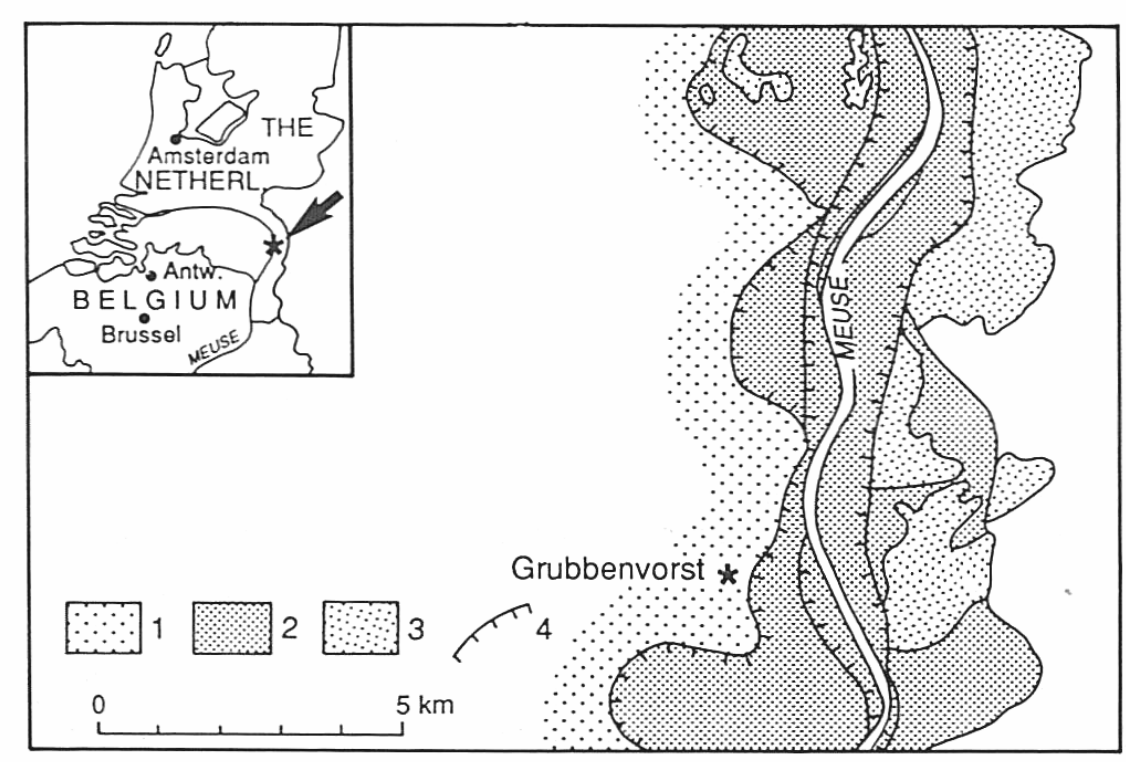

Figure 5.1: Geomorphological setting of the study area (from Mol et al., 1993). 1: Late Pleniglacial terrace; 2: Late-glacial and Holocene terraces; 3: Late-glacial river dunes; 4: terrace scarp.

At Grubbenvorst, the outcrops overlying the terrace consist of a 4 to 6 m thick sequence of purely aeolian sands grading downward into fluvio-aeolian and purely fluvial sand deposits. Such a type of succession is widespread in the Pleistocene lowlands of northwestern Europe (Schwan, 1988).

The fluvial sands are located at the base of the exposure. The sedimentary characteristics of this unit point to deposition in a braided river environment (Mol et al., 1993), which is characteristic of the periglacial fluvial regime (see e.g. Ehlers, 1996). A braided river consists of a network of interwoven small channels and resembles the strands of a complicated braid. The whole system is usually shallow and its drainage behaviour

resembles that of glacial meltwater streams. In winter, drainage comes almost to a complete standstill, but in spring and summer, when thawing sets in, the system becomes highly energetic, which can result in the mobilisation of an enormous amount of sedimentary material. Within the fluvial unit, a truncated ice-wedge cast has been observed by Mol et al. (1993), indicating permafrost conditions in the floodplain.

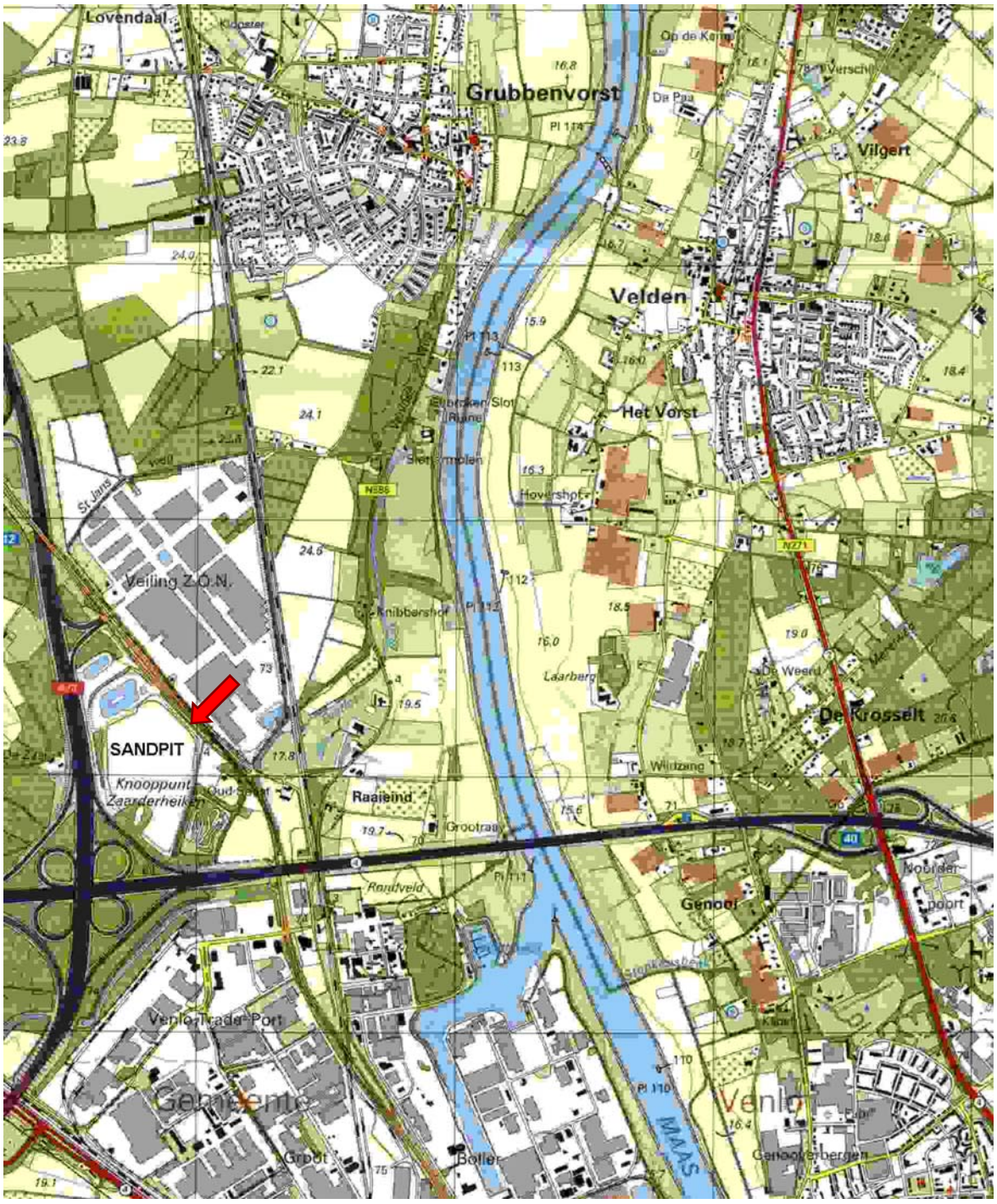

Figure 5.2: Location of the investigated site. The sandpit is located south of Grubbenvorst at the western side of the Meuse, and is indicated by the red arrow.

The fluvial deposits are overlain by the Older Coversand I sedimentary unit. This unit is composed of sediments that were deposited through a combination of aeolian and fluvial processes, owing to the existence of permafrost. The presence of ice-wedge casts in this unit (e.g. Mol et al., 1993; see also Section 5.3) points indeed to conditions of continuous permafrost prevailing in the entire region during deposition of the sediments. In such conditions, the ground is continuously frozen and cannot be penetrated by water. Consequently, in spring and summer, rain and meltwater resulted in floods, and the windblown sediments, loosely covering the permafrost as a sheet, could be readily remobilised. The sediments were then transported via shallow channels and overland flows towards valleys, where they accumulated. Aeolian activity also directly supplied sediment to the water bodies. Consequently, despite a strong aeolian activity, aeolian deposits were not frequently preserved. The reworked aeolian sediments alternate locally with primary aeolian layers and the whole has therefore been described as fluvio-aeolian. The outcrops in Grubbenvorst are mainly built up by this type of deposits. Going from the bottom upwards, there is a decrease in fluvial activity (Kasse et al., 1995). The change in depositional regime, i.e. from a fluvial to a fluvio-aeolian one (and ultimately to an aeolian one; see further), is possibly caused by an increased aridity (Schwan and Vandenberghe, 1991; Kasse et al., 1995).

The Older Coversand I unit is overlain by a thin pebble layer. This has been correlated with the Beuningen Gravel Bed, an important and widespread stratigraphic marker that can be found in the Netherlands, Belgium and Germany. It is considered as a “desert pavement” (i.e formed during a hyperarid phase with predominance of wind activity), where the finer material was blown away by the wind and the coarser gravel was left behind. It can indeed be seen by the naked eye that the pebbles have been abraded by the wind. The Beuningen Gravel Bed is often a constituent of a larger complex (together with the Beuningen Soil or surface; Van der hammen and Wijmstra, 1971; Kolstrup, 1980). In the sampled exposure, however, this complex seems to have been less well developed. Only the gravel bed could be recognised, which consisted of a quasi-continuous string of gravel. This layer was only one pebble thick, and was overlain by coarser sand that also contained some pebbles.

The Beuningen Gravel Bed separates the Older Coversand I unit from the Older Coversand II unit. The latter consists of primary aeolian sediments. In fact, all the sediments overlying the Beuningen Gravel Bed are purely aeolian in origin, and the whole can be interpreted, as mentioned above, as caused by an increased climatic aridity. On top

of the Older Coversands II, fragmentary exposures of a sedimentary unit were observed at the time of sampling, possibly representing the Younger Coversand I.
The Older Coversands II are overlain by a reddish brown sandy silt. On stratigraphical grounds, the soil has been interpreted as being equivalent with the Usselo Soil of Allerød age. The soil has a different appearance than the one at Ossendrecht (see Section 4.2). In Grubbenvorst, it also seems less developed, which may be related to different environmental conditions (moisture), and it contains no datable organic material. The soil indicates a phase of local surface stability but whether it also indicates a stop in the aeolian activity is not clear. Locally, the intercalated soil is not a single bed of sandy silt, but rather an interval with alternate bedding of fine sand and silt. Hence, rather than a period of complete absence of aeolian deposition and associated soil formation, this alternating bedding suggests a period of decreased aeolian deposition (Schwan and Vandenberghe, 1991).
Finally, the top of the sampled exposure, overlying the Allerød soil, consists of sediments belonging to the Younger Coversand II unit.

As such, the sediments exposed in Grubbenvorst form a relatively complete record of the three phases of aeolian sand deposition in west and central Europe that were proposed by Kasse (1999; phase I: Older Coversands I, phase II: Older Coversand II and Younger Coversand I, phase III: Younger Coversand II). This illustrates the importance of the Grubbenvorst exposure for palaeoclimatic research. For a more detailed description of the deposits exposed in Grubbenvorst, reference is made to Schwan and Vandenberghe (1991), Mol et al. (1993) and Kasse et al. (1995). Finally, it can be understood from the foregoing that the sediments overlying the Beuningen Gravel Bed (i.e. the Older Coversands II and the Younger Coversands I & II) in Grubbenvorst can be considered as contemporaneous with the sediments observed in Ossendrecht (see Section 4.2).

5.3. Independent age information

There is a general absence of datable organic material in the exposed sediments in Grubbenvorst. The age of the deposits is consequently not well established and is mainly based on correlation and palaeoclimate indicators.
About 4 km NW of Grubbenvorst, at a level somewhat below the base of the sand pit, a peat layer was encountered in a drill core. Radiocarbon dating of its base and top yielded conventional radiocarbon dates of 26.13 ± 0.18 ka BP and 25.20 ± 0.18 ka BP,

respectively (Westerhoff and Broertjes, 1990). The overlying sedimentary units are therefore younger. The radiocarbon dates extend beyond the calibration curve of the OxCal program, but using the calibration data of Kitagawa and Van Der Plicht (1998) and Voelker et al. (1998) the age of the sediments can be constrained to ~28-29 ka before AD 2000, i.e. the Late Pleniglacial and possibly Late-glacial. It should be noted that in the following all ^{14}C and OSL dates are expressed as ka before AD 2000.

In the fluvio-aeolian unit, large ice-wedge casts have been observed. Ice wedges are considered as diagnostic structures of permafrost. They form where thermal contraction in winter opens vertical cracks in the permafrost table into which water seeps and subsequently freezes (Lowe and Walker, 1997). The wedges grow as more ice accumulates. Ice-wedge casts were also visible at the time of sampling, and an example is shown in Figure 5.3. Furthermore, cryturbation structures (deformations or crumples in the sediments) are present in this unit. As these occur in association with the ice-wedge casts, they can be confidently interpreted as frozen ground phenomena (Lowe and Walker, 1997). The occurrence of all these periglacial phenomena is correlated with the maximum cold of the last glacial (between ~28-29 and 18 ka; Kasse, 1999), which is in agreement with the age information derived from the radiocarbon dates.

As mentioned previously, a gravel string is found overlying the fluvio-aeolian deposits, which has been correlated with the Beuningen Gravel Bed. Due to the lack of datable organic material, a radiocarbon age is not available for this gravel bed. Following Kolstrup (1980), it has generally been assumed that the formation of the Beuningen Complex should be placed between ~25 and 16.9 ka. Kolstrup (1980) further suggested a two-phase development for this complex. A first phase consisted of a dominant fluvial activity, with a prevailed deposition of coarse sand and gravel. Later, the wind may have become the main agent. In Grubbenvorst, it is probably this later phase that is of relevance, as this resulted in the formation of the gravel bed. According to Kolstrup (1980), the later phase of this development may have taken place mainly between 18.6 ka and 16.9 ka.

On top of the section, a soil is present which is assumed to be of Allerød age. This means that it should have been formed at about 13.1 ka (Hoek, 1997; see also Section 4.3).

Combining all the arguments mentioned above, the age of the fluvio-aeolian sediments can be constrained between 16.9 and ~28.5 ka. The deposition of the aeolian sediments belonging to the Older Coversand II unit, which is intercalated between the Beuningen Gravel Bed and the Allerød soil, can be placed between 16.8 and ~13.1 ka. The Younger

Coversand II unit overlying the Allerød soil should then have been deposited no longer than ~13.1 ka ago. Consequently, on the basis of these arguments, a Late Weichselian Pleniglacial to Weichselian Late-glacial age has been attributed to the section under consideration (Schwan and Vandenberghe, 1991).

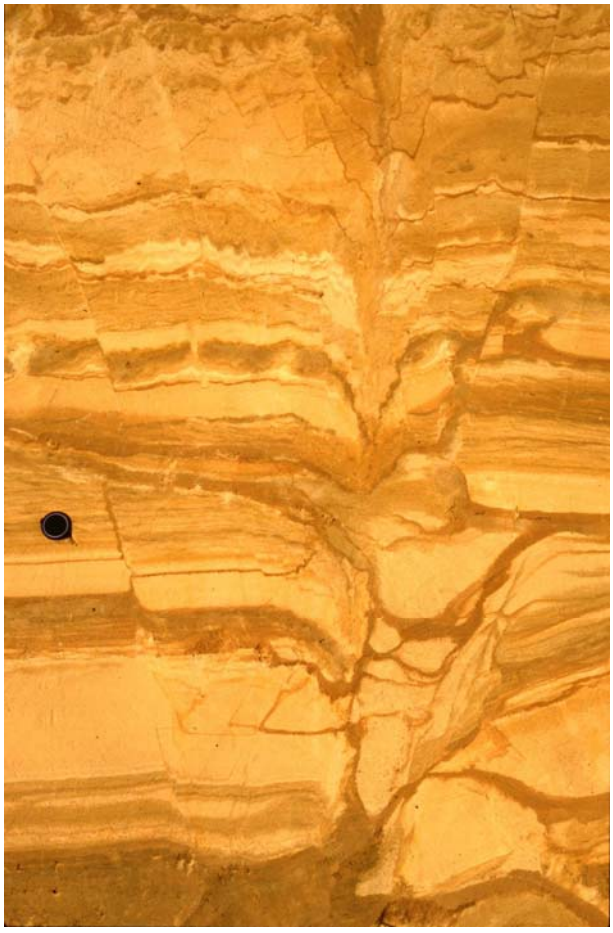

Figure 5.3: Illustration of an ice-wedge cast in the Older Coversands I stratigraphic unit, as observed in the Grubbenvorst sand pit at the time of sampling. The black spot is the lens cover of the camera.

Besides the age information summarised above, three unpublished OSL ages are available for the sediments of Grubbenvorst. Bateman et al. dated a sample from the fluvial sediments at the base of the exposure at 34.8 ± 2.4 ka. For a sample from the sediments immediately underlying the Beuningen Gravel Bed (the Older Coversands I), they obtained an age of 20.7 ± 1.2. Bateman et al. also sampled the sediments immediately overlying the Beuningen Gravel Bed (the Older Coversands II) and found an age of 19.8 ± 1.2 ka. With the exception of the OSL age for the Older Coversand I unit, it appears that these OSL ages are rather old compared to the expected ones (see above). Bateman et al. acknowledge these apparent overestimations but point out that correlations over large

distances should be treated with caution, and that the older age of 19.8 ka might reflect an earlier start of the coversand deposition in Grubbenvorst. However, they used single and multiple-aliquot additive-dose techniques for D_e determination in quartz, two techniques that do not take into account the occurrence of sensitivity changes.

It can finally be added that, if the stratigraphic correlations are correct, the OSL ages obtained for the Ossendrecht samples (Section 4.7) also bear some relevance here; the sediments observed in Ossendrecht are thought to be contemporaneous with those overlying the Beuningen Gravel Bed in Grubbenvorst (see Section 5.2). In Ossendrecht, an age of 12.2 ± 0.7 ka was found for the Younger Coversands II and an age of 15.0 ± 0.9 for the Older Coversands II (or Younger Coversands I; see Section 4.7).

5.4. Sampling and field measurements

An overview of the exposure sampled in Grubbenvorst is shown in Figure 5.4. A large profile of about 5-6 m deep was available for sampling.

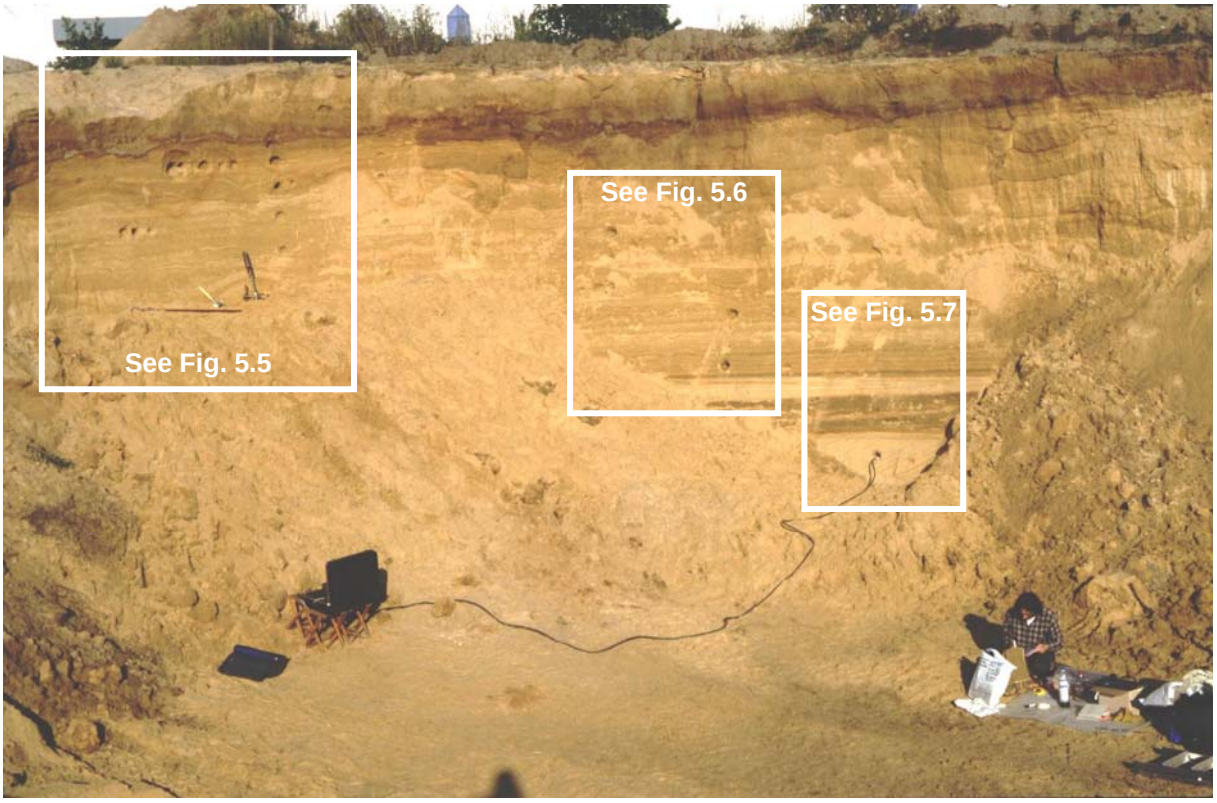

Figure 5.4: Overview of the exposure sampled in the Grubbenvorst sand pit (total depth: ~5-6 m). It also illustrates the field gamma-ray spectrometry that was carried out in the fluvial sediments at the base of the exposure (at the location of sample G10, see also Figure 5.7). Clearly visible near the top is a brownish soil, which on stratigraphic grounds may be equivalent with the Usselo Soil (Schwan and Vandenberghe, 1991).

Twenty-three samples in total were taken by hammering stainless steel or PVC cylinders into freshly cleaned exposures. One sample (G13) was taken from the Younger Coversand II unit overlying the Usselo Soil. Five samples (G14, G22, G9, G23 and G15) were taken from the coversands intercalated between the Usselo Soil and the Beuningen Gravel Bed. Four of these (G22, G9, G23, and G15) can be ascribed to the Older Coversand II sedimentary unit, while sample G14 may belong to the Younger Coversand I unit; the boundary between these two distinct lithostratigraphic units is, however, obscure. Nine samples (G1, G7, G16, G17, G11, G6, G5, G8 G12) were taken from the fluvio-aeolian sediments underlying the Beuningen Gravel Bed (the Older Coversand I unit). Figure 5.5 shows the top part of the sampled sequence to some greater detail. The different lithostratigraphic units are indicated for clarification. Moving further downward, the fluvio-aeolian sediments merge into clearly fluvial sediments. There is no clear boundary between the two units, and samples G3 and G4 were taken from the transition region. Figure 5.6 shows the base of the fluvio-aeolian unit and illustrates how it grades into the fluvial deposits. The base of the sampled exposure consists of purely fluvial deposits (Figure 5.7). At the top of this unit, a succession of coarser sandy and finer silty layers was found. Samples G2, G18 and G19 were taken from the sandy layers, while sample G20 was taken from a prominent intercalated silty layer. The basal part of this section consists of clearly coarse cross-bedded sands, and here samples G10 and G21 were taken.

A schematic overview of the whole of sampling in the Grubbenvorst sandpit is given in Figure 5.8. It must be emphasized that the whole profile was sampled with great detail; several samples were taken from each stratigraphic horizon (with the exception of the Younger Coversands II) to check for consistency.

Samples for low-level gamma-ray spectrometry were taken in the immediate vicinity of the samples G1, G7, G9, G10, G13, G14 taken for luminescence analyses. Some material was also collected from in between the samples G17 and G18. Three additional samples of sediment were taken for the determination of moisture content (in the Older Coversands I and II, and in the coarse fluvial sands at the bottom of the exposure; see Figure 5.8).

Field gamma-ray spectrometry was carried out at the location of samples G1, G7, G9 and G10, using the system described in Section 4.6.1.1.

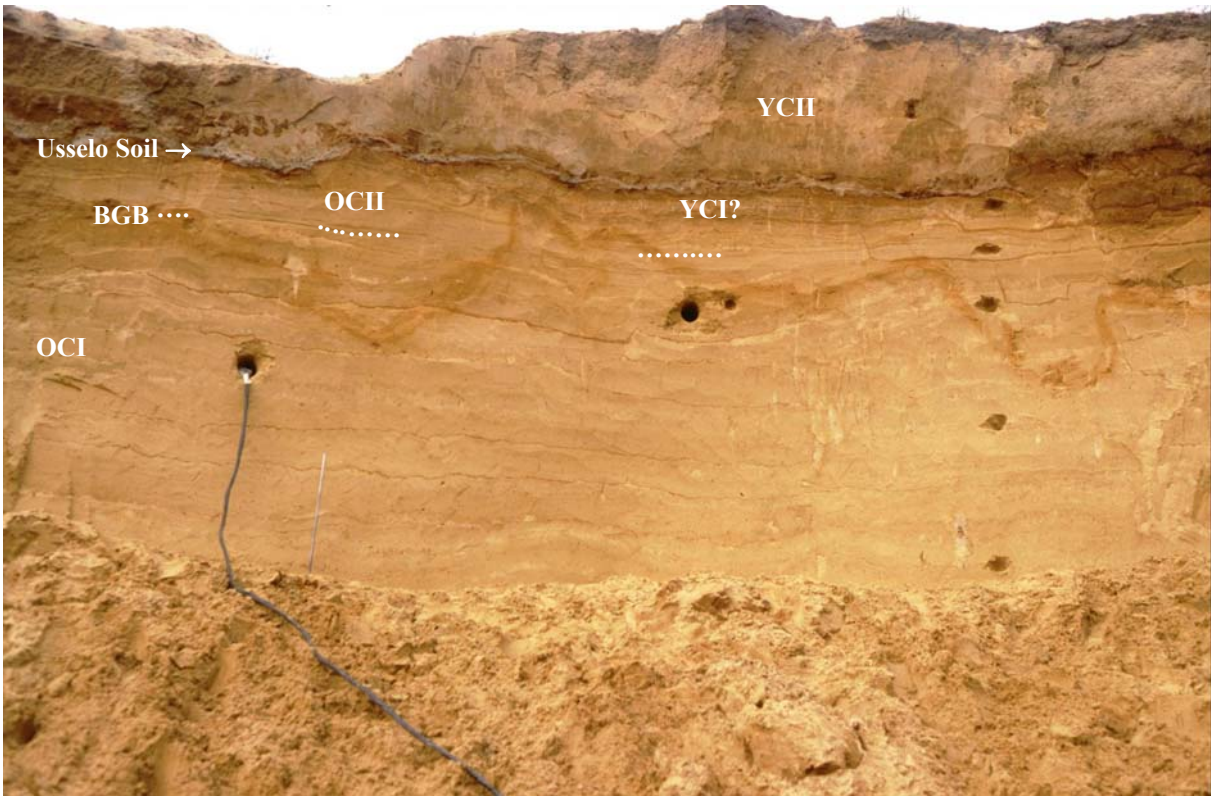

Figure 5.5: Upper part of the sampled exposure in the Grubbenvorst sand pit. The total height of the profile is about 3 m. The thin loamy horizon near the top is the Usselo Soil. It is overlain by the Younger Coversand II (YCII) unit and here sample G13 was taken. The sediments making up the Older Coversands II (OCII) stratigraphic unit are intercalated between the Usselo soil and a thin string of gravel that has been correlated with the Beuningen Gravel Bed (BGB). The latter is not visible on the photograph, but is indicated by the white dotted lines. Samples G9, G15, G22 and G23 were taken from the OCII unit. Directly below the Usselo layer, the Younger Coversand I (YCI) unit is possibly present. Here, a sample was taken as well (G14). The YCI unit could not be identified unambiguously and was not present over the entire width of the sampled profile. All the sediments overlying the BGB are aeolian. At Grubbenvorst, the exposed sediments mainly lie below the BGB and make up the Older Coversand I stratigraphic unit. It is composed of fluvio-aeolian sands grading downward into fluvial deposits (not shown in this picture). Four samples from this unit were taken from the part of the exposure shown here (G1, G7, G16 and G17; see Figures 5.6 and 5.8 for the additional samples). The photograph also illustrates one of the field gamma-ray spectrometry measurements carried out in the upper part of the Older Coversands I (at the location of sample G7). To give a notion of the dimensions, the diameter of the borehole is approximately 8 cm.

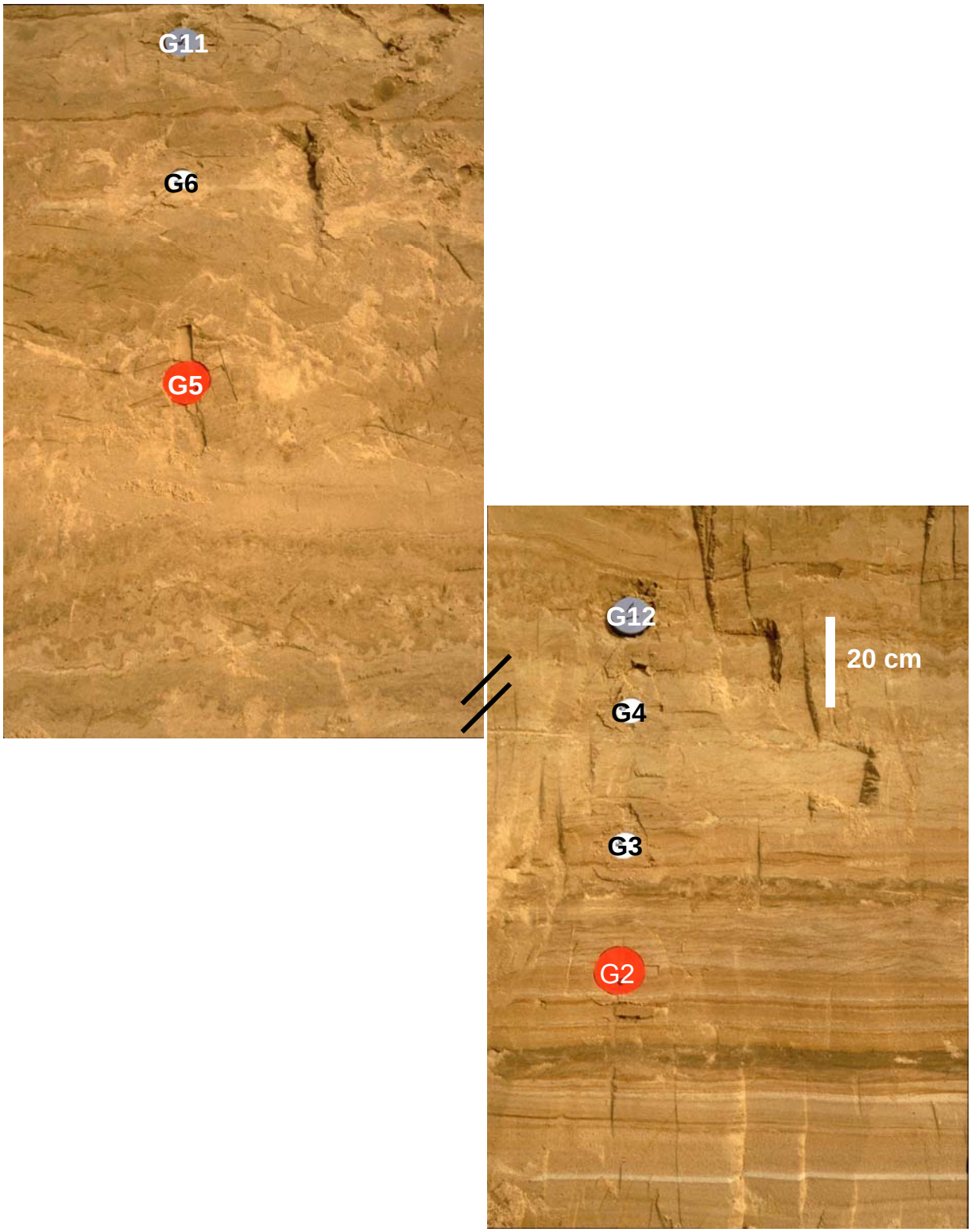

Figure 5.6: Detail showing the fluvio-aeolian sediments (the Older Coversands I), the upper part of the fluvial sediments, and the transition zone between the two. Samples G11, G6, G5 and G12 are fluvio-aeolian, while G3 and G4 were taken from the transition region between the fluvio-aeolian and the purely fluvial sediments. Sample G2 was taken from the top of the fluvial unit, which consists of alternating silty and sandy layers (see also Figure 5.7). The break between the two photographs represents a horizontal separation of 1.60 m between the two sampling locations (see Figure 5.8).

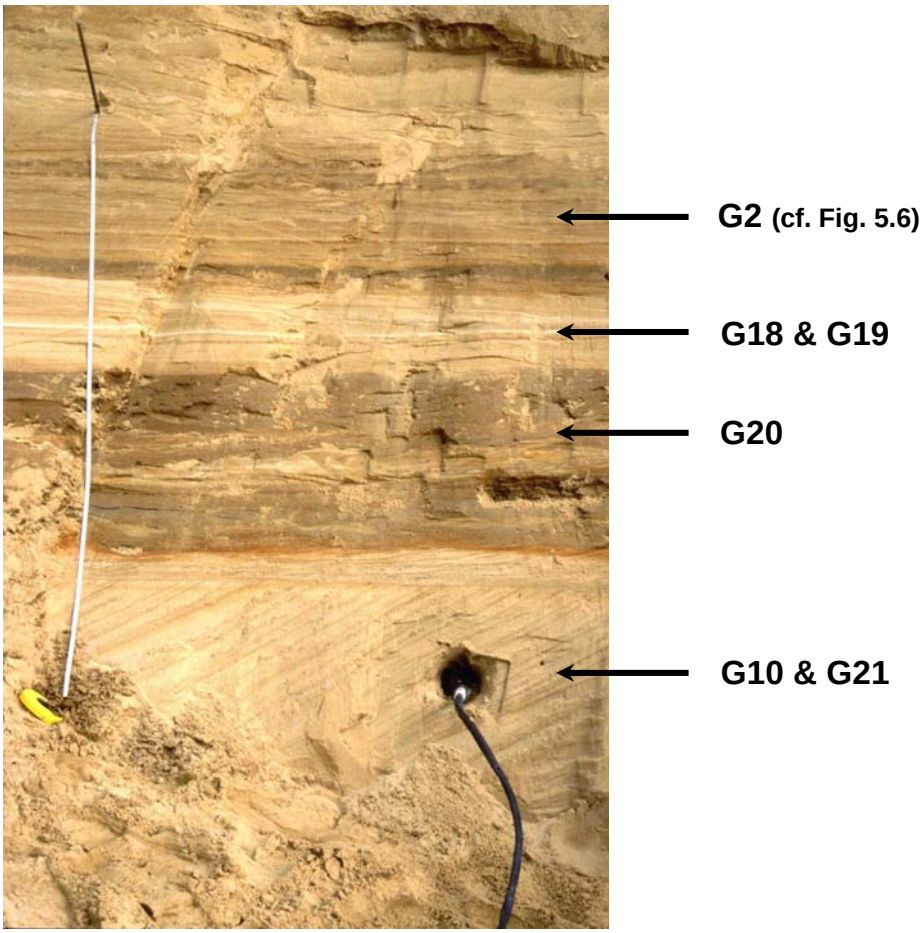

Figure 5.7: Detail of the fluvial sediments sampled in the Grubbenvorst sand pit. The top of the section consists of alternating silty and sandy layers (see also at the bottom right of Figure 5.6). Samples G18 and G19 were taken from an intercalated sandy layer, while sample G20 was taken from a prominent silt layer. The basal part (where the NaI detector is inserted) consists of coarse-grained cross-bedded sands. From these sediments, samples G10 [at the exact location of the borehole (Ø ≈ 8 cm)] and G21 were taken.

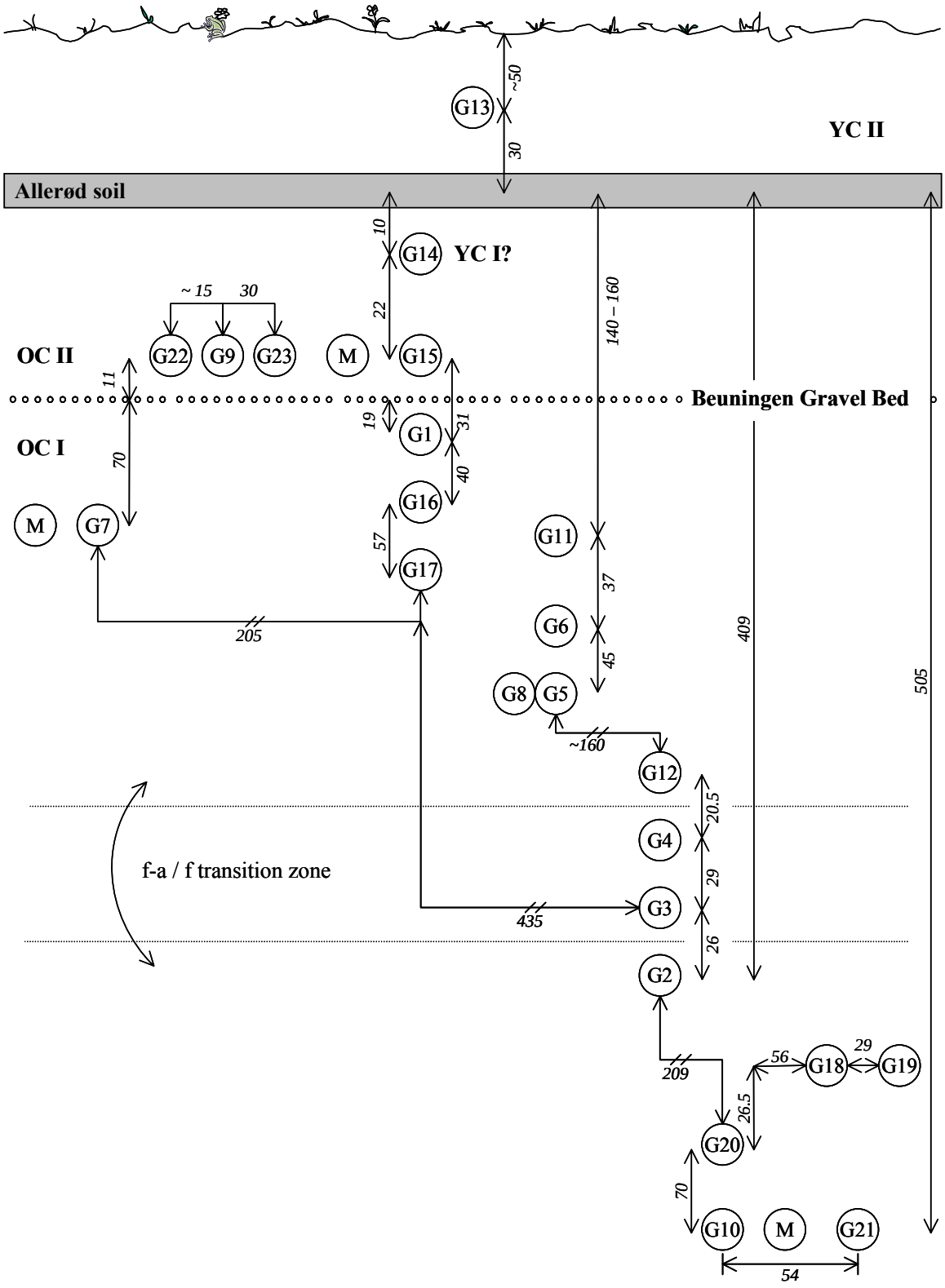

Figuur 5.8: Schematic overview of the sampling in the Grubbenvorst sandpit. The samples denoted with "M" are those that were taken for the determination of the moisture content. The numbers in italics are distances in cm. YC: Younger Coversand; OC: Older Coversand; f-a: fluvio-aeolian; f: fluvial. The fluvial deposits are located at the base, and are overlain by the fluvio-aeolian sands from the Older Coversand I unit. The purely aeolian sediments overly the Beuningen Gravel Bed.

5.5. Equivalent dose determination

5.5.1. Sample preparation

Coarse quartz grains (90-125 μm) were extracted from the samples as outlined in Section 4.5.1 (i.e. by sieving, HCl, H_2O_2, magnetic separation, heavy liquids and 40 min etching in 48% HF; see also Section 4.5.3). No coarse quartz grains were found in sample G20, which was taken from a silty layer near the bottom of the profile (see Figure 5.7). Therefore, this sample was not dealt with in this work.

The purity of the samples was checked using their infrared stimulated luminescence response at room temperature to a large regenerative β-dose (see Section 4.5.3). All samples passed the 10% (IRSL/OSL ratio) acceptance criterion, and hence the sample preparation procedure was considered as adequate. The IRSL check was also performed on each aliquot, after all the principal measurements (e.g. for D_e determination) were completed, to eliminate any aliquots with significant feldspar contamination from the analysis. It was only exceptionally that an aliquot had to be rejected for this reason.

5.5.2. Aliquot preparation and presentation

As already mentioned in Section 4.5.2, the procedure for preparing the aliquots was quite cumbersome. Therefore, an alternative procedure was applied (Aitken, 1985).

This second approach uses flat stainless steel discs of 0.5 mm thick and 9.7 mm* in diameter. As before, the discs are coated with silicon oil from an aerosol spray, but now use is made of a spray mask. The spray mask is placed over the discs and is constructed in such a way that only the centre of the discs is wetted with oil. After removing the spray mask, the discs are then inverted and simply dropped on a small pile of quartz grains. In this way, a monolayer of quartz grains could be fixed to the central part of each disc. The surplus of grains not sticking to the disc is removed by gently tapping it.

* The slightly smaller diameter of the discs (previously, 10 mm diameter discs were used; see Section 4.5.2) ensures an exact fit to the dimensions of the turntable and the lift/heating mechanism of the luminescence reader (Christiansen H., private communication).

This recipe for making the aliquots is very simple, time saving and quite reproducible (although the latter is not a crucial requirement when using single-aliquot protocols). Also, cleaning of the discs is straightforward and fast. By choosing the diameter of the holes in the spray mask, aliquots of varying size (i.e. containing various amounts of quartz grains) can easily be prepared. In the following, all measurements were carried out on 7 mm diameter aliquots, with the exception of the measurements for constructing dose distributions (see Section 5.5.3.4), for which a 2 mm mask was used.

5.5.3. Equivalent dose determination

The work on the samples from Ossendrecht (Chapter 4) showed the SAR protocol to be the technique of choice for equivalent dose determination. As a consequence, SAR was used for all the samples from Grubbenvorst. For all samples, the dependence of the D_e on the preheat conditions was investigated first. Subsequently, the dependence of the D_e on the size of the test dose was investigated for a few selected samples. For each sample, the suitability of the experimental measurement conditions was checked using dose recovery tests. Finally, equivalent dose distributions were constructed for one aeolian and some of the fluvio-aeolian and fluvial samples.
The measurement facilities that were used have been described in Section 4.5.6.

5.5.3.1. Influence of the preheat temperature on the D_e

The dependence of the equivalent dose on the preheat temperature was investigated for all samples. For each sample, 24 aliquots were prepared (as outlined in Section 5.5.2) and divided into eight groups of three. Each group received one of eight different preheats (10s at 160-300°C, in 20°C intervals), but otherwise all measurement conditions were equal for each group. Equivalent doses were determined using SAR as outlined in Table 3.3 and described in Section 4.5.7.3. For each aliquot, the complete growth curve was constructed. This consisted of the measurement of 5 regenerative dose points (the highest at ~2.5 times the D_e), a zero dose point and a repeated dose point (the 'recycling' point), each of these followed by the measurement of the corresponding test-dose signal. Stimulation was for 40 s at 125°C using the blue diodes, the test-dose cut heat was up to

160°C and the size of the test dose was about 10-15% of the estimated D_e. The results are shown in Figure 5.9.

In general, the D_e is clearly independent of preheat temperatures up to 260°C for all samples. At higher preheat temperatures, thermal erosion of the signal became progressively more important, and at a preheat of 300°C the growth curves were poorly defined. Nevertheless, with the exception of sample G23, it was still possible to calculate equivalent doses from the datasets obtained at this highest preheat. These D_e values are higher and, in general, more scattered compared to those obtained at lower preheat temperatures.

To illustrate the behaviour of the samples in the SAR protocol, recycling ratios and recuperation (expressed as a percentage of the corresponding corrected natural OSL signal) are also included in Figure 5.9. All samples can be seen to behave well over the preheat temperature range up to 260°C. Over this temperature range, recycling ratios fall within the range 0.90-1.10 suggested by Murray and Wintle (2000a) as a possible criterion for acceptance, while recuperation amounts to 3-4% at most. Also, the growth curve data (not shown) could be well approximated by a single saturating exponential function. It is only at preheat temperatures exceeding 260°C that the sensitivity correction does not always appear to be working well and that recuperation becomes a larger fraction of the corrected natural OSL signal. For sample G23, these disturbing effects are already taking place for preheat temperatures higher than 240°C.

The plateau region was, therefore, defined from 160 to 240°C for sample G23; for all other samples this extended to 260°C. The insensitivity of the equivalent dose to the preheat temperature indicates that thermal transfer is unimportant for these samples. These observations are similar to those made for the Ossendrecht samples (Section 4.5.7.3, Figure 4.15), as well as those reported in the literature (see e.g. Murray and Olley, 1999; Murray and Wintle, 2000a; Strickertsson et al., 2001).

The average D_e across the preheat plateau region (± 1 standard error) is indicated in the figures and was used in the final age calculations (see Section 5.7).

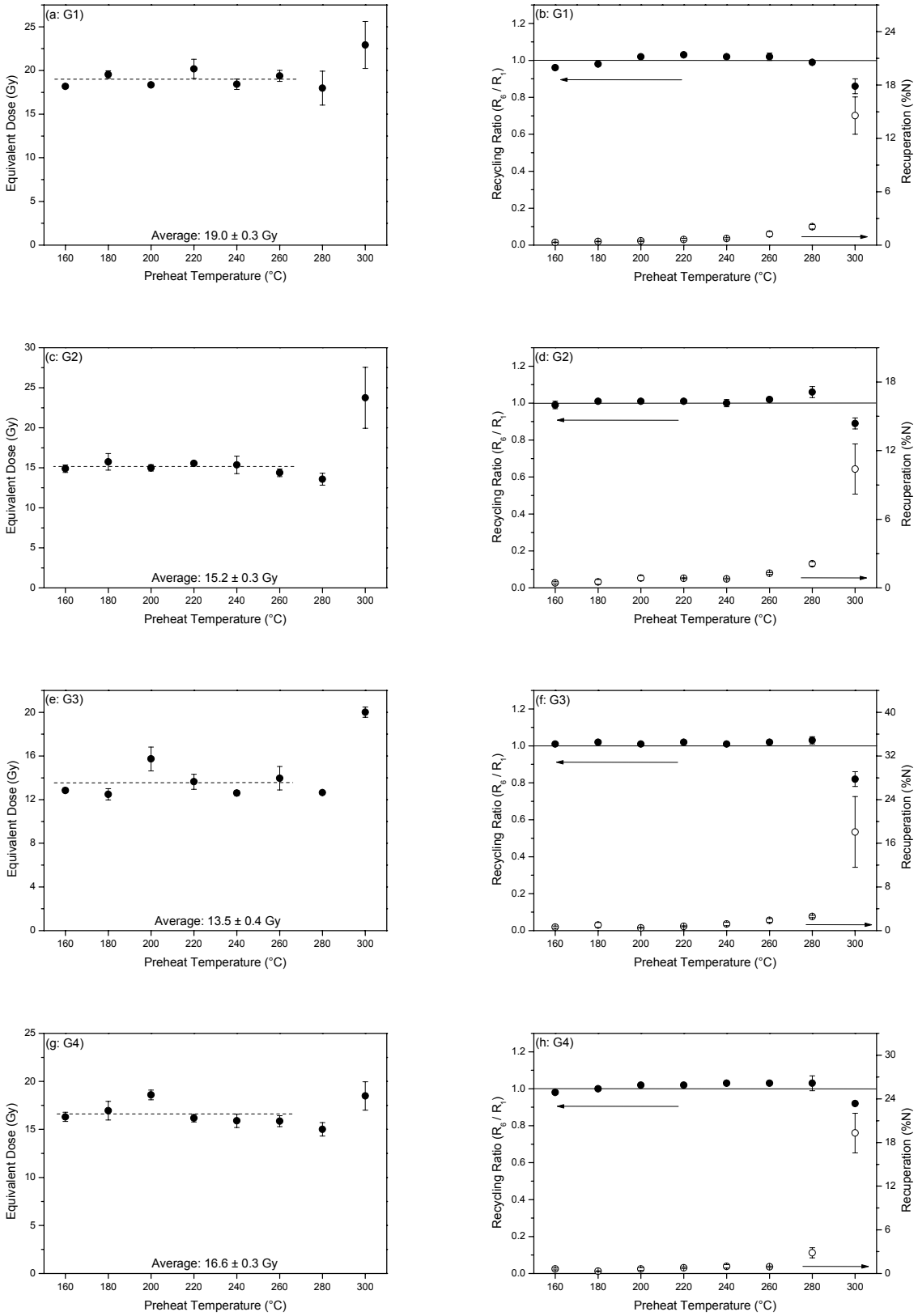

Figure 5.9: Dependence of the D_e on the preheat temperature; continued on the next page.

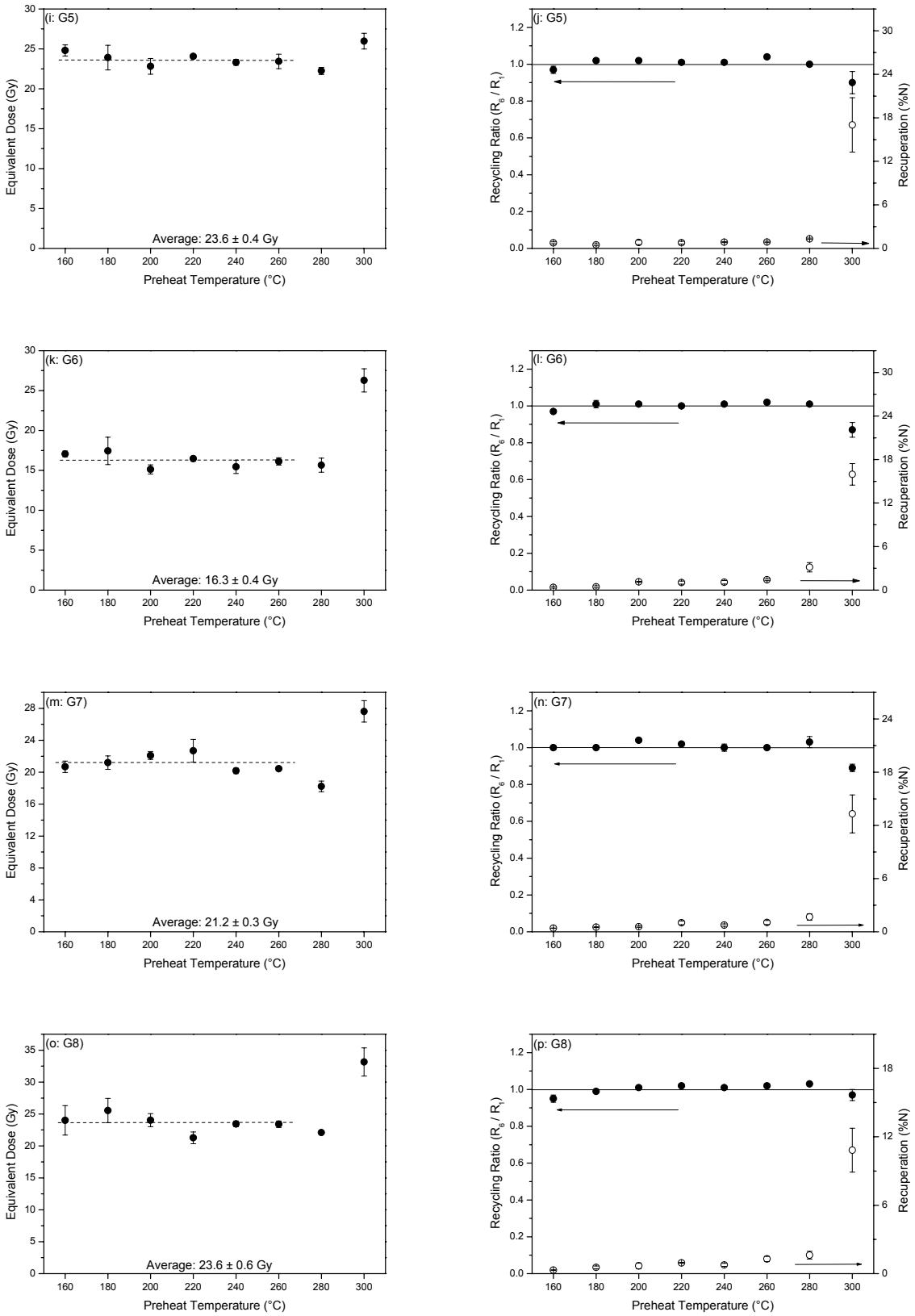

Figure 5.9 (continued): Dependence of the D_e on the preheat temperature; continued on the next page.

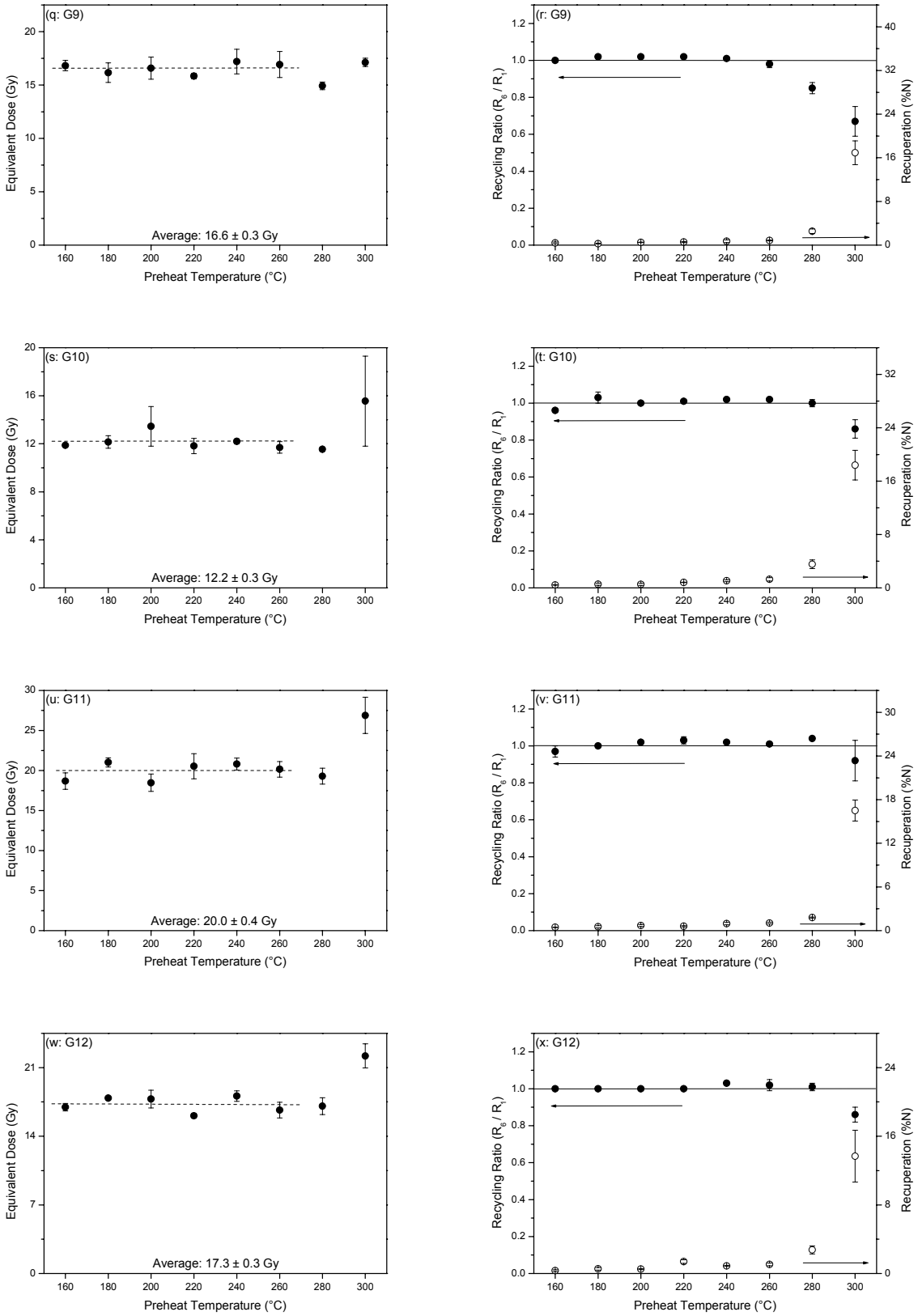

Figure 5.9 (continued): Dependence of the D_e on the preheat temperature; continued on the next page.

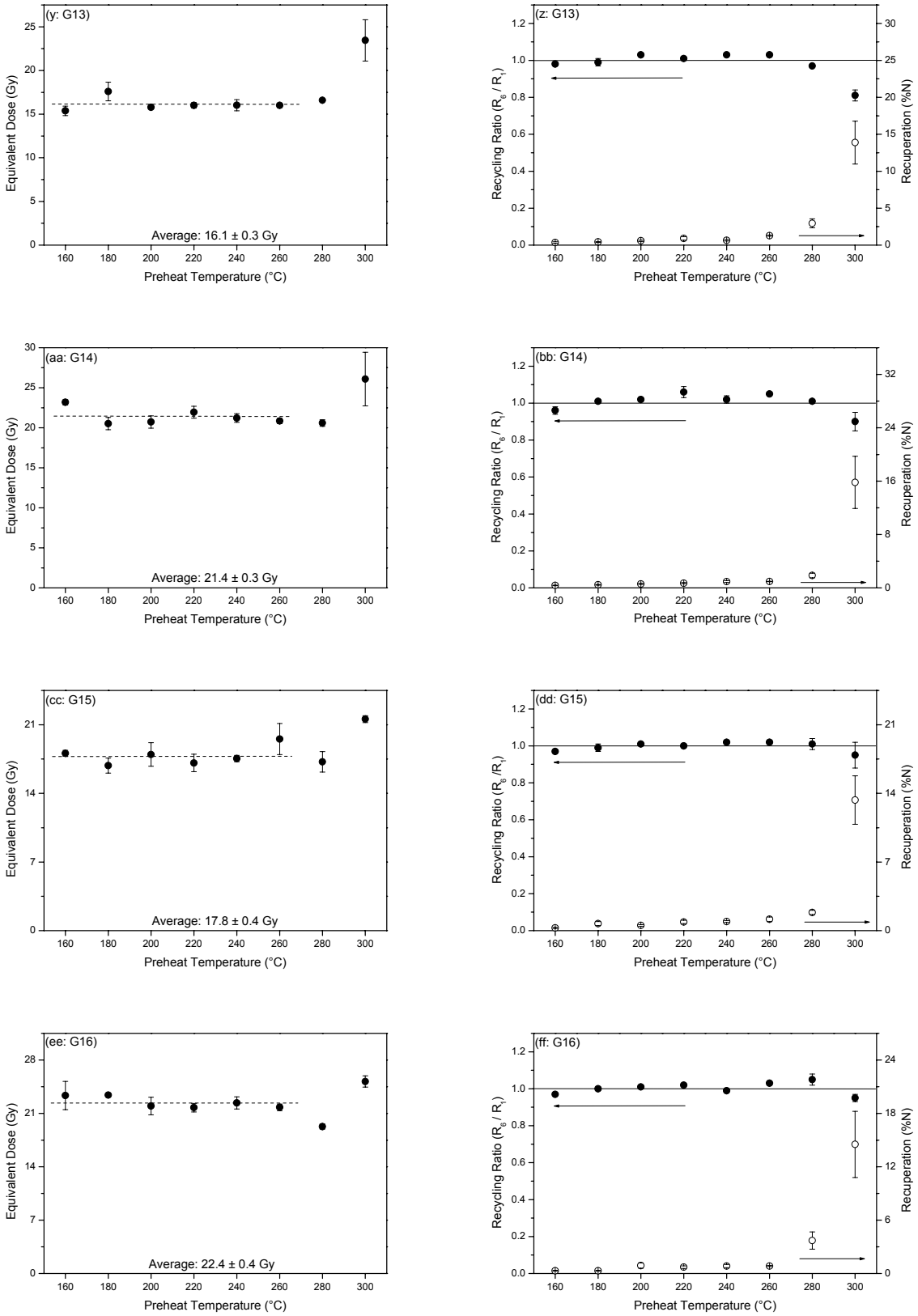

Figure 5.9 (continued): Dependence of the D_e on the preheat temperature; continued on the next page.

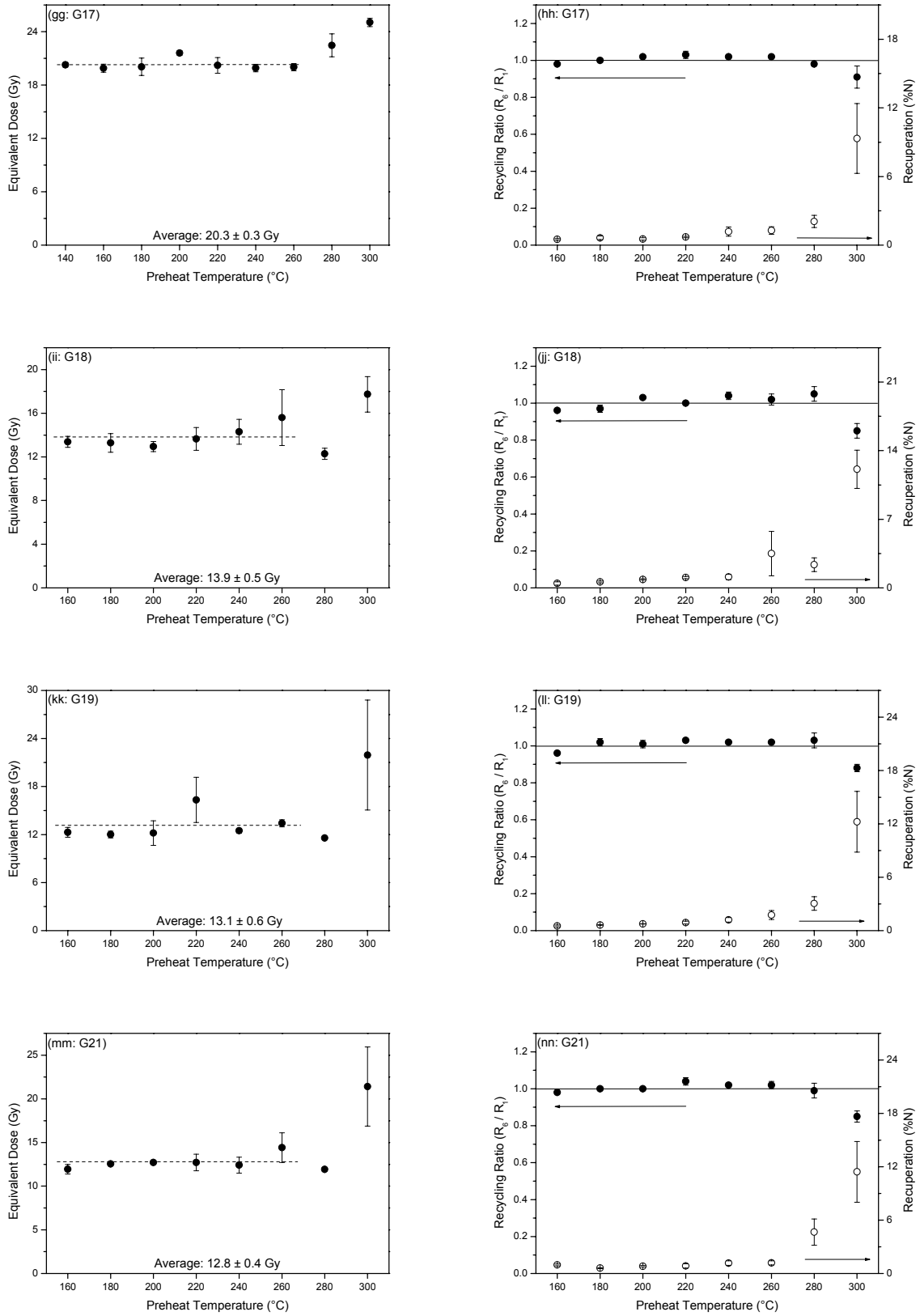

Figure 5.9 (continued): Dependence of the D_e on the preheat temperature; continued on the next page.

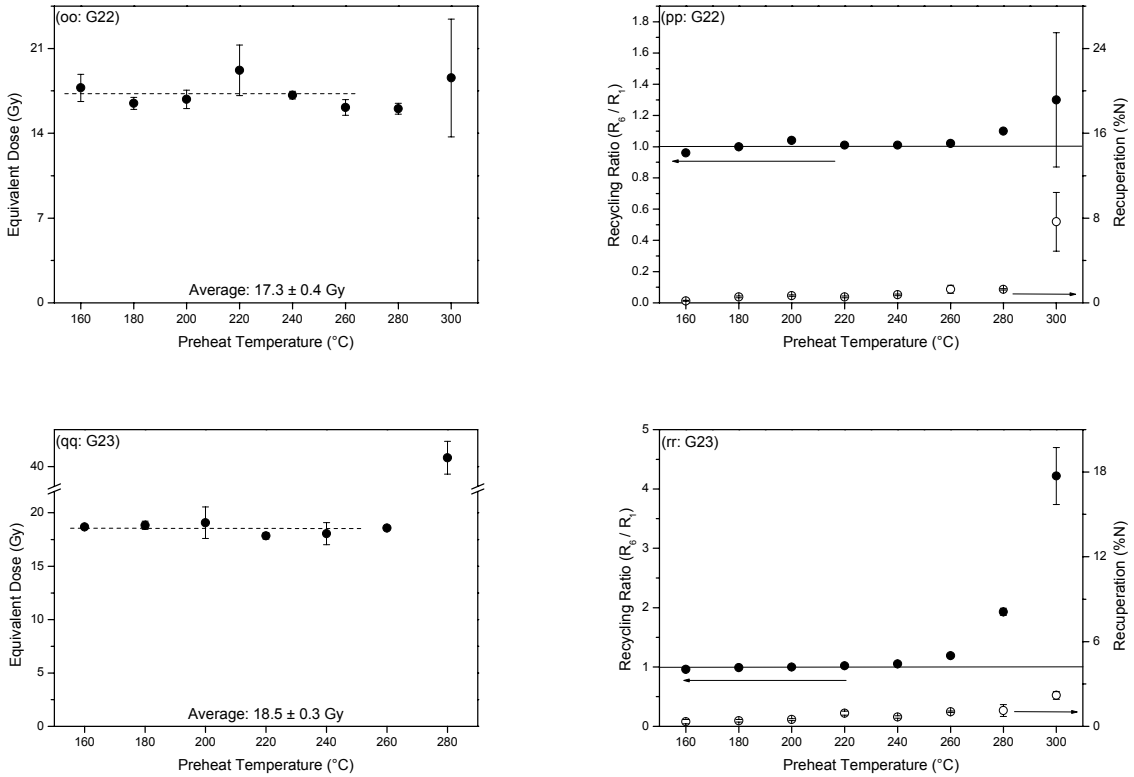

Figure 5.9 (continued): The figures on the left show the dependence of the equivalent dose on the preheat temperature ('preheat plateau' tests) for the 22 samples from Grubbenvorst. Sample identification is given in the upper left corner of each figure. The measurements were carried out following the SAR protocol (Murray and Wintle, 2000a; see also Table 3.3 and Section 4.5.7.3). Each data point represents the average of three D_e determinations; the error bars are 1 standard error. The dashed line represents the unweighted average over the indicated temperature region, and its value (± 1 standard error) is also shown in the figures. The figures on the right show the corresponding recycling ratios (solid circles) and recuperation (expressed as % of the corrected natural OSL signal; open circles). The solid line at a recycling ratio equal to unity is meant as an eye guide.

5.5.3.2. Influence of the size of the test dose on the D_e

The influence of the size of the test dose on the D_e was investigated for an aeolian (G9), a fluvio-aeolian (G9) and a fluvial (G10) sample (see Section 5.4 for a description of the samples). Three aliquots were used for each test dose, the size of which increased up to 5-6 times the estimated equivalent dose. A preheat temperature of 10s at 240°C was used, chosen from the plateau region observed in the D_e versus preheat temperature plots (Figure 5.9). Otherwise, the measurement conditions were the same as previously. The results are shown in Figure 5.10.

For sample G10, the D_e appears to be rather insensitive to the size of the test dose, but the scatter in the data may mask any trend. For samples G7 and G9, on the other hand, the data indicate a decrease in equivalent dose with increasing test dose size. It can be recalled that a similar observation was made for one of the Ossendrecht samples (sample OS-4, Figure 4.16e). Murray and Wintle (2000a; their Figure 5b) also reported a drop in D_e at high test dose/D_e ratios. The detectable decrease at higher values of the test dose suggests that some disturbing process is taking place for the two samples. This process could be a thermal transfer of charge inserted into light-insensitive traps by the test dose, during a subsequent high temperature preheat. This is consistent with the observed increase in the recuperation shown in the corresponding figures on the right. The recuperation in sample G10 also increases with the size of the test dose, but does not appear to produce a detectable effect on the D_e. In all three samples, the recuperation is, however, relatively small: even at the highest test dose, it does not exceed 5%. It can be noted that the recycling ratios, on the other hand, do not show any systematic variation. On the overall, they are slightly higher than the ideal value of unity, but remain well within the range 0.90-1.10.

As pointed out by Murray and Wintle (2000a), the interaction between recuperation and D_e is not well understood and it may not be the sole reason for the observed trend. As for the Ossendrecht samples, the test dose was therefore, out of caution, kept relative small, i.e. at about 10-15% of the equivalent dose. The resulting test dose signals could be measured with adequate precision.

It should be pointed out that for the three investigated samples a natural heterogeneity in D_e's might influence the appearance of the datasets, and hence might mask any systematic

effects. To avoid this source of scatter, perhaps a dose recovery test would be more appropriate to investigate the influence of the size of the test dose. Unfortunately, for the samples from Grubbenvorst, this fell outside the time available for this work.

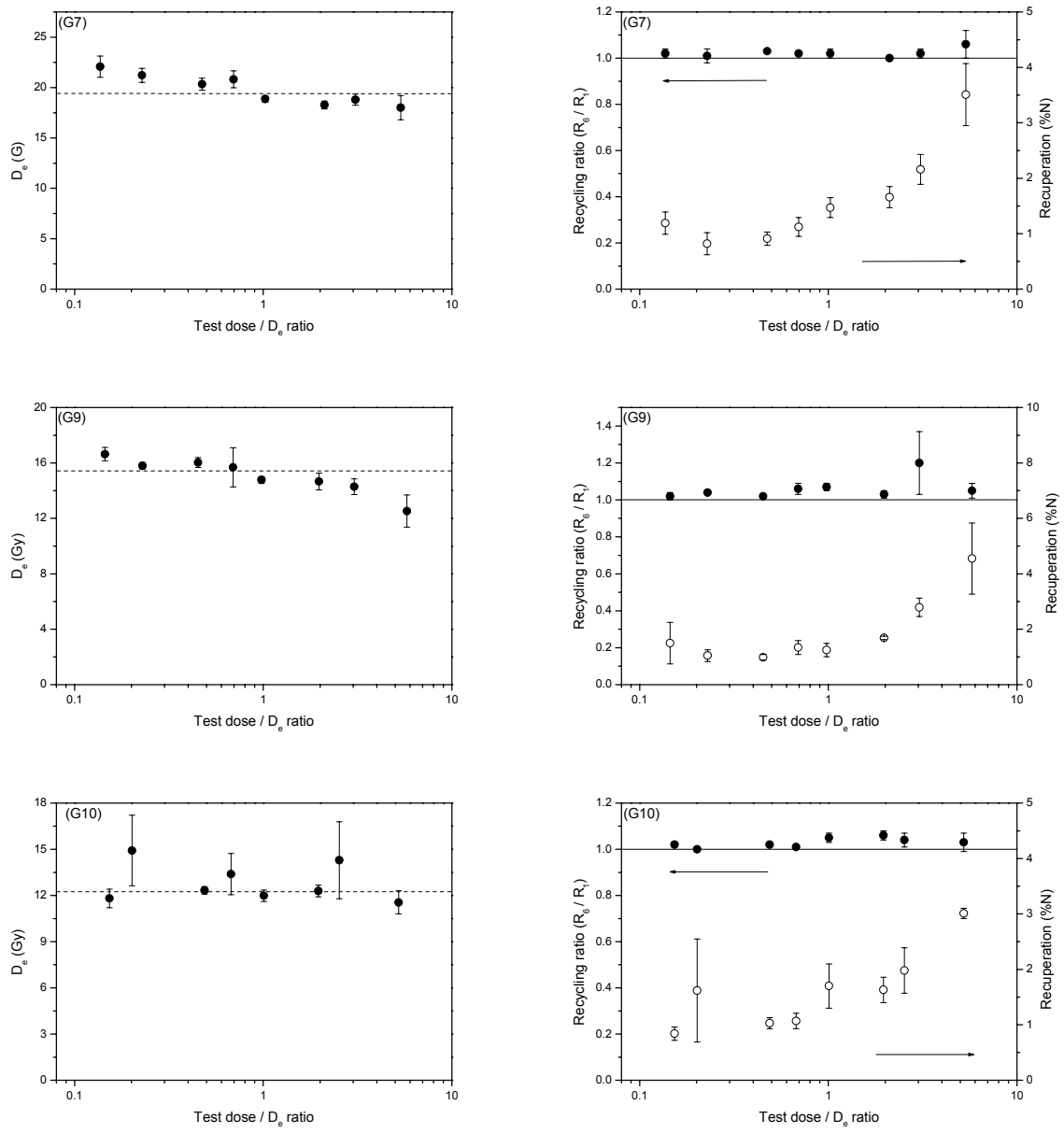

Figure 5.10: The figures on the left show the variation in D_e as a function of the size of the test dose for three selected samples from Grubbenvorst (G7, G9 and G10). Note that the test dose size is expressed relative to the D_e, on a logarithmic axis. Each data point represents the average of three determinations and the error bars are the associated standard errors (1s). The dashed line represents the weighted average of all 24 aliquots. The figures on the right show the corresponding recycling ratios (solid circles) and recuperation (expressed as percentage of the corrected natural OSL signal; open circles). The solid line at a recycling ratio equal to unity is meant as an eye guide.

5.5.3.3. Dose recovery tests

Each sample was tested too see if SAR was able to recover a known laboratory dose given to an aliquot after it had been optically bleached. These dose recovery tests were conducted in the same way as outlined in Section 4.5.7.3. After the natural OSL signal was removed by stimulating with the blue diodes for 100 s at room temperature, groups of three aliquots each received one of eight different doses. The given doses varied from ~0.5 to ~2 times the natural D_e. The SAR protocol was then applied using a preheat temperature of 10s at 240°C for all aliquots and samples (based on the D_e versus preheat temperature plots shown in Figure 5.9), but otherwise identical measurement conditions as outlined in Section 5.5.3.1 (test dose cut heat at 160°C, test dose size ~15% of the given dose, etc…). The results are shown in Figure 5.11.

As was previously observed (Section 4.5.7.3, Figure 4.17), there seems to be a general tendency of a small overestimation at lower given doses, and a small underestimation at higher given doses. However, with occasional exceptions at the lowest given dose, the given doses could be recovered to within 5% for all samples, and the overall ratios over the entire dose range are consistent with unity. Focussing on the dose range likely to be encountered in the natural samples (10-25 Gy), the given dose can, in general, be recovered to within 2.5%. It is concluded, therefore, that for these samples acceptable dose recoveries could be achieved. These observations enhance the confidence that can be put in the suitability of the SAR protocol for accurate equivalent dose determination. It should be noted that any pattern in the measured/given dose ratio is not followed by the recycling ratios. These latter lie for all samples and given doses within the range 0.95-1.05, most of them being consistent with unity. The recuperation, on the other hand, is small, with the highest values (of ~2%) usually being observed at the lowest given doses. There seems to be no clear relation between the observed amount of recuperation and the ability to recover a dose [compare e.g. Figures 5.11(k) and (l), Figures 5.11(m) and (n) and Figures 5.11(y) and (z)].

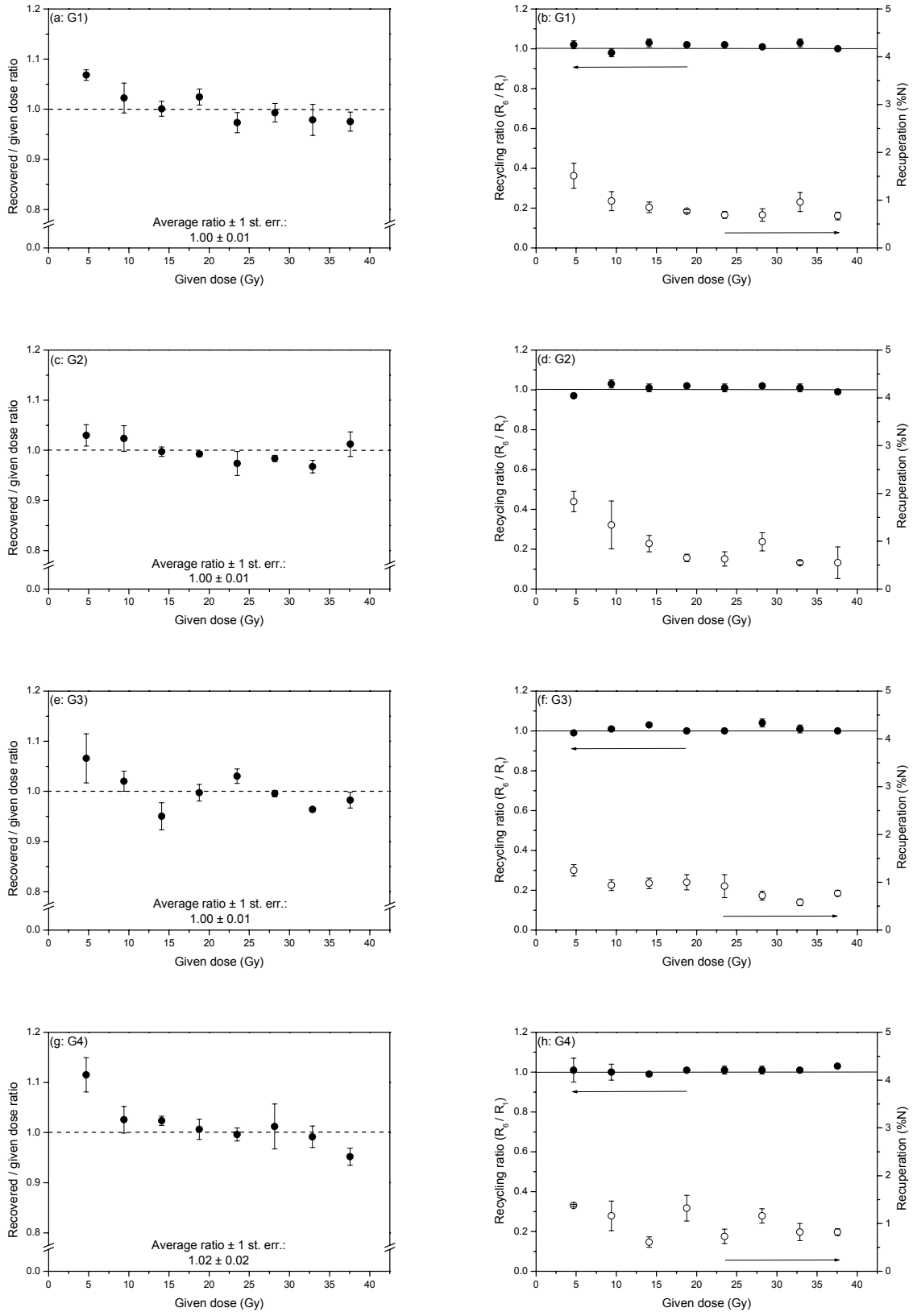

Figure 5.11: Data obtained from the dose recovery experiments; continued on the next page.

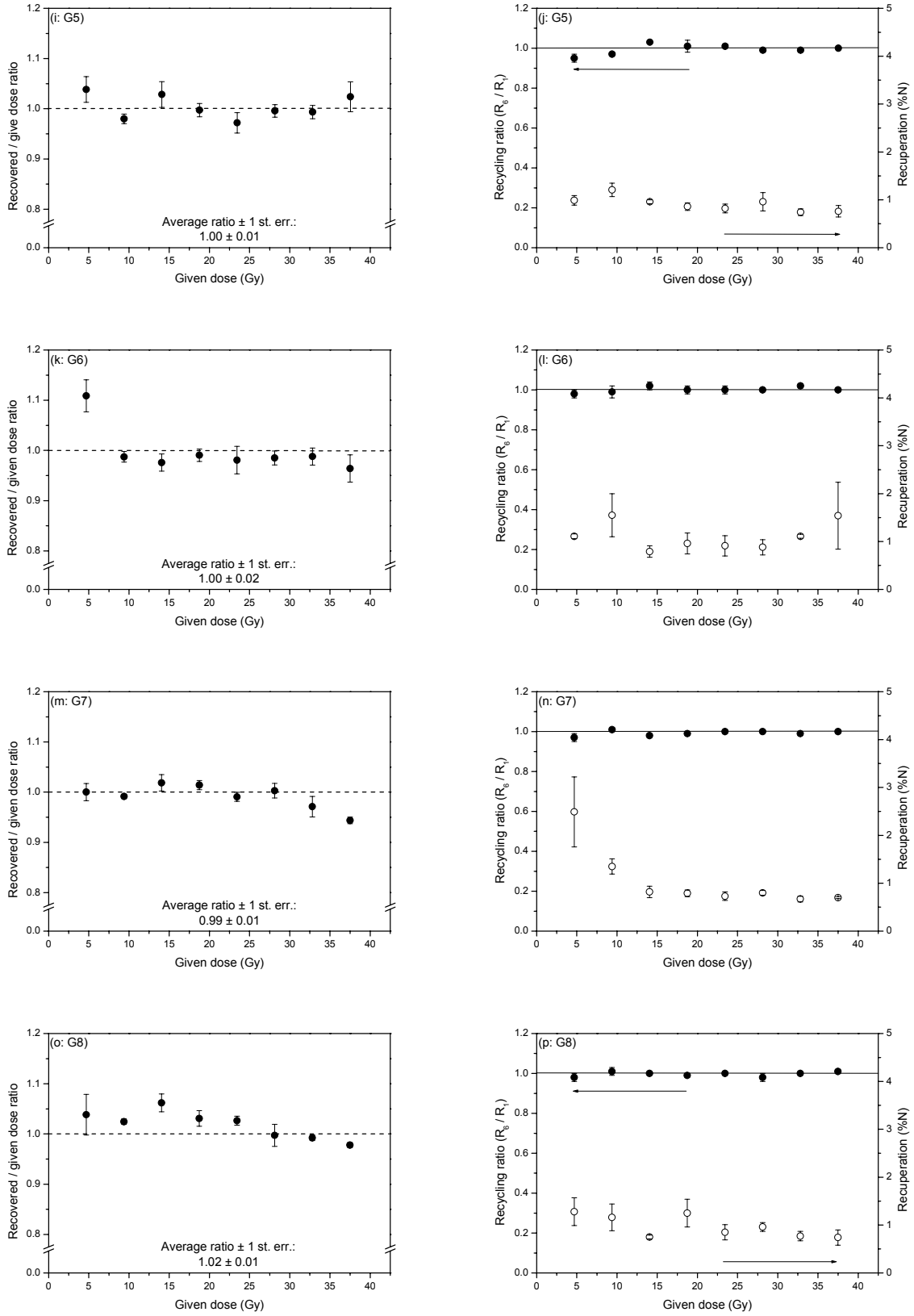

Figure 5.11 (continued): Data obtained from the dose recovery experiments; continued on the next page.

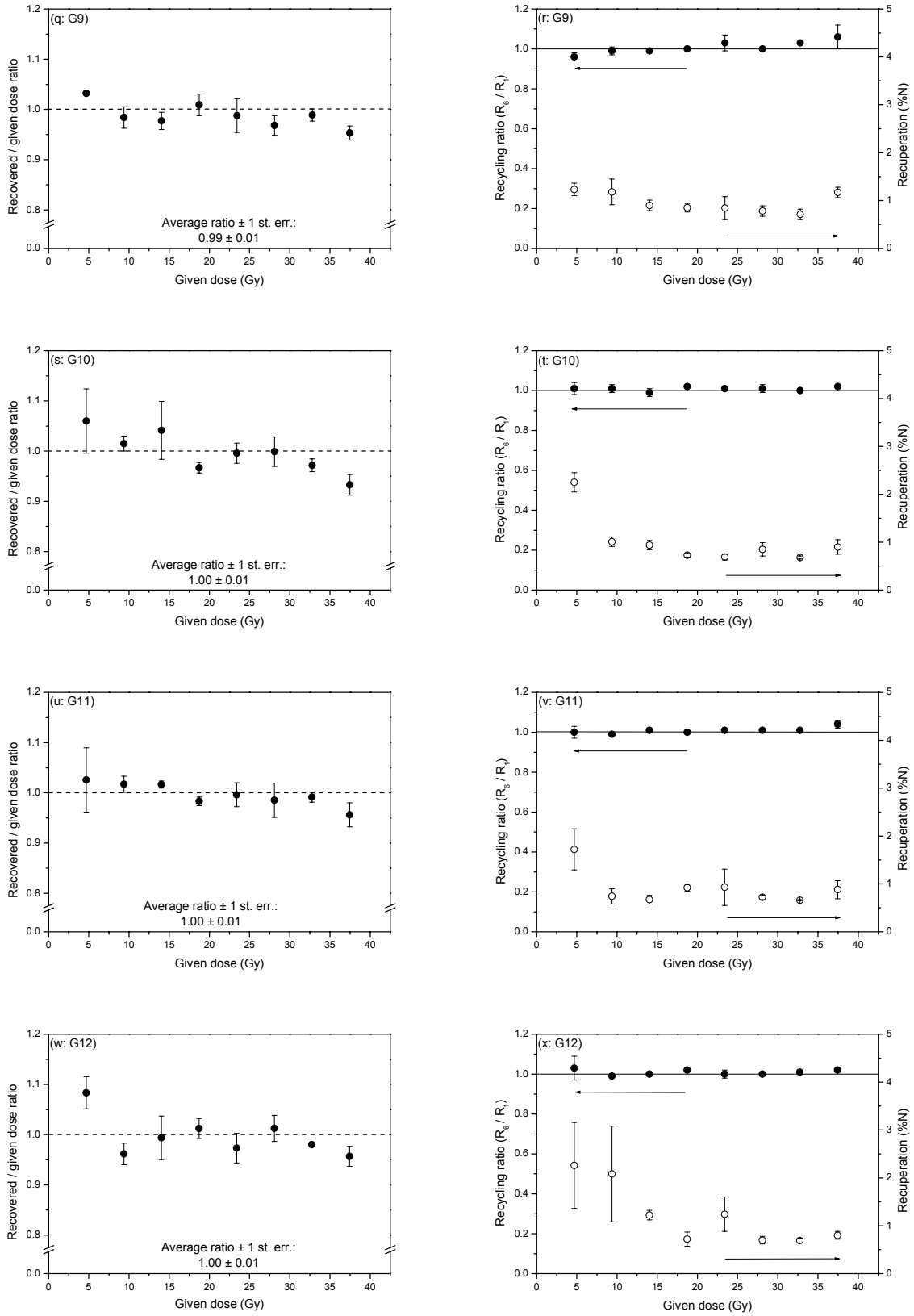

Figure 5.11 (continued): Data obtained from the dose recovery experiments; continued on the next page.

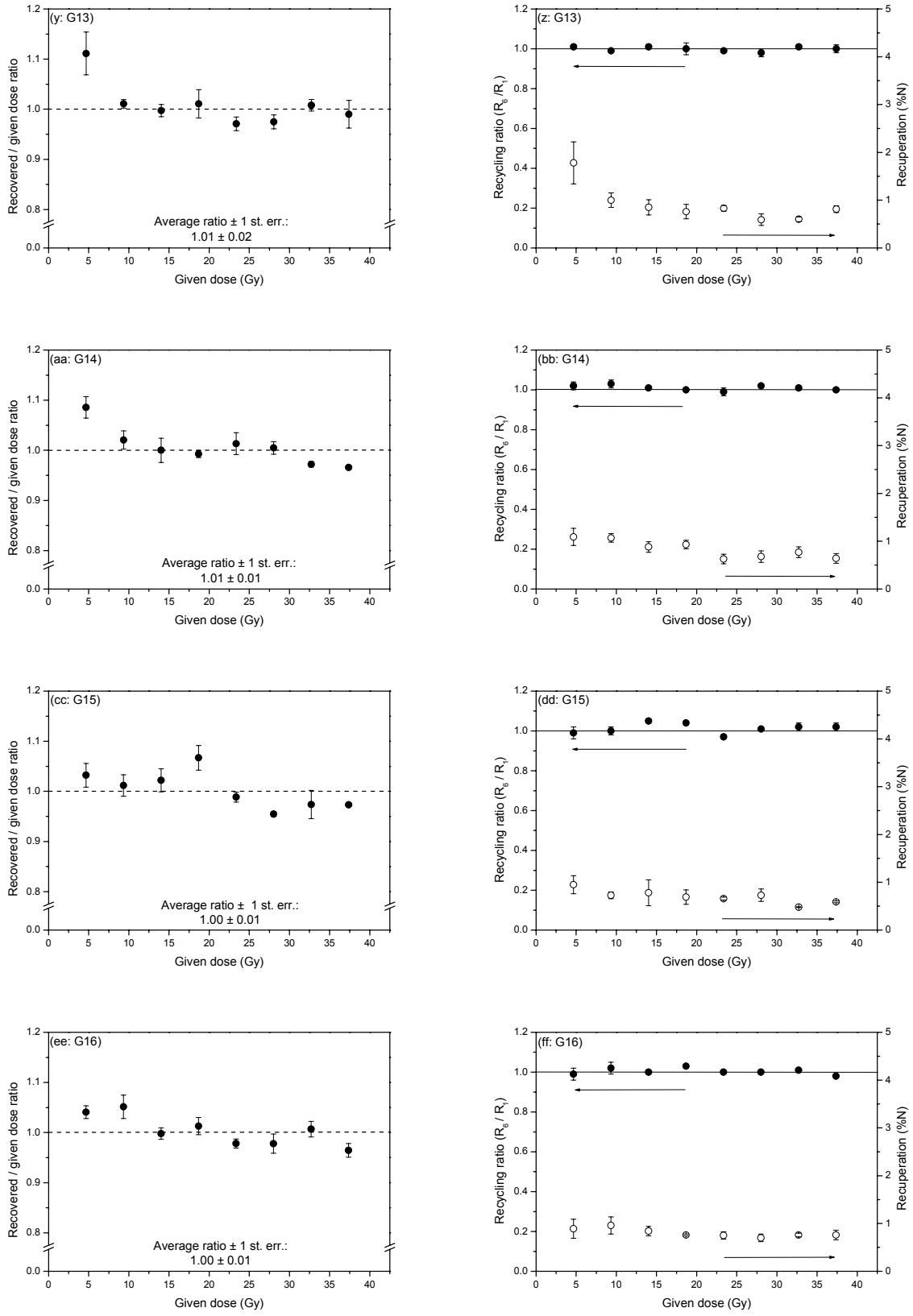

Figure 5.11 (continued): Data obtained from the dose recovery experiments; continued on the next page.

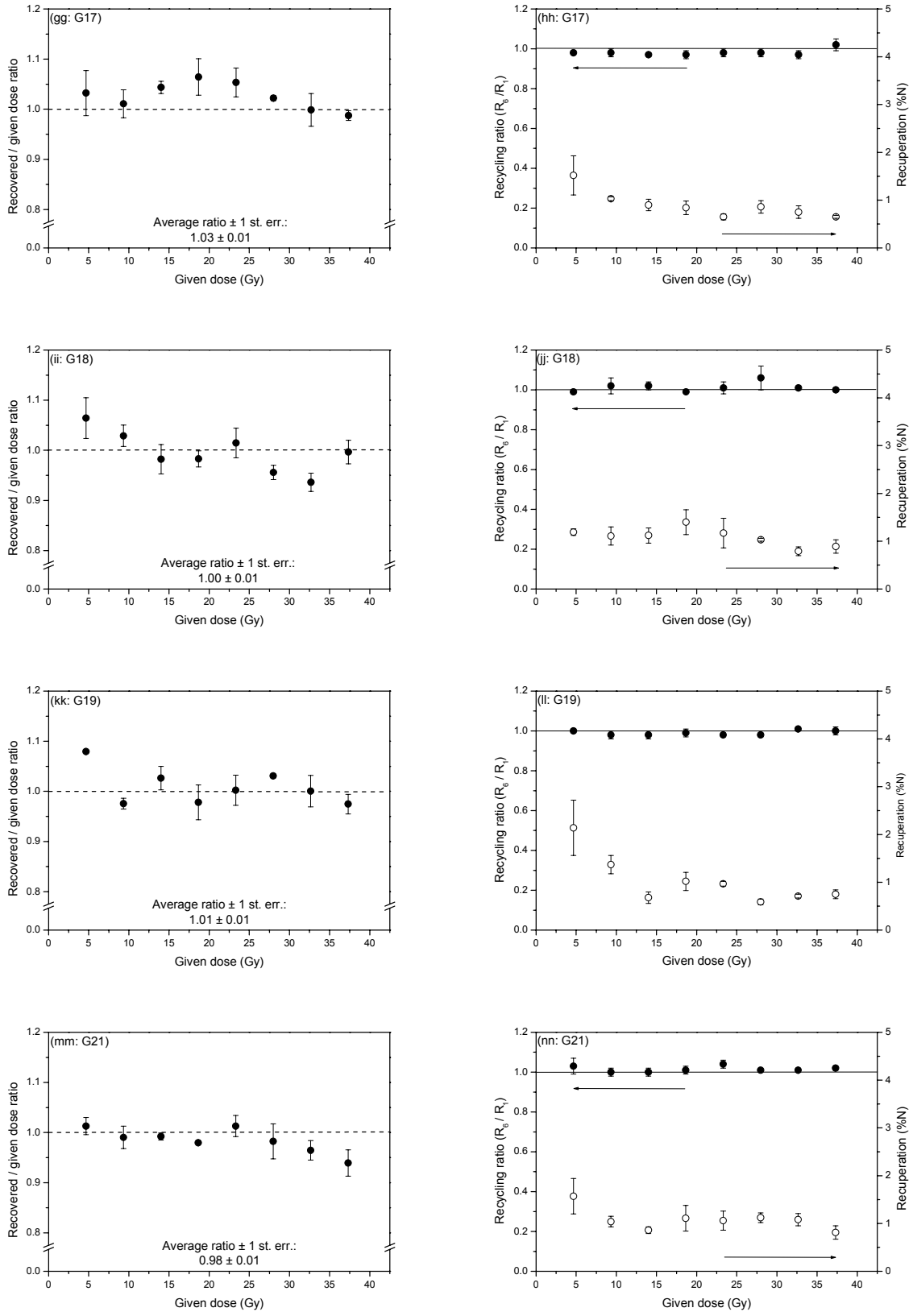

Figure 5.11 (continued): Data obtained from the dose recovery experiments; continued on the next page.

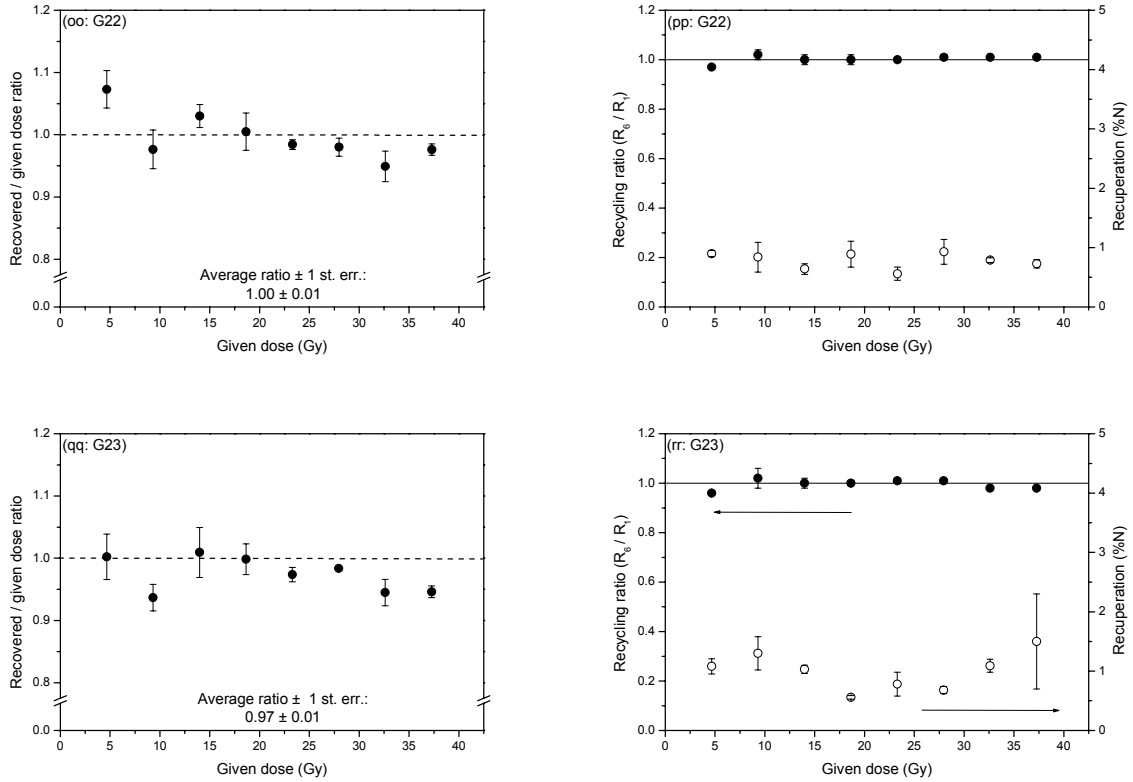

Figure 5.11 (continued): The figures on the left show the results of the dose recovery tests for the 22 samples from Grubbenvorst. Sample identification is given in the upper left corner of each figure. Three aliquots were measured for each given dose; the average recovered dose (expressed as the ratio versus the given dose) and one standard error are shown in the figures. The average ratio (± 1s) over the entire given dose range is also indicated in each figure. The dotted line is meant as an eye guide and represents the ideal recovered/given dose ratio equal to unity. The figures on the right show the corresponding recycling ratios (solid symbols) and recuperation (expressed as percentage of the corrected "natural" OSL signal; open symbols). The solid line indicating a recycling ratio equal to unity is meant as an eye guide.

5.5.3.4. Equivalent dose distributions

The D_e distribution was examined for one aeolian sample (G9), three fluvio-aeolian samples (G1, G7, G8) and two fluvial samples (G10 and G19), as well as for the two samples taken from the fluvio-aeolian to fluvial transition region (G3 and G4). For each sample, at least 96 "small" aliquots were prepared, using the spray mask with 2 mm diameter holes (see Section 5.5.2). The smaller amount of grains thus mounted on each aliquot should accentuate any heterogeneity in D_e. The equivalent doses were determined using the SAR protocol, in exactly the same way as outlined previously. The preheat temperature used was 10 s at 240°C for all samples, based on the preheat plateau plots shown in Figure 5.9. An equivalent dose was accepted if the recycling ratio was within the range of 0.90 – 1.10, if recuperation was less than 10% of the corrected natural OSL signal, and if the IRSL/OSL ratio (see Section 4.5.3) was ≤ 10%. Only a few aliquots had to be rejected.

5.5.3.4.1. Dose distribution in the aeolian sample (G9)

The results for sample G9 are shown as a histogram in Figure 5.12a. The distribution is similar in shape to the distributions observed for the samples from Ossendrecht (Figure 4.25). It is broad and quite symmetric, with a relative standard deviation of ~16%. The unweighted average D_e is 16.0 Gy, which is in acceptable agreement with the value of 16.6 ± 0.3 Gy that was obtained from the preheat plateau test [Figure 5.9(q)] The uncertainty arising from counting statistics on the natural signal is for the majority of the aliquots less than 5%. Hence, it seems unlikely that measurement precision alone can account for the width of the distribution. The precision of the measurement procedures was further assessed by treating the recycling dose (7.4 Gy) for each of the 95 aliquots as an unknown dose (cf. Section 4.8.2.1). The uncertainty on the sensitivity corrected recycled OSL signals due to counting statistics is typically about 5%, comparable to the natural dataset. However, a much tighter distribution was now obtained, with an unweighted mean of 7.7 Gy and a relative standard deviation of only ~7% (Figure 5.12b).

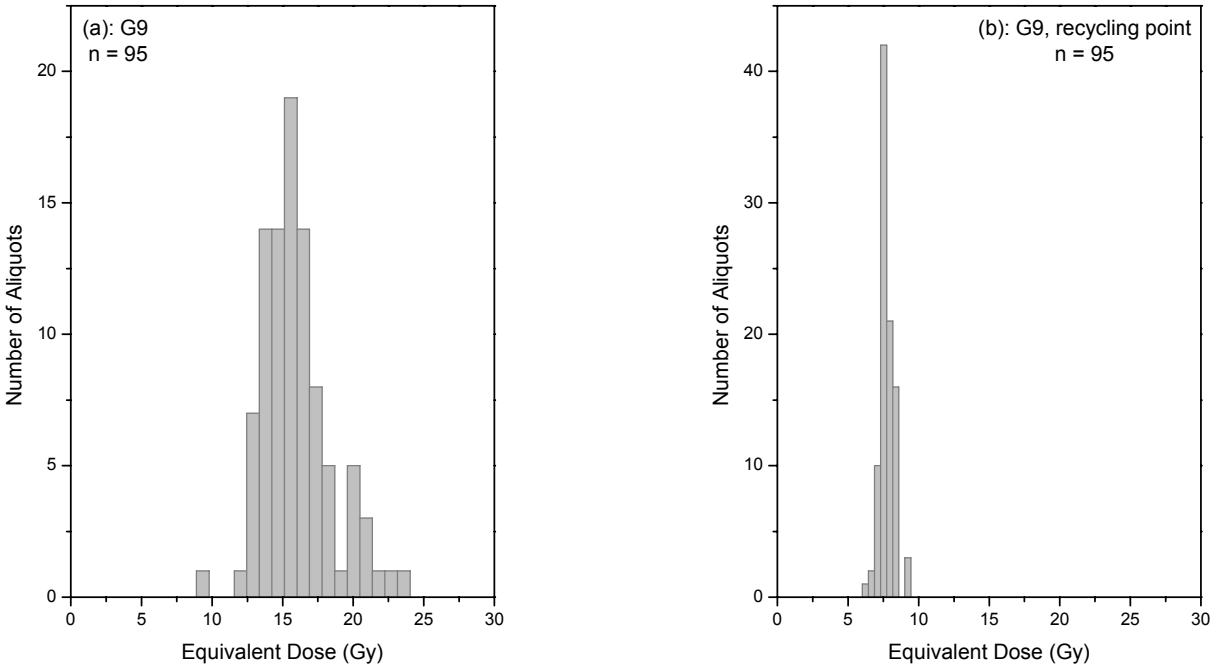

Figure 5.12 (a): D_e results from 95 small aliquots of the aeolian sample G9, presented as a histogram. Of the 96 aliquots that were analysed, only one had to be rejected. (b): D_e's obtained when for each aliquot of (a), the recycling dose was treated as an unknown.

So far, only the uncertainty on the natural (or recycled) OSL signal has been considered. The precision by which an individual D_e can be determined, however, is also influenced by the precision by which the data points of the growth curve have been measured. In other words, the total uncertainty on an individual D_e should also include a contribution from the fitting procedure. To get a notion of the magnitude of this total 'combined' uncertainty, use was made of Monte Carlo simulations. This well-known mathematical technique was chosen because of its simplicity, and because the calculations could easily be completely automated in Excel. Without going into details, the technique was applied as follows. The frequency distribution of each data point of the growth curve (and the natural OSL signal) was represented by a Gaussian distribution with as the mean the sensitivity corrected OSL signal and as the standard deviation the uncertainty on this OSL signal (obtained via conventional rules of error propagation). Using this distribution model and the random generator of Microsoft Excel, 5000 simulations were carried out for each data point, leading to 5000 growth curves and hence to 5000 solutions for the equivalent dose for each aliquot. A D_e and its associated total uncertainty were then obtained as the average and standard deviation of these 5000 solutions.

Processing the data for sample G9 in this manner, allowed constructing the radial plot shown in Figure 5.13. It can be seen that the majority of the D_e's bear a total uncertainty of less than 10% based on photon counting statistics. The radial plot also more appropriately represents the relationship between measurement precision and scatter. It clearly illustrates that equivalent doses on both extreme ends of the distribution can be obtained with an analytical precision of better than 5%. Hence, it is concluded that the width of the distribution cannot be explained by a poor measurement precision alone.

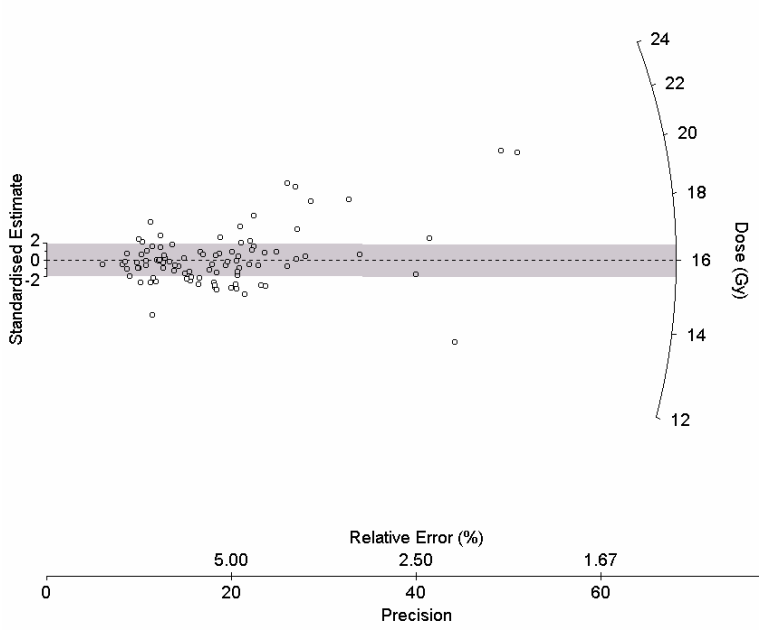

Figure 5.13: Radial plot of the data shown in Figure 5.12a. Uncertainties include those arising from the fit. The dashed line indicates the unweighted average of 16.0 Gy.

The observed equivalent doses range from 9 Gy up to 24 Gy, and this variation is quite symmetric around the unweighted mean. Sample G9 has an aeolian origin (Older Coversand II), and, hence, is expected to have been well bleached during transport. Furthermore, as the most easily bleachable part of the OSL signal was used for D_e calculation (the initial 0.32 s), partial bleaching is not really considered as a plausible explanation for the observed distribution. Nevertheless, this possibility was investigated into some greater detail by applying the SAR $D_e(t)$ technique (Bailey, 2003a; see also Sections 3.2.3.4.2 and 4.8.2.2) to the aliquots that yielded both relatively high and precise equivalent doses. At this point, it is worth recalling that recent investigations by Singarayer and Bailey (2004) have shown that the fast and medium components of the OSL signal bleach at the same rate under UV illumination. As this UV component is

significant in daylight, the SAR $D_e(t)$ technique is therefore not expected to identify partial bleaching in aeolian sediments. Indeed, for the SAR $D_e(t)$ technique to work, it is not only necessary that the OSL signal consists of different components, but also that these have been bleached to different degrees during transport. In other words, whether there is partial bleaching or not, SAR $D_e(t)$ plots for windblown sediments are likely to be flat.

However, the interpretation of the SAR $D_e(t)$ data was found not to be straightforward. At later stimulation time intervals, the recuperation increased to levels exceeding the 10% level that was set as a criterion for acceptance of an equivalent dose. To get a more detailed view on the variation in D_e and recuperation with stimulation time, the data were reprocessed with an increased resolution. The following stimulation time intervals were now used: 0 – 0.32 s, 0.32 – 0.8 s, 0.8 – 1.4 s, 1.4 – 2.4 s and 2.4 – 4 s (previously, the intervals 0 – 0.32 s, 0.32 – 2.4 s and 2.4 – 4 s were used; see Section 4.8.2.2). After 4 s of stimulation, the OSL signal had been reduced to ~1-5% of its initial intensity. An increasing width of the intervals was chosen to minimize the loss in precision that is associated with the reduction in the signal as the stimulation proceeds. Apart from that, the intervals were chosen completely arbitrarily; which intervals yielded the best counting statistics and/or result in the best separation of the different OSL components was not investigated.

Two representative examples are shown in Figure 5.14. For the first aliquot [Figure 5.14(a)], the natural D_e increases with stimulation time (solid circles). The replacement plot [i.e. the $D_e(t)$ plot for the recycling point treated as an unknown signal; open circles], however, is not flat. For the second aliquot [Figure 5.14(c)], the natural $D_e(t)$ data rather exhibit a decreasing trend, while a flat plot can be observed for the replacement data. Note that the uncertainties (1s) are quite large, especially at later stimulation time intervals.

The interpretation of the data becomes further complicated when the figures on the right are also considered [Figures 5.14(b) and (d)]. These show the corresponding variation in recycling ratio (solid circles) and recuperation (open circles) with stimulation time. Some deviation of the recycling ratios from unity can be seen, as well as a significant increase in recuperation with stimulation time. At the highest stimulation time interval, the recuperation reaches levels that are no longer negligible. Although about the same amount of recuperation is observed for both aliquots, their $D_e(t)$ data as well as the progress of

their recycling ratios with stimulation, are clearly different. Furthermore, the natural and regenerated signals behave differently. The effect of the recuperation on the SAR $D_e(t)$ data seems complicated and is poorly understood.

Over the whole of data collected for sample G9, an increase in recuperation with stimulation time is the general observation. It typically increased up to levels exceeding the 10% acceptance criterion. For some aliquots, it was even found to amount to levels as high as ~60% of the corresponding natural OSL signal. Some further discussion of these observations will be given at the end of this section.

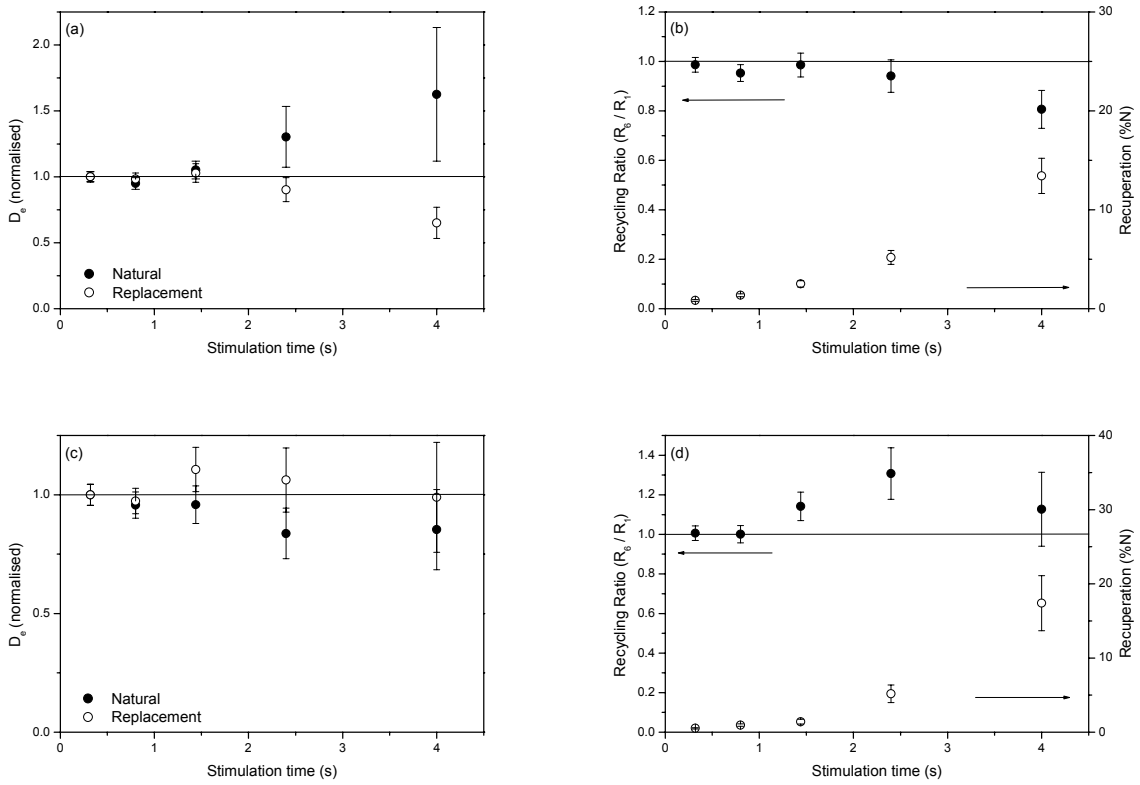

Figure 5.14 (a): SAR $D_e(t)$ plot for an aliquot of sample G9 yielding an equivalent dose of 22.7 ± 0.9 Gy. The solid circles refer to the natural dataset, the open circles to the replacement point (i.e. the recycling point was treated as an unknown signal). Error bars are 1s and were obtained through Monte Carlo simulations. The data have been normalised to the D_e obtained from the first stimulation time interval (0 – 0.32 s). The solid line is meant as an eye guide. (b): Recycling ratios (solid circles) and recuperation (expressed as percentage of the corrected natural OSL signal; open circles) as a function of the stimulation time. Error bars are 1s and arise from counting statistics only. (c) and (d): Same as in (a) and (b), respectively, for an aliquot of G9 yielding an equivalent dose of 20.2 ± 0.9 Gy.

5.5.3.4.2. Dose distributions in the fluvio-aeolian samples (G1, G7 and G8)

The dose distributions obtained for the fluvio-aeolian samples G1, G7 and G8 (taken from the Older Coversand I stratigraphic unit; see Figure 5.8) are shown as histograms in Figures 5.15 (a), (b) and (c), respectively. All three samples exhibit wide distributions. The unweighted average D_e's are 18.5 Gy (RSD: ~13%), 20.6 Gy (RSD: ~17%) and 22.3 Gy (RSD: ~17%) for samples G1, G7 and G8, respectively. These values are in acceptable agreement with the average D_e's across the preheat plateau region [G1: 19.0 ± 0.3 Gy, Figure 5.9(a); G7: 21.2 ± 0.3 Gy, Figure 5.9(m); G8: 23.6 ± 0.6 Gy, Figure 5.9(o)].
Proceeding with the analysis in the same way as for the aeolian sample (i.e. by looking at the spread of the recycled dose distribution, and by "quantifying" the uncertainty on each individual D_e through Monte Carlo simulations), showed that the precision of the measurements alone could not account for the observed spread in the data; the uncertainty on the D_e's arising from counting statistics was typically 5-6%
The Older Coversand I deposits have been interpreted as resulting from a complex interaction between aeolian and fluvial deposition in a periglacial environment (see Section 5.2). For instance, aeolian transport could directly supply sediments to the river system, from which they were subsequently deposited. Another possibility is that the sediments were first both transported and deposited by the action of the wind, and, only later on, reworked by fluvial processes. This reworking, however, is considered to have happened quite soon after the aeolian material had been deposited (deposition of the aeolian sands in winter, reworking and accumulation as fluvio-aeolian sands in spring and summer; Kasse, 1999; see also Section 5.2). In such conditions, any fluvial reworking and re-depositioning of the sediments should have taken place before a significant dose could accumulate in the grains. Furthermore, whatever the exact depositional mode was, the resetting of the OSL signal then most likely occurred in direct daylight. On the other hand, one cannot rule out that significantly older grains from previously deposited sediments were reworked, and became partially bleached. Indeed, during the cold Late Pleniglacial period, vegetation was virtually absent and hence, river bank stability was probably low and sediment supply towards the river large (Kasse et al., 1995). If these grains were completely bleached, which is possible as fluvial activity in a braided river system usually involves shallow water bodies, than there is obviously no problem. On the other hand, the high sediment load of the river adversely affects the bleaching conditions.

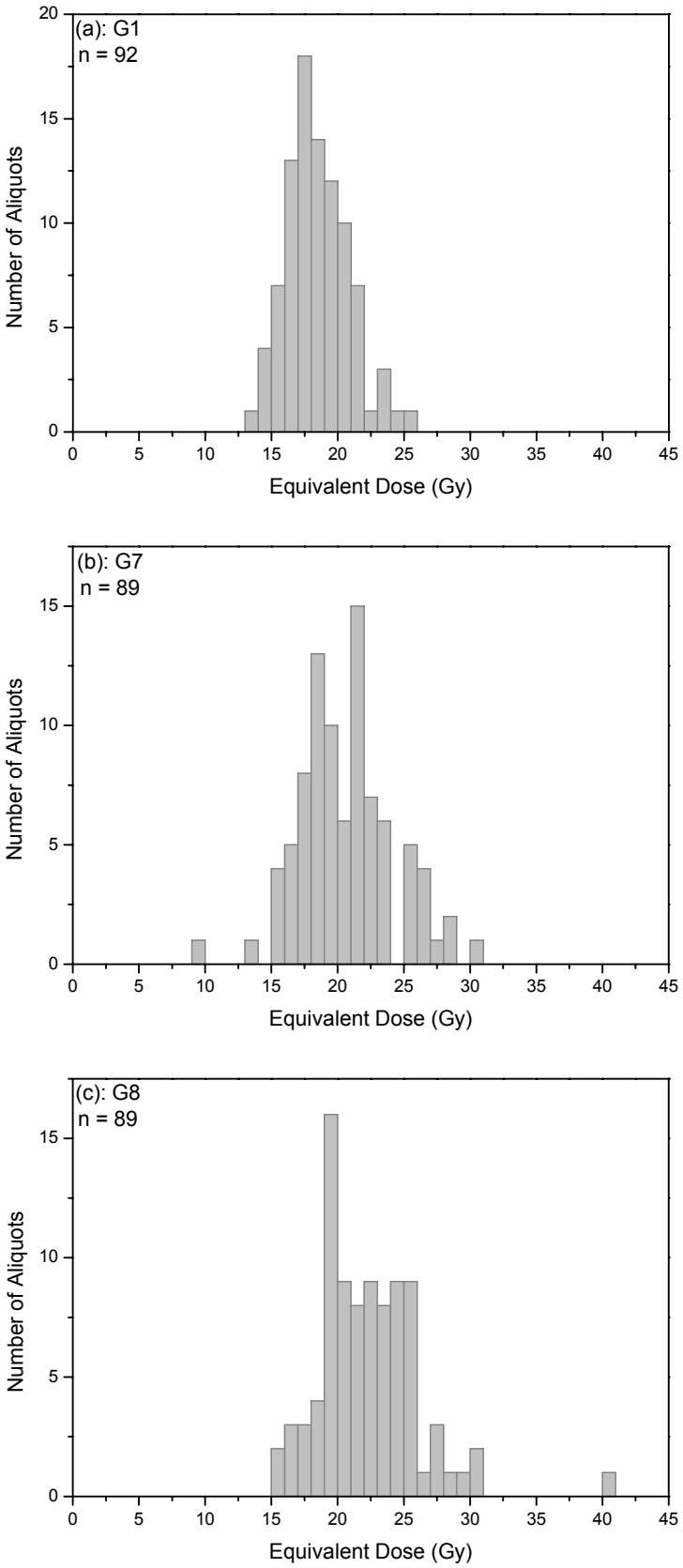

Figure 5.15: Equivalent dose distributions for fluvio-aeolian samples G1 (a), G7 (b) and G8 (c), respectively. For each sample, 96 aliquots were analysed; the number of aliquots that passed the criteria for acceptance (n) is indicated in the upper left corner of each figure.

The SAR $D_e(t)$ technique may yield some more objective information into the bleaching history of these samples. Therefore, it was applied to the datasets shown in Figure 5.15. Some illustrative results are shown in Figure 5.16.

For the four examples given, no significant increase in $D_e(t)$ can be seen. For one of the aliquots [Figure 5.16 (g)], the natural $D_e(t)$ plot instead shows a pronounced decrease. The replacement points, on the other hand, yield approximately constant $D_e(t)$'s, although some deviations are visible at the 1s level [see e.g. Figure 5.16 (e)]. The figures on the right show the corresponding variations in recycling ratio and recuperation. As for the aeolian sample, some variation of the recycling ratios around unity can be observed, as well as an increase of the recuperation with stimulation time. A dramatic increase in recuperation can be observed in Figure 5.16(h), where it reaches a value of about 60% of the corrected natural OSL. In this case, the increase is followed by a decrease of the natural $D_e(t)$ data [Figure 5.16(g)]. As was noted previously, the natural and regenerated data behave different.

The examples shown in Figure 5.16 are representative of all the SAR $D_e(t)$ results obtained for the fluvio-aeolian samples. For all investigated aliquots and for all three samples, an increase in $D_e(t)$ for the zero dose point was observed. At later stimulation times, the recuperation generally reached values of ~15 to 60% of the corrected natural OSL signal. In some cases, the recuperation at the latest stimulation time interval was observed to even exceed the natural signal. The effect on the $D_e(t)$ data (natural and regenerated) and recycling ratios varied between the aliquots. Only for a few aliquots were the 10% criteria (for recycling ratio and recuperation) met over the entire 4 s of stimulation that was examined. Here, no increasing $D_e(t)$ plots were observed.

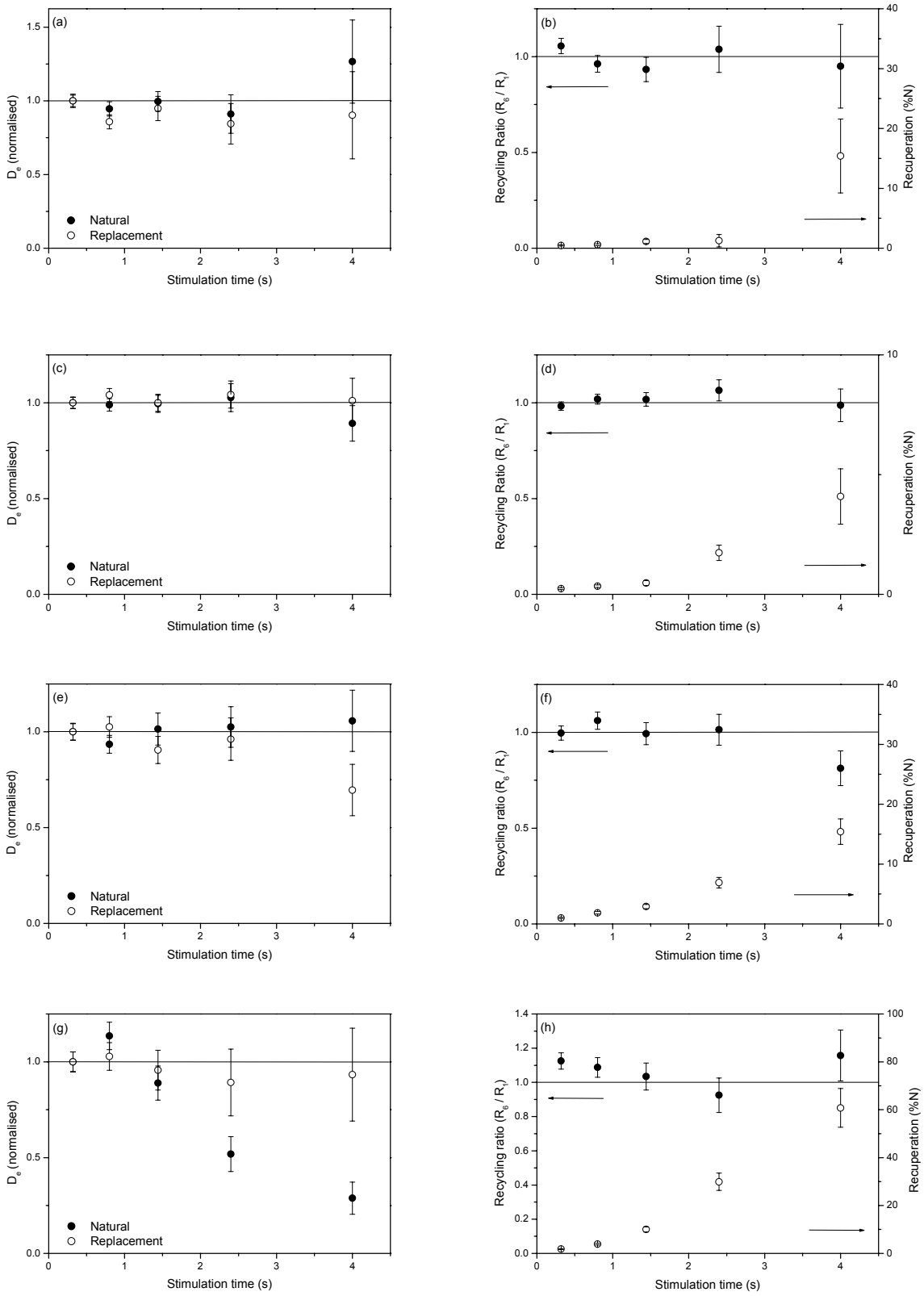

Figure 5.16: The figures on the left show the SAR $D_e(t)$ plot for an aliquot of sample G1 yielding a D_e of 25.4 ± 1.0 Gy (a), for an aliquot of sample G7 yielding a D_e of 30.1 ± 0.9 (c), and for two aliquots of sample G8 yielding D_e's of 30.4 ± 1.3 Gy (e) and 29.9 ± 1.5 Gy (f). The figures on the right show the corresponding variations in recycling ratio and recuperation. The meaning of the symbols is the same as in Figure 5.14.

5.5.3.4.3. Dose distributions in the fluvio-aeolian / fluvial samples (G3 and G4)

The D_e distributions obtained for samples G3 and G4 (taken from the transition region between the fluvio-aeolian and the fluvial samples; see Figure 5.8) are shown in Figure 5.17 (a) and (b), respectively.

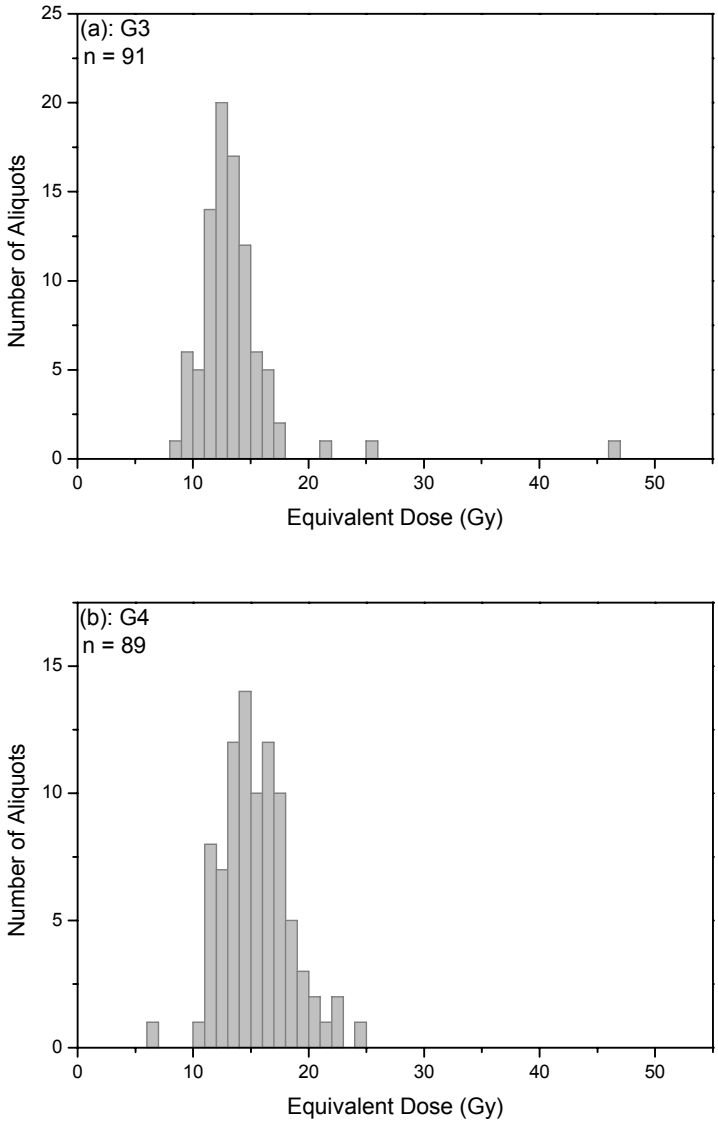

Figure 5.17: D_e distributions for samples G3 (a) and G4 (b). These samples were taken from the transition zone between the fluvio-aeolian and fluvial deposits (see Figure 5.8). For each sample, 96 small aliquots were measured and the number that passed the criteria for acceptance (n) is mentioned in the upper left corner of each figure.

A wide range of equivalent doses was obtained. The unweighted average D_e's are 13.6 Gy (RSD: 32%) and 15.4 Gy (RSD: 19%) for samples G3 and G4, respectively, which is in acceptable agreement with the average D_e's derived from the plateau region in the D_e versus preheat temperature plots [G3: 13.5 ± 0.4, Figure 5.9(e); G4: 16.6 ± 0.3 Gy, Figure 5.9(f)].

Again, the precision by which the individual D_e's were determined could not account for the observed variations. The uncertainty on the D_e's arising from counting statistics was typically 9-12% for sample G3 and 6-8% for sample G4. The samples were therefore examined for signal resetting by looking for an increase in D_e with stimulation time. Some arbitrarily chosen examples are shown in Figure 5.18.

None of the aliquots show rising $D_e(t)$ plots. The two results shown for sample G3 [Figures 5.18(a) and (c)] are somewhat scattered, but also carry quite large uncertainties. If any trend is to be discerned, it would rather be a slightly decreasing one. In the given examples for sample G4 [Figures 5.18 (f) and (h)], recuperation remains within acceptable limits (≤ 10%) and the $D_e(t)$ data are relatively flat. Nevertheless, recuperation does increase with stimulation time. Figure 5.18(b) illustrates that high levels of recuperation (> 10%) were observed for these samples as well. Whereas the increase in recuperation does not seem to affect the replacement data (and recycling ratios), it is followed by a significant drop in the natural $D_e(t)$ data [Figure 5.18(a)]. From Figure 5.18(d), it can be seen that recuperation might not be sole factor complicating the interpretation of a $D_e(t)$ plot. In this case, the recuperation meets the 10% criterion (within analytical uncertainties), but there is a marked drop in recycling ratio at the latest stimulation time interval. This indicates that the sensitivity correction is no longer working as intended. Additional factors that might influence the shape of a $D_e(t)$ plot will receive some attention at the end of this section.

Once more, these observations are considered to be representative for the entire dataset. Indeed, over the first 4 s of the OSL shine down curve that was studied, the recuperation increased with stimulation time for all aliquots. A large inter-aliquot variability in amount of recuperation, in shape of the $D_e(t)$ plots and behaviour of the natural and regenerated data was observed. No unambiguously rising $D_e(t)$ plots were encountered.

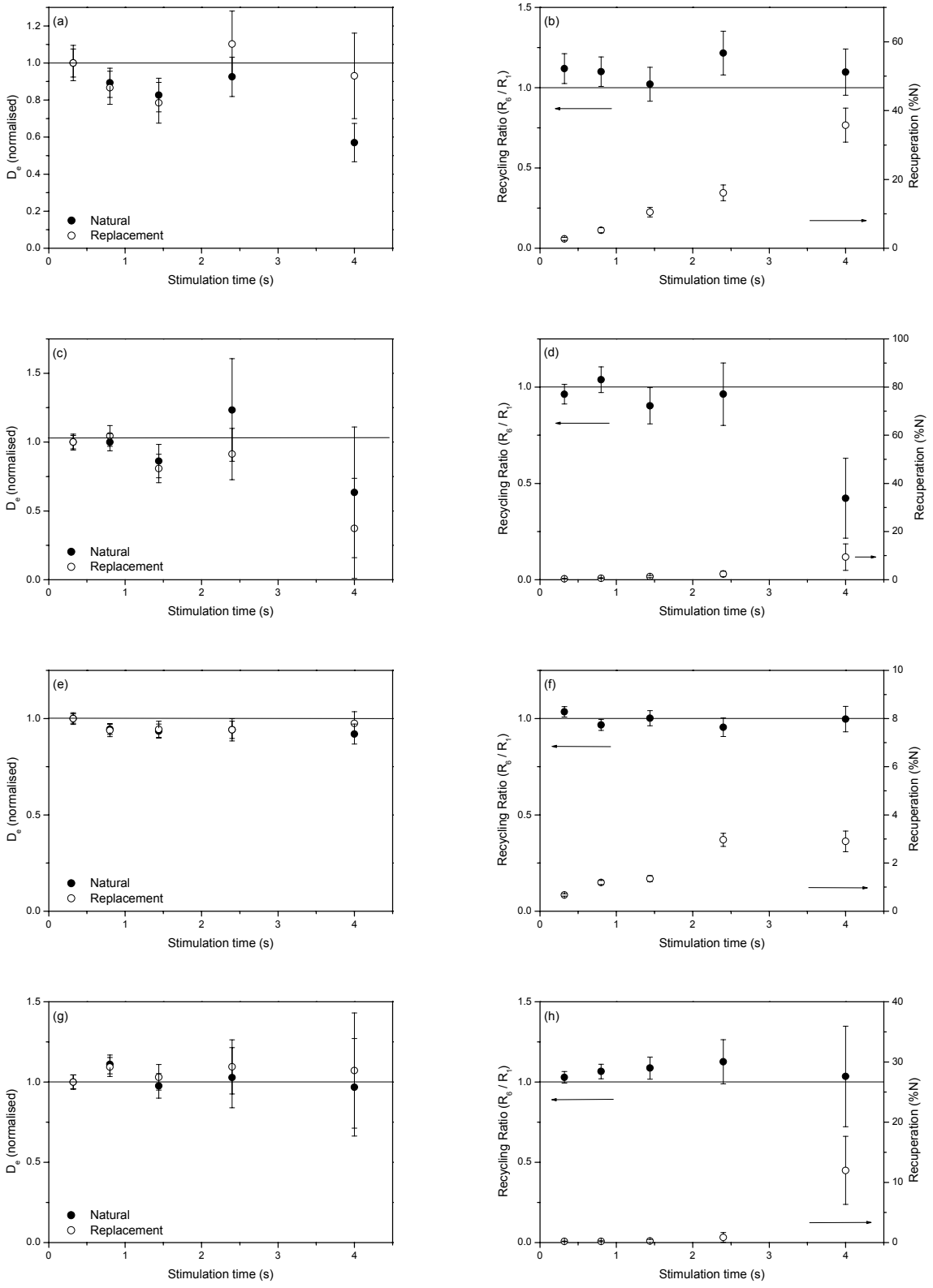

Figure 5.18: The figures on the left show the SAR $D_e(t)$ plots for two aliquots of sample G3 yielding a D_e of 25.9 ± 2.0 Gy (a) and 21.5 ± 1.0 Gy (c) and for two aliquots of sample G4 yielding a D_e of 22.7 ± 0.6 Gy (e) and 22.1 ± 1.0 Gy (g). The figures on the right show the corresponding variation in recycling ratio and recuperation. The meaning of the symbols is the same as previously.

5.5.3.4.4. Dose distributions in the fluvial samples (G10 and G21)

Finally, the D_e distribution data for the fluvial samples G10 and G19 are plotted as histograms in Figures 5.19(a) and (b), respectively. The unweighted average D_e's are 12.6 Gy (RSD: ~24%) and 12.8 Gy (RSD: ~30%) for G10 and G19, respectively, which are consistent with the average D_e's obtained using large aliquots [G10: 12.2 ± 0.3 Gy, Figure 5.8(s); G19: 13.1 ± 0.6 Gy, Figure 5.8(kk)].

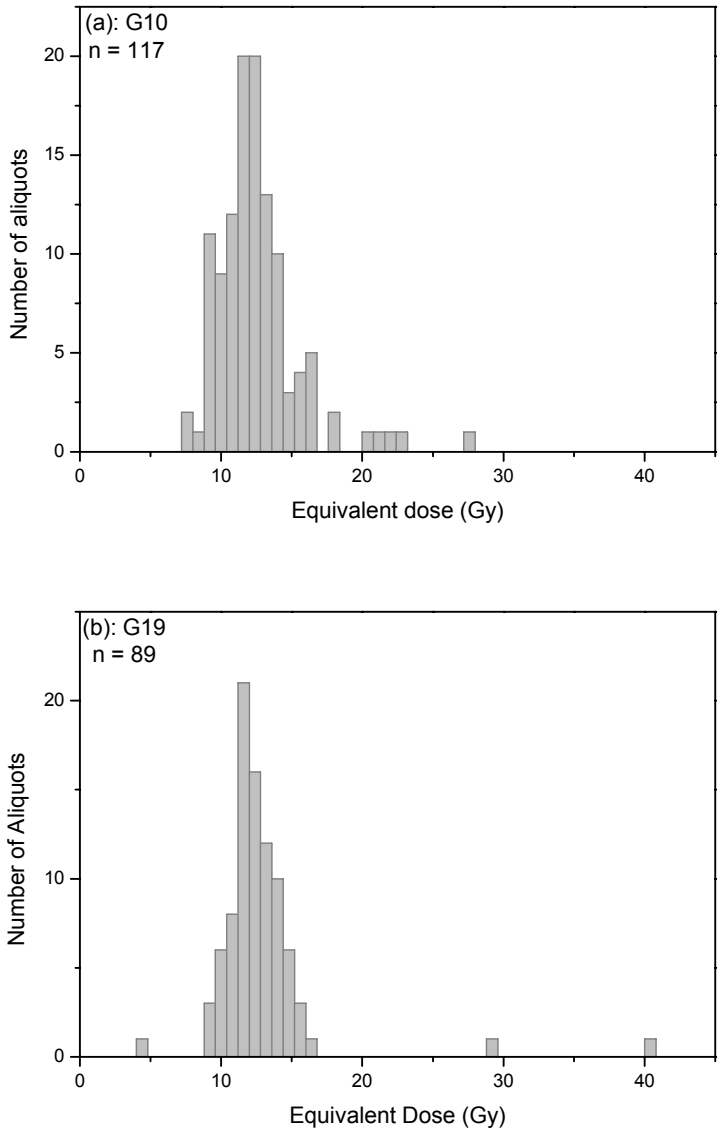

Figure 5.19: Equivalent dose distributions for small aliquots of quartz extracted from the fluvial samples G10 (a) and G19 (b). For sample G10, 120 aliquots were analysed, while for sample G19 only 96 aliquots were measured. The number of aliquots (n) that passed the criteria for acceptance is given in the upper left corner of each histogram.

The doses again cover a wide range and are now slightly more asymmetrically distributed (especially for sample G10). A few aliquots yield distinctly low or high equivalent doses, which is not the result of a poor measurement precision. The observations once more suggest the presence in these samples of a mixture of grains containing different doses.

In fluvial environments, sediments are much less likely to be completely reset. Evidence for incomplete resetting in fluvial environments, resulting in wide and asymmetric dose distributions, has been presented by a number of authors (e.g. Murray et al., 1995; Olley et al., 1998). The distributions observed for the fluvial samples G10 and G19 might therefore truly reflect a heterogeneous and incomplete resetting process. The fluvial sediments, however, represent so-called braided river deposits, and were transported and deposited in shallow, highly energetic and turbulent conditions (see Section 5.2). In such a regime complete resetting is more likely. If the sediment grains were carried close to the surface (due to the turbulent transport or simply because the water was shallow), they were exposed to daylight that still contained a significant portion of the UV component. The slow and medium OSL components will then bleach at about the same rate (Singarayer and Bailey, 2004) and the SAR $D_e(t)$ technique will not be able to detect partial bleaching. This is not necessarily a problem, if the grains were exposed to enough light for their OSL signal to be completely removed. However, as the river probably carried a high sediment load, partial bleaching cannot be ruled out.

To get a better insight on the degree of signal resetting in these samples, the SAR $D_e(t)$ technique was applied here as well. Some examples are shown in Figure 5.20.

For both samples, the $D_e(t)$ plots do not present any unambiguous evidence for partial bleaching in these aliquots. The results shown in Figure 5.20(e), for instance, suggest a rise in the D_e as stimulation proceeds, but the variation in the data for the replacement point questions the reliability of this observation. Figure 5.20(a), on the other hand, shows another example of a falling $D_e(t)$ plot. The figures on the right illustrate that also for these samples recuperation increases with stimulation time, and can reach relatively high levels [Figure 5.20(b)]. Also, even if an aliquot passed the 10% acceptance criterion for recuperation, its $D_e(t)$ plot was not necessarily observed to behave as intended. This is illustrated in Figure 5.20g (replacement point) and 5.20h (recycling ratio). Although the results are rather imprecise, both the replacement point and the recycling ratio show a significant drop at the latest stimulation time.

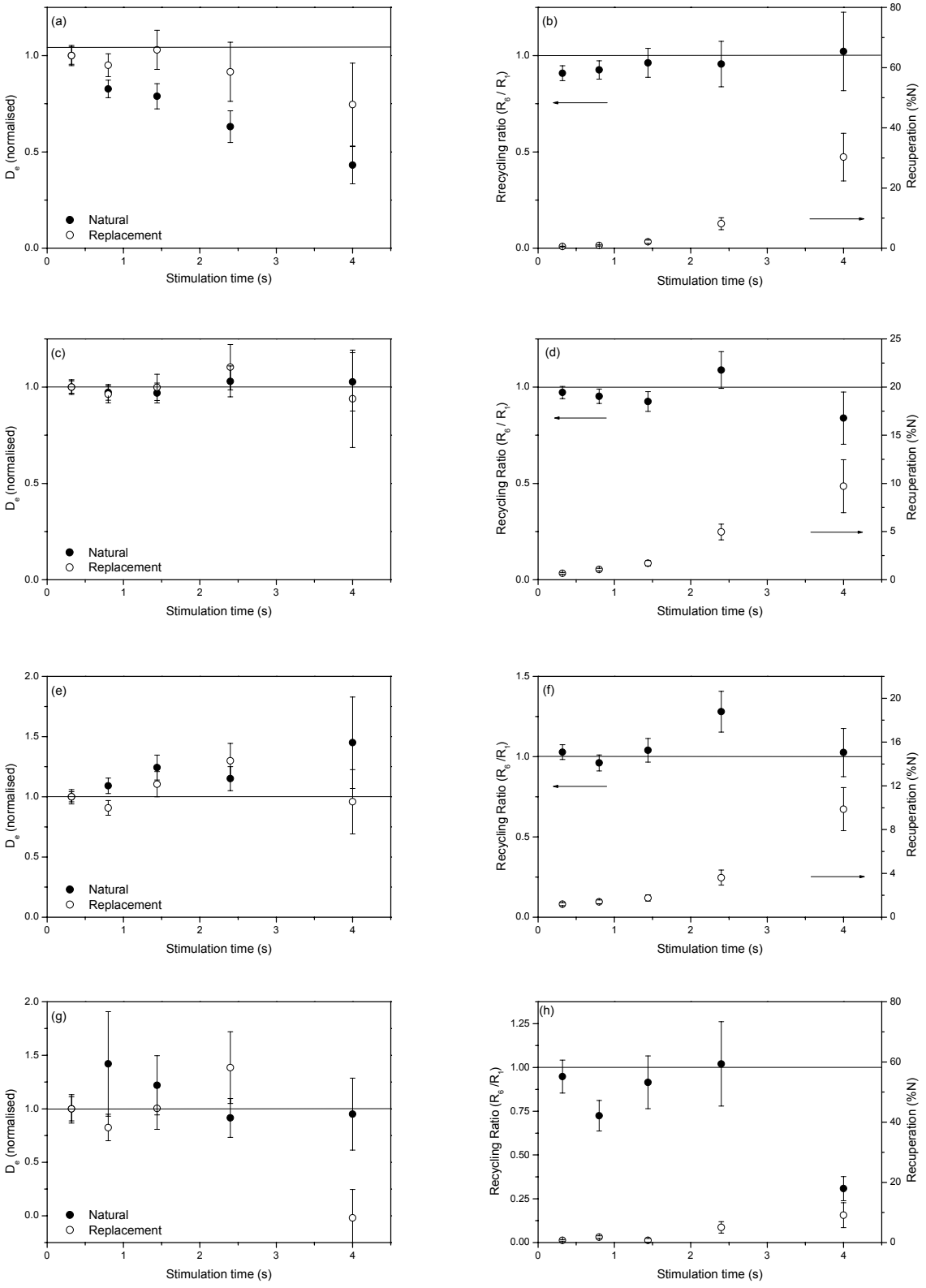

Figure 5.20: The figures on the right show SAR $D_e(t)$ plots for two aliquots of sample G10 yielding D_e's of 21.6 ± 1.0 Gy (a) and 18.0 ± 0.6Gy (c), and for two aliquots of sample G19 yielding D_e's of 29.5 ± 1.3 Gy (e) and 40.0 ± 5.3 Gy (g). The figures on the right show the corresponding variation in recycling ratio and recuperation. The symbols mean the same as previously.

Observations similar to those shown in Figure 5.20 were made for other aliquots of these samples. The plots for the natural signal were flat [cf. Figure 5.20(c)], falling [cf. Figure 5.20(a)] or slightly rising [cf. Figure 5.20(e)], but could, in combination with the replacement data (and/or the acceptance criteria for recuperation and recycling ratio), not be convincingly attributed to partial bleaching.

5.5.3.4.5. Discussion

For all samples wide D_e distributions were observed, exhibiting some degree of asymmetry. The large spread in equivalent doses could not be attributed to limitations in measurement precision alone. Non-linearity of the growth curves may contribute to the shape (both width and high-dose tailing) of the dose distributions (Murray et al., 2002; Murray and Funder, 2003). In the dose range under consideration here, however, the interpolation involved that region of the saturating exponential growth curve where the curvature is still small. Nevertheless, large variations in dose response characteristics between aliquots were observed, comparable to the findings for the Ossendrecht samples (Figure 4.24). For some aliquots, the growth curves reached earlier saturation than for others, and so the effect is probably not entirely negligible.

Another possibility accounting for both higher as well as scattered D_e values is that of inter-aliquot variations in thermal transfer (see Section 3.2.2). However, as was shown in Figure 5.9, the D_e is quite insensitive to the preheat temperature. This indicates that thermal transfer is not important in these samples. Note that the D_e measurements described in the present section used a preheat temperature (10 s at 240°C) that was chosen from the preheat plateau region.

The major contributory factor to the shape of the distributions is, therefore, thought to be that the samples are truly composed of grains containing different doses. Considering the depositional history of the samples, one would not really expect partial bleaching to play a significant role. However, to get a better insight into this matter, the SAR $D_e(t)$ technique was applied to the datasets. Although only a few examples could be given here, which were chosen as to be representative for the whole of $D_e(t)$ plots available, they illustrate the inter-aliquot variability and the complications that were encountered. One common feature, however, could be clearly recognised for all aliquots and for all samples: a detectable increase in recuperation with stimulation time. In many cases, this ultimately reached levels largely exceeding 10% of the corrected natural OSL signal.

Recuperation is usually attributed to transfer of charge in one way or another (see Section 3.2.2.2). In this case, the rise in $D_e(t)$ for the zero dose points would suggest a progressively more significant transfer of charge into the less bleachable components of the OSL signal. These observations are consistent with the results of the more detailed investigations recently presented by Jain et al. (2003; see also Murray and Wintle, 2003). Using linearly modulated OSL, they found no detectable recuperation of the fast component of the quartz OSL signal (this is comparable to the results obtained in this work using the OSL signal integrated over the initial 0.32 s of stimulation), while significant recuperation was observed for the slower OSL components, the amount being greater as the components become more difficult to bleach.

It appears that the effect of recuperation on $D_e(t)$ can manifest itself in a different direction for the regenerated and the natural signals, or in no effect at all. Although this might represent reality, it must be pointed out, however, that also other factors (alone or in combination with each other) can determine the appearance of a $D_e(t)$ plot. These factors are related to the thermal stability of the different OSL components and their saturation characteristics, the actual composition of the OSL signal, the magnitude of any residual signal and the exact spectral composition of the daylight during the bleaching. A falling $D_e(t)$ plot, for instance, can alternatively be attributed to the disturbing interference of one of the slow components of the quartz OSL signal. This component has been found to be thermally unstable and saturates at much lower doses than the other components (component S2; Singarayer and Bailey, 2003). For further details, reference can be made to Bailey (2003a, b), Singarayer and Bailey (2003), Bailey et al. (2003) and Jain et al. (2003).

Considering all these potential complications, as well as the possibility that each interval of the shine-down that was used actually may be composed of more than one component, would suggest that any trend in a SAR $D_e(t)$ plot (rising, falling or constant) can originate from a combination of causes. The interpretation of such a plot is consequently far from simple and the usefulness of the technique rather limited. The observations made in this work do not support the conclusion made by Bailey et al (2003), that the SAR $D_e(t)$ technique provides a useful tool in the identification of incompletely bleached sedimentary quartz samples. It is worth emphasizing that even if the SAR $D_e(t)$ technique would accurately identify partial bleaching, this identification relates to the slow components. It gives no information as to the degree of resetting of the fast OSL

component (the initial 0.32 s of stimulation), which is the component usually employed for dating.
In any case, none of all investigated aliquots exhibited a rising SAR $D_e(t)$ plot that could unambiguously be attributed to partial bleaching. It is concluded that if incomplete resetting is responsible for the observed dose distributions, signal analysis could not identify it in the samples from Grubbenvorst, regardless of whether the samples had an aeolian, fluvio-aeolian or fluvial nature.

If partial bleaching is indeed responsible for the observed distributions, then the D_e values at the lowest end of the dose distribution are expected to yield the most accurate ages. As will be shown in Section 5.7, the overall unweighted average D_e's calculated from the preheat plateau plots, however, yield ages in quite good agreement with the geological expectation. No serious age overestimation could be detected. The use of a simplified leading edge approach, e.g. by using the average D_e calculated from the 5% of the aliquots that yield the lowest D_e values (Olley et al., 1998), would rather lead to age underestimations. Combining all the evidence leads to the conclusion that the observed variation in equivalent doses cannot convincingly be attributed to partial bleaching.
According to Rieser and Smith (2003; see also Section 3.2.3.2), partial bleaching is a rare event, and they argue that the primary cause for scatter in most dose distributions is an inhomogeneous radiation field. Variations in microdosimetry could indeed give rise to a sample consisting of a mixture of grains containing different doses. Although this possibility was not explicitly investigated, it will be shown in the next section that the sedimentary profile in Grubbenvorst consists of a succession of layers with different radioactivity characteristics. Hence, it is concluded that microdosimetric variations form a sensible explanation for the observations made on the Grubbenvorst samples. It is acknowledged that this deduction is mostly substantiated by the lack of other clearly apparent causes. However, it can be recalled that differences in radioactivity on a very small scale were found to the most likely explanation for the scatter observed in the dose distributions of the Ossendrecht samples (Section 4.8).
It can finally be pointed out once more that acceptable ages were obtained for these samples (Section 5.7.). Consequently, whatever the causes of the distributions are, they do not seem to have a major implication towards the accuracy of the age determination. This is in support of the hypothesis that the distributions do not originate from incomplete resetting, as in such a case, averaging would lead to age overestimations.

5.6. Annual dose determination

Determination of the annual dose was based on the same analytical techniques as outlined in Section 4.6 (i.e. in-situ gamma-ray spectrometry, low-level gamma-ray spectrometry, neutron activation analysis and thick source alpha counting). Some minor refinements or modifications were made to the experimental procedures and these are reported in the following, together with the analytical results and their interpretation.

5.6.1. Gamma-ray spectrometry

5.6.1.1. Field NaI(Tl) gamma-ray spectrometry

In-situ gamma-ray spectrometry was carried out at the position of the dating samples G1, G7, G9 and G10 (Section 5.4). Data processing was exactly as previously outlined (Section 4.6.1.1; see also Hossain, 2003), employing the "Heidelberg" calibration for converting the measured count-rates to concentrations. To eliminate any subjectivity between analysts*, which is inevitably always present to some degree in the fitting of the spectra, the calibration spectra were reprocessed as well. Table 5.1 summarises the results of this exercise.

	Concentration [a]	**s** [b]	**Count-rate** [c] **(cps)**	**s** [d]	**Calibration factor**	**s**
K	4.08 %	0.11	32.1	0.5	7.86 cps/%	0.24
U	18.8 mg kg^{-1}	1.3	6.2	0.6	0.33 cps/ mg kg^{-1}	0.04
Th	14.0 mg kg^{-1}	0.9	3.1	0.1	0.22 cps/ mg kg^{-1}	0.02

Table 5.1: a: weighted average of AAS and NAA results obtained for the inner and the outer part of the drill core that was retained when the auger hole in the "Flossi" granite block was made (Rieser, 1991). b: standard error. c: average of three calibration measurements. d: largest of the observed (scatter) and expected (counting statistics) uncertainty. All uncertainties are 1s.

* See Section 4.6.1.1: the results obtained via field gamma-ray spectrometry in Ossendrecht (Table 4.3) are those obtained by Hossain (2003), corrected for the difference in composition and packing density between the sand and the granite calibration block (following De Corte et al., 2003).

The calibration factors given in Table 5.1 were used further throughout this work. The last column of the table shows the systematic uncertainties associated with this technique. It can be seen that they are relatively large for U and Th (12% and 7%, respectively).
The K, U and Th concentrations obtained for the four field measurements in Grubbenvorst are given in Table 5.2.

	K (%)	**U** (mg kg^{-1})	***Th*** (mg kg^{-1})
G1	0.663 ± 0.006	0.92 ± 0.05	2.21 ± 0.04
G7	0.688 ± 0.007	0.97 ± 0.07	2.31 ± 0.05
G9	0.668 ± 0.004	1.32 ± 0.06	2.83 ± 0.05
G10	0.255 ± 0.002	0.34 ± 0.03	0.93 ± 0.03

Table 5.2: K, U and Th concentrations obtained via in-situ gamma-ray spectrometry. Uncertainties are 1s and arise from counting statistics only; no systematic uncertainties are included. The concentrations given are on a dry weight basis by making allowance for the "as found" moisture content and have been corrected for the difference in composition and packing density between calibrant and sample (De Corte et al., 2003a).

5.6.1.2. Low-background Ge gamma-ray spectrometry

Low-background gamma-ray spectrometry was carried out as described in Section 4.6.1.2. It was not applied to all samples for reasons of instrument availability. Furthermore, due to electricity renovation works in the building where the measurement apparatus is located, some spectra got lost or were rendered completely useless by intolerably high levels of electronic noise. This might cause the dataset reported below to appear as somewhat incoherent.

All measurements were carried out on ~ 60-200 g of dried material (at 110°C, until constant weight). Samples were gently rubbed in a mortar to remove larger agglomerates and, by doing so, to ensure a more reproducible packing in the container. As well as the sediment samples specifically taken in the field for gamma-ray spectrometry (see Section 5.4), in some cases the outer material that had been discarded from the sampling tubes

was also measured. In these cases, the material was crushed to a grain size < 63 μm in a ball-mill. After filling and sealing the sample container, it was stored for at least one month to allow ^{222}Rn, which might have escaped during sample preparation, to build up again. All samples were measured in a "Bluecap" geometry (a simple plastic container with a screw-cap). The system had already been calibrated for these measurement geometries (in a relative way versus IAEA standards RGK-1, RGU-1 and RGTh-1), but as for the field gamma-ray spectrometry, the previously recorded calibration spectra were reprocessed. Samples were typically measured for 1 week, in some exceptional cases for two weeks, as a compromise between instrument occupation and obtaining acceptable counting statistics. As it was impractical to determine the elemental composition of each sample, the average elemental composition of the coversands from Ossendrecht (see Table 5.3) was used for all detection efficiency calculations. No corrections for true-coincidence (COI-factors) were performed in the calculation of concentrations, as the differences in these factors between standard and sample were negligible. The differences in COI were also negligible in the corrections for spectral interference.

Element	%
Si	39.76
Ti	0.12
Al	0.70
Fe	0.22
Mn	0.005
Ca	0.02
Na	0.17
K	0.49
P	0.005
H	1.40
O	57.11

Table 5.3: The elemental composition (of the coversands from Ossendrecht) that was used in all detection efficiency calculations.

The K concentrations obtained via low-level gamma-ray spectrometry are summarised in Figure 5.21. A clear concentration variation can be observed throughout the profile. Sample G14 yields a distinctly higher K concentration, while the lowest concentrations were found for the coarse fluvial sands at the base of the exposure. It can also be noted that samples from the same stratigraphic position (i.e. G15, G22, G9 & G23, and G10 & G21) yield approximately the same K concentration.

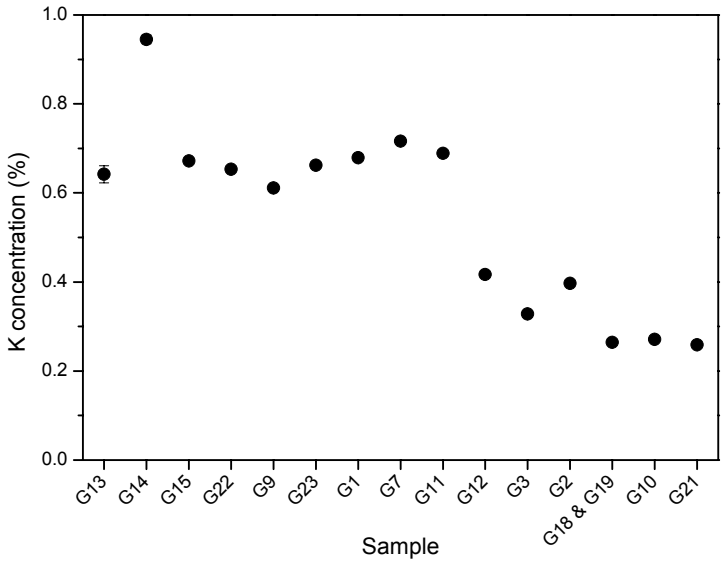

Figure 5.21: K concentrations obtained via low-level gamma-ray spectrometry in the laboratory. Uncertainties are 1s (counting statistics only) and are in most cases smaller than the symbols. Note that the samples have been arranged according to their stratigraphic position.

The results for U and Th are graphically represented in Figure 5.22. The gamma-ray energies in the ^{238}U decay series are, from left to right: 63.3 keV (^{234}Th), 295.0 keV (^{214}Pb), 351.9 keV (^{214}Pb), 609.3 keV (^{214}Bi), 1764.5 keV (^{214}Bi) and 46.5 keV (^{210}Pb). The gamma-ray energies in the ^{232}Th decay series are, from left to right: 338.3 keV (^{228}Ac), 911.2 keV (^{228}Ac), 969.0 keV (^{228}Ac), 238.6 keV (^{212}Pb), 583.2 keV (^{208}Tl) and 2614.5 keV (^{208}Tl). The results for samples G1, G7, G9, G10, G13, G14 and for the sample denoted by // G18&G19 are for sediment that was collected from the immediate surroundings of the samples that were taken for luminescence analysis (see Section 5.4). All other results are for the material that was kept aside from the dating samples themselves (i.e. the material from the outer edges of the sampling tubes which had been exposed to sunlight).

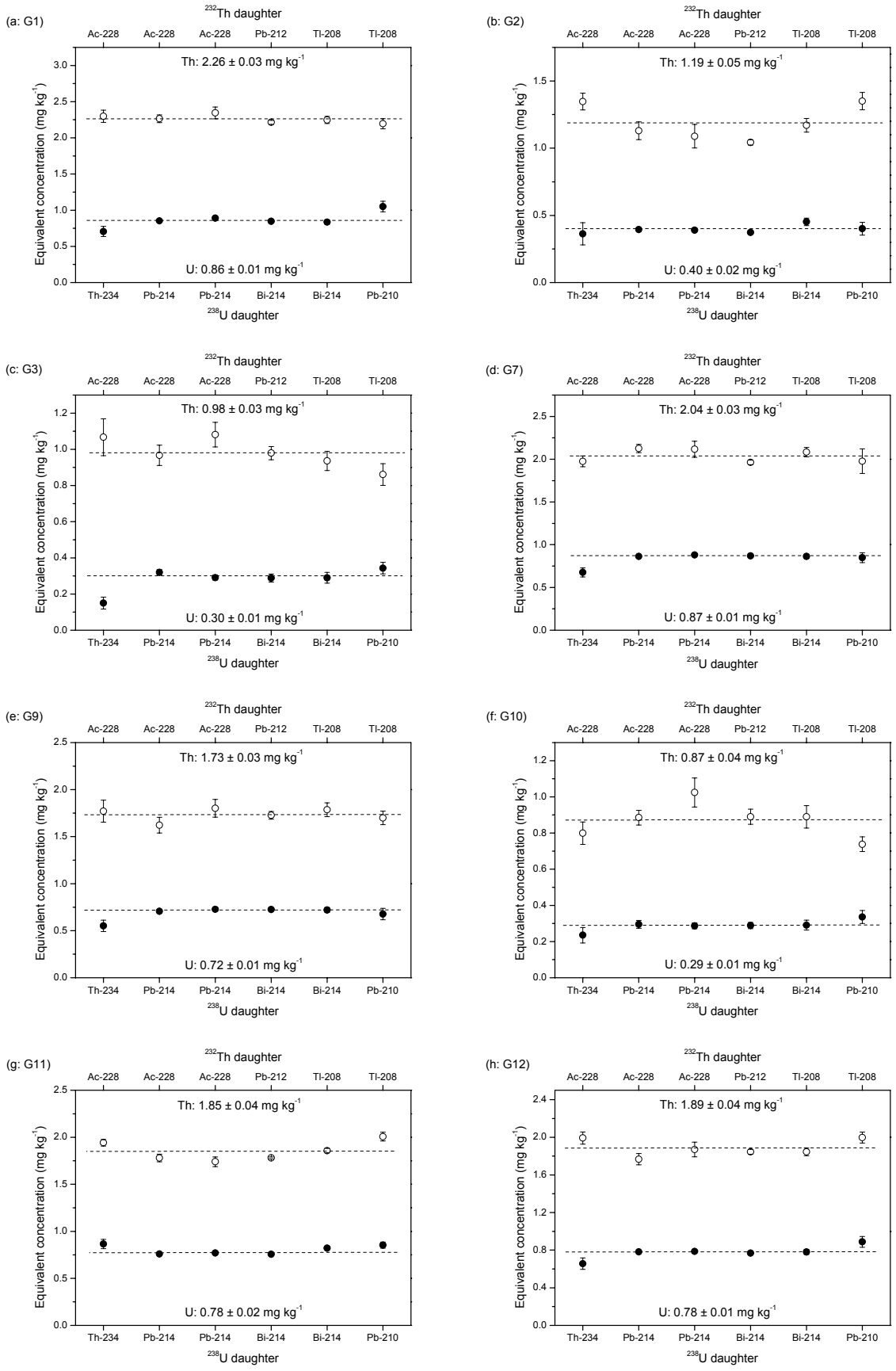

Figure 5.22: Equivalent U (solid circles) and Th (open circles) concentrations obtained via low-level γ-spectrometry. Error bars represent 1s and are derived from counting statistics only. The dashed lines indicate the unweighted average, and the values are shown in the figures as well (continued on the next page).

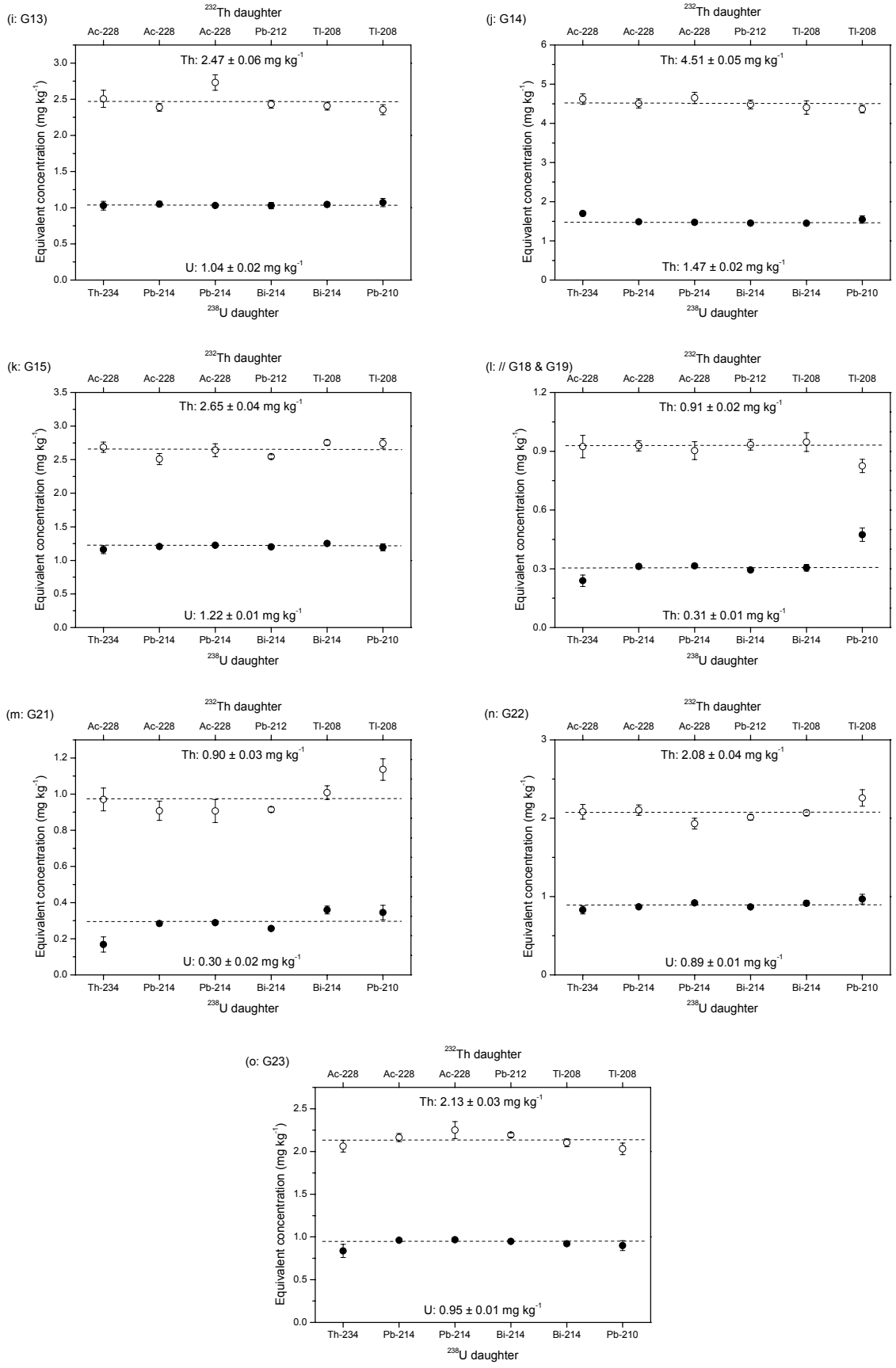

Figure 5.22 (continued): For the ^{232}Th decay series, all daughters were taken into account for calculating the average; for the ^{238}U decay series, only ^{214}Pb and ^{214}Bi. Sample identification is given in the upper left corner of each figure. Figure 5.22(l) shows the results for a sample that was taken from in between the dating samples G18 and G19 (see Section 5.4).

For each sample, the different ^{232}Th daughter isotopes and their gamma lines (open circles) give rather consistent results. Any deviations that can be observed are not related to a radionuclide but to one of the γ-lines of a radionuclide, and are also not systematic. It is therefore concluded that for all samples the ^{232}Th decay chain is in equilibrium.

The data, on the other hand, suggest the presence of a disequilibrium in the ^{238}U decay series in some of the samples (solid circles). This is indicated by the U concentration obtained via ^{214}Pb and ^{214}Bi (indicated by the dotted line in the figures) being significantly higher than that derived from ^{234}Th (see, for instance, the results for samples G3, G7, G9 and G21). To allow a clearer visualisation, the ratio of the average U concentration obtained via ^{214}Pb and ^{214}Bi to that derived from ^{234}Th is given in Figure 5.23 for all samples.

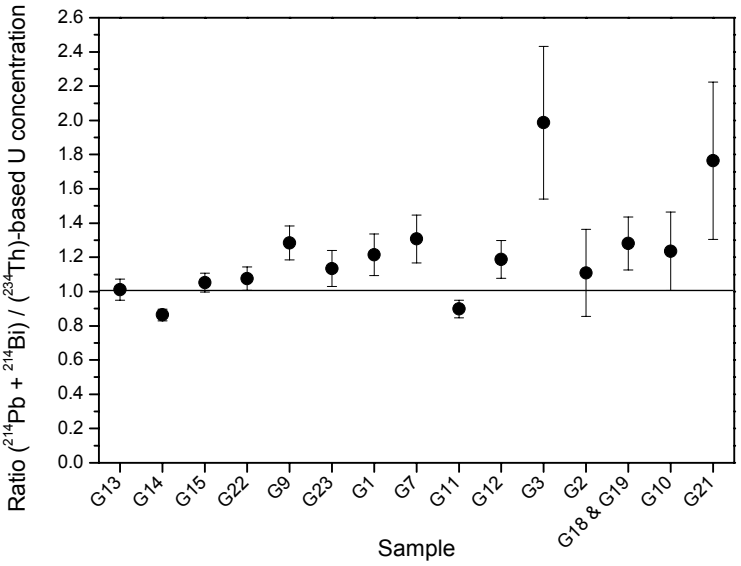

Figure 5.23: Ratios of the U concentration derived from ^{214}Pb and ^{214}Bi to that obtained via ^{234}Th. The error bars represent 1s. Note that the samples have been arranged according to their stratigraphic position. The solid line at a ratio equal to unity is meant as an eye guide.

For the majority of the samples, a radium enrichment can be seen of typically about 20%, while for two samples the deviation from equilibrium even exceeds 80%. The results for samples G14 and G11 rather indicate a radium depletion. Only a few of the measured samples appear to be in equilibrium.

The uncertainty on the U concentration derived from ^{234}Th is unfortunately rather large (because of poor counting statistics) and thus the interpretation of the data is not

straightforward. Indeed, when considering the 2s level, the majority of the samples yield ratios consistent with unity. For samples G3, G7, G9, G11 and G14 a small but statistically significant deviation from unity remains. Also, the large uncertainties complicate the comparison of the ratios between samples taken from the same stratigraphic level (compare, for instance, the absolute deviation from unity for sample G21 with that for sample G10). An attempt towards a more precise quantification of the observed disequilibria, making use of the parent concentrations obtained via neutron activation analysis, will be presented in Section 5.6.4, together with a further discussion.
In some samples (G1, G11, G12, G18&G19), an increased ^{210}Pb activity is also present. This is more clearly illustrated in Figure 5.24, where the U concentration derived from ^{214}Bi and ^{214}Pb is compared with that derived from ^{210}Pb.

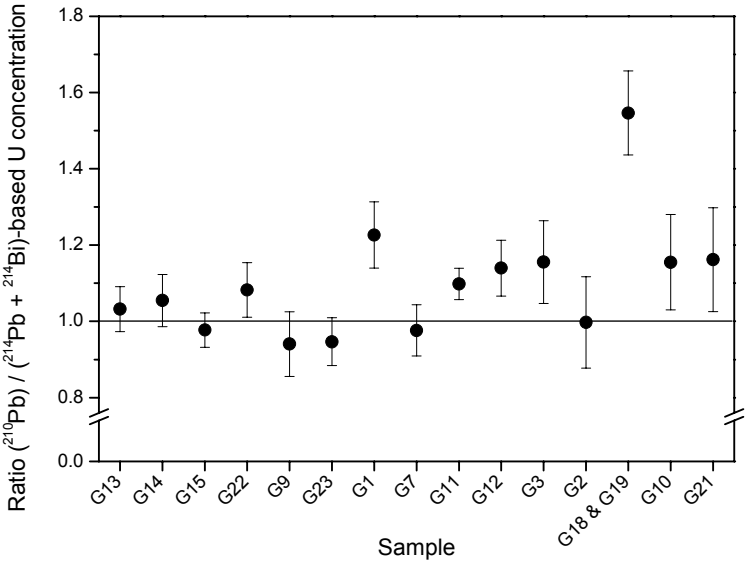

Figure 5.24: Ratios of the U concentration derived from ^{210}Pb to that obtained via ^{214}Pb and ^{214}Bi. The error bars represent 1s. Note that the samples have been arranged according to their stratigraphic position. The solid line at a ratio equal to unity is meant as an eye guide.

For the majority of the samples the excess is insignificant, while for samples G11 and especially G1 and G18&G19, the ratio remains significantly higher than unity at the 2s level. It is not clear where this apparent ^{210}Pb excess in the three samples comes from. The process usually quoted in the literature is atmospheric fallout (following the decay of its gaseous parent ^{222}Rn) and subsequent incorporation into the sediments. One should then expect the enrichment to be visible in other samples as well, especially in those from the

top of the sediment profile (G13 and G14). This is clearly not the case. Any ^{210}Pb excess is, however, thought to be only of minor importance with regard to the annual dose. It is probably caused by a recent process [$T_{1/2}$ (^{210}Pb) = 22.2a], and as the dose rate derived from ^{210}Pb and its daughters is small (~3%; Olley et al., 1996), it can be safely ignored.

It must be pointed out that De Corte et al. (2004) recently showed that serious inaccuracies can be introduced in the concentration derived from low energetic gamma lines (i.e. the ^{210}Pb 46.5 keV and the ^{234}Th 63.3 keV lines) if no allowance is made for a difference in composition between sample and calibrant which is significant, especially when it comes to elements with low or high mass number. Depending on the deviation between the true composition and that introduced in the calculations (Table 5.3), the U concentrations derived from ^{234}Th and ^{210}Pb could be systematically wrong (too high or too low), and would lead to a discrepancy when comparing them with the U concentrations derived from more energetic gamma lines (such as the ^{214}Pb and ^{214}Bi lines). Comparison of Figure 5.23 and 5.24 does not suggest such a systematic effect, but it may be masked by the presence of disequilibria. The chemical composition of the Grubbenvorst sands, however, is not expected to differ significantly from that from the Ossendrecht sands with respect to "upsetting" elements such as Ca. Although it cannot be completely ruled out, any effect is probably much smaller than the uncertainties on the "low-energy" concentrations that arise from counting statistics. Hence, it probably also has no significant implications towards the interpretation of Figures 5.23 and 5.24.

It can finally be noted that for samples G15, G22, G9 and G23, which were all taken from exactly the same stratigraphic level (i.e. at a depth of ~30 cm below the Usselo layer, and just above the Beuningen gravel bed; see Section 5.4), quite different U and Th concentrations were found. The fact that the sand layer immediately above the Beuningen layer contains small pebbles might perhaps account for these differences. For these samples, there is also some scatter in the degree of apparent Ra enrichment. For samples G10 and G21, on the other hand, which were both taken in the coarse-grained fluvial sand at a depth of approximately 5 m below the Usselo layer, quite consistent concentration results were obtained. However, here as well, there is some uncertainty about the extent of the disequilibrium.

5.6.2. Neutron activation analysis

Neutron activation analysis was carried out along the same experimental lines as described in Section 4.6.2. It was, however, not always possible to follow the "classical" measurement scheme described by Vancraeynest (1998) and Hossain (2003). The measurement for uranium, which is usually carried out after a decay time of 6-7 days, could for some samples now only be performed after a longer decay time of up to two weeks. This led to spectral interferences of the γ-line from ^{239}Np at 228.1 keV (by the 229.3 keV line from ^{182}Ta, and the 228.2 keV line from ^{132}Te) of such a magnitude, that they could no longer be accurately corrected for. Therefore, for all samples, the U concentration was derived solely from the γ-line of ^{239}Np at 277.6 keV.

All the analyses were carried out on dried (at 110°C, until constant weight) and pulverised (< 63 μm, using a ball-mill) material that was kept aside from the dating samples. When it was practically possible, the material that had been measured via alpha counting was recovered, and was subsequently also used for NAA. The idea behind this was that an analysis of exactly the same material as had been used in both techniques, would enable a more direct comparison between the results. It is realised that a substantial difference in scale of analysis between the two techniques remains (of the ~3 gram of sample put on the ZnS screen, only about 0.2 gram effectively contributes to the measured count-rate). Nevertheless, the results so obtained should still be more directly comparable than when two separate sets of samples had been used.

For each sample, the analysis was carried out in threefold, with each sub-sample weighing ~1 gram. It can finally be mentioned that the elemental composition given in Table 5.3 was used for the calculation of the detection efficiencies.

The concentrations of K, U and Th obtained via neutron activation analysis are shown in Table 5.4. The uncertainties quoted are 1 standard error and are the larger of the observed and expected uncertainties. Again, a notable difference in radionuclide content can be noted between the samples G9 and G15, which were taken from the same stratigraphic level, while the results for samples G10 and G21 are quite consistent.

	K (%)	***U*** (mg kg^{-1})	Th (mg kg^{-1})
G1	0.672 ± 0.002	0.87 ± 0.01	2.29 ± 0.02
G2	0.383 ± 0.024	0.34 ± 0.01	1.10 ± 0.01
G3	0.318 ± 0.001	0.25 ± 0.01	0.91 ± 0.01
G4	0.387 ± 0.002	0.54 ± 0.01	1.41 ± 0.02
G5$^{\bullet}$	0.564 ± 0.002	1.17 ± 0.04	2.69 ± 0.04
G6	0.432 ± 0.003	0.37 ± 0.01	1.13 ± 0.01
G7	0.672 ± 0.005	0.73 ± 0.01	1.86 ± 0.01
G8$^{\bullet}$	0.550 ± 0.003	1.40 ± 0.01	2.79 ± 0.04
G9*	0.613 ± 0.002	0.61 ± 0.01	1.58 ± 0.02
G10$^{\nabla}$	0.246 ± 0.003	0.26 ± 0.01	0.83 ± 0.01
G11$^{\otimes}$	0.668 ± 0.003	0.72 ± 0.01	1.80 ± 0.01
G12	n.a.	n.a.	n.a.
G13	0.644 ± 0.006	0.84 ± 0.01	2.18 ± 0.01
G14	0.912 ± 0.005	1.50 ± 0.02	4.04 ± 0.04
G15*	0.650 ± 0.015	1.25 ± 0.01	2.56 ± 0.01
G16	0.742 ± 0.003	0.84 ± 0.01	2.09 ± 0.03
G17$^{\otimes}$	0.663 ± 0.006	0.89 ± 0.01	2.06 ± 0.02
G18$^{\blacklozenge}$	n.a.	n.a.	n.a.
G19$^{\blacklozenge}$	0.256 ± 0.001	0.27 ± 0.01	0.88 ± 0.02
G21$^{\nabla}$	0.259 ± 0.001	0.27 ± 0.01	0.80 ± 0.01
G22*	n.a.	n.a.	n.a.
G23*	n.a.	n.a.	n.a.

Table 5.4: K, U and Th concentrations obtained via k_0-NAA. Uncertainties represent 1 standard error, the largest of the expected and the observed uncertainty being adopted. All the analyses were carried out in threefold, each sub-sample containing about 1 gram of sediment. n.a.: not analysed. Samples denoted by the same subscript were taken from the same stratigraphic level.

5.6.3. Thick source alpha counting

Thick source alpha counting was carried out for every sample, with the exception of G19. The outer material that was kept aside from the dating samples was used for this purpose. It was first dried (at 110°C, until constant weight) and subsequently pulverised (< 63 μm, using a ball-mill), before a small portion (~3 g) of it was retained for the measurement (see Section 4.6.3). Counting times amounted typically to about one month. This yielded a total number of counts between 4500 and 6000, while about 100 slow pairs were registered. Attention was paid to these slow pairs because, as outlined in the Appendix, the pairs counting technique was expected to yield annual doses that are more accurate and almost equally precise compared to those derived from the integral count-rate. The experimental efforts were consequently completely directed towards the realisation of such an improvement in the technique. It can be pointed out that, whether using the integral alpha or the pairs counting technique, annual doses derived from the count-rates will only be accurate in the absence of disturbing effects such as overcounting. However, using the more conventional "integral" alpha counting technique, Vancraeynest (1998) and Hossain (2003) obtained annual doses in good agreement with those obtained via other analytical techniques. Their encouraging results formed the prime motivation for the investigations on the pairs counting technique reported in this work.

Before each sample was counted, a background count-rate was recorded without a sample. The screen was covered with a plexiglass disc to shield it from air in the holder. The sample holder itself was sealed as well. This was done to avoid counting any radioactivity from the air. As the screens might previously have absorbed some airborne radioactivity, they were stored in the sealed sample holder for at least a few days before being counted. In view of the low U and Th contents anticipated in most of the samples, an individual background measurement was carried out, rather than using a fixed background count-rate for each counter.

To detect any radioactive disequilibria owing to radon emanation, two measurements were performed for each sample. A first measurement was carried out with the sample holder open ("unsealed" counting). This was followed by a second measurement that was started immediately after the lid had been screwed on the container ("sealed"counting). This is a classic counting procedure (Aitken, 1985), but note that this procedure differs from the

one described by Vancraeynest (1998) and Hossain (2003), who carried out both measurements on sealed containers, one immediately after sealing and one after the sample had been sealed for at least one month. Such an approach clearly dilutes the ability of the alpha counting technique for detecting radon emanation, especially if long counting times are required.

The observed unsealed and sealed alpha count-rates, and their ratio, are given in Table 5.5. For most samples, the ratio of the sealed to the unsealed count-rate does not deviate more than 10% from unity, within analytical uncertainties (a 10% increase is usually taken as the warning level; Aitken, 1985). It is therefore concluded that for the majority of the samples no significant radon loss was detected. The only exception to this is sample G3, for which an increase of the sealed to the unsealed count-rate well above the 10% warning level was observed (ratio sealed/unsealed: 1.22 ± 0.04).

All ratios of sealed to unsealed count-rates are nevertheless systematically higher than unity. Omitting sample G3, the overall ratio ± 1 standard error is 1.06 ± 0.01, which suggests that there is always a slight degree of radon escape. Significant radon loss in nature, especially to a degree as found for sample G3, would be reflected by a depletion of ^{210}Pb in the gamma-ray spectrometry results. However, the level of ^{210}Pb as determined via low-level gamma-ray spectrometry (Figure 5.24) does not follow this trend, indicating that the degree of Rn loss observed via alpha counting is not representative for that which might have occurred during burial of the samples. It is therefore suggested that the observed loss is either caused by a relatively recent process, or, is induced by the sample preparation (i.e. the pulverising).

The slow pairs-rates (arising in the ^{232}Th decay series) observed during the unsealed and the sealed counting are given in Table 5.6. It can be noted that the uncertainties on the pairs-rates are relatively large (~10%, 1s), owing to the relatively low number of pairs being registered (~100). These uncertainties are, however, largely diluted upon calculation of annual doses (see the Appendix).

	unsealed count-rate	s	sealed count-rate	s	ratio sealed / unsealed	s
G1	26.3	0.4	27.5	0.4	1.05	0.02
G2	12.6	0.2	13.1	0.2	1.04	0.03
	12.7	0.2	14.2	0.2	1.11	0.03
G3	8.9	0.2	10.8	0.2	1.22	0.04
G4	16.2	0.3	17.1	0.3	1.06	0.03
G5	36.5	0.5	40.5	0.6	1.11	0.02
G6	12.6	0.2	13.2	0.2	1.05	0.02
G7	22.0	0.3	23.4	0.4	1.06	0.02
G8	41.1	0.6	43.7	0.6	1.06	0.02
	36.2	0.5	38.4	0.5	1.06	0.02
G9	18.8	0.3	20.3	0.3	1.08	0.02
G10	9.6	0.2	9.9	0.2	1.03	0.02
G11	25.8	0.4	27.8	0.4	1.08	0.02
G12	22.0	0.4	23.5	0.4	1.07	0.03
G13	28.0	0.4	28.4	0.4	1.01	0.02
G14	48.1	0.6	50.3	0.8	1.04	0.02
G15	33.8	0.5	34.8	0.5	1.03	0.02
G16	24.3	0.4	26.8	0.4	1.10	0.03
G17	24.1	0.4	25.5	0.4	1.06	0.02
G18	10.1	0.2	10.6	0.2	1.05	0.03
G19	n.m.	-	n.m.	-	-	-
G21	11.9	0.3	12.2	0.2	1.03	0.03
G22	25.8	0.4	29.0	0.4	1.12	0.02
G23	32.2	0.5	34.0	0.5	1.06	0.02

Table 5.5: Unsealed and sealed count-rates (counts per 10 ks) for the samples from Grubbenvorst as obtained via thick source alpha counting, and their ratio. The uncertainty (s) is one standard deviation. n.m.: not measured.

	unsealed slow pairs-rate	s	sealed slow pairs-rate	s
G1	0.48	0.05	0.48	0.05
G2	0.25	0.03	0.26	0.03
	0.30	0.03	0.34	0.03
G3	0.16	0.02	0.27	0.03
G4	0.27	0.04	0.33	0.04
G5	0.69	0.08	0.69	0.08
G6	0.24	0.03	0.25	0.03
G7	0.43	0.05	0.42	0.05
G8	0.71	0.07	0.92	0.09
	0.61	0.07	0.68	0.07
G9	0.27	0.03	0.43	0.04
G10	0.18	0.02	0.23	0.02
G11	0.51	0.05	0.49	0.05
G12	0.47	0.05	0.57	0.06
G13	0.48	0.06	0.55	0.06
G14	0.89	0.09	0.98	0.11
G15	0.53	0.06	0.64	0.06
G16	0.49	0.05	0.59	0.06
G17	0.42	0.05	0.44	0.05
G18	0.19	0.03	0.29	0.03
G19	n.m.	-	n.m.	-
G21	0.24	0.03	0.29	0.03
G22	0.41	0.05	0.63	0.06
G23	0.62	0.07	0.63	0.07

Table 5.6: Slow pairs count-rates (counts per 10 ks) observed during the unsealed and sealed measurements. The uncertainty ("s") is one standard deviation. n.m.: not measured. The slow pairs arise from the decay of ^{220}Rn (T½ = 55.6 s) into ^{216}Po (T½ = 0.145 s) in the ^{232}Th series.

5.6.4. Comparison and evaluation of the results

5.6.4.1. Comparison of field with low-level gamma-ray spectrometry

Figure 5.25 compares the results obtained via field gamma-ray spectrometry with those obtained via low-level gamma-ray spectrometry. The comparison is between concentrations obtained via the same daughter isotopes (^{40}K for K, ^{214}Bi for U and ^{208}Tl for Th). Error bars are 1s, and take the systematic uncertainties into account (see Table 5.1 for field gamma-ray spectrometry, with an additional 2% being introduced to allow for the uncertainty associated with the "composition correction" factors; a systematic uncertainty of 2.5% was adopted for the laboratory measurements).

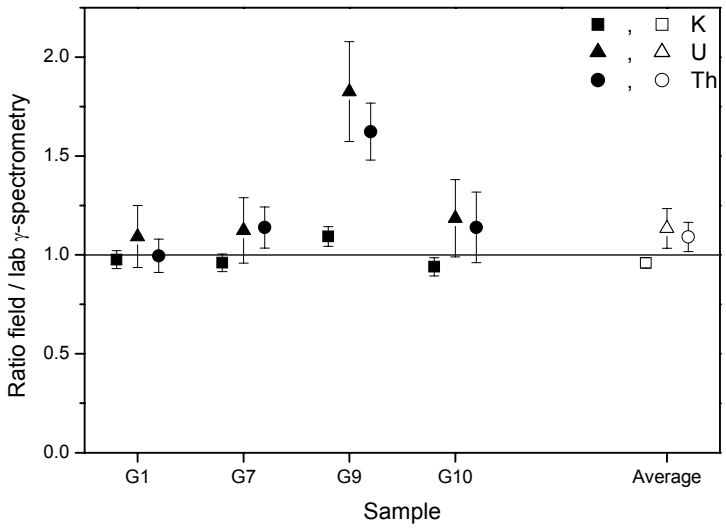

Figure 5.25: Comparison between the K, U and Th concentrations obtained via field gamma-ray spectrometry and low-level gamma-ray spectrometry. K was obtained via the ^{40}K gamma line at 1460.8 keV, U via the ^{214}Bi gamma line at 1764.5 keV and Th via the gamma line at 2614.5 keV from ^{208}Tl. For the laboratory measurements, the results obtained via the ^{214}Bi gamma line at 609.3 keV and the ^{208}Tl gamma line at 583.2 keV are included as well. Sample G9 was omitted to calculate the unweighted average ratios (indicated by the open symbols). The solid line at a ratio equal to unity is meant as an eye guide. Error bars represent 1s and take the systematic uncertainties into account.

It can be seen that for samples G1, G7 and G10 an acceptable to good agreement is found for K, U and Th. The average ratio obtained for these three samples is indicated in the figure by the open symbols, and is, within 2s, consistent with unity. For sample G9, on the

other hand, field gamma-ray spectrometry indicates a much larger U and Th concentration. This discrepancy is interpreted as reflecting radioactive heterogeneity in the sediment overlying the Beuningen Gravel Bed. This is supported by the horizontal variation in radionuclide content observed via gamma-ray spectrometry for samples G9, G15, G22 and G23, which were all taken from exactly the same stratigraphic level (see Section 5.6.1.2), as well as via NAA (see Section 5.6.2; samples G9 and G15 only).

5.6.4.2. Comparison of k_0-NAA with low-level gamma-ray spectrometry

A comparison of the results obtained via neutron activation analysis and low-level gamma-ray spectrometry is shown in Figure 5.26(a), (b) and (c), for K, U and Th respectively.

For K, low-background γ-spectrometry yields somewhat higher results than NAA (3%, on the average). Nevertheless, there is generally a good agreement between the two techniques, all individual ratios being equal to unity within 2s (note that only 1s is indicated in Figure 5.26).

The results for U are more scattered around the ideal ratio of unity. Let us first make the comparison of NAA with the U concentration derived from ^{234}Th (indicated by the circles). This should enable a more direct comparison. Indeed, neutron activation determines the parent concentration, and ^{234}Th is the first daughter in the ^{238}U decay series that can be measured via low-level γ-spectrometry. Assuming that no disequilibrium occurred at this stage, both methods should consequently yield indistinguishable results. Considering 2s confidence intervals, the majority of the samples do indeed yield ratios consistent with unity. Only for sample G13, a significantly lower U concentration was found via NAA. The overall ratio is consistent with unity as well, within 2s. As was pointed out previously, the uncertainty on the ^{234}Th concentrations is large (for some samples > 20%). To allow a more precise comparison and to confirm, or otherwise, the observations on the disequilibria previously made in Figures 5.23 and 5.24, a second comparison, indicated by the star symbols, is included in Figure 5.26(b). Here, the U concentration as determined by NAA is compared to that derived from the ^{214}Pb and ^{214}Bi daughters. It can be seen that for samples G3, G7, G9, G10, G19 and G21 the suggestion of radium enrichment by ~10-15% is supported. For samples G1, G11 and G14, NAA is

in better agreement with the average concentration derived from the ^{214}Pb and ^{214}Bi daughters. Samples G15, G2 and G13 were found to be in equilibrium (Figure 5.23), which is confirmed by the NAA results. For the latter two samples, however, there is a significant difference in the U concentration obtained via NAA and low-level gamma-ray spectrometry. It remains somewhat confusing to find an apparent radium enrichment in sample G9, while it is not observed for sample G15, which was taken from the same stratigraphic level.

The comparison between the results obtained for Th via NAA and low-level gamma-ray spectrometry in the laboratory is shown in Figure 5.26(c). As no disequilibria were detected in the ^{232}Th decay series, the Th concentrations adopted for low-level gamma-ray spectrometry are the averages calculated from all the daughter isotopes. Both techniques yield the same results for the majority of the samples, provided that the 2s level is considered. For samples G13, G14, G7 and G21 a small but statistically significant deviation from unity remains. The overall average ratio indicates that Th concentrations obtained via NAA are lower (or that the laboratory measurements are higher) by about 7%.

In general, the differences between the NAA and γ-spectrometry results can probably be explained in terms of sample inhomogeneity. Indeed, whereas the low-level gamma-ray spectrometry was performed on an amount of material varying between 60 to 200 g, the NAA results refer to the average of 3 analyses of ~1 g sub-samples. Although these NAA sub-samples were randomly taken from a larger amount of pulverised and mixed material, one cannot rule out that this “averaging” process was not fully completed. It can be noted that if the differences between NAA and γ-spectrometry had a systematic origin, the same discrepancies would have been observed for the Ossendrecht samples as well. This was not the case. Due to the sample heterogeneity, the comparison for U between the results obtained via NAA and via the ^{214}Pb and ^{214}Bi daughters does not allow a more precise quantification of the degree of disequilibrium observed in the ^{238}U decay series.

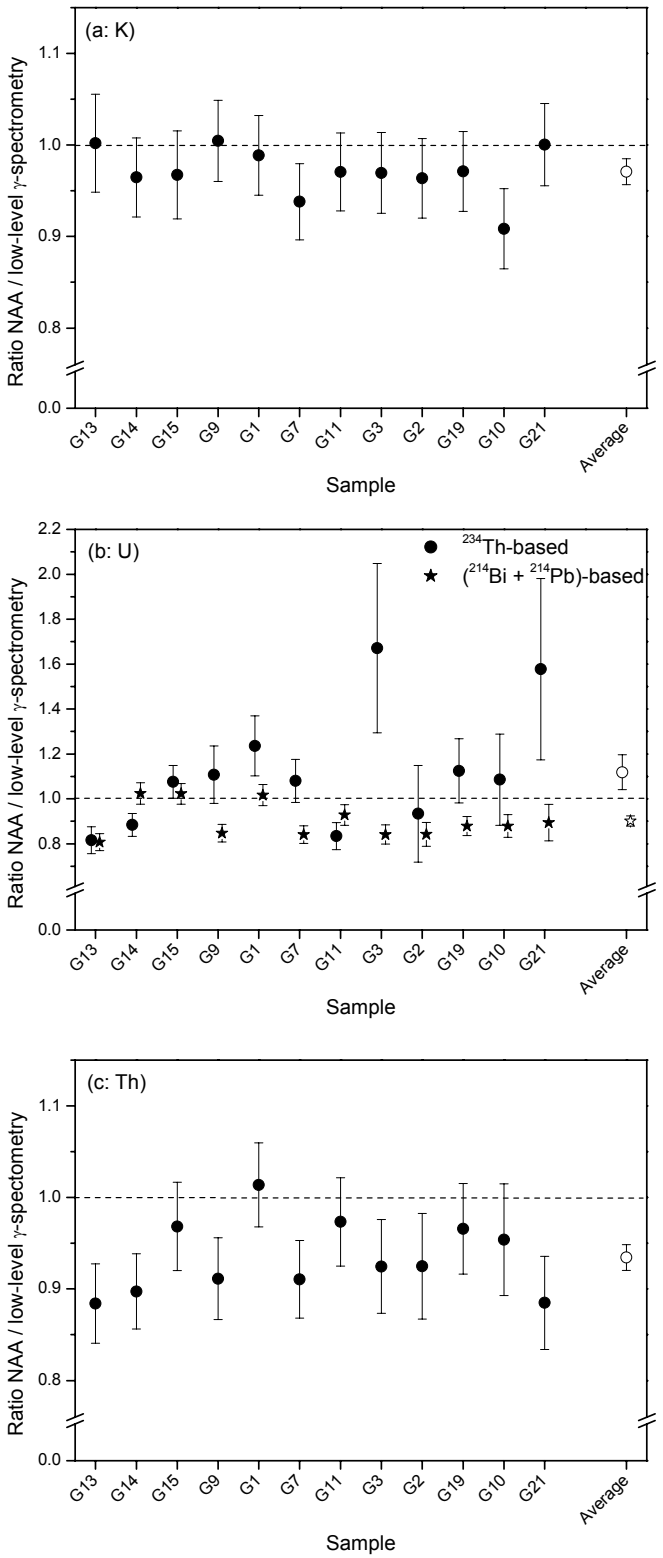

Figure 5.26: Comparison of the results obtained via NAA and low-level gamma-ray spectrometry for K (a), U (b) and Th (c). The error bars are 1s and include both random and systematic uncertainties. The dashed line at a ratio equal to unity is meant as an eye guide. In Figure 5.26 (b) the NAA results are compared with those derived from ^{234}Th (circles), as well as with the average U concentrations calculated from ^{214}Bi and ^{214}Pb (stars). The samples have been arranged according to their stratigraphic position.

Figure 5.22 suggests a ^{226}Ra enrichment of typically between 10-20%, that is mainly situated in the fluvio-aeolian and fluvial part of the sediment succession. These sediments have always been in saturated water conditions, until the river Meuse shifted its watercourse to the east (Kasse, private communication; Kasse et al., 1995). This is thought to have happened around the very end of the Late Pleniglacial (i.e. ~15 ka ago). From this moment on, the sediments have been drying up until the present moisture content was reached, which is low (~5%). The current ground water-level is low as well. Assume now that the fluvial and fluvio-aeolian sediments were deposited in an open system, which remained open until the moment of diversion of the river Meuse. ^{226}Ra is mobile because of its solubility and hence the wet conditions could be responsible for the observed ^{226}Ra enrichment. From the moment the system closed, the excess of ^{226}Ra then started to decay slowly towards a condition of radioactive equilibrium. Assuming that ^{238}U always was in equilibrium with its daughters up to ^{226}Ra, then it is possible to calculate what the initial level of ^{226}Ra would have been from its current activity using the following equation (Olley et al., 1996):

$$^{226}a_t = {}^{230}a + \left[{}^{226}a_0 - {}^{230}a\right]e^{-\lambda_{226}t}$$

in which $^{226}a_0$ and $^{226}a_t$ are the activities of ^{226}Ra at time t=0 and t respectively, ^{230}a is the activity of ^{230}Th (equal to the parent activity in the case of secular equilibrium) and λ_{226} is the decay constant for ^{226}Ra ($T½ = 1.600$ ka; $\lambda = 4.332 \times 10^{-1}$ ka).

Solving this equation using a current ^{226}Ra excess of ~15%, yields an initial ^{226}Ra excess 15 ka ago of about a factor 100. This cannot be considered as realistic. Olley et al. (1996) investigated modern sediments from a variety of fluvial depositional environments and found most of the samples to be within 50% of equilibrium. If the sediments remained in a chemically closed environment over the last 15 ka, it seems consequently quite unlikely that a ^{226}Ra excess of 20%, or even 10%, would have been detected at the present day.
Another possibility is that the sediments were deposited in a chemically open environment and that the currently observed disequilibrium conditions have prevailed during the entire burial time, i.e. the system remained open. However, what has then been the transporting agent for the ^{226}Ra? To remain at an approximately constant level, there should have been

a continuous input of ^{226}Ra. The sediments, however, have been drying up for the last 15 ka.

A sensible explanation to arrive at a present day excess of 20% would be that element mobility occurred quite recently. The excess of ^{210}Pb that was observed in some of the samples (see Figure 5.24) points indeed to a recent process. Maybe the ^{226}Ra was incorporated into the sediment by taking it up from surface waters seeping of the profile wall, or maybe the disequilibria were triggered by human activity (such as the excavations in the quarry). However, in these cases, the ^{226}Ra excess would have prevailed only over a relatively short period of the entire burial period, with a minimal effect on the dose-rate.

There is obviously no straightforward answer to the issue of the observed ^{226}Ra excess (note that the same reasoning applies to the apparent 10-20% ^{226}Ra depletion that was observed for samples G11 and G14; see Figure 5.23). Consequently, to arrive at dose-rates, some assumptions have to be made. Following the above, it was opted for assuming that the ^{226}Ra disequilibria have not prevailed during the entire burial period of the samples. Instead, it was assumed that the ^{238}U decay series has always been in equilibrium, with an activity as indicated by NAA and the ^{234}Th isotope. It is worth recalling that the disequilibria are not significant at the 2s level for the majority of the samples (Section 5.6.1.2). As the ^{234}Th results carry large analytical uncertainties, only those obtained via NAA were actually adopted for calculating the contribution from U to the annual dose.

Depending on the degree by which the assumption of equilibrium is false, some overestimation of the true age of the sediments is to be expected (neglecting a Ra excess implies an underestimation of the annual dose). It can finally be pointed out that the contribution from the ^{238}U series to the dose-rate, and any uncertainty associated with it, is diluted by the contributions from Th and K.

5.6.4.3. Comparison of observed with predicted alpha count-rates

The last comparison to be discussed is that between alpha counting and NAA. The measured unsealed alpha count-rates are compared in Figure 5.28 with those predicted from the U and Th concentrations obtained via neutron activation analysis. It can be

recalled that for many samples the comparison is as direct as possible, as exactly the same material had been used for both analyses.

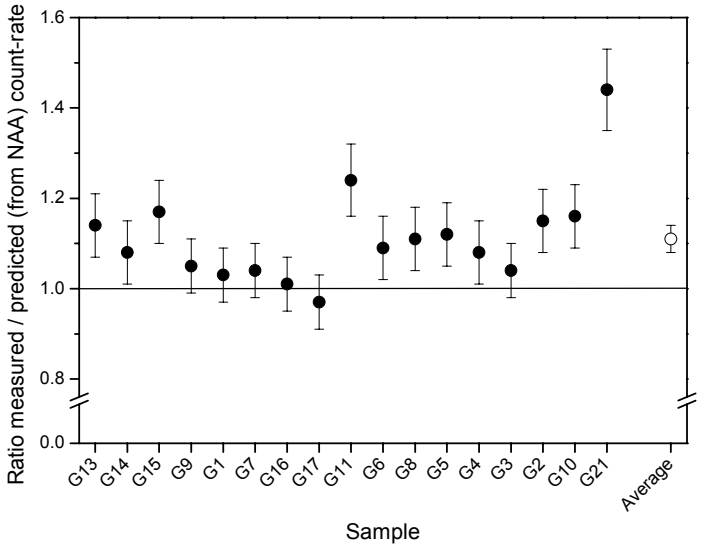

Figure 5.28: Comparison of measured ("unsealed") alpha count-rates and predicted ones (from the U and Th concentrations obtained via NAA). Error bars are 1s and include both random and systematic uncertainties. The solid line at a ratio equal to unity is meant as an eye guide.

At the 2s level, the majority of the samples yield a ratio consistent with unity (note that the error bars in the figure represent 1s). However, the overall ratio is significantly higher than unity (unweighted average: 1.11 ± 0.03). Sample G21 exhibits the highest deviation, exceeding 40%. This apparent "overcounting" can clearly not be ascribed to radon build-up in the container, as the observed unsealed count-rate was used to perform the comparison. It should be noted that NAA only determines parent concentrations, and in the derivation of predicted alpha count-rates from these values, the decay chains have been assumed to be in equilibrium. If a disequilibrium is present in which there is an excess of daughters, the predicted count-rate will be underestimated.

In the following, therefore, the observed alpha count-rates are compared to those predicted from the results obtained via low-level gamma-ray spectrometry. In this comparison the ^{238}U decay series was assumed to be in equilibrium and to be present in an activity as indicated by the ^{214}Bi and ^{214}Pb daughters. As γ-spectrometry also yielded the highest Th results [see Figure 5.26(c)], the expected count-rates so obtained can be considered as an upper limit for the calculated alpha count-rates. If the observed count-rates still exceed this "upper prediction level", true overcounting effects are the most likely explanation.

The comparison is shown in Figure 5.29 for the samples for which both alpha counting and low-level gamma-ray spectrometry has been performed.

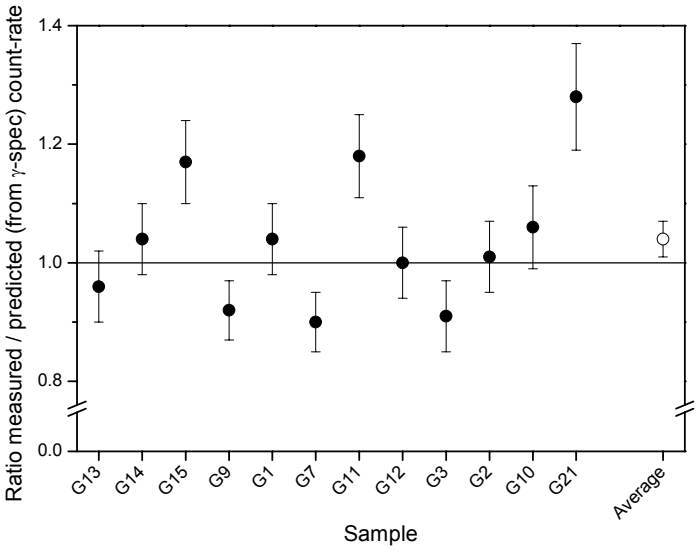

Figure 5.29: Simplified comparison between the observed unsealed alpha count-rates and those predicted from low-level gamma-ray spectrometry (see text for more details). Error bars represent 1s and take both random and systematic uncertainties into account. The solid line at an ideal ratio of 1 is meant as an eye guide.

The situation now clearly has improved, but, on the overall, it is still not considered as satisfactory. Although for some samples alpha counting may yield accurate results, for others significant overcounting clearly has occurred. Indeed, as outlined above, the predicted count-rate is considered as an upper limit, and should in fact rather be an overestimation. Consequently, ratios of measured to predicted count-rates equal to unity can even be regarded as an overestimate. Perhaps the least complex example is given by sample G15. For this sample no disequilibrium or significant inhomogenity effects were observed [see figures 5.26(b) and (c)]. The predicted count-rate is, however, significantly lower than the observed one.

In the foregoing, some differences were observed between the results obtained via NAA and gamma-ray spectrometry, which were attributed to sample inhomogeneity. One should, consequently, not overlook the possibility that this heterogeneity affects the present comparisons as well. Indeed, only a thin layer of 0.2 g actually contributes to the measured alpha count-rate, while a much larger amount is used by the other analytical techniques (NAA: 3*1 g; γ-spec: 60-200 g). However, if the samples are already

inhomogeneous at the 0.2 g level, one can wonder how representative the dose-rate derived from this small amount of sample will be for the dose-rate a dating sample actually receives.

Apart from these considerations (possible overcounting, and the effect of sample inhomogeneity), it was also argued in the above that the dose-rate derived from the ^{238}U daughters is not representative of that experienced by the samples during their entire burial time. Hence, alpha-counting, even if it were accurate, would not yield the annual doses appropriate to the assumptions previously made. Therefore, the results obtained via alpha-counting were not considered further.

5.7. Age calculation, optical ages and discussion

Table 5.7 summarises all the analytical data from Sections 5.5 and 5.6, and includes the final optical dates.

The K, U and Th results for samples G4, G5, G6, G8, G16 and G17 are derived from k_0-NAA solely (as for these samples no other data are available), while for samples G12, G18, G22 and G23 only the results from low-level gamma-ray spectrometry are available. For the latter, the U activity quoted in Table 5.7 refers to that obtained via the ^{234}Th daughter. For samples G13 and G15, the averages of the radionuclide concentrations obtained via k_0-NAA and low-level gamma-spectrometry have been adopted (note that for these samples, no disequilibria in the ^{238}U decay series were detected; see Figure 5.23). For the other samples, the contribution from K and Th to the annual dose was calculated from the averages of the radionuclide concentrations obtained via field gamma-ray spectrometry (only for samples G1, G7 and G10), low-level gamma-ray spectrometry and k_0-NAA. For the reasons outlined in the previous section, the U activities specified for these samples are based on k_0-NAA solely. Sample G9 was treated in another way. For this sample, a non-uniformity in the radioactive environment was encountered (see Figure 5.25). Therefore, the beta dose rate was derived from laboratory gamma-ray spectrometry (K and Th) and k_0-NAA (K, U and Th), while the gamma dose rate was derived from the field gamma-ray spectrometry (K and Th) and k_0-NAA (U).

As outlined in Section 4.6.5, annual doses were calculated using the conversion factors of Adamiec and Aitken (1998). The external beta dose-rate was corrected for the effect of

attenuation and etching (see Section 3.3.7), and both the gamma and beta contributions were corrected for the effect of moisture (see Section 3.3.5). For the sands overlying the Beuningen layer, the 'as found' present moisture content has been assumed to be representative for that prevailing throughout the whole burial period. For the samples underlying the Beuningen layer, it was taken into account that they have always been saturated with water, until the river Meuse shifted its watercourse away from the investigated site about 15 ka ago (Kasse et al., 1995). During the remainder of the burial period, the sediments were assumed to have been half at saturation for half of the time and at their present moisture content for the other half. This is to be considered as a simplified approximation of the drying up conditions. The external dose rates given in Table 5.7 include the contribution from cosmic rays, which was calculated according to Prescott and Hutton (1994), assuming an uncertainty of 15% (see Section 3.3.3). The cosmic dose-rate ranged from ~0.18 Gy ka^{-1} (G13) to ~0.11 Gy ka^{-1} (G10 and G21). Its relative contribution was highest for the fluvial sands at the base of the exposure, where it amounted to ~25% of the total dose-rate. Investigations on any internal activity in the quartz grains are ongoing at present and, for the time being, an internal contribution of 0.035 Gy ka^{-1} was assumed. This value falls within the range of internal dose-rates that were experimentally determined for the Ossendrecht samples (see Section 4.7). An associated systematic uncertainty of 50% was adopted.

The equivalent doses given in Table 5.7 represent the average D_e's across the plateau region in the SAR D_e versus preheat temperature plots (Figure 5.9). The ages were then obtained according to equation 3.1. Uncertainties on the luminescence ages were calculated as previously (i.e. following Aitken and Alldred, 1972 and Aitken, 1976; see Section 4.7) All the sources of uncertainty involved have been quantified previously (see e.g. Section 4.7). It can be seen from Table 5.7 that the systematic uncertainty is dominant in the overall uncertainty on the ages, as was also the case for the Ossendrecht samples (see Table 4.7). The total uncertainty typically amounts to ~7-8% and, within this uncertainty, all ages are stratigraphically consistent (note that the samples have been arranged according to their stratigraphic position in Table 5.7). For easy visualisation, the OSL ages are also shown in Figure 5.30. It can be seen that the ages increase with depth, and that, within uncertainties, quite consistent ages were obtained for samples from the same stratigraphic level (indicated by the braces in Figure 5.30).

	Natural U *(Bq kg^{-1})*	*^{232}Th* *(Bq kg^{-1})*	*^{40}K* *(Bg kg^{-1})*	*F*W*	*External Dose rate (Gy ka^{-1})*	*Internal Dose rate (Gy ka^{-1})*	*D_e (Gy)*	*Age (ka)*	*Random Uncertainty (%)*	*Systematic Uncertainty (%)*	*Total Uncertainty*	
											(%)	*(ka)*
G13	12.13 ± 1.31	9.44 ± 0.58	194.5 ± 3.1	0.044	1.134 ± 0.026	0.035	16.1 ± 0.3	13.8	2.30	6.59	6.98	1.0
G14	19.47 ± 0.27	17.35 ± 0.94	280.9 ± 5.1	0.044	1.647 ± 0.022	0.035	21.4 ± 0.3	12.7	1.94	6.64	6.92	0.9
G15	15.84 ± 0.27	10.57 ± 0.17	200.0 ± 3.3	0.044	1.223 ± 0.011	0.035	17.8 ± 0.3	14.1	2.14	6.59	6.93	1.0
G9	7.87 ± 0.06	β: 6.73 ± 0.31 γ:. 11.49 ± 0.21	β: 185.1 ± 0.4 γ: 202.0 ± 1.2	0.044	1.036 ± 0.004	0.035	16.6 ± 0.3	15.5	1.96	6.29	6.59	1.0
G22	10.71 ± 0.66	8.43 ± 0.02	197.5 ± 1.5	0.044	1.087 ± 0.012	0.035	17.3 ± 0.4	15.4	2.73	6.62	7.16	1.1
G23	10.80 ± 0.99	8.66 ± 0.14	200.3 ± 1.5	0.044	1.100 ± 0.018	0.035	18.5 ± 0.3	16.3	2.42	6.62	7.05	1.1
G1	11.24 ± 0.10	9.15 ± 0.10	203.1 ± 1.4	0.094	1.068 ± 0.004	0.035	19.0 ± 0.3	17.2	1.48	6.67	6.84	1.2
G7	9.43 ± 0.13	8.40 ± 0.53	209.3 ± 3.9	0.094	1.035 ± 0.014	0.035	21.2 ± 0.3	19.8	2.05	6.70	7.01	1.4
G16	10.78 ± 0.16	8.48 ± 0.13	224.5 ± 0.8	0.094	1.102 ± 0.004	0.035	22.4 ± 0.4	19.7	1.68	6.71	6.91	1.4
G11	9.30 ± 0.14	7.42 ± 0.10	205.2 ± 3.1	0.094	0.996 ± 0.009	0.035	20.0 ± 0.4	19.4	2.27	6.72	7.09	1.4
G17	11.48 ± 0.07	8.38 ± 0.08	200.4 ± 1.9	0.094	1.035 ± 0.005	0.035	20.3 ± 0.3	18.9	1.34	6.70	6.83	1.3

Table 5.7: Summary of analytical data (uncertainties represent 1s), estimates of past moisture content expressed as F*W, calculated dose rates, D_e values, ages, and random, systematic and total uncertainties. W is the porosity, calculated as the ratio of the mass of water that the sample takes up at full saturation to the mass of the dry sample; F is the fraction of saturation corresponding to the assumed average water content over the entire burial period (see Section 3.3.5). The uncertainties mentioned with the D_e and dosimetry data are random. See the text for more details (continued on the next page).

	Natural U (Bq kg^{-1})	*^{232}Th* (Bq kg^{-1})	*^{40}K* (Bg kg^{-1})	*F*W*	*External Dose rate* (Gy ka^{-1})	*Internal Dose rate* (Gy ka^{-1})	*D_e* (Gy)	*Age* (ka)	*Random Uncertainty* (%)	*Systematic Uncertainty* (%)	*Total Uncertainty* (%)	(ka)
G6	4.75 ± 0.03	4.60 ± 0.03	128.0 ± 0.9	0.094	0.658 ± 0.002	0.035	16.3 ± 0.3	23.5	2.10	6.88	7.19	1.7
G8	18.06 ± 0.17	11.34 ± 0.18	166.4 ± 1.3	0.094	1.093 ± 0.005	0.035	23.6 ± 0.5	20.9	2.36	6.65	7.05	1.5
G5	15.14 ± 0.47	10.91 ± 0.17	170.6 ± 0.5	0.094	1.049 ± 0.008	0.035	23.6 ± 0.3	21.8	1.67	6.66	6.86	1.5
G12	8.46 ± 0.79	7.66 ± 0.15	126.1 ± 1.2	0.094	0.752 ± 0.013	0.035	17.3 ± 0.3	22.0	2.43	6.73	7.15	1.6
G4	6.92 ± 0.12	5.74 ± 0.08	117.1 ± 0.5	0.094	0.666 ± 0.003	0.035	16.6 ± 0.3	23.7	1.84	6.81	7.05	1.7
G3	3.23 ± 0.03	3.84 ± 0.15	97.6 ± 1.5	0.126	0.503 ± 0.004	0.035	13.5 ± 0.3	25.2	2.63	7.42	7.87	2.0
G2	4.37 ± 0.08	4.64 ± 0.18	117.9 ± 2.2	0.126	0.586 ± 0.006	0.035	15.2 ± 0.2	24.4	1.96	7.26	7.51	1.8
G18	3.08 ± 0.37	3.69 ± 0.07	79.9 ± 0.9	0.126	0.447 ± 0.006	0.035	13.9 ± 0.5	28.8	3.62	7.57	8.39	2.4
G19	3.47 ± 0.02	3.57 ± 0.07	77.6 ± 0.2	0.126	0.445 ± 0.001	0.035	13.1 ± 0.6	27.2	4.21	7.57	8.66	2.4
G10	3.30 ± 0.04	3.56 ± 0.11	77.8 ± 2.2	0.126	0.431 ± 0.006	0.035	12.2 ± 0.2	26.2	2.67	7.58	8.04	2.1
G21	3.43 ± 0.11	3.44 ± 0.21	78.3 ± 0.5	0.126	0.433 ± 0.004	0.035	12.8 ± 0.3	27.3	2.77	7.58	8.07	2.2

Table 5.7 (continued): Summary of analytical data (uncertainties represent 1s), estimates of past moisture content expressed as F*W, calculated dose rates, D_e values, ages, and random, systematic and total uncertainties. The uncertainties mentioned with the D_e and dosimetry data are random. See the text for more details.

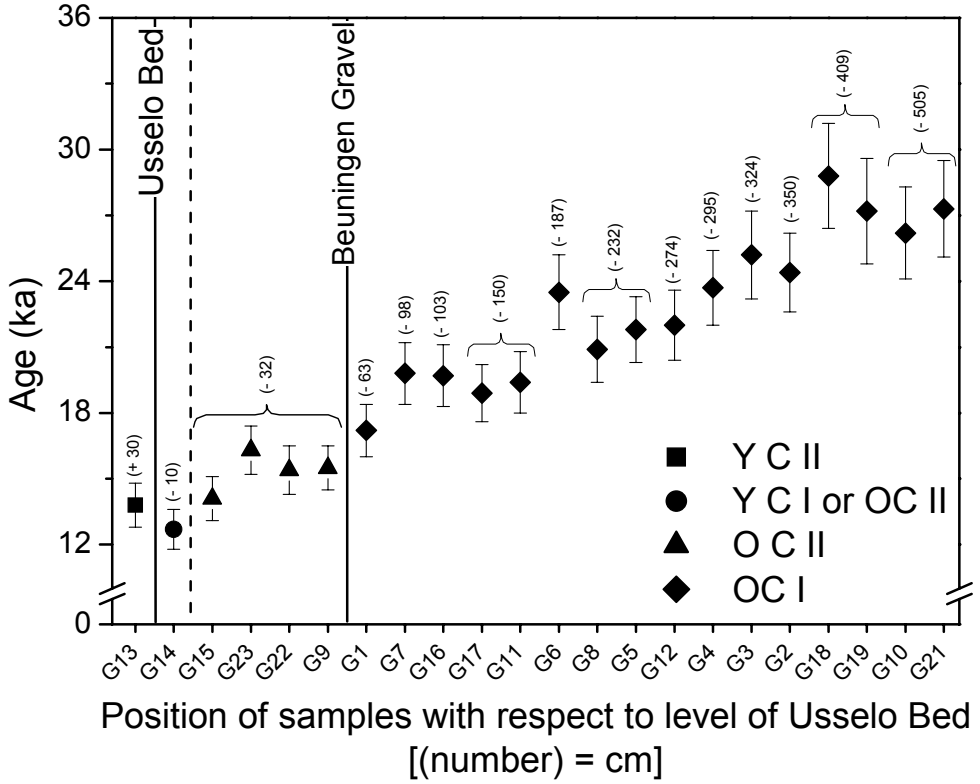

Figure 5.30: Summary of the dating results presented in Table 5.7. The samples are ordered according to the level of the Usselo layer, the stratigraphic distances (in cm) to which are given by the numbers between brackets. Samples from the same stratigraphic level are indicated by the braces. YC: Younger Coversand II; OC: Older Coversand.

No precise independent age information is available to evaluate the accuracy of the optical ages. However, they agree well with the age information that is based on correlation using (radiocarbon dated) stratigraphic markers and palaeoclimate indicators (summarised in Section 5.3).

The weighted mean OSL age (see Section 4.7) for the four fluvial samples from the base of the exposure (samples G18, G19, G10 & G21) is 27.3 ± 2.1 ka. This is in good agreement with the radiocarbon age of ~28-29 ka before AD 2000 that was obtained for the top of the peat layer underlying the base of the sand pit. However, the peat bed was encountered at several kilometres distance from the quarry and correlations over such distances should be considered with caution.

Owing to the occurrence of different types of cryoturbations (e.g. ice-wedge casts) in the fluvio-aeolian sands (and because of the above radiocarbon date), this unit has been

interpreted as being deposited during the maximum cold of the Last-glacial (between ~18 and 28 ka before AD 2000; Kasse, 1999). The optical ages obtained for the fluvio-aeolian sand unit range from 17.2 ± 1.2 ka (sample G1) to 23.7 ± 1.7 ka (sample G4), which is consistent with this interpretation. The overall average age obtained for all ten samples of the Older Coversand I unit is 20.3 ± 1.3 ka.

Radiocarbon dates of the Beuningen Gravel Bed are not available, owing to the absence of datable organic material. Kolstrup (1980), however, radiocarbon dated the start of the deposition of the sands making up the Coversand II unit at 16.9 ± 0.7 ka before AD 2000. The formation of the Usselo soil, on the other hand, can be placed at around 13.1 ka before AD 2000 (Section 5.3). The optical ages obtained for the sediments intercalated between the Beuningen Gravel Bed and the Usselo soil, are consistent with this age information. The weighted average OSL age for the four samples immediately overlying the Beuningen Gravel Bed (samples G15, G9, G22 & G23) is 15.3 ± 1.0 ka. This indicates that the sediments were deposited at the Late Pleniglacial to Late-glacial transition. The top of the Older Coversand II unit (sample G14) yields a slightly younger age of 12.7 ± 0.9 ka. This could suggest that the sample was indeed taken from the Younger Coversand I unit. However, the Older Dryas (during which the Younger Coversands I were deposited) covers only a time period of about 200 years. In view of the uncertainty on the optical age, distinguishing phases of aeolian coversand deposition during the Older Dryas and the Bølling (Older Coversand II) is actually impossible. It is worth pointing out that for a clear distiction to made between the different phases of the Late-glacial (Bølling, Older Dryas, Allerød and Younger Drays), a relatively high resolution is required. Indeed, the whole of the Late-glacial only covers a period of about 3 ka. Taking into account that the uncertainty on an optical age typically amounts to 1 ka, makes it rather difficult to reliably distinguish the different chronostratigraphic periods from each other by optical dating alone. It is owing to the physical presence of stratigraphic markers (such as the Usselo Soil) that a more reliable division is possible.

For the Younger Coversands II overlying the Usselo Soil, an age of 13.8 ± 1.0 ka was obtained (sample G13). Within analytical uncertainties, this is consistent with the radiocarbon age of the Soil.

The optical ages for the coversands overlying the Beuningen Gravel Bed also agree well with the age of contemporaneous sediments observed in Ossendrecht (Section 4.7). There, the Younger Coversands I were dated at 12.7 ± 0.7 ka and the Older Coversands II at 15.0 ± 0.9 ka.

Bateman and Van Huissteden (1999) obtained OSL ages on stratigraphically equivalent deposits exposed in the Lutterzand section (Dinkel valley, E. Netherlands). Using quartz and the single-aliquot additive-dose technique, they obtained an average age of 12.5 ± 1.1 ka for the so-called Wierden member (which represents the Younger Coversands I and II). For the Older Coversands II, they found an average age of 15.8 ± 1.8 ka, while the Older Coversands I were dated at 21.9 ± 1.9 ka. The SAR-based ages obtained in this work, are consistent with these SAAD-based ages. Dijkmans and Wintle (1991) also dated the coversands from the Lutterzand section. They used TL and coarse-grained feldspars. It was noted previously (see Section 4.3 and Table 4.1), however, that these TL-ages are systematically too low (by about 20-40%) compared to the radiocarbon ages. For the sake of completion, it can be added that Dijkmans and Wintle (1991) obtained ages of 10.3 ± 0.8 ka and 11.8 ± 1.0 ka for the Older Coversands I.

Comparison of the OSL ages of Table 5.7 with the independent luminescence chronology established by Bateman et al. for the Grubbenvorst site (unpublished; see section 5.3) indicates some notable differences. Their dates of 19.8 ± 1.2 ka for the coversands overlying the Beuningen Gravel Bed and of 34.8 ± 2.4 ka for the fluvial sediments at the base of the exposure are older than the ages obtained in this work. The latter, however, are consistent with the geological expectations and the luminescence ages obtained for the Ossendrecht sands. For a sample that was taken from the sediments just below the Beuningen Gravel Bed (the Older Coversands I), Bateman et al. obtained an age of 20.7 ± 1.2 ka. Although this falls within the range of optical ages obtained for the fluvio-aeolian sand unit in this work, the age is older than the age of 17.2 ± 1.2 ka that was found for sample G1, which was also taken from just below the gravel bed. It is suggested that the higher ages obtained by Bateman et al. are, at least in part, owing to their use of the single-aliquot additive-dose protocol, which does not correct for sensitivity changes. The SAR-based equivalent doses are considered to be more accurate. A detailed discussion and comparison of both datasets is probably not appropriate, but it can be pointed out that they also exhibit significant differences in the dose rates.

This brings us back to the discussion on the ^{226}Ra excess that was conducted in the previous section. The ages presented in Table 5.7 fit in rather well with the constraints imposed by the stratigraphic markers, the palaeoclimate indicators and the radiocarbon age. More generally, they are in good accordance with the established interpretations on the timing of the deposition of the coversands (see e.g. Kasse, 1999). From this good agreement, one can conclude that the results can be looked upon with a certain degree of confidence. This implies that neglecting the ^{226}Ra excess did not result in a detectable error in the age. It is acknowledged that independent age information is lacking that could confirm with absolute certainty the accuracy of the ages, and hence would allow a validation of the assumptions that were made with regard to the dose rate. However, if serious errors had been committed, it is, to our opinion, unlikely that such a sound degree of consistency in the results had been obtained for all 22 samples.

5.8. Conclusions

The fluvial and fluvio-aeolian sands exposed in Grubbenvorst have been interpreted as Upper Pleniglacial. This is confirmed by the optical ages. More specifically, the deposition of the Older Coversands I can be bracketed between ~17 and ~25 ka. The start of the deposition of the sediments belonging to the Older Coversand II stratigraphic unit was dated at 15.3 ± 1.0 ka, i.e. at the Late-Pleniglacial to Late-glacial transition. The top of this unit was dated at 12.7 ± 0.9 ka. The Younger Coversands II overlying the Usselo Soil were dated at 13.8 ± 1.0 ka. All ages are stratigraphically consistent, and agree well with the geological expectation. For the purely aeolian coversands, the ages are also consistent with the OSL ages of contemporaneous sediments observed in Ossendrecht.
As previously no absolute age information was available for the sediments of the Grubbenvorst section, it can be concluded that an improved chronology for this site could be established. It must be pointed out, however, that optical dating alone cannot strictly distinguish between the two phases of aeolian sand deposition date that, following Kasse (1999), should have occurred during the Late-glacial. With respect to the dating methodology, a few outstanding issues remain to be solved, namely the origin of the dose distributions and that of the apparent radium enrichment.

SUMMARY AND CONCLUSIONS

Luminescence dating is used increasingly as a means of establishing the deposition chronology of sediment (sand, loess). The method is unique because it uses the constituent mineral grains of the sediment itself (quartz, feldspars) instead of the associated material (such as radiocarbon). It covers a wide and important age range (10^0-10^6 a), and yields the ages directly in calendar years. There are two variants of luminescence dating, namely thermoluminescence (TL) and optically stimulated luminescence (OSL or optical) dating, depending on whether the luminescence signal is set free from the minerals by exposing them to heat or light, respectively. Optical dating is a better method for dating sediments, because the OSL signal is more completely and more rapidly reset than the TL signal, and also offers several practical and methodological advantages. As a consequence, optical dating relatively rapidly gained in popularity since it was first introduced in 1985 for solving geological dating problems. Nowadays, the method has replaced the use of TL almost completely.

Until a few years ago, all dating work in the Ghent luminescence laboratory was still carried out using TL. Although the TL age results contributed significantly to palaeoclimatic research in Belgium, our laboratory did lag behind on the immense progress being made in luminescence dating technology. Therefore, the main scope of this thesis was to try catching up with all these developments, and to realize a laboratory that performs luminescence dating according to the state of the art. In essence, this consisted of the implementation of the optical dating method, and of an investigation of its applicability to the Young-Quaternary sandy deposits of our West-European lowlands.

The implementation was started by upgrading the available luminescence measurement apparatus (a Risø TL/OSL-DA-12 system). In a later stage of the investigations, a second reader (a Risø TL/OSL-DA-15 system) was installed. In both systems, the stimulation of OSL can be either by blue light (for quartz or feldspars) or by infrared light (for feldspars). To determine the dose-response curves, two new beta irradiator attachments (equipped with calibrated ^{90}Sr sources) were put into use. Complete measurement sequences can now be carried out fully automated.

In this work, all analyses were based on the optically (blue light) stimulated luminescence signals from quartz. Over the last few years, quartz has become the preferred mineral for dating, and its luminescence properties are understood best. There are a multitude of techniques that can be used for equivalent dose (D_e) determination in the optical dating of quartz. However, none of them had yet proven to be universally applicable. The first step in our research, therefore, consisted of a study of three such measurement protocols, namely the single-aliquot regenerative-dose technique (SAR), the single-aliquot additive-dose technique (SAAD) and the multiple-aliquot additive-dose technique (MAAD). For this purpose, quartz grains were extracted from a sequence of Upper-Pleniglacial to Late-glacial coversands exposed at the locality of Ossendrecht in the southwestern Netherlands. This site was chosen because both radiocarbon ages and earlier luminescence are available that provide independent age control.

Of the three D_e-determination protocols that were investigated, SAR was found to be the technique of choice. All samples behaved well in this SAR protocol. Recycling ratios were within the range of 0.90-1.10 and recuperation was small (less than a few percent of the corrected natural OSL signal). No significant variation in D_e with preheat temperature was detected in the range of 160°C to 260-280°C. The D_e was also rather insensitive to the size of the test dose. Dose recovery tests were carried out to test the overall applicability of the measurement procedures. For all samples, the individual given doses (ranging from ~5 to ~40 Gy) could be recovered to within 5%, and the overall average recovered/given dose ratios were equal to unity. The implementation of the SAR protocol was further investigated by setting up a small interlaboratory comparison (Ghent, Heidelberg and Risø) of SAR-based D_e determinations. The results were in acceptable overall agreement, giving confidence in the implementation of the SAR technique at the Ghent luminescence dating laboratory.

Annual dose determination is the same for TL and OSL dating and the following well-established techniques were used: in-situ NaI(Tl) gamma-ray spectrometry, low-level Ge gamma-ray spectrometry, neutron activation analysis and thick source alpha counting. The results obtained via alpha counting and field γ-spectrometry were not considered further, for reasons of overcounting and a poor documentation of the measurements, respectively. As a consequence, only the concentration results obtained via k_0-NAA and low-level γ-spectrometry were adopted for annual dose calculation. Some discrepancies were

observed between the results obtained via these two techniques, which were attributed to sample inhomogeneity. No radioactive disequilibria were detected.
The optical ages obtained were stratigraphically consistent and in good agreement with the independent age information available for the same and equivalent deposits. More specifically, a mean OSL age of 12.2 ± 0.7 ka was obtained for the Younger Coversand II stratigraphic unit, while the Older Coversand II (or Younger coversand I) unit was dated at 15.0 ± 0.9 ka. From the good agreement between the SAR-based ages and the independent age information, it was concluded that SAR yields accurate dating results. Uncertainties on the individual ages amounted typically to about 6.5%, and arose predominantly from systematic effects. This improvement compared to the relative uncertainty on a TL age result, which is typically 10-15%, is owing to the very high precision by which equivalent doses can be determined using the SAR protocol.

In the course of the optical dating of the coversands from Ossendrecht, the distribution of equivalent doses within a few of the samples was examined more explicitly, by applying the SAR protocol to small aliquots containing 0.5-1 mg of quartz grains. Broad dose distributions with relative standard deviations of 11-12% were observed. This was not expected, given the windblown nature of the deposits.
A study was subsequently carried out to find the cause of the broad dose distributions. Investigations were made as to whether the spread might be related to the measurement procedures, but no evidence for this was found. The possibility of partial bleaching was investigated using the SAR $D_e(t)$ technique. After proving the method to be able to identify artificially partially bleached samples, it was applied to the natural dataset. No evidence for partial bleaching was found, but the $D_e(t)$ plots for the natural samples did not entirely support the positive laboratory findings concerning the applicability of this technique. However, it was not thought to be very likely that these samples had been incompletely reset, because of their windblown nature. Therefore, the possibility of small-scale variations in annual dose was investigated next, by performing NAA on small amounts (0.5-1 g) of sediment. A large scatter in U and Th concentrations throughout the profile, and within each sample, was found. Furthermore, NAA of etched quartz extracts showed a non-negligible internal radioactivity. It was concluded that small-scale differences in the annual dose rate are likely to be the main cause for the observed

distributions, although it could not be established whether internal or external variations in microdosimetry are the dominant factor. The effect of such variations on the age determination was thought to be minor, as a good agreement was found between the OSL ages and the independent radiocarbon ages.

A next step in our research consisted of the application of the optical dating method to a sequence of Upper-Weichselian aeolian, fluvio-aeolian and fluvial sediments exposed near the locality of Grubbenvorst in the southeastern Netherlands. The sediments represent a quasi-complete record of the climatic fluctuations that occurred in this region between the Last Glacial Maximum and the early Holocene. The site is therefore considered as important for the stratigraphy of the southern Netherlands. However, the only age information available for the sediments of the Grubbenvorst section was based on correlation; no absolute ages were available. To improve the chronology of this site, optical dating was applied to these sediments.

Based on the findings for the Ossendrecht samples, the SAR protocol was used for equivalent dose determination. All samples behaved well, with recycling ratios within a range of 0.90-1.10, and with recuperation less than a few percent of the corrected natural OSL signal. In general, there was no systematic dependency of the D_e on preheat temperatures of up to 260-280°C. For one aeolian, one fluvio-aeolian and one fluvial sample, the dependency of the D_e on the test dose size was investigated as well. For the fluvial sample, the D_e was very insensitive to the size of the test dose. For the two other samples, on the other hand, the D_e was observed to decrease as the test dose size increased from ~0.15 to ~6 times the D_e. The causes for the drop in D_e are not understood. For all samples, dose recovery tests were subsequently carried out, which yielded satisfactory results. A range of given doses that bracketed the natural dose (10-25 Gy) could be recovered to within 2.5%. This indicated that the selected SAR measurement parameters (a preheat temperature chosen from the plateau region in the D_e versus preheat temperature plot, and a test dose size of ~ 15% of the D_e) were suitable for analyzing the samples.

The distribution of equivalent doses in one aeolian, three fluvio-aeolian and two fluvial samples was then examined. Two samples that were taken from the fluvio-aeolian to fluvial transition region were analyzed as well. For all samples, broad dose distributions

were found, which could not be attributed to a lack in measurement precision. The possibility of partial bleaching was investigated using the SAR $D_e(t)$ technique. However, several factors were found to complicate the interpretation of the $D_e(t)$ data. One common feature could be clearly recognized for all aliquots and for all samples, namely a significant increase of recuperation in progressively harder to bleach components of the OSL signal. A large inter-aliquot variability was observed as to the amount of recuperation ultimately reached, but in general it amounted to more than 10% of the corrected natural OSL signal. The whole of empirical observations did not support the strong recommendation that was previously made in the literature of using the SAR $D_e(t)$ technique as a tool for identifying partially bleached samples. The possibility of small-scale variations in annual dose was not explicitly investigated. However, a comparison of the concentration results obtained via field γ-spectrometry, low-level γ-spectrometry and NAA indicated a heterogeneous distribution of radionuclides within and surrounding the samples. It was therefore concluded that microdosimetric variations could offer an explanation for the observed D_e distributions.

For the majority of the samples, a ^{226}Ra excess of typically about 20% was detected. Additionally, an increased ^{210}Pb content was observed in some samples. It was considered most likely that these disequilibria had been caused by some recent process. Therefore, for those samples that showed a disequilibrium in the ^{238}U decay series, the contribution from U to the annual dose was derived from the parent activity only. The results from alpha counting were consequently not used for calculating annual doses. Moreover, these results were considered as unreliable as, at least for some samples, evidence was found for the occurrence of alpha overcounting. For K and Th, the averages of all other available results were used.

Within analytical uncertainties, the obtained optical ages increase with depth, and consistent ages were obtained for samples that were taken from the same stratigraphic level. Based on correlation (using stratigraphic markers, palaeoclimate indicators and a radiocarbon age), a Late Weichselian Pleniglacial to Weichselian Late-glacial age had previously been attributed to the Grubbenvorst section. This was confirmed by the optical ages. The fluvial deposits at the base of the section were dated at 27.3 ± 2.1 ka. The deposition of the overlying fluvio-aeolian unit (the Older Coversands I) was bracketed between 17.2 ± 1.2 and 23.7 ± 1.7 ka. The start of the deposition of the sediments

intercalated between the Beuningen Gravel Bed and the Usselo Soil (i.e. the Older Coversand II unit) was dated at 15.3 ± 1.0 ka, while the top of this sedimentary unit (possibly the Younger Coversand I unit) was dated at 12.7 ± 0.9 ka. Finally, an optical age of 13.8 ± 1.0 ka was obtained for the Younger Coversands II. The ages for the aeolian sands that overlie the Beuningen Gravel Bed were quite consistent with the optical ages obtained for the contemporaneous sediments exposed in Ossendrecht.
As previously no absolute age information was available for the sediments exposed in Grubbenvorst, it was concluded that an improved chronology for this site could be established through optical dating.

It is generally concluded that the implementation of the optical dating method in our laboratory has been successful, and proceeded without any significant problems. The case-study of Grubbenvorst clearly illustrates the important contribution that optical dating can deliver to palaeoclimatic research in Belgium and the Netherlands. The implemented dating procedures allow an accurate and, in comparison to TL, also relatively rapid and precise (6-8%) age determination of sediments that were deposited sometime during the Late-Weichselian and the last glacial – interglacial transition. It is worth adding that, although this work could not be included in this thesis, optical dating of quartz was also successfully applied, for instance, for the timing of the different phases of drift sand formation that occurred in the southern Netherlands during the Holocene.

Future dating applications and methodological challenges lie, as it were, ready to hand. Indeed, the demand for absolute age determinations is high, as well in Belgium as abroad. Optical dating of sediments can also aid in solving archaeological problems, and there is no impediment in putting the optical dating method in use for the dating or the authenticity testing of heated materials. Recent developments in measurement technology (such as single-grain readers, X-ray irradiation sources, linear modulation, and radioluminescence facilities) have further created a wide variety of research perspectives. It is hoped that, through the work presented in this thesis, the foundations have been laid for making such routine dating and innovative methodological research possible at the Ghent luminescence laboratory.

– APPENDIX –

A NOTE ON PAIRS COUNTING

Thick source alpha counting is routinely used in our laboratory for the determination of the annual alpha, beta and gamma dose (Vancraeynest, 1998; Van den haute et al., 1998; Hossain, 2003; Van den haute et al., 2003). This is because the technique is sensitive, relatively cheap and requires a minimum of sample preparation or other effort from the analyst. From the registered alpha count-rate (i.e. the integral count-rate) the desired dose-rates are calculated using tabulated conversion factors. In this conversion, however, it is implicitly assumed that the samples contain equal activities of the uranium and thorium series. The maximum errors introduced by not taking into account the real activity ratio are 5% for the alpha dose-rate and ~20% for the beta and gamma dose-rate. These maximum errors refer to samples containing only the uranium series or only the thorium series. As this situation is quite unlikely to be encountered in the dating of sediments, the errors introduced are in reality smaller. Furthermore, the dependence of the beta dose-rate on the U/Th ratio is in the opposite sense than that of the gamma dose-rate. As a consequence, one error will, for the greater part, cancel the other, if both the beta and the gamma component are derived from alpha counting. It is quite common, however, to use another analytical technique for determining one of the components. To obtain the gamma dose-rate, for instance, one might prefer a technique that samples a larger volume of sediment. If, on the other hand, a separate evaluation is made of the alpha activity of the dating sample and of its surroundings, then it cannot be assumed that both have the same U/Th ratio. In these cases, it is clearly desirable to introduce the actual activity ratio in the calculations.

The U/Th activity ratio can be derived from the results obtained via other analytical techniques but this would obviously make alpha counting less self-contained, even superfluous. However, the alpha counting itself also yields information on the U/Th ratio. Indeed, in the Th decay chain about 3% of the registered counts occur in pairs (meaning that two alpha particles are emitted and detected in quick succession). ^{216}Po has a half-life of only 0.145 s, and decays by α-emission almost immediately after the decay of the

previous daughter ^{220}Rn, which is also an alpha emitter (the decay scheme of ^{232}Th is shown in Figure 3.21). The same happens in the ^{235}U series, where an alpha particle is emitted from ^{215}Po ($T_{1/2} = 1.78 \times 10^{-3}$ s) in rapid succession with that emitted by its predecessor ^{219}Rn (see Figure 3.19). Using appropriate coincidence circuitry, it is consequently possible to count and distinct between the slow pairs from the ^{232}Th series and the fast pairs from the ^{235}U series and consequently, to determine the U/Th ratio in a sample. The Elsec 7286 low-level alpha counting systems that are in use in our laboratory automatically keep track not only of the total number of counts, but also of the number of counts occurring within 0.004 s (fast ^{235}U pairs) and those occurring between 0.02 and 0.40 s (slow ^{232}Th pairs). This information is thus available without any extra effort.

It has been pointed out by Vancraeynest (1998) and Hossain (2003) that pairs counting is not suitable for practical use because of the low number of pairs that is registered, and hence the large statistical uncertainty on the final result. The purpose of this note is to point out that this is a misconception. The following will show that the pairs technique yields dose-rates that are no longer subjected to the inherent “equal activity” assumption, and are thus more accurate – with a minimum loss in precision. This is especially relevant to the coarse-grain technique, where the error introduced by unknown activity ratios is less diluted compared to the fine grain technique.

The a priori assumption is that alpha counting is indeed able to provide accurate annual doses. The good results previously obtained by Vancraeynest (1998) and, more recently, by Hossain (2003) suggested this to be so, which is why the technique was also incorporated in this work. The results presented in Sections 4.6.4 and 5.6.4.3, however, question the reliability of the alpha counting technique, as evidence was found for “overcounting” to occur. This problem will perhaps be overcome in future, and the following might then be of some use.

It can be shown (Aitken, 1985; the conversion factors will be discussed later) that the beta dose-rate from U and Th can be calculated from the measured alpha count-rate using the following relation:

$$D_\beta = 7.20\,\dot{\alpha} \qquad \text{(A.1)}$$

in which D_β is the beta dose-rate in mGy ka^{-1} and $\dot{\alpha}$ is the total alpha count-rate (counts per 10 ks). This is in the assumption of equal activities of the Th and U series. This expression is derived from:

$$D_\beta = 8.74\,\dot{\alpha}_U + 5.65\,\dot{\alpha}_{Th} \tag{A.2}$$

in which $\dot{\alpha}_U$ and $\dot{\alpha}_{Th}$ are the counts per 10 ks from the U and Th series, respectively. As $\dot{\alpha} = \dot{\alpha}_U + \dot{\alpha}_{Th}$, the equation can be rewritten as:

$$D_\beta = 8.74\,\dot{\alpha} - 3.09\,\dot{\alpha}_{Th} \tag{A.3}$$

The count-rate from the thorium series can be obtained from the measured slow pairs count-rate:

$$\dot{\alpha}_{Th} = 21.0\,\dot{p} \tag{A.4}$$

in which $\dot{p}$ is the net true slow pairs count-rate (pairs per 10 ks), with a correction for random coincidence. The latter can be performed by subtracting the random coincidence pairs-rate $\dot{r}$ from the observed pairs-rate $\dot{p}_{meas}$:

$$\dot{p} = \dot{p}_{meas} - \dot{r} \tag{A.5}$$

The number of pairs caused by coincidence per unit of time (10 ks) can be calculated from:

$$r = 0.38\,\dot{\alpha}^2 \tag{A.6}$$

The factor 0.38 refers to the time that the coincidence window is open. Consequently, the probability that another alpha particle will arrive within this time is given by $0.38\,\dot{\alpha}$, and the number of random pairs occurring per measurement period is as in the above equation.

As a practical note, it is perhaps worth pointing out that the probability is dimensionless $\left(= 0.38\,(\mathrm{s}) \,.\, \frac{\text{number of alpha counts observed on average in a period}}{\text{duration of the period (s)}} \right)$.

Turning back now to the expression for the beta dose-rate, substitution of equation A.4 into equation A.3 yields:

$$D_\beta = 8.74\,\dot{\alpha} - 64.89\,\dot{p} \tag{A.7}$$

The absolute uncertainty s_a on D_β is obtained following the conventional rules of error propagation:

$$s_a\left(D_\beta\right) = s_a\sqrt{\left[s_a\left(8.74\,\dot{\alpha}\right)\right]^2 + \left[s_a\left(64.89\,\dot{p}\right)\right]^2} \tag{A.8}$$

Note that the slow pairs are used, rather than the fast pairs from the ^{235}U series, as the latter are measured with less precision (~10% of the Th pairs or less).

The gamma dose-rate can be obtained via pairs counting in a similar manner. The equation assuming equal activities is:

$$D_\gamma = 8.31\,\dot{\alpha} \tag{A.9}$$

This expression is derived from:

$$D_\gamma = 6.76\,\dot{\alpha}_U + 9.86\,\dot{\alpha}_{Th} \tag{A.10}$$

Using $\dot{\alpha} = \dot{\alpha}_U + \dot{\alpha}_{Th}$, the equation can be rewritten as:

$$D_\gamma = 6.76\,\dot{\alpha} + 3.10\,\dot{\alpha}_{Th} \tag{A.11}$$

Substitution of the count-rate from the thorium series using equation A.4 gives the gamma dose-rate:

$$D_\gamma = 6.76\,\dot{\alpha} + 65.1\,\dot{p} \qquad \text{(A.12)}$$

The absolute uncertainty s_a on D_γ is obtained following the conventional rules of error propagation:

$$s_a\left(D_\gamma\right) = s_a\sqrt{\left[s_a\left(6.76\,\dot{\alpha}\right)\right]^2 + \left[s_a\left(65.1\,\dot{p}\right)\right]^2} \qquad \text{(A.13)}$$

Let us now, for the sake of clarity, have a look at an elaborate example. For sample G7 (a fluvio-aeolian sample from Grubbenvorst; see Section 5.4), a total number of 5273 alpha counts and 102 pairs were registered over a total counting time of 2230000 s. The background yielded 290 alpha counts and 1 pair in 1750000 s. This leads to the net count-rates (counts per 10 ks) of 21.99 ± 0.34 and 0.45 ± 0.05 for the alphas and the pairs, respectively. The uncertainties are obtained following the conventional rules of error propagation. Subtraction of the random pairs-rate from the measured net pairs-rate yields a true pairs-rate of 0.43 ± 0.05. Solving equations A.7 and A.8, and A.12 and A.13 gives the corresponding beta and gamma dose-rates of 164 ± 4 mGy ka^{-1} and 177 ± 4 mGy ka^{-1}. The dose-rates calculated from the integral alpha count-rate are 158 ± 2 mGy $ka^{-1}$and 183 ± 3 mGy ka^{-1} for the beta and the gamma component, respectively.
The relative uncertainty on the beta and gamma dose-rate is 2.6% and 2.1 %, respectively, when using the pairs counting technique, and ~1.5% when using the integral count-rate. It is clear that the use of pairs counting does not lead to a significant loss in precision. For this sample, the use of the integral count-rate would not lead to a significantly wrong dose-rate, but this cannot be assumed for all samples.

It is concluded that pairs counting is a useful technique for determining the dose-rate, suitable for routine determination of the annual beta and gamma dose in the coarse-grain technique. Compared to the use of the integral count-rate, this should lead to a negligible small loss in precision but an improved accuracy of the results. All this is in the

assumption that no other effects, such as overcounting, interfere with the accuracy. It must be pointed out that this conclusion is in no way epoch-making, as the same remark was already put to paper by Aitken (1990) more than a decade ago. To all probability, many experienced alpha counting practitioners already acknowledge the usefulness of pairs counting.

All the necessary conversion factors for performing the above calculations are given in Tables A.1 and A.2 (see further) with the exception of the one required for obtaining the contribution of the Th series to the total alpha count-rate from the measured slow pairs. In fact, the last appearance of this factor in the literature dates back to 1985 (Aitken, 1985). Although the value of this factor was not expected to change much when calculating it from more recent nuclear data, it was recalculated nevertheless, just to set the empiricist's mind at ease.

It can be shown (Aitken, 1985) that the measured slow pairs count-rate (pairs per 10 ks) is related to the specific activity of the Th series according to the following relation:

$$\dot{p}_{Th} = \frac{P}{1.2} . A . (R_1 - \delta R) . \rho . a_{Th} . \left(1 + \frac{1}{2} . \frac{R_2 - R_1}{(R_2 - \delta R)}\right) \qquad (A.14)$$

in which $\dot{p}_{Th}$ is the measured slow pairs count-rate, A the area of the ZnS scintillation screen (1385 mm^2), a_{Th} the specific ^{232}Th activity (Bq/kg), δR a residual range corresponding to the minimum energy an alpha particle requires to be detected (= 0.15 × average range), R_1 the range of the α-particles emitted by ^{220}Rn, R_2 the range of those emitted by ^{216}Po and ρ the density of the sample (g cm^{-3}). P expresses the probability that a second alpha particle will be emitted within a time τ after the first particle was emitted. This probability is given by $(1 - \exp(-\lambda\tau))$ in which λ is the decay constant of ^{216}Po (4.78 s^{-1}). In ELSEC equipment, the coincidence window for the slow pairs is open from 0.02 to 0.4 s after each count. Hence, the probability that two alpha particles occur as a pair within this window is $[(1 - \exp(-4.78\times0.4) - (1 - \exp(-4.78\times0.02)]$, that is, 0.761.

Adamiec and Aitken (1998) give the average ranges for the natural decay series, but not the individual values for R_1 and R_2 that are required to complete equation A.14. These values can, however, be readily obtained when repeating their calculations following the

same working method. Adamiec and Aitken (1998) obtained the ranges by adding 2% to the ranges evaluated for quartz by Brennan and Lyons (1989). Figure A.1 shows these data as solid circles; note that the ranges are expressed as ρ.R (mg cm^{-2}). Following the practice of Brennan and Lyons (1989), a third order polynomial was chosen to approximate the data. The fit (shown as the solid line in Figure A.1) was excellent, as was indicated by the residuals (not shown in the figure) lying within an error band of less than 0.5%. For all energies from 1 to 10 MeV, the corresponding ranges can then be obtained using the equation given in the caption of the figure. In this manner, the ranges were obtained for all the alpha particles involved in the ^{232}Th decay series, yielding an average alpha range of 67.3 μg mm^{-2}. This value is indistinguishable from the value of 67.4 μg mm^{-2} that is given by Adamiec and Aitken (1998). This good agreement suggests that individual alpha ranges can be obtained from Figure A.1 with sufficient accuracy. For ^{220}Rn a range of 70.9 μg mm^{-2} was found, for ^{216}Po of 79.5 μg mm^{-2}.

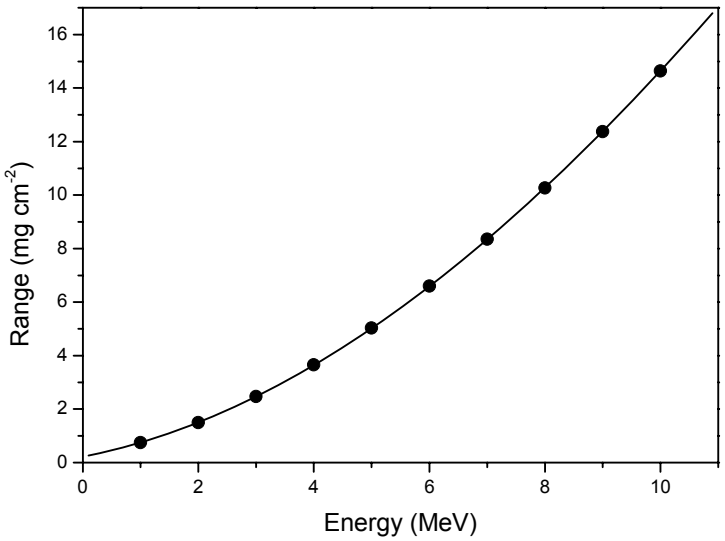

Figure A.1: Range as a function of energy. The ranges used (solid circle) were obtained by adding 2% to the ranges evaluated for quartz by Brennan and Lyons (1989); the extra 2 % is on account of the greater range in typical sediment. This follows the practice by Adamiec and Aitken (1998). Only the energy range 1 – 10 MeV was used. The solid line results from a third order polynomial with equation: Range = 0.221 + 0.415*E + 0.116*E^2 – 0.001*E^3.

Using these new values for δR (0.15×67.3 = 10.1 μg mm^{-2}), R_1 (70.9 μg mm^{-2}) and R_2 (79.5 μg mm^{-2}), equation A.14 is reduced to:

$$\dot{p}_{Th} = 0.057\ a_{Th} \qquad (A.15)$$

Making use of the relationship between the alpha count-rate (cts per 10 ks) and the specific activity (Bq per kg):

$$\dot{\alpha}_{Th} = 1.19\ a_{Th} \qquad (A.16)$$

it is possible to express the relationship between the pairs count-rate and the alpha count-rate as:

$$\dot{\alpha}_{Th} = 21.0\ \dot{p}_{Th} \qquad (A.17 = A.4)$$

This value is not significantly different from the previously tabulated value of 21.1 (Aitken, 1985, p. 302).

A last note concerns the conversion factors that are necessary to obtain dose-rates from measured alpha count-rates. Conversion factors have been reported from time to time in the literature, the different factors being revised as nuclear data tables are updated. Although the overall effect on an age is usually small, it is obviously desirable to use the most recent ones from the literature, which at the time of writing are those tabulated by Adamiec and Aitken (1998). The dose-rate data tabulated by Aitken (1998) for beta and gamma radiation are those from Adamiec and Aitken (1998), but this is not the case for alpha radiation. This is on account of the use by Adamiec and Aitken (1998) of the more recently evaluated alpha ranges by Brennan and Lyons (1989). The difference in conversion factors related to alpha counting is illustrated in Table A.1 and A.2; only those relevant to coarse-grain dating are considered.

It can be pointed out that, although the use of the more recent conversion factors does not influence the calibration settings of the counters (the high voltage plateau is not influenced, and the error introduced in the threshold setting is estimated at ~0.1%), it does compromise some of the previously reported comparisons of observed and measured count-rates. Indeed, the latest set of conversion factors for calculating alpha count-rates

from concentrations are on average ~6.5% lower than those tabulated by Aitken (1998). The predicted count-rate will decrease correspondingly, which might very well upset some previously observed "within analytical uncertainty"-consistencies with the measured count-rate (see e.g. Section 4.6.4). This is perhaps a matter worthy of further consideration.

	Beta		Gamma		Ratio	
	A. & A.	A.	A. & A.	A.	Beta	Gamma
^{232}Th	5.65	5.31	9.86	9.31	1.064	1.059
Natural uranium	8.74	8.15	6.76	6.35	1.072	1.065

Table A.1: Comparison of the conversion factors (dose rate in mGy ka^{-1} for an alpha count-rate of 1 per 10 ks) by A. & A.: Adamiec and Aitken (1998) and A.: Aitken (1998).

	α count-rate (counts/10ks) per Bq kg^{-1} of parent		Ratio
	A. & A.	A.	
^{232}Th	1.19	1.26	0.94
Natural uranium	1.29	1.38	0.93

Table A.2: Comparison of the factors to obtain the alpha count-rate (in counts per 10 ks) per Bq kg^{-1} of parent; A.: Aitken (1998); A. & A.: Adamiec and Aitken (1998).

NEDERLANDSE SAMENVATTING

De luminescentiedateringsmethode is een radiometrische dateringsmethode die gebaseerd is op de tijdsafhankelijke accumulatie van stralingsschade in mineralen. De stralingsschade is het gevolg van blootstelling van de mineralen aan natuurlijke radioactiviteit. Hoe langer de mineralen blootgesteld worden aan de ioniserende straling, hoe groter de stralingsschade. De intensiteit van de stralingsschade is bijgevolg een maat voor de totale stralingsdosis die de mineralen hebben ontvangen over een bepaalde tijdspanne.

In de luminescentiedateringsmethode wordt de stralingsschade terug vrijgesteld onder de vorm van een klein maar meetbaar lichtsignaal: het luminescent signaal. Het vrijstellen (= het op nul zetten) van de luminescentie gebeurt door de mineralen te stimuleren met warmte of licht (TL en OSL, zie verder). In het specifieke geval van sedimenten bijvoorbeeld, vindt dergelijke op nul zetting plaats in de natuur tijdens het transport van de mineraalkorrels. Hierbij worden ze immers blootgesteld aan daglicht. Eenmaal de korrels opnieuw afgezet en vervolgens begraven worden onder andere korrels, kan het luminescent signaal opnieuw aangroeien onder invloed van de natuurlijke radioactieve straling.

De luminescentie kan op dezelfde manier (met behulp van warmte of licht) ook in het laboratorium vrijgesteld en gemeten worden. De intensiteit van het gemeten luminescent signaal is evenredig met de totale stralingsdosis die in de mineralen opgeslagen werd sinds de vorige op nul zetting. Voor sedimenten is dit dus de laatste blootstelling aan daglicht net voor ze begraven werden. Als ook bepaald wordt aan welk tempo de mineralen de stralingsdosis (en dus luminescentie) absorbeerden (de jaarlijkse stralingsdosis) kan een ouderdom bepaald worden. In de context van de datering van sedimenten is de ouderdom bijgevolg gelijk aan de tijd die verstreken is tussen het moment waarop het sediment werd afgezet en begraven, en het moment waarop het luminescent signaal in het laboratorium wordt gemeten.

De luminescentiedateringsmethode wordt wereldwijd in toenemende mate gebruikt om het tijdstip te bepalen waarop sedimenten (zand, loess) werden afgezet en waarop dus

sedimentaire landschapsvormen ontstaan zijn. Uniek aan de methode is dat ze gebruik maakt van de triviale bestanddelen (kwarts, veldspaat) van een gewoon sediment en niet van geassocieerd materiaal (zoals bijvoorbeeld ^{14}C) dat doorgaans schaarser en/of onbetrouwbaarder is. De methode bestrijkt een groot en belangrijk tijdsvenster (10^0-10^6 jaar) dat veel breder is dan dat van de ^{14}C-dateringsmethode (tot ~40 ka). Aangezien het vrijstellen van luminescentie op twee manieren kan gebeuren, zijn er ook twee varianten van de dateringsmethode. Als de mineralen thermisch gestimuleerd worden noemt men het resulterende lichtsignaal thermoluminescentie (TL); worden de mineralen blootgesteld aan licht van een welbepaalde golflengte, dan spreekt men van optisch gestimuleerde luminescentie of OSL. De OSL-methode is een betere methode om sedimenten te dateren. Het OSL-signaal wordt sneller en volledig op nul gesteld (in tegenstelling tot het TL-signaal, waar steeds nog een residusignaal aanwezig blijft), en het biedt bovendien praktische en methodologische voordelen. De populariteit van de OSL-methode groeide dan ook snel sinds ze werd voorgesteld in 1985 door Huntley et al. voor het dateren van geologische materialen. Tegenwoordig heeft de OSL-methode het gebruik van TL bijna volledig vervangen en vooral voor wat de chronometrie van de laatste honderdduizend jaar betreft lijkt ze een echte doorbraak teweeg te brengen.

Tot voor een aantal jaar werden alle luminescentiedateringen in ons laboratorium uitgevoerd met behulp van de TL-methode. Alhoewel de bekomen TL-ouderdommen een significante bijdrage leverden aan het paleoklimatologisch onderzoek in België, liep ons laboratorium achter op de enorme vooruitgang die ondertussen werd geboekt op het gebied van de dateringsmethode. De doelstelling van dit werk bestond er dan ook in bij te benen met deze ontwikkelingen om zo luminescentie-ouderdommen te kunnen produceren volgens de “state of the art”, en om de toepasbaarheid te onderzoeken van de OSL-methode voor het dateren van de jong Kwartaire zanderige afzettingen van de West-Europese lage landen.

In een eerste stap van dit werk werd de reeds aanwezige apparatuur (een Risø TL/OSL-DA-12 meetsysteem) gemoderniseerd om het meten van optisch gestimuleerde luminescentiesignalen mogelijk te maken. In een later stadium werd ook een tweede, meer recent ontwikkeld meetsysteem geïnstalleerd (een Risø TL/OSL-DA-15). In beide

toestellen kan, naast het verhitten van monsters (voor TL of een voorverhittingsbehandeling), de stimulatie van luminescentie gebeuren met behulp van blauw licht (voor kwarts of veldspaten) of infrarood licht (voor veldspaten). Om de aangroei van het OSL-signaal als functie van de stralingdosis te karakteriseren, werden twee nieuwe β-bestralingseenheden in gebruik genomen. Elk systeem werd uitgerust met een $^{90}Sr/^{90}Y$ bron en rechtstreeks op een meettoestel gemonteerd. Vervolgens werden de β-bronnen gekalibreerd. Met de toestellen in deze configuratie kunnen volledige meetsequenties nu volautomatisch uitgevoerd worden.

In dit werk werd voor alle analyses gebruik gemaakt van het luminescent signaal dat met behulp van blauw licht uit kwarts gestimuleerd werd. Kwarts is de voorbije jaren het mineraal bij uitstek voor datering geworden en zijn luminescentie-eigenschappen zijn het best gekend. Er is een hele waaier aan meetprocedures beschikbaar om de door kwarts geabsorbeerde stralingsdosis (de equivalente dosis of D_e) te bepalen aan de hand van OSL-signalen. Niet alle technieken zijn echter even geschikt voor het dateren van een gegeven type sediment. De eerste fase van het onderzoek bestond er in om drie van deze technieken te onderzoeken: het “single-aliquot additive-dose” (SAAD) protocol, het “single-aliquot regenerative-dose” (SAR) protocol, en het “multiple-aliquot additive-dose” (MAAD) protocol. Hiervoor werden kwartskorrels afgezonderd uit een sequentie van Pleni- tot Laatglaciale zanden die bemonsterd werden te Ossendrecht (ZW Nederland). Deze site werd gekozen omdat de ouderdom van de sedimenten goed gekend is door middel van ^{14}C-dateringen en vroegere TL- en OSL-dateringen door andere onderzoekers. Dit zou toelaten om de meetprocedures, en de resultaten die ze uiteindelijk opleveren, te evalueren met betrekking tot hun accuratesse.
Van de drie technieken die onderzocht werden bleek het SAR-protocol de beste techniek. De correctie voor sensitiviteitsveranderingen werkte uitstekend. Veranderingen in voorverhittingstemperatuur en grootte van de testdosis hadden geen significante invloed op de D_e’s bekomen via het SAR-protocol. Zogenaamde “dose recovery” testen bevestigden de geschiktheid van de experimentele procedures. Hierbij werden in het laboratorium gekende stralingsdosissen (van 5 tot 40 Gy) toegediend aan op nul gezette monsters, waarna deze stralingsdosissen met de SAR procedure bepaald werden. De afwijking tussen de bepaalde en de gekende toegediende dosissen bedroeg niet meer dan

5%. Over het hele onderzochte dosisbereik was de gemiddelde verhouding bepaalde/toegediende dosis gelijk aan 1. Hieruit besloten we dat het SAR-protocol betrouwbaar is. De implementatie van de SAR techniek in ons laboratorium werd onderzocht door een kleine interlaboratoriumvergelijking (Risø en Heidelberg). Door elk laboratorium werd voor een aantal monsters de D_e bepaald met behulp van de SAR techniek. De resultaten waren in goede overeenstemming, wat vertrouwen gaf in onze implementatie van dit meetprotocol.

Het bepalen van de jaarlijkse stralingsdosis is zowel voor de TL als de OSL-dateringsmethode hetzelfde, en omtrent dit luik was al een ruime ervaring aanwezig in ons laboratorium. De volgende analytische technieken werden gebruikt: in situ NaI(Tl) γ-spectrometrie, lage-achtergrond Ge γ-spectrometrie, neutronenactiveringsanalyse en alfa-telling. De resultaten bekomen via alfa-telling en in situ γ-spectrometrie werden niet gebruikt om de jaarlijkse dosis te berekenen. Bij alfa-telling omwille van "overcounting"; bij γ-spectrometrie omwille van een gebrek aan informatie met betrekking tot de exacte locatie van de metingen. Bijgevolg werden enkel de resultaten gebruikt die bekomen werden via NAA en lage-achtergrond γ-spectrometrie. De resultaten bekomen via deze twee methoden waren niet volledig in overeenstemming. Dit was toe te schrijven aan een inhomogeniteit van de monsters. Er werden geen radioactive onevenwichten vastgesteld.

De OSL-ouderdommen bekomen voor de Ossendrecht zanden waren stratigrafisch consistent. Meer bepaald werd voor het zogenaamde Jong Dekzand II een (gemiddelde) OSL-ouderdom bekomen van 12,2 ± 0,7 ka. De ouderdom bekomen voor het onderliggende Oud Dekzand II (of Jong Dekzand I) was 15,0 ± 0,9 ka. Deze ouderdommen waren in goede overeenstemming met de onafhankelijke ouderdomsinformatie die beschikbaar was. Hieruit besloten we dat het SAR-protocol tot accurate dateringsresultaten leidt. De onzekerheid op een individuele ouderdom bedroeg typisch ongeveer 6,5%, en vond zijn oorsprong voornamelijk in systematische effecten. In vergelijking met de onzekerheid op een TL-ouderdom, die typisch 10-15% bedraagt, is dit een aanzienlijke verbetering. Dit is te danken aan de zeer hoge precisie waarmee de equivalente dosis kan worden bepaald met het SAR-protocol.

De distributie van equivalente dosissen in een aantal monsters werd expliciet onderzocht door het SAR-protocol toe te passen op kleine aliquots bestaande uit slechts 0,5 – 1 mg

kwartskorrels. Brede dosisdistributies met een relatieve standaarddeviatie van 11-12% werden geobserveerd.

Nadien werd een onderzoek uitgevoerd om de oorsprong van deze spreiding te achterhalen. Eerst werd nagegaan of de spreiding een verband had met de experimentele meetprocedures of met een gebrek in de precisie van de bepalingen. Dit was niet het geval. Een onvolledige op nul zetting van het OSL-signaal in het verleden was een tweede mogelijkheid. Om dit na te gaan werd de SAR $D_e(t)$ techniek gebruikt. Eerst werd aangetoond dat deze techniek kunstmatig onvolledig op nul gezette monsters correct kon identificeren. Daarna werd ze toegepast op de natuurlijke data. Er werd geen aanwijzing gevonden voor een onvolledige op nul zetting van het OSL-signaal in de monsters. Bij toepassing van de SAR $D_e(t)$ techniek op de natuurlijke data werden echter een aantal complicaties vastgesteld die, in tegenstelling tot de veelbelovende resultaten van de simulaties in het laboratorium, eerder een beperkte toepasbaarheid van de $D_e(t)$ techniek suggereerden. Een onvolledige op nul zetting van het OSL signaal in deze monsters was in ieder geval niet waarschijnlijk, omdat deze dekzanden door de wind getransporteerd werden en hierbij normaal gezien aan voldoende licht waren blootgesteld. Daarom werd een derde mogelijkheid onderzocht, namelijk die van variaties in de jaarlijkse dosis op een zeer kleine schaal. Hiervoor werden kleine hoeveelheden sediment (0,5 – 1 g) geanalyseerd met behulp van neutronenactiveringsanalyse. Er werd een grote spreiding in de U en Th concentraties gevonden, niet alleen doorheen het volledige profiel, maar ook in elk monster zelf. Ook zuiver kwarts dat uit het sediment werd geëxtraheerd, werd geanalyseerd met NAA. De resultaten van deze experimenten duidden op een niet verwaarloosbare inwendige radioactiviteit. Er werd besloten dat variaties in jaarlijkse dosis op een zeer kleine schaal de hoofdoorzaak zijn van de geobserveerde spreidingen. Er kon echter niet vastgesteld worden of het inwendige (in de kwartskorrels zelf) of uitwendige variaties in de jaarlijkse stralingsdosis waren die de brede spreiding in equivalente dosissen veroorzaakten. De invloed van deze variaties op de ouderdomsbepalingen leek verwaarloosbaar klein, of in ieder geval voldoende uitgemiddeld te worden, omwille van de goede overeenkomst van de bekomen OSL-ouderdommen met de onafhankelijke ouderdomscontrole.

In de laatste fase van het onderzoek werd de OSL-dateringsmethode toegepast op een sequentie van eolische, fluvio-eolische en fluviatiele sedimenten die werden bemonsterd

in een zandgroeve nabij Grubbenvorst (ZO Nederland). De sedimenten vertegenwoordigen een quasi volledige opname van de klimaatschommelingen die in deze regio plaatsvonden tussen het Laatste Glaciaal Maximum en het vroege Holoceen. De site wordt bijgevolg beschouwd als een belangrijke type-localiteit. De enige ouderdomsinformatie die beschikbaar was voor de sedimenten van de Grubbenvorst site was echter gebaseerd op correlatie. Er waren geen absolute ouderdommen beschikbaar.

Voortbouwend op de ervaring met de dekzand monsters uit Ossendrecht, werd het SAR protocol gebruikt om de equivalente dosis te bepalen. De correctie voor sensitiviteitsveranderingen werkte naar behoren. Voor alle monsters had de voorverhittingsprocedure geen significante invloed op de waarde van de equivalente dosis. Voorverhittingen variërend van 160°C tot 260-280°C (elk met een duur van 10s) gaven hetzelfde resultaat. Voor één windgeblazen monster, één fluvio-eolisch monster en één fluviatiel monster werd ook de invloed van de grootte van de testdosis op de D_e-bepaling onderzocht. Voor het fluviatiel monster werd geen verband tussen beide vastgesteld. Voor de twee andere monsters daarentegen daalde de D_e naarmate de testdosis groter werd. De oorzaak hiervoor is niet bekend. Om de geschiktheid van de meetprocedures (en in het bijzonder de grootte van de testdosis) te evalueren, werden voor alle monsters dose recovery testen uitgevoerd. Gebruik makend van een testdosis van ~15% van de te bepalen stralingsdosis, konden alle in het laboratorium toegediende dosissen correct worden bepaald. Hieruit werd besloten dat de SAR meetprocedure tot een accurate D_e-bepaling leidt.

We onderzochten de distributie van equivalente dosissen in één eolisch, drie fluvio-eolische en twee fluviatiele monsters. Ook twee monsters uit de overgangszone van de fluvio-eolische naar de fluviatiele sedimenten werden geanalyseerd. Voor alle monsters werden brede distributies bekomen, wat niet kon toegeschreven worden aan een gebrek in meetprecisie. Aan de hand van de SAR $D_e(t)$ techniek werd nagegaan of de strooiing te wijten kon zijn aan een onvolledige op nul zetting van het OSL signaal in het verleden. Verschillende factoren bemoeilijkten de interpretatie van deze plots, zoals vroeger al werd aangegeven bij de analyse van de monsters uit Ossendrecht. Voor alle aliquots en alle monsters kon nu één gemeenschappelijke complicatie opgemerkt worden, namelijk een toename van de recuperatie in de moeilijker bleekbare componenten van het OSL signaal. De absolute hoeveelheid recuperatie varieerde sterk van aliquot tot aliquot, maar bedroeg

in het algemeen uiteindelijk meer dan 10% van het overeenkomstig natuurlijk OSL signaal. Het geheel van empirische observaties suggereert dat de SAR $D_e(t)$ techniek eerder beperkt is als hulpmiddel voor de identificatie van partieel gebleekte monsters, en dus niet tegemoet komt aan de verwachtingen die in de literatuur beschreven staan. De mogelijkheid van variaties in jaarlijkse dosis op microschaal werd niet expliciet onderzocht. Uit een vergelijking tussen de concentratieresultaten bekomen via in-situ γ-spectrometrie, lage-achtergrond γ-spectrometrie en neutronenactiveringsanalyse kon afgeleid worden dat de radionucliden heterogeen verdeeld zijn in en rond de monsters. Er werd besloten dat dit een mogelijke verklaring kan bieden voor de geobserveerde dosis distributies.

Voor het merendeel van de monsters werd een ^{226}Ra aanrijking vastgesteld van ongeveer 20%. In sommige monsters was ook het ^{210}Pb-gehalte verhoogd. Er werd aangenomen dat deze onevenwichten het gevolg zijn van een recent proces. Voor de monsters waarvoor het onevenwicht vastgesteld werd, werd bijgevolg de bijdrage van U tot de jaarlijkse dosis enkel afgeleid uit de concentratie van de ^{238}U-moeder. De resultaten bekomen via alfa-telling konden dus niet in rekening gebracht worden. Deze resultaten werden hoe dan ook verworpen aangezien de accuratesse ervan twijfelachtig was omwille van “overcounting”. Voor K en Th werd het gemiddelde van alle beschikbare resultaten gebruikt.

De bekomen OSL ouderdommen waren stratigrafisch consistent. Voor monsters van hetzelfde stratigrafische niveau werden bovendien dezelfde ouderdommen gevonden. Op basis van correlatie (aan de hand van stratigrafische markers, paleoklimaatsindicatoren en een ^{14}C ouderdom van een veenlaagje uit een boorkern in de buurt van de groeve) werd vroeger een Pleni- tot Laatglaciale ouderdom toegeschreven aan de Grubbenvorst sectie. De OSL-ouderdommen ondersteunen deze interpretatie volledig. De fluviatiele afzettingen aan de basis van de sectie werden gedateerd op 27,3 ± 2,1 ka. De ouderdommen verkregen voor de erboven liggende fluvio-eolische zandlaag (Oud Dekzand I) varieerden van 17,2 ± 1,2 ka tot 23,7 ± 1,7 ka. De aanvang van de depositie van de sedimenten die tussen de Beuningen grindlaag en de Usselo bodem liggen (Oud Dekzand II) werd bepaald op 15,3 ± 1,0 ka, terwijl de top van deze laag (mogelijk Jong Dekzand I) werd gedateerd op 12,7 ± 0,9 ka. Tot slot werd een ouderdom bekomen van 13,8 ± 1,0 ka voor het Jong Dekzand II dat boven op de Usselo laag ligt. De ouderdommen voor de eolische zanden boven de Beuningen grindlaag waren consistent

(binnen de analytische onzekerheden) met de OSL-ouderdommen voor de sedimenten ontsloten te Ossendrecht.

De dateringen van de Grubbenvorst site tonen duidelijk aan dat de OSL dateringsmethode een belangrijke bijdrage kan leveren tot het paleoklimatologisch onderzoek in België en Nederland. De geïmplementeerde dateringsprocedures laten een accurate en, in vergelijking met TL, ook relatief snelle en precieze ouderdomsbepaling toe van sedimenten die werden afgezet tijdens het Laat-Pleistoceen en Laatglaciaal.

Toekomstige toepassingen en methodologische uitdagingen liggen voor de hand. De vraag naar absolute dateringen is groot, zowel in binnen- als buitenland. OSL-datering van sedimenten kan ook helpen bij het oplossen van archeologische vraagstukken en er is geen reden om de methode niet in te zetten voor het dateren van verhitte materialen, of voor het bepalen van de authenticiteit ervan. Al het onderzoeksmateriaal kan hierbij eigen methodologische problemen geven. Recente ontwikkelingen in instrumentatie en meet-technologie (zoals single-grain meettoestellen, X-stralen bestralingsbronnen, lineaire modulatie en radioluminescentie) hebben een brede waaier aan onderzoeksperspectieven gecreëerd. Hopelijk levert het werk voorgesteld in deze thesis een basis voor zowel routinematig dateren als fundamenteel en vernieuwend methodologisch onderzoek in het Gentse luminescentiedateringslaboratorium.

– REFERENCES –

Adamiec G. (2000).
Variations in luminescence properties of single quartz grains and their consequences for equivalent dose estimation.
Radiation Measurements **32**, 427-432.

Adamiec G. and Aitken M. (1998).
Dose-rate conversion factors: update.
Ancient TL **16**, 37-50.

Agersnap Larsen N., Bulur E., Bøtter-Jensen L. and McKeever S.W.S. (2000).
Use of the LM-OSL technique for the detection of partial bleaching in quartz.
Radiation Measurements **32**, 419-425.

Aitken M.J. (1976).
Thermoluminescent age evaluation and assessment of error limits: revised system.
Archaeometry **18**, 233-238.

Aitken M.J. (1985).
Thermoluminescence Dating.
Academic Press, London, 359p., ISBN: 0-12-046380-6.

Aitken M.J. (1992).
Optical Dating.
Quaternary Science Reviews **11**, 127-131.

Aitken M.J. (1994).
Optical dating: a non-specialist review.
Quaternary Geochronology (Quaternary Science Reviews) **13**, 503-508.

Aitken M.J. (1998).
An introduction to optical dating .The Dating of Quaternary Sediments by the Use of Photon-Stimulated Luminescence.
Oxford University Press, Oxford, 267p., ISBN: 0-19-854092-2.

Aitken M.J. and Alldred J.C. (1972).
The assessment of error limits in thermoluminescent dating.
Archaeometry **14**, 257-267.

Aitken M.J. and Bowman S.G.E. (1975).
Thermoluminescent dating: assessment of alpha particle contribution.
Archaeometry **17**, 132-138.

Aitken M.J. and Smith B.W. (1988).
Optical dating: recuperation after bleaching.
Quaternary Science Reviews **7**, 387-393.

Aitken M.J. and Xie J. (1990).
Moisture correction for annual gamma dose.
Ancient TL, **8**, 6-9.

Aitken M.J., Tite M.S. and Reid J. (1964).
Thermoluminescent dating of ancient ceramics.
Nature **202**, 1032-1033.

Aitken M.J., Zimmerman D.W. and Fleming S.J. (1968).
Thermoluminescent dating of ancient pottery.
Nature **219**, 442-444.

Aitken M.J., Huxtable J. and Debenham N.C. (1986).
Thermoluminescence dating in the Palaeolithic: burnt flint, stalagmitic calcite and sediment.
Supplément au Bulletin de l'Association Française pour l'étude du Quaternaire **26**, 7-14.

Andersen C.E., Bøtter-Jensen L. and Murray A.S. (2003).
A mini X-ray generator as an alternative to a $^{90}Sr/^{90}Y$ beta source in luminescence dating.
Radiation Measurements **37**, 557-561.

Armitage S.J., Duller G.A.T. and Wintle A.G. (2000).
Quartz from southern Africa: sensitivity changes as a results of thermal pre-treatment.
Radiation Measurements **32**, 571-577.

Auclair M., Lamothe M. and Huot S. (2003).
Measurement of anomalous fading for feldspar IRSL using SAR.
Radiation Measurements **37**, 487-492.

Bailey R.M. (1997).
Optical detrapping of charge from the 110°C quartz TL region.
Ancient TL **15**, 7-10.

Bailey R.M. (1998).
Depletion of the quartz OSL signal using low photon energy stimulation.
Ancient TL **16**, 33-36.

Bailey R.M. (2000).
The interpretation of quartz optically stimulated luminescence equivalent dose versus time plots.
Radiation Measurements **32**, 129-140.

Bailey R.M. (2001).
Towards a general kinetic model for optically and thermally stimulated luminescence of quartz.
Radiation Measurements **33**, 17-45.

Bailey R.M. (2002).
Simulations of variability in the luminescence characteristics of natural quartz and its implications for estimations of the absorbed dose.
Radiation Protection Dosimetry **100**, 33-38.

Bailey R.M. (2003a).
Paper I: The use of measurement-time dependent single-aliquot equivalent-dose estimates from quartz in the identification of incomplete signal resetting.
Radiation Measurements **37**, 673-683.

Bailey R.M. (2003b).
Paper II: The interpretation of measurement-time-dependent single-aliquot equivalent-dose estimates using predictions from a simple empirical model.
Radiation Measurements **37**, 685-691

Bailey R.M., Smith B.W. and Rhodes E.J. (1997).
Partial bleaching and the decay form characteristics of quartz OSL.
Radiation Measurements **27**, 126-126.

Bailey R.M., Adamiec G. and Rhodes E.J. (2000).
OSL properties of NaCl relative to dating and dosimetry.
Radiation Measurements 32, 717-723.

Bailey R.M., Singarayer J.S., Ward S. and Stokes S. (2003).
Identification of partial resetting using D_e as a function of illumination time.
Radiation Measurements **37**, 511-518.

Bailey S.D., Wintle A.G., Duller G.A.T. and Bristow C.S. (2001).
Sand deposition during the last millennium at Aberffraw, Anglesey, North Wales as determined by OSL dating of quartz.
Quaternary Science Reviews **20**, 701-704.

Bailiff I.K., Bowman S.G.E., Mobbs S.F. and Aitken M.J. (1977).
The phototransfer technique and its use in thermoluminescence dating.
Journal of Electrostatics **3**, 269-280.

Ballarini M., Wallinga J., Murray A.S., van Heteren S., Oost A.P., Bos A.J.J. and van Eijk C.W.E. (2003).
Optical dating of young coastal dunes on a decadal time scale.
Quaternary Science Reviews **22**, 1011-1017.

Banerjee D. (2000).
Thermal transfer and recuperation in quartz OSL and their consequences regarding luminescence dating procedures.
In: Luminescence and its applications, eds: Murthy KVR, Sastry MD, Joshi TR, Prasad LHH, Page AG, Patel NG, Luminescence Society of India. 86-93.

Banerjee D., Bøtter-Jensen L. and Murray A.S. (1999).
Retrospective dosimetry: preliminary use of the single aliquot regeneration (SAR) protocol for the measurement of quartz dose in young house bricks.
Radiation Protection Dosimetry **84**, 421-426.

Banerjee D., Bøtter-Jensen L. and Murray A.S. (2000).
Retrospective dosimetry: estimation of the dose to quartz using the single-aliquot regenerative-dose protocol.
Applied Radiation and Isotopes **52**, 831-844.

Banerjee D., Murray A.S., Bøtter-Jensen L. and Lang A. (2001a).
Equivalent dose estimation using a single aliquot of polymineral fine grains.
Radiation Measurements **33**, 73-94.

Banerjee D., Murray A.S. and Foster I.D.L. (2001b).
Scilly Isles, UK: optical dating of a possible tsunami deposit from the 1755 Lisbon earthquake.
Quaternary Science Reviews **20**, 718-718.

Banerjee D., Blair M., Lepper K. and McKeever S.W.S. (2002).
Optically stimulated luminescence signals of polymineral fine grains in the JSC Mars-1 soil simulant sample.
Radiation Protection Dosimetry **101**, 321-326.

Baran J., Murray A.S. and Häggström L.
Estimating the age of stone structures using OSL: the potential of entrapped sediment.
Quaternary Science Reviews **22**, 1265-1271.

Bateman M.D. and Van Huissteden J. (1999).
The timing of last-periglacial and aeolian events, Twente, eastern Netherlands.
Journal of Quaternary Science **14**, 277-283.

Bateman M.D., Frederick C.D., Jaiswal M.K. and Singhvi A.K. (2003).
Investigations into the potential effects of pedoturbation on luminescence dating.
Quaternary Science Reviews **22**, 1169-1176.

Bell W.T. (1979).
Attenuation factors for the absorbed radiation dose in quartz inclusions for thermoluminescence dating.
Ancient TL **8**, 2-13.

Bell W.T. (1980).
Alpha dose attenuation in quartz grains for thermoluminescence dating.
Ancient TL **12**, 4-8.

Bell W.T. and Zimmerman D.W. (1978).
The effect of HF acid etching on the morphology of quartz inclusions for thermoluminescence dating.
Archaeometry **20**, 63-65.

Benkö L. (1983).
TL properties of individual quartz grains.
PACT **9**, 175-181.

Berger G.W. (1990).
Effectiveness of natural zeroing of the thermoluminescence in sediments.
Journal of Geophysical Research **95**, 12375-12397.

Berger G.W. (1995).
Progress in luminescence dating methods for Quaternary sediments.
In: Dating Methods for Quaternary Deposits, Geological Association of Canada, *GEOtext* **2**, Rutter N.W. and Catto N.R. (eds.), 81-104.

Berger G.W. and Huntley D.J. (1994).
Tests for optically stimulated luminescence from tephra glass.
Quaternary Geochronology (Quaternary Science Reviews) **13**, 509-511.

Berger G.W. and Neil P.A. (1999).
Photon-stimulated-luminescence (PSL) dating tests of glass-rich volcanic ash.
Book of Abstract LED99: 138.

Bohncke S., Vandenberghe J. and Huijzer A.S. (1993).
Periglacial environments during the Weichselian Late Glacial in the Maas valley, the Netherlands.
Geologie en Mijnbouw **72**, 193-210.

Bortolot V.J. (1997).
Improved OSL excitation with fiberoptics and focused lamps.
Radiation Measurements **27**, 101-106.

Bortolot V.J. (2000).
A new modular high capacity OSL reader system.
Radiation Measurements **32**, 751-757.

Bowall L., Frean R., McKeogh K.J., Rendell H.M. and Townsend P.D. (1987).
Sensitivity changes in the TL of quartz and feldspar after bleaching.
Crystal Lattice Defects and Amorphous Materials **16**, 37-43.

Bøtter-Jensen L. (1988).
The automated Risø TL dating reader system.
Nuclear Tracks and Radiation Measurements **14**, 177-180.

Bøtter-Jensen L. (1997).
Luminescence techniques: instrumentation and methods.
Radiation Measurements **27**, 749-768.

Bøtter-Jensen L. and Duller G.A.T. (1992).
A new system for measuring optically stimulated luminescence from quartz samples.
Nuclear Tracks and Radiation Measurements **20**, 549-553.

Bøtter-Jensen L. and Murray A.S. (1999).
Developments in optically stimulated luminescence techniques for dating and retrospective dosimetry.
Radiation Protection Dosimetry **84**, 307-315.

Bøtter-Jensen L., Duller G.A.T. and Poolton N.R.J. (1994).
Excitation and emission spectrometry of stimulated luminescence from quartz and feldspars.
Radiation Measurements **23**, 613-616.

Bøtter-Jensen L., Mejdahl V. and Murray A.S. (1999a).
New light on OSL.
Quaternary Geochronology **18**, 303-309.

Bøtter-Jensen L., Duller G.A.T., Murray A.S. and Banerjee D. (1999b).
Blue light emitting diodes for optical stimulation of quartz in retrospective dosimetry and dating.
Radiation Protection Dosimetry **84**, 335-340.

Bøtter-Jensen L., McKeever S.W.S. and Wintle A.G. (2003a).
Optically Stimulated Luminescence Dosimetry.
Elsevier Science, The Netherlands, 355p., ISBN: 0-444-50684-5.

Bøtter-Jensen L., Andersen C.E., Duller G.A.T. and Murray A.S. (2003b).
Developments in radiation, stimulation and observation facilities in luminescence measurements.
Radiation Measurements **37**, 535-541.

Brennan B.J. and Lyons R.G. (1989).
Ranges of alpha particles in various media.
Ancient TL **7**, 32-37.

Bronk Ramsey C. (1995).
Radiocarbon calibration and analysis of stratigraphy: the OxCal program.
Radiocarbon **37**, 425-430.

Bronk Ramsey C. (1998).
Probability and dating.
Radiocarbon **40**, 461-474.

Bulur E. (1996).
An alternative technique for optically stimulated luminescence (OSL) experiment.
Radiation Measurements **26**, 701-709.

Bulur E. (2000).
A simple transformation for converting CW-OSL curves to LM-OSL curves.
Radiation Measurements **32**, 141-145.

Bulur E., Bøtter-Jensen L. and Murray A.S. (2000).
Optically stimulated luminescence from quartz measured using the linear modulation technique.
Radiation Measurements **32**, 407-411.

Bulur E., Bøtter-Jensen L. and Murray A.S. (2001).
LM-OSL signals from some insulators: an analysis of the dependency of the detrapping probability on stimulation light intensity.
Radiation Measurements **33**, 715-719.

Bulur E., Duller G.A.T., Solongo S., Bøtter-Jensen L. and Murray A.S. (2002).
LM-OSL from single grains of quartz: a preliminary study.
Radiation Measurements **35**, 79-85.

Buylaert J.-P., Vandenberghe D., De Corte F. and Van den haute P. (2003).
Testing the MAAD-IRSL and double SAR procedures for D_e determination on the (Upper Pleniglacial) Brabant loess: first results.
Book of Abstracts of the UL Luminescence and ESR Meeting, 8-10th September 2003, University of Wales, Aberystwyth, United Kingdom, p. 20.

Chen G. and Li S.-H. (2000).
Studies of quartz 110°C thermoluminescence peak sensitivity change and its relevance to optically stimulated luminescence dating.
Journal of Physics D: Applied Physics **33**, 437-443.

Chen R. (1976).
Methods for kinetic analysis of thermally stimulated processes.
Journal of Materials Science **11**, 1521-1541.

Chen R. and McKeever S.W.S. (1997).
Theory of thermoluminescence and related phenomena.
World Scientific Publishing, Singapore, 559p., ISBN: 9810222955.

Choi J.H., Murray A.S., Cheong C.S., Hong D.H. and Chang H.W. (2003a).
The resolution of stratigraphic inconsistency in the luminescence ages of marine terrace sediments from Korea.
Quaternary Science Reviews **22**, 1201-1206.

Choi J.H., Murray A.S., Jain M., Cheong S.H. and Chang H.W. (2003b).
Luminescence dating of well-sorted marine terrace sediments on the southeastern coast of Korea.
Quaternary Science Reviews **22**, 407-421.

Chu S.Y., Nordberg H., Firestone R.B. and Ekström L.P. (1999).
Isotope Explorer, Version 2.23.

Clark P.A. and Templer R.H. (1988).
Thermoluminescence dating of materials which exhibit anomalous fading.
Archaeometry **30**, 19-36.

Clarke M.L. (1996).
IRSL dating of sands: bleaching characteristics at deposition inferred from the use of single aliquots.
Radiation Measurements **26**, 611-620.

Clarke M.L., Rendell H.M. and Wintle A.G. (1999).
Quality assurance in luminescence dating.
Geomorphology **29**, 173-185.

Colls A.E.L. (1999).
Optical dating of fluvial sediments from the Loire Valley, France.
Unpublished Master of Science thesis, University of Oxford, Oxford.

De Corte F. (1987).
The traceability of the neutron activation analysis (NAA) k_0-standardization method.
Journal of Trace and Microprobe Techniques **5**, 115-134.

De Corte F. (2001a).
The standardization of standardless NAA.
Journal of Radioanalytical and Nuclear Chemistry **248**, 13-20.

De Corte F. (2001b).
Methods for quality control/quality assurance of k0-assisted neutron activation analysis.
In: Applications of Accelerators in Research and Industry – Sixteenth International Conference, 1-5 November 2000, Denton, Texas, USA. Duggan J.L., Morgan I.L. (eds.). CP**576**, 495-498.

De Corte F., Simonits A., De Wispelaere A. and Hoste J. (1987).
Accuracy and applicability of the k_0-standardization method.
Journal of Radioanalytical and Nuclear Chemistry **113**, 145-161.

De Corte F., Hossain S.M., Jovanovič S., Dlabač A., De Wispelaere A., vandenberghe D. and Van den haute P. (2003).
Introduction of Marinelli effective solid angles for correcting the calibration of NaI(Tl) field gamma-ray spectrometry in TL/OSL dating.
Journal of Radioanalytical and Nuclear Chemistry **257**, 551-555.

De Corte F., Vandenberghe D., Hossain S.M., De Wispelaere A. and Van den haute P. (2004).
The effect of different sample-calibrant composition in gamma-ray spectrometry for the assessment of the radiation dose rate in the luminescence dating of sediments.
Journal of Radioanalytical and Nuclear Chemistry, submitted.

Dijkmans J.W.A. and Wintle A.G. (1991).
Methodological problems in thermoluminescence dating of Weichselian coversand and late Holocene drift sand from the Lutterzand area, E. Netherlands.
Geologie en Mijnbouw **70**, 21-33.

Dijkmans J.W.A., Wintle A.G. and Mejdahl V. (1988).
Some thermoluminescence properties and dating of eolian sands from the Netherlands.
Quaternary Science Reviews **7**, 349-355.

Dijkmans J.W.A., van Mourik J.M. and Wintle A.G. (1992).
Thermoluminescence dating of Aeolian sands from polycyclic soil profiles in the southern Netherlands.
Quaternary Science Reviews **11**, 85-92.

Ditlefsen C. and Huntley D.J. (1994).
Optical excitation of trapped charges in quartz, potassium feldspars and mixed silicates: the dependence on photon energy.
Radiation Measurements **23**, 675-682.

Dricot E.M. (1961).
Microstratigraphie des Argiles de Campine.
Bulletin de la Société belge de géologie, paléontologie et d'hydrologie **70**, 113-141.

Duller G.A.T. (1991).
Equivalent dose determination using single aliquots.
Nuclear Tracks and Radiation Measurements **18**, 371-378.

Duller G.A.T. (1994a).
Luminescence dating of sediments using single aliquots: new procedures.
Quaternary Geochronology (Quaternary Science Reviews) **13**, 149-156.

Duller G.A.T. (1994b).
Luminescence dating of poorly bleached sediments from Scotland.
Quaternary Geochronology (Quaternary Science Reviews) **13**, 521-524.

Duller G.A.T. (1995).
Luminescence dating using single aliquots: methods and applications.
Radiation Measurements **24**, 217-226.

Duller G.A.T. (1996).
Recent developments in luminescence dating of Quaternary sediments.
Progress in Physical Geography **20**, 127-145.

Duller G.A.T., Wintle A.G. and Hall A.M. (1995).
Luminescence dating and its application to key Pre-Late Devensian sites in Scotland.
Quaternary Science Reviews **14**, 495-519.

Duller G.A.T., Bøtter-Jensen L., Murray A.S. and Truscott A.J. (1999a).
Single gain laser luminescence (SGLL) measurements using a novel automated reader.
Nuclear Instruments and Methods in Physics Research B **155**, 506-514.

Duller G.A.T., Bøtter-Jensen L., Kohsiek P. and Murray A.S. (1999b).
A high sensitivity optically stimulated luminescence scanning system for measurement of single sand-sized grains.
Radiation Protection Dosimetry **84**, 325-330.

Duller G.A.T., Bøtter-Jensen L. and Mejdahl V. (1999c).
An automated iterative procedure for determining palaeodoses using the SARA method.
Quaternary Geochronology **18**, 293-301.

Duller G.A.T., Bøtter-Jensen L. and Murray A.S. (2000).
Optical dating of single sand-sized grains of quartz: sources of variability.
Radiation Measurements **32**, 453-457.

Duller G.A.T., Bøtter-Jensen L. and Murray A.S. (2003).
Combining infrared- and green-laser stimulation sources in single-grain luminescence measurements of feldspar and quartz.
Radiation Measurements **37**, 543-550.

Ehlers J. (1996).
Quaternary and glacial geology.
John Wiley & Sons Ltd., Chichester, England. 578p. ISBN 0-471-95576-0.

Erfurt G. (2003).
Radiolumineszenzspektroskopie und –dosimetrie an Feldspäten und synthetischen Luminophoren für die geochronometrische Anwendung.
Ph.D. thesis, Technischen Univeristät Bergakademie Freiberg.

Fazekas B., Molnàr G., Belgya T., Dabolczi L. and Simonits A. (1997).
Introducing HYPERMET-PC for automatic analysis of complex gamma-ray spectra.
Journal of Radioanalytical and Nuclear Chemistry **215**, 271-277.

Feathers J.K. (2003).
Single-grain OSL dating of sediments from the Southern High Plains, USA.
Quaternary Science Reviews **22**, 1035-1042.

Feathers J. K. and Migliorini E. (2001).
Luminescence dating at Katanda – a reassessment.
Quaternary Science Reviews **20**, 961-966.

Felix C. and Singhvi A.K. (1997).
Study of non-linear luminescence-dose growth curves for the estimation of the paleodose in luminescence dating: results of Monte Carlo simulations.
Radiation Measurements 27, 599-609.

Fink T. (2000).
Lumineszenzdatierung eines spätglazialen und holozänen Dünenprofils bei Ossendrecht (Niederlande). Methodische Untersuchungen des Multiple und Single Aliquot-Regerierungsprotokolls für Quartze.
Diplomarbeit, Universität zu Köln.

Fleming S.J. (1966).
Study of thermoluminescence of crystalline extracts from pottery.
Archaeometry **9**, 170-173.

Fleming S.J. (1970).
Thermoluminescence dating: refinement of the quartz inclusion method.
Archaeometry **12**, 133-145.

Fragoulis D. and Stoebe T.G. (1990).
Relationship of anomalous fading to feldspar inclusions in quartz.
Radiation Protection Dosimetry **34**, 65-68.

Fragoulis D.V. and Readhead M.L. (1991).
Feldspar inclusions and the anomalous fading and enhancement of thermoluminescence in quartz grains.
Nuclear Tracks and Radiation Measurements **18**, 291-296.

Franklin A.D. and Hornyak W.F. (1990).
Isolation of the rapidly bleaching peak in quartz TL glow curves.
Ancient TL **8**, 29-31.

Franklin A.D., Prescott J.R. and Scholefield R.B. (1995).
The mechanism of thermoluminescence in an Australian quartz.
Journal of Luminescence **63**, 317-326.

Fuchs M. (2001).
Die OSL-Datierung von Archäeosedimenten zur Rekonstruktion anthropogen bedingter Sedimentumlagerung. Geoarchäeologische Untersuchungen im Becken von Phlious, NE-Peloponnes, Griechenland.
Ibidem-Verlag, Stuttgart.

Fuchs M. and Lang A. (2001).
OSL dating of coarse-grain fluvial quartz using single-aliquot protocols on sediments from NE Peloponnese, Greece.
Quaternary Science Reviews **20**, 783-787.

Galbraith R.F. (1988).
Graphical display of estimates having different standard errors.
Technometrics **30**, 271-281.

Galbraith R.F. (1990).
The radial plot: graphical assessment of spread in ages.
Nuclear Tracks and Radiation Measurements **17**, 207-214.

Galbraith R.F. (1994).
Some applications of radial plots.
Journal of the American Statistical Association **89**, 1232-1242.

Galbraith R.F., Roberts R.G., Laslett G.M., Yoshida H. and Olley J.M. (1999).
Optical dating of single and multiple grains of quartz from Jinmium rock shelter, northern Australia: Part I, experimental design and statistical models.
Archaeometry **41**, 339-364.

Galloway R.B. (1993).
Stimulation of luminescence using green light emitting diodes.
Radiation Protection Dosimetry **47**, 679-682.

Galloway R.B. (1994).
On the stimulation of luminescence with green light emitting diodes.
Radiation Measurements **23**, 547-540.

Galloway R.B. (1996).
Equivalent dose determination using only one sample: alternative analysis of data obtained from infrared stimulation of feldspars.
Radiation Measurements **26**, 103-106.

Galloway R.B., Hong D.G. and Napier H.J. (1997).
A substantially improved green-light-emitting diode system for luminescence stimulation.
Measurement Science and Technology **8**, 267-271.

Godfrey-Smith D.I. and Cada M. (1996).
IR stimulation spectroscopy of plagioclase and potassium feldspar, and quartz.
Radiation Protection Dosimetry **66**, 379-385.

Godfrey-Smith D.I., Huntley D.J. and Chen W.-H. (1988).
Optical dating studies of quartz and feldspar sediment extracts.
Quaternary Science Reviews **7**, 373-380.

Goethals F. (2003)
Geochronologisch onderzoek met de OSL-methode van de Boven-Pleniglaciale dekzanden te Grubbenvorst (Nederland).
Licentiate Thesis, Ghent University.

Hashimoto T., Nakagawa T., Hong D.-G. and Takano M. (2002).
An automated system for both red/blue thermoluminescence and optically stimulated luminescent measurement.
Journal of Nuclear Science and Technology **39**, 108-109.

Hilgers A. (2004)
The chronology and reconstruction of the Late Glacial and Holocene dune development in the European sand belt, based on luminescence dating results from the Netherlands, Germany and Poland.
PhD Thesis, University of Cologne.

Hoek W.Z. (1997).
Palaeogeography of Lateglacial vegetations. Aspects of Lateglacial and Early Holocene vegetation, abiotic landscape, and climate in the Netherlands.
Thesis, Vrije Universiteit Amsterdam. Drukkerij Elinkwijk: Utrecht.

Hong D.-G. and Galloway R.B. (2000).
Comparison of equivalent dose values determined by luminescence stimulation using blue and green light.
Nuclear Instruments and Methods in Physics Research B **160**, 59-64.

Hong D.-G., Galloway R. and Hashimoto T. (2000).
Additive Dose Single and Multiple Aliquot Methods of Equivalent Dose Determination Compared for Quartz Luminescence Stimulated by Green Light.
Japanese Journal of Applied Physics **39**, 4209-4216.

Hossain S.M. (2003)
A critical comparison and evaluation of methods for the annual radiation dose determination in the luminescence dating of sediments.
Ph. D. thesis, Ghent University.

Hossain S.M. and De Corte F. (1999).
Determination of K, Th and U via k_0-NAA in samples (Flossi A and Flossi B) from the Flossenbürger granite block placed at the MPI, Heidelberg for the calibration of γ-spectrometers.
Analysis Report, Laboratory for Analytical Chemistry, Institute for Nuclear Sciences, Ghent University. 2p.

Huntley D.J. and Hancock R.G.V. (2001).
The Rb contents of the K-feldspar grains being measured in optical dating.
Ancient TL **19**, 43-46.

Huntley D.J. and Prescott J.R. (2001).
Improved methodology and new thermoluminescence ages for the dune sequence in south-east South Australia.
Quaternary Science Reviews **20**, 687-699.

Huntley D.J., Godfrey-Smith D.I. and Thewalt M.L.W. (1985).
Optical dating of sediments.
Nature, **313**, 105-107.

Huntley D.J., Berger G.W. and Bowman S.G.E. (1988).
Thermoluminescence responses to alpha and beta irradiation, and age determination when the high dose response is non-linear.
Radiation Effects **105**, 279-284.

Huntley D.J., Godfrey-Smith D.I. and Haskell E.H. (1991).
Light-induced emission spectra from some quartz and feldspars.
Nuclear Tracks and Radiation Measurements **18**, 127-131.

Huntley D.J., Hutton J.T. and Prescott J.R. (1993).
The stranded beach-dune sequence of south-east South Australia: A test of thermoluminescence dating, 0-800 ka.
Quaternary Science Reviews **12**, 1-20.

Huntley D.J., Hutton J.T. and Prescott J.R. (1994).
Further thermoluminescence dates from the dune sequence in the southeast of South Australia.
Quaternary Science Reviews **13**, 201-207.

Huntley D.J., Short M.A. and Dunphy K. (1996).
Deep traps in quartz and their use for optical dating.
Canadian Journal of Physics **74**, 81-91.

Huntley D.J., McMullan W.G., Godfrey-Smith D.I. and Thewalt M.L.W. (1989).
Time-dependent recombination spectra arising from optical ejection of trapped charges in feldspars.
Journal of Luminescence **44**, 41-46.

Hütt G., Jaek I. And Tchonka J. (1988).
Optical dating: K-feldspars optical response stimulation spectra.
Quaternary Science Reviews **7**, 381-385.

Ingelbrecht C., Peetermans F., de Corte F., De Wispelaere A., Vandecasteele C., Courtijn E. and D'Hondt P. (1991).
Aluminium-gold reference material for the k_0-standardisation of neutron activation analysis.
Nuclear Instruments and Methods in Physics Research A **303**, 119-122

Isarin R.F.B., Renssen H. and Koster E.A. (1997).
Surface wind climate during the Younger Dryas in Europe as inferred from aeolian records and model simulations.
Palaeogeography, Palaeoclimatology, Palaeoecology **134**, 127-148.

Jacobs Z., Duller G.A.T. and Wintle A.G. (2003a).
Optical dating of dune sand from Blombos Cave, South Africa: II – single grain data.
Journal of Human Evolution **44**, 613-625.

Jacobs Z., Wintle A.G. and Duller G.A.T. (2003b).
Optical dating of dune sand from Blombos Cave, South Africa: I – multiple grain data.
Journal of Human Evolution **44**, 599-612.

Jain M., Murray A.S. and Bøtter-Jensen L. (2003).
Characterisation of blue-light stimulated luminescence components in different quartz samples: implications for dose measurements.
Radiation Measurements **37**, 441-449.

Jovanović S, Mihaljević N., De Corte F., Vancraeynest L., Faltejsek J., Vukotić P., Dapčević S., Kučera J., De Wispelaere A., Carrot F., Dardenne-Deschamps C. and Deschamps N. (1992).
Experimental test of "MARSANGLE", a computer code to calculate detection efficiencies of Ge-detectors for Marinelli sources.
In: *Proceedings of the International k_0 Users Workshop Gent* (De Corte F., ed.), 30 September – 2 October 1992, Deinze, Belgium. 59-62.

Jungner H. and Bøtter-Jensen L. (1994).
Study of sensitivity change of OSL signals from quartz and feldspars as a function of preheat temperature.
Radiation Measurements **23**, 621-624.

Kalchgruber R., Fuchs M., Murray A.S. and Wagner G.A. (2003).
Evaluating dose-rate distributions in natural sediments using α-Al_2O_3:C grains.
Radiation Measurements **37**, 293-297.

Kasse C. (1988).
Early-Pleistocene tidal and fluviatile environments in the southern Netherlands and northern Belgium.
Proefschrift Vrije Universiteit Amsterdam.

Kasse C. (1990).
Lithostratigraphy and provenance of the Early-Pleistocene deposits in the southern Netherlands and northern Belgium.
Geologie en Mijnbouw **69**, 327-340.

Kasse C. (1997).
Cold-climate sand-sheet formation in North-Western Europe (c. 14-12.4 ka); a response to permafrost degradation and increased aridity.
Permafrost and Periglacial Processes **8**, 295-311.

Kasse C. (1999).
Late Pleniglacial and Late Glacial aeolian phases in The Netherlands.
In: *Dunes and Fossil Soils*, Schirmer W. (ed.). *GeoArchaeoRhein* **3**, 61-82.

Kasse C., Vandenberghe J. and Bohncke S. (1995).
Climatic change and fluvial dynamics of the Maas during the late Weichselian and early Holocene.
In: "European river activity and climatic change during the Lateglacial and early Holocene", Frenzel B. (ed.), ESF Project European Palaeoclimate and Man, Special Issue 9. *Paläoklimaforschung/Palaeoclimate Research* **14**, 123-150.

Kaylor R.M., Feathers J., Hornyak W.F. and Franklin A.D. (1995).
Optically stimulated luminescence in Kalahari quartz: Bleaching of the 325°C peak as the source of the luminescence.
Journal of Luminescence **65**, 1-6.

KAYZERO/SOLCOI software for using the k0-standardization method, V. 5A.
Ghent University and DSM Research, 2003.

Kitagawa H. and van der Plicht J. (1998).
Atmospheric radiocarbon calibration to 45000 yr B.P.: Late Glacial fluctuations and cosmogenic isotope production.
Science **279**, 1187-1190.

Kolstrup E. (1980).
Climate and Stratigraphy in Northwestern Europe between 30,000 B.P. and 13,000 B.P., with special reference to The Netherlands.
Mededelingen Rijks Geologische Dienst, **32-15**, 181-253.

Koster E.A. (1988).
Ancient and modern cold-climate aeolian sand deposition: a review.
Journal of Quaternary Science **3**, 69-83.

Krbetschek M.R., Rieser U., Zöller L. and Heinicke J. (1994).
Radioactive disequilibria in palaeodosimetric dating of sediments.
Radiation Measurements **23**, 485-489, 1994.

Krbetschek M.R., Götze J., Dietrich A. and Trautman T. (1997).
Spectral information from minerals relevant for luminescence dating.
Radiation Measurements **27**, 695-748.

Kuhn R., Trautmann T., Singhvi A.K., Krbetschek M.R., Wagner G.A. and Stolz W. (2000).
A study of thermoluminescence emission spectra and optical stimulation spectra of quartz from different provenances.
Radiation Measurements **32**, 653-657.

Kuhns C.K., Agersnap Larsen N. and McKeever S.W.S. (2000).
Characteristics of LM-OSL from several different types of quartz.
Radiation Measurements **32**, 413-418.

Lamothe M., Auclair M., Hamzaoui C. and Huot S. (2003).
Towards a prediction of long-term anomalous fading of feldspar IRSL.
Radiation Measurements **37**, 493-498.

Lang A., Lindauer S., Kuhn R. and Wagner G.A. (1996).
Procedures used for Optically and Infrared Stimulated Luminescence Dating of Sediments in Heidelberg.
Ancient TL **14**, 7-11.

Lepper K. (2001).
Development of an objective dose distribution analysis method for OSL dating and pilot studies for planetary application.
Ph.D. thesis, Oklahoma State University, Stillwater, OK.

Lepper K., Agersnap Larsen N. and McKeever S.W.S. (2000).
Equivalent dose distribution analysis of Holocene Aeolian and fluvial quartz sands from Central Oklahoma.
Radiation Measurements **32**, 603-608.

Li S.-H. (1994).
Optical dating: insufficiently bleached sediments.
Radiation Measurements **23**, 563-567.

Li S.-H. and Wintle A.G. (1991).
Sensitivity changes of luminescence signals from colluvial sediments after different bleaching procedures.
Ancient TL **9**, 50-53.

Li S.-H. and Wintle A.G. (1992).
Luminescence sensitivity change due to bleaching of sediments.
Nuclear Tracks and Radiation Measurements **20**, 567-573.

Li S.-H., Tso M.-Y., Westaway K.E. and Chen G. (1999).
Choice of the most appropriate thermal treatment in optical dating of quartz.
Radiation Protection Dosimetry **84**, 495-498.

Lian O.B. and Huntley D.J. (2001).
Luminescence dating.
In: Tracking Environmental Change Using Lake Sediments. Volume 1: Basin Analysis, Coring and Chronological Techniques. Last W.M. and Smol J.P. (eds.). Kluwer Academic Publishers, Dordrecht, 261-282.

Liritzis I., Galloway R.B. and Hong D.G. (1997).
Single aliquot dating of ceramics by green light stimulation of luminescence from quartz.
Nuclear Instruments and methods in Physics Research B **132**, 457-467.

Lowe J.J. and Walker M.J.C. (1997).
Reconstructing Quaternary Environments.
Addison Wesley Longman Limited, England. 446 p. ISBN 0-582-10166-2.

Markey B.G., Bøtter-Jensen L. and Duller G.A.T. (1997).
A new flexible system for measuring thermally and optically stimulated luminescence.
Radiation Measurements **27**, 83-89.

Mauz B., Bode T., Mainz E., Blanchard H., Hilger W., Dikau R. and Zöller L. (2002).
The luminescence dating laboratory at the University of Bonn: equipment and procedures.
Ancient TL **20**, 53-61.

McCoy D.G., Prescott J.R. and Nation R.J. (2000).
Some aspects of single-grain luminescence dating.
Radiation Measurements **32**, 859-864.

McFee C.J. and Tite M.S. (1994).
Investigations into the thermoluminescence properties of single quartz grains using an imagining photon detector.
Radiation Measurements **23**, 355-360.

McFee C.J. and Tite M.S. (1998).
Luminescence dating of sediments – the detection of high equivalent dose grains using an imaging photon detector.
Archaeometry **40**, 153-168.

McKeever S.W.S. (1985).
Thermoluminescence of solids.
Cambridge University Press, London, 376p. ISBN: 0-521-36811-1.

McKeever S.W.S. (1991).
Mechanisms of tehrmoluminescence production: some problems and a few answers?
Nuclear Tracks and Radiation Measurements **18**, 5-12.

McKeever S.W.S. (1994).
Models for optical bleaching of thermoluminescence in sediments.
Radiation Measurements **23**, 267-275.

McKeever S.W.S. and Morris M.F. (1994).
Computer simulations of optical bleaching of TL and OSL signals.
Radiation Measurements **23**, 301-306.

McKeever S.W., Agersnap Larsen N., Bøtter-Jensen L. and Mejdahl V. (1997).
OSL sensitivity changes during single aliquot procedures: computer simulations.
Radiation Measurements **27**, 75-82.

Mejdahl V. (1969).
Thermoluminescence dating of ancient Danish ceramics.
Archaeometry **11**, 99-104.

Mejdahl V. (1979).
Thermoluminescence dating: beta-dose attenuation in quartz grains.
Archaeometry **21**, 61-72.

Mejdahl V. (1985).
Thermoluminescence dating based on feldspars.
Nuclear Tracks and Radiation Measurements **10**, 133-136.

Mejdahl V. (1987)
Internal radioactivity in quartz and feldspar grains.
Ancient TL 5, 10-17.

Mejdahl V. and Winther-Nielsen M. (1982).
TL dating based on feldpsar inclusions.
PACT **6**, 426-437.

Mejdahl V. and Bøtter-Jensen L. (1994).
Luminescence dating of archaeological materials using a new technique based on single aliquot measurements.
Quaternary Geochronology (Quaternary science Reviews) **13**, 551-554.

Mejdahl V. and Christiansen H.H. (1994).
Procedures used for luminescence dating of sediments.
Quaternary Geochronology (Quaternary Science Reviews) **13**, 403-406.

Mejdahl V. and Bøtter-Jensen L. (1997).
Experience with the SARA OSL method.
Radiation Measurements **27**, 291-294.

Miallier D., Sanzelle S. and Faïn J. (1983).
The use of flotation techniques to separate quartz from feldspar.
Ancient TL **1**, 5-6.

Mol. J., Vandenberghe J., Kasse K. and Stel H. (1993).
Periglacial microjointing and faulting in Weichselian fluvio-aeolian deposits.
Journal of Quaternary Science **8**, 15-30.

Munyikwa K. (2000).
Cosmic ray contribution to environmental dose rates with varying overburden thickness.
Ancient TL **18**, 27-34.

Munyikwa K., Van den haute P., Vandenberghe D. and De Corte F. (2000).
The age and palaeoenvironmental significance of the Kalahari Sands in western Zimbabwe from a thermoluminescence reconnaissance study.
Journal of African Earth Sciences **30**, 941-956.

Murray A.S. (1996a).
Developments in optically stimulated luminescence and photo-transferred thermoluminescence dating of young sediments: Application to a 2000-year sequence of flood deposits.
Geochimica et Cosmochimica Acta **60**, 565-576.

Murray A.S. (1996b).
Incomplete stimulation of luminescence in young quartz sediments and its effect on the regenerated signal.
Radiation Measurements **26**, 221-231.

Murray A.S. (2000).
Single Aliquot Protocols in Luminescence Dating.
In: Luminescence and its applications, eds: Murthy KVR, Sastry MD, Joshi TR, Prasad LHH, Page AG, Patel NG, Luminescence Society of India. 103-117

Murray A.S. and Roberts R.G. (1997).
Determining the burial time of single grains of quartz using optically stimulated luminescence.
Earth and Planetary Science Letters **152**, 163-180.

Murray A.S. and Roberts R.G. (1998).
Measurement of the equivalent dose in quartz using a regenerative-dose single-aliquot protocol.
Radiation Measurements **29**, 503-515.

Murray A.S. and Wintle A.G. (1998).
Factors controlling the shape of the OSL decay curve in quartz.
Radiation Measurements **29**, 65-79.

Murray A.S. and Mejdahl V. (1999).
Comparison of regenerative-dose single-aliquot and multiple-aliquot (SARA) protocols using heated quartz from archaeological sites.
Quaternary Geochronology **18**, 223-229.

Murray A.S. and Olley J.M. (1999).
Determining sedimentation rates using luminescence.
GeoResearch Forum **5**, 121-144.

Murray A.S. and Wintle A.G. (1999a).
Isothermal decay of optically stimulated luminescence in quartz.
Radiation Measurements **30**, 119-125.

Murray A.S. and Wintle A.G. (1999b).
Sensitisation and stability of quartz OSL: implications for interpretation of dose-response curves.
Radiation Protection Dosimetry **84**, 427-432.

Murray A.S. and Wintle A.G. (2000a).
Luminescence dating using an improved single-aliquot regenerative-dose protocol.
Radiation Measurements **32**, 57-73.

Murray A.S. and Wintle A.G. (2000b).
Application of the single-aliquot regenerative-dose protocol to the 375°C quartz TL signal.
Radiation Measurements **32**, 579-583.

Murray A.S. and Clemmensen L.B. (2001).
Luminescence dating of Holocene Aeolian sand movement, Thy, Denmark.
Quaternary Science Reviews **20**, 751-754.

Murray A.S. and Olley J.M. (2002).
Precision and accuracy in the optically stimulated luminescence dating of sedimentary quartz: a status review.
Geochronometria **21**, 1-16.

Murray A.S. and Funder S. (2003).
Optically stimulated luminescence dating of a Danish Eemian coastal marine deposit: a test of accuracy.
Quaternary Science Reviews **22**, 1177-1183.

Murray A.S. and Wintle A.G. (2003).
The single aliquot regenerative dose protocol: potential for improvements in reliability.
Radiation Measurements **37**, 377-381.

Murray A.S., Olley J.M. and Caithcheon G.G. (1995).
Measurement of equivalent doses in quartz from contemporary water-lain sediments using optically stimulated luminescence.
Quaternary Science Reviews (Quaternary Geochronology) **14**, 365-371.

Murray A.S., Roberts R.G. and Wintle A.G. (1997).
Equivalent dose measurement using a single aliquot of quartz.
Radiation Measurements **27**, 171-184.

Murray A.S., Wintle A.G. and Wallinga J. (2002).
Dose estimation using quartz OSL in the non-linear region of the growth curve.
Radiation Protection Dosimetry **101**, 371-374.

Nathan R.P., Thomas P.J., Jain M., Murray A.S. and Rhodes E.J. (2003).
Environmental dose rate heterogeneity of beta radiation and its implications for luminescence dating: Monte Carlo modelling and experimental validation.
Radiation Measurements **37**, 305-313.

Olley J.M., Murray A.S. and Roberts R.G. (1996).
The effects of disequilibria in the uranium and thorium decay chains on burial dose rates in fluvial sediments.
Quaternary Science Reviews (Quaternary Geochronology) **15**, 751-760.

Olley J.M., Caitcheon G. and Murray A. (1998).
The distribution of apparent dose as determined by optically stimulated luminescence in small aliquots of fluvial quartz: implications for dating young sediments.
Quaternary Geochronology **17**, 1033-1040.

Olley J.M., Caitcheon G.G. and Roberts R.G. (1999).
The origin of dose distributions in fluvial sediments, and the prospect of dating single grains from fluvial deposits using optically stimulated luminescence.
Radiation Measurements **30**, 207-217.

Perkins N.K. and Rhodes E.J. (1994).
Optical dating of fluvial sediments from Tattershall, U.K.
Quaternary Geochronology (Quaternary Science Reviews) **13**, 517-520.

Poolton N.R.J., Smith G.M., Riedi P.C., Bulur E., Bøtter-Jensen L., Murray A.S. and Adrian M. (2000).
Luminescence sensitivity changes in natural quartz induced by high temperature annealing: a high frequency EPR and OSL study.
Journal of Physics D: Applied Physics **33**, 1007-1017.

Poolton N.R.J., Bulur E., Wallinga J., Bøtter-Jensen L., Murray A.S. and Willumsen F. (2001).
An automated system for the analysis of variable temperature radioluminescence.
Nuclear Instruments and Methods in Physics Research B **179**, 575-584.

Prescott J.R. and Stephan L.G. (1982).
The contribution of cosmic radiation to the environmental dose for thermoluminescent dating. Latitude, altitude and depth dependences.
PACT **6**, 17-25.

Prescott J.R. and Hutton J.T. (1988).
Cosmic ray and gamma ray dosimetry for TL and ESR.
Nuclear Tracks and Radiation Measurements **14**, 223-227.

Prescott J.R. and Hutton J.T. (1994).
Cosmic ray contributions to dose rates for luminescence and ESR dating: large depths and long-term time variations.
Radiation Measurements **23**, 497-500.

Prescott J.R. and Hutton J.T. (1995).
Environmental dose rates and radioactive disequilibrium from some Australian luminescence dating sites.
Quaternary Science Reviews (Quaternary Geochronology) **14**, 439-448.

Prescott J.R. and Robertson G.B. (1997).
Sediment dating by luminescence: a review.
Radiation Measurements **27**, 893-922.

Prescott J.R., Huntley D.J. and Hutton J.T. (1993).
Estimation of equivalent dose in thermoluminescence dating – the *Australian slide* method.
Ancient TL **11**, 1-5.

Prescott J.R., Scholefield R.B. and Franklin A.D. (1995).
Three-dimensional thermoluminescence spectra and their application in the study of some sedimentary quartz.
Scanning Microscopy Supplement **9**, 245-254.

Quickert N.A., Godfrey-Smith D.I. and Casey J.L. (2003).
Optical and thermoluminescence dating of Middle Stone Age and Kintampo bearing sediments at Birimi, a multi-component archaeological site in Ghana.
Quaternary Science Reviews **22**, 1291-1297.

Readhead M.L. (1988).
Thermoluminescence dating study of quartz in aeolian sediments from southeastern Australia.
Quaternary Science Reviews **7**, 257-264.

Readhead M.L. (2002a).
Addendum to "Absorbed dose fraction for ^{87}Rb β particles".
Ancient TL **20**, 47.

Readhead M.L. (2002b).
Absorbed dose fraction for ^{87}Rb β particles.
Ancient TL **20**, 25-28.

Rees-Jones J. and Tite M.S. (1997).
Optical dating results for British archaeological sediments.
Archaeometry **39**, 177-187.

Rendell H.M. and Townsend P.D. (1988).
Thermoluminescence dating of a 10 m loess profile in Pakistan.
Quaternary Science Reviews **7**, 251-255.

Rhodes E.J. (1988).
Methodological considerations in the optical dating of quartz.
Quaternary Science Reviews **7**, 395-400.

Rich J. and Stokes J. (2001).
Optical dating of geoarchaeologically significant sites from the Southern High Plains and South Texas, USA.
Quaternary Science Reviews **20**, 949-959.

Rich J., Stokes S. and Wood W.W. (1999).
Holocene chronology for lunette dune deposition on the Southern High Plains, USA.
Zeitschrift für Geomorphologie Neue Folge, Supplement-Band **116**, 165-180.

Richardson C.A. (1994).
Effects of bleaching on the sensitivity to dose of the infrared-stimulated luminescence of potassium-rich feldspars from Ynyslas, Wales.
Radiation Measurements **23**, 587-591.

Rieser U. (1991).
Low-Level Gamma-Spektrometrie zum Zwecke der Dosisleistungbestimmung bei der Lumineszenz-Datierung.
Diplomarbeit, Ruprecht – Karls – Universität Heidelberg.

Rieser U. and Smith E.G.C. (2003).
On the interpretation of dose distributions.
Book of Abstracts of the UK Luminescence and ESR Meeting 2003, 8-10th September 2003, Aberystwyth, United Kingdom, p 56.

Roberts H.M. and Wintle A.G. (2001).
Equivalent dose determinations for polymineralic fine-grains using the SAR protocol: application to a Holocene sequence of the Chinese Loess Plateau.
Quaternary Science Reviews **20**, 859-863.

Roberts R.G. (1997).
Luminescence dating in archaeology: from origins to optical.
Radiation Measurements **27**, 819-892.

Roberts R.G., Spooner N.A. and Questiaux D.G. (1993).
Cautions on the use of extended duration preheats in the optical dating of quartz.
Ancient TL **11**, 47-54.

Roberts R.G., Jones R., Spooner N.A., Head M.J., Murray A.S. and Smith M.A. (1994a).
The human colonisation of Australia: optical dates of 53,000 and 60,000 years bracket human arrival at Deaf Adder George, Northern Territory.
Quaternary Geochronology (Quaternary Science Reviews) **13**, 575-583.

Roberts R.G., Spooner N.A. and Questiaux D.G. (1994b).
Palaeodose underestimates caused by extended-duration preheats in the optical dating of quartz.
Radiation Measurements **23**, 647-653.

Roberts R.G., Spooner N.A. and Questiaux D.G. (1994c).
Optical dating of quartz: A comment on Stokes and Gaylord.
Quaternary Research **42**, 108-109.

Roberts R., Yoshida H., Galbraith R., Laslett G., Jones R. and Smith M. (1998a).
Single-aliquot and single-grain optical dating confirm thermoluminescence age estimates at Malakunanja II rock shelter in northern Australia.
Ancient TL **16**, 19-24.

Roberts R., Bird M., Olley J., Galbraith R., Lawson E., Laslett G., Yoshida H., Jones R., Fullagar R., Jacobsen G. and Hua Q. (1998b).
Optical and radiocarbon dating at Jinmium rock shelter in northern Australia.
Nature **393**, 358-362.

Roberts R.G., Galbraith R.F., Olley J.M., Yoshida H. and Laslett G.M. (1999).
Optical dating of single and multiple grains of quartz from Jinmium rock shelter, northern Australia: Part II, results and implications.
Archaeometry **41**, 365-395.

Roberts R., Walsh G., Murray A., Olley J., Jones R., Morwood M., Tuniz C., Lawson E., Macphail M., Bowdery D. and Naumann I. (1997).
Luminescence dating of rock art and past environments using mud-wasp nests in northern Australia.
Nature **387**, 696-699.

Sanzelle S., Faïn J., Miallier D., Montret M. and Pilleyre Th. (1993).
Exponential regressions for TL/ESR using regenerated dose response curves.
Ancient TL **11**, 6-13.

Schilles T., Poolton N.R.J., Bulur E., Bøtter-Jensen L., Murray A.S., Smith G.M., Riedi P.C. and Wagner G.A. (2001).
A multi-spectroscopic study of luminescence sensitivity changes in natural quartz induced by high-temperature annealing.
Journal of Physics D: Applied Physics **34**, 722-731.

Schwan J. (1988).
Sedimentology of coversands in northwestern Europe.
Thesis, Vrije Universiteit, Amsterdam, 137 p.

Schwan J. (1991).
Palaeowetness indicators in a Weichselian Late Glacial to Holocene succession in the southwestern Netherlands.
Zeitschrift für Geomorphologie, Neue Folge, Supplement-Band **90**, 155-169.

Schwan J. and Vandenberghe J. (1991).
Weichselian Late Pleniglacial fluvio-aeolian deposits and cryogenic structures.
In: Excursion guide for the symposium on "Periglacial environments in relation to climatic change", 3-6 May 1991. IGU Commission on Frost Action Environments, IPA Working Group on Periglacial Environments, Vrije Universiteit, Amsterdam, 68-77.

Singarayer J.S. and Bailey R.M. (2003).
Further investigations of the quartz optically stimulated luminescence components using linear modulation.
Radiation Measurements **37**, 451-458.

Singarayer J.S. and Bailey R.M. (2004)
Component-resolved bleaching spectra of quartz optically stimulated luminescence: preliminary results and implications for optical dating.
Radiation Measurements **38**, 111-118.

Smith B.W. (1988).
Zircon from sediments: a combined OSL and TL auto-regenerative dating technique.
Quaternary Science Reviews **7**, 401-406.

Smith B.W. and Rhodes E.J. (1994).
Charge movements in quartz and their relevance to optical dating.
Radiation Measurements **23**, 329-333.

Smith B.W., Rhodes E.J., Stokes S. and Spooner N.A. (1990a).
The optical dating of sediments using quartz.
Radiation Protection Dosimetry **34**, 75-78.

Smith B.W., Aitken M.J., Rhodes E.J., Robinson P.D. and Geldard D.M. (1986).
Optical dating: methodological aspects.
Radiation Protection Dosimetry **17**, 229-233.

Smith B.W., Rhodes E.J., Stokes S., Spooner N.A. and Aitken M.J. (1990b).
Optical dating of sediments: initial quartz results from Oxford.
Archaeometry **32**, 19-31.

Spencer J.Q., Sanderson D.C.W., Deckers K. and Sommerville A.A. (2003).
Assessing mixed dose distributions in young sediments identified using small aliquots and a simple two-step SAR procedure: the F-statistic as a diagnostic tool.
Radiation Measurements **37**, 425-431.

Spooner N.A. (1992).
Optical dating: preliminary results on the anomalous fading of luminescence from feldspars.
Quaternary Science Reviews **11**, 139-145.

Spooner N.A. (1994a)
The anomalous fading of infra-red stimulated luminescence from feldspars.
Radiation Measurements **23**, 625-632.

Spooner N.A. (1994b).
On the optical dating signal from quartz.
Radiation Measurements **23**, 593-600.

Spooner N.A. and Allsop A. (2000).
The spatial variation of dose-rate from $^{90}Sr/^{90}Y$ beta sources for use in luminescence dating.
Radiation Measurements **32**, 49-55.

Spooner N.A. and Questiaux D.G. (2000).
Kinetics of red, blue and UV thermoluminescence and optically-stimulated luminescence from quartz.
Radiation Measurements **32**, 659-666.

Spooner N.A., Prescott J.R. and Hutton J.T. (1988).
The effect of illumination wavelength on the bleaching of the thermoluminescence (TL) of quartz.
Quaternary Science Reviews **7**, 325-329.

Stokes S. (1991).
Quartz based optical dating of Weichselian coversands from the eastern Netherlands.
Geologie en Mijnbouw **70**, 327-339.

Stokes S. (1992).
Optical dating of young (modern) sediments using quartz: results from a selection of depositional environments.
Quaternary Science Reviews **11**, 153-159.

Stokes S. (1994).
The timing of OSL sensitivity changes in a natural quartz.
Radiation Measurements **23**, 601-605.

Stokes S. (1996a).
Further comparisons of quartz OSL additive dose palaeodoses generated using long and short duration pre-heats.
Ancient TL **14**, 1-3.

Stokes S. (1996b).
Pre-heats, Palaeodoses and Paradigms in the Optical Dating of Quartz: Some Commens on Roberts et al. (1993) 'Cautions on the use of Extended Duration Pre-heats in the Optical Dating of Quartz'.
Ancient TL **14**, 5-8.

Stokes S. (1999).
Luminescence dating applications in geomorphological research.
Geomorphology **29**, 153-171.

Stokes S. and Gaylord D.R. (1994).
Reply to Roberts et al. (1994) Optical dating of quartz: A comment on Stokes and Gaylord (1993).
Quaternary Research **42**, 110-111.

Stokes S., Colls A.E.K., Fattahi M. and Rich J. (2000).
Investigations of the performance of quartz single aliquot D_e determination procedures.
Radiation Measurements 32, 585-594.

Stoneham D. (1991).
Authenticity testing.
In: *Scientific Dating Methods*, eds. H.Y. Göksu, M. Oberhofer and D. Regulla, *Eurocourses Advanced Scientific Techniques* **1**, 175-192, Kluwer Academic Publishers, Dordrecht.

Stoneham. D. and Stokes S. (1991).
An investigation of the relationship between the 110°C TL peak and optically stimulated luminescence in sedimentary quartz.
Nuclear Tracks and Radiation Measurements **18**, 119-123.

Strickertsson K. and Murray A.S. (1999).
Optically stimulated luminescence dates for Late Pleistocene and Holocene sediments from Nørre Lyngby, Northern Jutland, Denmark.
Quaternary Geochronology **18**, 169-178.

Strickertsson K., Murray A.S. and Lykke-Andersen H. (2001).
Optically stimulated luminescence dates for Late Pleistocene sediments from Stensnæs, Northern Jutland, Denmark.
Quaternary Science Reviews **20**, 755-759.

Sutton S.R. and Zimmerman D.W. (1978).
Thermoluminescence dating: radioactivity in quartz.
Archaeometry **20**, 67-69.

Thomas D.S.G., Brook G., Shaw P., Bateman M., Haberyan K., Appleton C., Nash D., McLaren S. and Davies F. (2003).
Late Pleistocene wetting and drying in the NW Kalahari: an integrated study from the Tsodilo Hills, Botswana.
Quaternary International **104**, 53-67.

Thomsen K.J., Bøtter-Jensen L. and Murray A.S. (2002).
Household and workplace chemicals as retrospective luminescence dosemeters.
Radiation Protection Dosimetry **101**, 515-518.

Thomsen K.J., Jain M., Bøtter-Jensen L., Murray A.S. and Jungner H. (2003).
Variation with depth of dose distributions in single grains of quartz extracted from an irradiated concrete block.
Radiation Measurements **37**, 315-321.

Turner R.C., Radley J.M. and Mayneord W.V. (1958).
The alpha-ray activity of human tissues.
The British Journal of Radiology **31**, 397-406.

Valladas G. and Gillot P.Y. (1978).
Dating of the Olby lava flow using heated quartz pebbles: some problems
PACT **2**, 141-150.

Valladas H. and Valladas G. (1982).
Effet de l'irradiation α sur des grains de quartz.
PACT **6**, 171-178.

Vancraeynest L. (1998).
Bijdrage tot de studie van de tehrmoluminescentie-dateringsmethode en toepassing op archeologisch keramiek en eolische sedimenten.
Doctoraatsthesis, Universiteit Gent.

Van Dam R.L. and Schlager W. (2000).
Identifying causes of ground-penetrating radar reflections using time-domain reflectrometry and sedimentological analyses.
Sedimentology **47**, 435-449.

Vandenberghe D., Kasse C., Hossain S.M., De Corte F., Van den haute P., Fuchs M. and Murray A.S. (2004).
Exploring the method of optical dating and comparison of optical and ^{14}C ages of Late Weichselian coversands in the southern Netherlands.
Journal of Quaternary Science **19**, 73-86.

Van den haute P., Vancraeynest L. and de Corte F. (1998).
The Late Pleistocene loess deposits of eastern Belgium New TL age determinations.
Journal of Quaternary Science **13**, 487-497.

Van den haute P., Frechen, M., Buylaert J.-P., Vandenberghe D. and De Corte F. (2003).
The Last Interglacial palaeosol in the Belgian loess belt: TL age record.
Quaternary Science Reviews **22**, 985-990.

Van der Hammen T. (1951).
Late-Glacial flora and periglacial phenomena in the Netherlands.
Thesis, Eduard Ijdo: Leiden.

Van der Hammen T. (1971).
The Upper Quaternary stratigraphy of the Dinkel Valley.
In: *The Upper Quaternary of the Dinkel Valley*, Van der Hammen T. and Wijmstra TA (eds). *Mededelingen Rijks Geologische Dienst, Nieuwe Serie* **22**, 59-72.

Van der Hammen T. and Wijmstra T.A. (editors). (1971).
The Upper Quaternary of the Dinkel Valley.
Mededelingen Rijks Geologische Dienst **22**, 55-214.

Van der Hammen T., Maarleveld G.C., Vogel J.C. and Zagwijn W.H. (1967).
Stratigraphy, climatic successions and radiocarbon dating of the last glacial in the Netherlands.
Geologie en Mijnbouw **46**, 79-95.

Van Geel B., Coope G.R., Van der Hammen T. (1989).
Palaeoecology and stratigraphy of the Lateglacial type section at Usselo (The Netherlands).
Review of Palaeobotany and Palynology **60**, 25-129.

Van Huissteden J., Vandenberghe J., Van der Hammen T. and Laan W. (2000).
Fluvial and aeolian interaction under permafrost conditions: Weichselian Late Pleniglacial, Twente, eastern Netherlands.
Catena **40**, 307-311.

Van Huissteden J., Schwan J.C.G. and Bateman M.D. (2001).
Environmental conditions and paleowind directions at the end of the Weichselian Late Pleniglacial recorded in aeolian sediments and geomorphology (Twente, Eastern Netherlands).
Geologie en Mijnbouw / Netherlands Journal of Geosciences **80**, 1-18.

Vartanian E., Guibert P., Roque C., Bechtel F. and Schvoerer M. (2000).
Changes in OSL properties by preheating: an interpretation.
Radiation Measurements **32**, 647-652.

Visocekas R. (2000).
Monitoring anomalous fading of TL of feldspars by using far-red emission as a gauge.
Radiation Measurements **32**, 499-504.

Voelker A.H.L., Sarnthein M., Grootes P.M., Erlenkeuser H., Laj C., Mazaud A., Nadeau M.-J., Schleicher M. (1998).
Correlation of marine 14C ages from the Nordic seas with the GISP2 isotope record: implications for radiocarbon calibration beyond 25 ka BP.
Radiocarbon **40**, 517-534.

Wagner G.A. (1995).
Altersbestimmung von jungen Gesteinen und Artefakten: Physikalische und chemische Uhren in Quartärgeologie und Archäologie.
Enke-Verlag, Stuttgart, 277p., ISBN: 3-432-26411-9.

Wagner G.A. (1998).
Age determination of young rocks and artifacts: physical and chemical clocks in Quaternary geology and archaeology.
Springer-Verlag Berlin Heidelberg, 466p., ISBN: 3-540-63436-3.

Wallinga J. (2002a).
Optically stimulated luminescence dating of fluvial deposits: a review.
Boreas **31**, 303-322.

Wallinga J. (2002b).
On the detection of OSL age overestimation using single-aliquot techniques.
Geochronometria **21**, 17-26.

Wallinga J., Murray A.S. and Wintle A.G. (2000a).
The single-aliquot regenerative-dose (SAR) protocol applied to coarse-grain feldspar.
Radiation Measurements **32**, 529-533.

Wallinga J., Murray A.S. and Duller G.A.T. (2000b).
Underestimation of equivalent dose in single-aliquot optical dating of feldspars caused by preheating.
Radiation Measurements **32**, 691-695.

Wallner G., Wild E., Aref-Azar H., Hille P. and Schmidt W.F.O. (1990).
Dating of Austrian loess deposits.
Radiation Protection Dosimetry **34**, 69-72.

Warren S.E. (1978).
Thermoluminescence dating of pottery: an assessment of the dose-rate from rubidium.
Archaeometry **20**, 69-70.

Westerhoff W.and Dobma W. (1995).
Landschap en geologie van de Brabantse Wal.
Grondboor en Hamer **3/4**, 72-73.

Westerhoff W.E. and Broertjes J.P. (1990).
Excursiegids 30e Belgisch-Nederlandse palynologendagen, 4-5 Oktober 1990, Arcen.
Rijks Geologische Dienst, distrikt Zuid, kantoor Nuenen, 54 p.

Wintle A.G. (1973).
Anomalous fading of thermoluminescence in mineral samples.
Nature **245**, 143-144.

Wintle A.G. (1975).
Thermal quenching of thermoluminescence in quartz.
Geophysical Journal of the Royal Astronomical Society **41**, 107-113.

Wintle A.G. (1977).
Detailed study of a thermoluminescent mineral exhibiting anomalous fading.
Journal of Luminescence **15**, 385-393.

Wintle A.G. (1985)
Sensitization of TL signal by exposure to light.
Ancient TL **3**, 16-21.

Wintle A.G. (1997).
Luminescence dating: laboratory procedures and protocols.
Radiation Measurements **27**, 769-817.

Wintle A.G. and Huntley D.J. (1979).
Thermoluminescence dating of a deep-sea sediment core.
Nature **279**, 710-712.

Wintle A.G. and Huntley D.J. (1980).
Thermoluminescence dating of ocean sediments.
Canadian Journal of Earth Sciences **17**, 348-360.

Wintle A.G. and Murray A.S. (1997).
The relationship between quartz thermoluminescence, photo-transferred thermoluminescence, and optically stimulated luminescence.
Radiation Measurements **27**, 611-624.

Wintle A.G. and Murray A.S. (1998).
Towards the development of a preheat procedure for OSL dating of quartz.
Radiation Measurements **29**, 81-94.

Wintle A.G. and Murray A.S. (1999).
Luminescence sensitivity changes in quartz.
Radiation Measurements **30**, 107-118.

Wintle A.G. and Murray A.S. (2000).
Quartz OSL: Effects of thermal treatment and their relevance to laboratory procedures.
Radiation Measurements **32**, 387-400.

Wintle A.G., Aitken M.J. and Huxtable J. (1971).
Abnormal thermoluminescence fading characteristics.
In: Proceedings of the third international conference on luminescence dosimetry (ed.: Mejdahl V.), 14/11/1974, Risø, Denmark. Risø Report **249**, 105-131.

Wintle A.G., Li S.-H., Botha G.A. and Vogel J.C. (1995).
Evaluation of luminescence-dating procedures applied to late-Holocene colluvium near St. Paul's Mission, Natal, South Africa.
The Holocene **5**, 97-102.

Wolfe S.A., Huntley D.J. and Ollerhead J. (1995).
Recent and late Holocene sand dune activity in asouthwestern Sakatchewan.
In: Current Research 1995-B; Geological Survey of Canada, 131-140.

Wood P.B. (1994).
Optically stimulated luminescence dating of a late Quaternary shoreline deposit, Tunisia.
Quaternary Geochronology (Quaternary Science reviews) **13**, 513-516.

Yang X.H. and McKeever S.W.S. (1990a).
The pre-dose effect in crystalline quartz.
Journal of Physics D: Applied Physics **23**, 237-244.

Yang X.H. and McKeever S.W.S. (1990b).
Point defects and the pre-dose effect in quartz.
Radiation Protection Dosimetry **33**, 27-30.

Yoshida H., Roberts R.G., Olley J.M., Laslett G.M. and Galbraith R.F. (2000).
Extending the age range of optical dating using single 'supergrains' of quartz.
Radiation Measurements **32**, 439-446.

Yoshida H., Roberts R.G. and Olley J.M. (2003).
Progress towards single-grain optical dating of fossil mud-wasp nests and associated rock art in northern Australia.
Quaternary Science Reviews **22**, 1273-1278.

Zagwijn W.H. (1974).
Vegetation, climate and radiocarbon datings in the Late Pleistocene of the Netherlands. Part II: Middle Weichselian.
Mededelingen Rijks Geologische Dienst, Nieuwe Serie **25**: 101-111.

Zander A., Duller G.A.T. and Wintle A.G. (2000).
Multiple and single aliquot luminescence dating techniques applied to quartz extracted from Middle and Upper Weichselian loess, Zemechy, Czech Republic.
Journal of Quaternary Science **15**, 51-60.

Zhou L.P. and Wintle A.G. (1994).
Sensitivity change of thermoluminescence signals after laboratory optical bleaching: experiments with loess fine grains.
Quaternary Geochronology (Quaternary Science Reviews) **13**, 457-463.

Zimmerman D.W. (1967).
Thermoluminescence from fine grains from ancient pottery.
Archaeometry **10**, 26-28.

Zimmerman D.W. (1971).
Thermoluminescence dating using fine grains from pottery.
Archaeometry **13**, 29-52.

Zimmerman J. (1971).
The radiation-induced increase of the 100°C thermoluminescence sensitivity of fired quartz.
Journal of Physics C: Solid State Physics **4**, 3265-3276.

Zimmerman D.W. (1972)
Relative thermoluminescence effects of alpha- and beta radiation.
Radiation Effects **14**, 81-92.